

# Magnetic Buoyancy Instability in the Solar Tachocline



Daniela Frances Motycka Weston

School of Mathematics

University of Leeds

A thesis submitted for the degree of

*Doctor of Philosophy*



---

To my family.

## **Acknowledgements**

Firstly I would like to thank my supervisors, Professor David Hughes and Professor Steven Tobias, for all their invaluable guidance over the course of my PhD. Without their consistent support and advice this work would not have been possible, and I am very grateful indeed to have had the chance to work with them. I would also like to thank my parents for their support throughout my education, and for helping me to arrive where I am now. This work has been funded by a grant from the Science and Technology Facilities Council, to whom I would also like to extend my thanks.

## Abstract

Magnetic buoyancy has been suggested as a probable mechanism for the rise of flux tubes through the solar convection zone to emerge as the structures we observe at the surface. The large scale of these structures, however, implies that rising flux interacts with the effects of the small-scale, turbulent convection in the region through which they pass in such a way as to preserve the large scale variation. With this motivation, we consider the linear stability of a horizontal layer to magnetic buoyancy, as a model for the escape of field from the solar tachocline.

We assume a turbulent region in the upper part of the layer and a non-turbulent region below. The effects of turbulent convective motion are captured via the turbulent pumping and turbulent diffusion effects implied by mean field dynamo theory. We produce a self-consistent equilibrium state given these effects, and solve for linear perturbations to this state. We consider the effects of parameter changes and of the vertical profiles of the turbulent effects on the growth rate, horizontal scale, and vertical variation of perturbations. We find that for stronger turbulent effects in the upper part of the layer, 2D interchange modes are preferred over 3D modes. We also apply the turbulent pumping and turbulent diffusion preferentially to larger horizontal scales, in light of the assumption of mean field theory. However, we find that the primary effect of the turbulent pumping and diffusion on stability for our parameters is via their influence on the initial equilibrium field gradient, as opposed to their action directly on the perturbations.

In addition, following the asymptotic approach of Gilman (1970), we consider the non-diffusive case for modes with small spatial scale, to derive an analytic expression for the growth rate, given the effect of mean field turbulent pumping. In the small-scale, non-diffusive limit we find that, when the turbulent pumping is included, the stability is no longer determined by an effective vertically dependent dispersion relation but instead by a second order ODE for 3D modes, and first order for interchange. We focus on the interchange case and compare with the more general non-diffusive case, with no small-scale assumption, and find a third order eigenvalue problem for interchange modes. We consider two third order model problems in relation to this system, which we solve asymptotically in the limit of small turbulent pumping. We then consider a local approximation to the non-diffusive linear system and derive dispersion relations for the cases of first an isothermal and then an adiabatic system.

# Contents

<b>1</b>	<b>Introduction</b>	<b>1</b>
1.1	The Sun . . . . .	1
1.2	The Solar Cycle . . . . .	3
1.2.1	Solar Structure and the Effects of Differential Rotation . .	4
1.3	Magnetic Buoyancy . . . . .	8
1.3.1	Linear Magnetic Buoyancy Instability . . . . .	9
1.3.2	Diffusive Case . . . . .	11
1.3.3	Linear magnetic buoyancy instability: previous work . . .	12
1.3.4	Nonlinear simulation . . . . .	14
1.3.5	Rising flux tubes in the convection zone . . . . .	15
1.4	Mean Field Dynamo Theory . . . . .	16
1.4.1	Motivation: the Solar Dynamo Problem . . . . .	16
1.4.2	The Kinematic Dynamo Problem . . . . .	17
1.4.3	Implications of differential rotation . . . . .	18
1.4.4	Mean Field Turbulence: Mathematical Formulation . . . .	20
1.4.5	Past work on mean field turbulent effects . . . . .	22
1.5	Mathematical Formulation . . . . .	26
1.5.1	Coordinate system . . . . .	26
1.5.2	MHD Equations . . . . .	26
1.5.3	Dimensionless Form . . . . .	27
<b>2</b>	<b>Equilibrium Basic State</b>	<b>31</b>
2.1	Equilibrium States of the System . . . . .	31
2.2	Choice of $\gamma(z)$ and $\beta(z)$ profiles . . . . .	33
2.2.1	Standard “step” functional form of $\gamma$ and $\beta$ . . . . .	33

## CONTENTS

---

2.2.2	“Top hat” functional form of $\gamma(z)$ and $\beta(z)$ . . . . .	34
2.3	Choice of Boundary Conditions . . . . .	34
2.4	$\bar{B}'(0) = 1, \bar{B}(0) = 0$ . . . . .	36
2.5	$\bar{B}'(0) = 1, \phi(1) = 1$ . . . . .	38
2.6	$\bar{B}'(0) = 0, \phi(1) = 1$ . . . . .	39
2.6.1	Analytic solution for step functions $\gamma = \beta, \bar{B}'(0) = 0,$ $\phi(1) = 1$ . . . . .	41
2.7	$\bar{B}(0) = 0, \phi(1) = 1$ . . . . .	47
2.7.1	Semi-analytic comparison for $\bar{B}(0) = 0, \phi(1) = 1$ . . . . .	48
2.7.2	Analytic form of the equilibrium field for $\bar{B}(0) = 0, \phi(1) = 1$ . . . . .	49
2.8	$\bar{B}'(1) = 1, \phi(1) = 1$ . . . . .	53
2.8.1	Semi-analytic comparison for $\bar{B}'(1) = 1, \phi(1) = 1$ . . . . .	53
2.9	$\bar{B}'(1) = 0, \phi(1) = 1$ . . . . .	55
2.9.1	Semi-analytic comparison for $\bar{B}'(1) = 0, \phi(1) = 1$ . . . . .	55
2.10	Shifting the interfaces of $\gamma$ and $\beta$ in the $z$ -direction . . . . .	56
2.10.1	$\bar{B}'(0) = 0, \phi(1) = 1$ . . . . .	57
2.10.2	$\bar{B}'(1) = 1, \phi(1) = 1$ . . . . .	61
2.11	Constant $\beta$ : numerical and analytical results . . . . .	63
2.11.1	Constant $\beta = \gamma_m$ with $\bar{B}'(0) = 0, \phi(1) = 1$ . . . . .	63
2.11.2	Constant $\beta, \bar{B}'(0) = 1, \phi(1) = 1$ . . . . .	65
2.11.3	Constant $\beta, \bar{B}'(1) = 1, \phi(1) = 1$ . . . . .	66
2.12	Finding $\gamma$ required to produce a given field, given $\beta$ . . . . .	66
2.13	Other Basic States of the System . . . . .	73
2.13.1	Temperature Equilibrium State . . . . .	74
2.13.2	Density Equilibrium State . . . . .	76
2.14	Summary and Conclusions . . . . .	76
<b>3</b>	<b>Linear Stability of Equilibrium Basic States</b> . . . . .	<b>81</b>
3.1	Linear Stability Analysis . . . . .	81
3.1.1	Linearised System . . . . .	83
3.2	Parameters . . . . .	85
3.3	Linear stability for $\gamma = \beta = 0$ . . . . .	85
3.4	$\gamma = \beta \neq 0$ . . . . .	88

3.4.1	$F = 10^{-3}$ . . . . .	89
3.4.2	$F = 10^{-5}$ . . . . .	93
3.5	Effect of varying $F$ . . . . .	98
3.6	Separating the effects of $\gamma$ and $\beta$ . . . . .	101
3.6.1	$\beta = 0$ . . . . .	103
3.6.2	$\gamma = 0$ . . . . .	105
3.6.3	$\beta > \gamma$ . . . . .	108
3.6.4	$\beta < \gamma$ . . . . .	108
3.7	Summary . . . . .	113
<b>4</b>	<b>Scale Dependence of the Instability</b> . . . . .	<b>115</b>
4.1	Effect of $\gamma$ and $\beta$ on the basic state versus the perturbations . . . . .	115
4.2	Applying $\gamma$ and $\beta$ only to the basic state . . . . .	117
4.2.1	High $F$ Regime . . . . .	118
4.2.2	Low $F$ Regime . . . . .	121
4.3	Scale-dependent $\gamma$ and $\beta$ . . . . .	121
4.4	Prescribed Basic States . . . . .	126
4.4.1	$\bar{B} = 2z$ . . . . .	126
4.4.2	Magnetic slab between $z = 0.6$ and $z = 0.8$ . . . . .	130
4.5	Conclusions . . . . .	134
<b>5</b>	<b>An Analytic Approach to the Diffusionless Instability</b> . . . . .	<b>137</b>
5.1	Large $k_y$ limit . . . . .	137
5.1.1	Diffusionless case, in the limit $k_y \rightarrow \infty$ . . . . .	138
5.1.2	3D system, with $\gamma = 0$ . . . . .	140
5.1.3	Interchange system with $\gamma \neq 0$ . . . . .	141
5.2	Comparison with the diffusionless interchange system for finite $k_y$ . . . . .	142
5.2.1	Interchange case . . . . .	143
5.3	Model problem . . . . .	146
5.3.1	Simplified third order eigenvalue model problem . . . . .	146
5.3.2	Numerical solution to (5.61) for $y'(0) = 0$ . . . . .	151
5.3.3	Numerical solution to (5.61) for $y'(1) = 0$ . . . . .	154
5.4	A more complex third order model problem . . . . .	156
5.4.1	Numerical solution . . . . .	159

## CONTENTS

---

5.5	Local Approximation . . . . .	164
5.5.1	Isothermal, interchange system . . . . .	165
5.5.2	Isothermal 3D system . . . . .	168
5.5.3	Adiabatic, interchange system . . . . .	169
5.5.4	Applicability of the Local Approximation . . . . .	174
5.6	Conclusions . . . . .	175
<b>6</b>	<b>Conclusions and Discussion</b>	<b>179</b>
6.1	Equilibrium Basic States . . . . .	180
6.2	Linear Stability Analysis: Conclusions . . . . .	180
6.2.1	Action of $\gamma = \beta$ on the basic state and perturbed quantities in combination . . . . .	180
6.2.2	Effect of varying field strength $F$ . . . . .	181
6.2.3	Varying the relative strength of $\gamma$ and $\beta$ . . . . .	181
6.2.4	Scale dependence of the instability . . . . .	181
6.2.5	Prescribed basic states . . . . .	182
6.3	Diffusionless Case: Conclusions . . . . .	183
6.3.1	Diffusionless, small scale limit . . . . .	183
6.3.2	Diffusionless interchange instability . . . . .	184
6.3.3	Local Analysis . . . . .	184
6.4	Limitations . . . . .	186
6.4.1	Parameter Regime . . . . .	186
6.4.2	Validity of the Mean Field Approximation . . . . .	186
6.4.3	Basic state boundary conditions . . . . .	187
6.5	Extensions of the Research . . . . .	188
6.5.1	Rotation . . . . .	188
6.5.2	$\alpha$ Effect . . . . .	189
6.5.3	Nonlinear Regime . . . . .	189
6.6	Concluding Remarks . . . . .	189
<b>A</b>	<b>Analytic solution for step functions <math>\gamma = \beta</math>, <math>\bar{B}'(0) = \lambda</math>, <math>\phi(1) = 1</math></b>	<b>191</b>
<b>B</b>	<b>Coefficients of the dispersion relation for the 3D isothermal in- stability</b>	<b>193</b>

## CONTENTS

---

References	211
------------	-----

## CONTENTS

---

# List of Figures

1.1	Sunspot butterfly diagram (Royal Observatory Greenwich/NOAA), showing the change in the average latitude of sunspots over the course of the solar cycle. Note that the magnetic field switches polarity with each sunspot cycle, giving rise to the full twenty-two year magnetic cycle. . . . .	4
1.2	Observed differential rotation velocity of the solar convection zone, from helioseismological measurements averaged over the period 1995-2009 (NSO/GONG, 2009). . . . .	5
2.1	The vertical $\gamma(z)$ profile given by (2.4), with $\gamma_m = 0.1$ , $a = 30$ , and $z_i = 0.5$ . . . . .	34
2.2	The modified form of $\gamma$ given by (2.6), with $\gamma_m = 0.1$ , $a = 30$ , $z_{i1} = 0.1$ , and $z_{i2} = 0.5$ . . . . .	35
2.3	Variation of equilibrium field for $\bar{B}'(0) = 1$ and $\bar{B}(0) = 0$ , $\gamma = \beta$ with varying amplitude given by (2.4) and (2.5). . . . .	36
2.4	Variation of equilibrium field for $\bar{B}'(0) = 1$ and $\bar{B}(0) = 0$ , $\gamma = \beta$ with varying amplitude given by (2.6) and (2.7), with $z_{i1} = 0.1$ and $z_{i2} = 0.5$ . . . . .	37
2.5	Variation of equilibrium field for $\bar{B}'(0) = 1$ and constant flux, $\gamma = \beta$ with varying amplitude, for (a) step profile and (b) top hat profile with $z_{i1} = 0.1$ and $z_{i2} = 0.5$ . . . . .	39
2.6	Variation of equilibrium field for $\bar{B}'(0) = 0$ and constant flux, $\gamma = \beta$ with varying amplitude, for (a) step profile and (b) top hat profile with $z_{i1} = 0.1$ and $z_{i2} = 0.5$ . . . . .	40

## LIST OF FIGURES

---

2.7	The variation of the equilibrium field, calculated numerically for $\bar{B}'(0) = 0$ and constant flux boundary conditions, and pumping and turbulent diffusion $\gamma = \beta$ given by Equation (2.4), with parameters $z_i = 0.5$ and $a = 1000$ . Compare with the numerical result for a step-like $\gamma$ and $\beta$ for the same boundary conditions, presented in Figure 2.6a. . . . .	44
2.8	Semi-analytic field profiles for $\bar{B}'(0) = 0$ , constant flux boundary conditions, with $\gamma = \beta$ given by (a) step function and (b) top hat function between $z_{i1} = 0.1$ and $z_{i2} = 0.5$ . . . . .	45
2.9	Numerically calculated profiles for $\bar{B}'(0) = 0$ , constant flux, and top hat $\gamma$ , with $a = 1000$ . . . . .	46
2.10	Variation of equilibrium field for $\bar{B}(0) = 0$ and constant flux, $\gamma = \beta$ with varying amplitude, for (a) step profile and (b) top hat profile with $z_{i1} = 0.1$ and $z_{i2} = 0.5$ . . . . .	48
2.11	Semi-analytic field profiles for $\bar{B}(0) = 0$ , constant flux boundary conditions, with $\gamma = \beta$ given by (a) step function and (b) top hat function between $z_{i1} = 0.1$ and $z_{i2} = 0.5$ . . . . .	49
2.12	Coefficients $P$ , $Q$ , $R$ , and $S$ as a function of $\gamma_m$ in the case of constant flux and $\bar{B}(0) = 0$ boundary conditions, assuming a step function form for $\gamma = \beta$ , with $\zeta_o = 0.01$ and $C_k = 0.01$ . . . . .	52
2.13	Absolute values of coefficients $P$ , $Q$ , $S$ , and $R$ as a function of small $\gamma_m$ , compared with their full analytic forms, (2.20) – (2.23), in the limit $\gamma_m \rightarrow 0$ . . . . .	52
2.14	Variation of equilibrium field for $\bar{B}'(1) = 1$ and constant flux, $\gamma = \beta$ with varying amplitude, for (a) step profile and (b) top hat profile with $z_{i1} = 0.1$ and $z_{i2} = 0.5$ . . . . .	53
2.15	Semi-analytic field profiles for $\bar{B}'(1) = 1$ , constant flux boundary conditions, with $\gamma = \beta$ given by (a) step function and (b) top hat function between $z_{i1} = 0.1$ and $z_{i2} = 0.5$ . . . . .	54
2.16	Variation of equilibrium field for $\bar{B}'(1) = 0$ and constant flux, $\gamma = \beta$ with varying amplitude, for (a) step profile and (b) top hat profile with $z_{i1} = 0.1$ and $z_{i2} = 0.5$ . . . . .	55

## LIST OF FIGURES

---

2.17	Semi-analytic field profiles for $\bar{B}'(1) = 0$ , constant flux boundary conditions, with $\gamma = \beta$ given by (a) step function and (b) top hat function between $z_{i1} = 0.1$ and $z_{i2} = 0.5$ . . . . .	56
2.18	Numerically calculated equilibrium fields for $z_{i\gamma} = 0.25$ , with constant flux and $\bar{B}'(0) = 0$ boundary conditions. . . . .	58
2.19	Numerically calculated equilibrium fields for $z_{i\gamma} = 0.75$ , with constant flux and $\bar{B}'(0) = 0$ boundary conditions. . . . .	60
2.20	Numerically calculated equilibrium fields for $z_{i\gamma} = 0.25$ , with constant flux and $\bar{B}'(1) = 1$ boundary conditions. . . . .	61
2.21	Numerically calculated equilibrium fields for $z_{i\gamma} = 0.75$ , with constant flux and $\bar{B}'(1) = 1$ boundary conditions. . . . .	62
2.22	Numerically calculated equilibrium fields for constant $\beta = \gamma_m = 0.1$ , with variable $z_{i\gamma}$ , and $\bar{B}'(0) = 0$ and constant flux boundary conditions. . . . .	63
2.23	Numerically calculated equilibrium fields for constant $\beta = \gamma_m = 0.1$ , with variable $z_{i\gamma}$ , and $\bar{B}'(0) = 1$ and constant flux boundary conditions. . . . .	65
2.24	Equilibrium fields for constant $\beta = \gamma_m = 0.1$ , with variable $z_{i\gamma}$ , and $\bar{B}'(1) = 1$ and constant flux boundary conditions. . . . .	66
2.25	The three forms of $\bar{B}$ involved in the inverse analysis. Upper: top hat profile, middle: step profile, lower: sandwich profile. . . . .	67
2.26	$\gamma$ required to produce a step field, given various forms of $\beta$ . From top to bottom: with tanh, exponential, linear $\beta$ . . . . .	69
2.27	$\gamma$ required to produce a top hat field, given various forms of $\beta$ . From top to bottom: with tanh, exponential, linear $\beta$ . . . . .	70
2.28	$\gamma$ required to produce a sandwich field, given various forms of $\beta$ . From top to bottom: with tanh, exponential, linear $\beta$ . . . . .	70
2.29	(a) Temperature, density and pressure equilibrium states for $\gamma_m = 0$ , and (b) difference in equilibrium states for non-zero $\gamma = \beta$ , for $F = 0.001$ . . . . .	74
2.30	(a) Temperature, density and pressure equilibrium states for $\gamma_m = 0$ , and (b) difference in equilibrium states for non-zero $\gamma = \beta$ , for $F = 0.00001$ . . . . .	75

## LIST OF FIGURES

---

3.1	$F$ -dependence of the scale and growth rate of the most unstable mode, when $\gamma = \beta = 0$ . (a), (b): horizontal wavenumbers $k_x$ and $k_y$ , (c): growth rate $Re(s)$ of the most unstable mode, as a function of $F$ . . . . .	87
3.2	Normalised $\hat{b}_x$ for the most unstable mode, with $\gamma = \beta = 0$ . . . . .	87
3.3	Growth rate $\Re(s)$ as a function of $k_x$ and $k_y$ for various values of $\gamma_m$ , for $F = 10^{-3}$ , with $\gamma = \beta$ applied to the basic states and equally to perturbations of all scales. . . . .	90
3.4	Basic states for $\zeta_o = 0.01$ , $C_k = 0.01$ , with $\gamma = \beta$ . . . . .	91
3.5	Normalised $\hat{b}_x$ perturbations for the mode of maximum growth rate, for $F = 10^{-3}$ , $\gamma = \beta$ (contour plots shown in Figure 3.3). . . . .	91
3.6	Growth rate $\Re(s)$ as a function of $k_x$ and $k_y$ for various values of $\gamma_m$ , for $F = 10^{-3}$ , with $\gamma = \beta$ applied to the basic states and equally to perturbations of all scales, and $\gamma_m \leq 10^{-3}$ . . . . .	94
3.7	Basic states for $\zeta_o = 0.01$ , $C_k = 0.01$ , with $\gamma = \beta$ and $\gamma_m \leq 10^{-3}$ . . . . .	95
3.8	Normalised $\hat{b}_x$ perturbations for the mode of maximum growth rate, for $F = 10^{-3}$ , $\gamma = \beta$ , with $\gamma_m \leq 10^{-3}$ (contour plots shown in Figure 3.6). . . . .	95
3.9	Growth rate $\Re(s)$ as a function of $k_x$ and $k_y$ with various values of $\gamma_m$ , for $F = 10^{-5}$ , with $\gamma = \beta$ applied to the basic states and equally to perturbations of all scales. . . . .	96
3.10	Normalised $\hat{b}_x$ perturbations for the mode of maximum growth rate, for $F = 10^{-5}$ , $\gamma = \beta$ . . . . .	97
3.11	Horizontal scale of the most unstable mode for various values of $F$ , for comparison with equivalent contour plots shown in Figures 3.3 for $F = 10^{-3}$ and 3.9 for $F = 10^{-5}$ . . . . .	99
3.12	(a) $k_x$ and (b) $k_y$ of the most unstable mode as a function of $\gamma_m$ , for various values $F$ . Note that $\gamma_m = 0$ values are plotted with circles on the vertical axis. Note also that in (a), the value of $k_x$ is zero for all $\gamma_m$ in the cases of $F = 10^{-1}, 10^{-2}, 10^{-3}$ , as in these cases the most unstable mode is interchange. . . . .	100
3.13	Growth rate of the most unstable mode as a function of $\gamma_m$ . Note that $\gamma_m = 0$ values are plotted with circles on the vertical axis. . . . .	101

## LIST OF FIGURES

---

3.14	Growth rates of the most unstable mode for the case of $\beta = q\gamma$ , with the additional case of $\gamma = 0$ , with fixed $F = 10^{-3}$ . . . . .	102
3.15	(a) $k_x$ and (b) $k_y$ for the most unstable mode in the case $\beta = q\gamma$ , with the additional case of $\gamma = 0$ , for $F = 10^{-3}$ . . . . .	103
3.16	Growth rate $\Re(s)$ as a function of $k_x$ and $k_y$ at various values of $\gamma_m$ with $\beta = 0$ , for $F = 10^{-3}$ . . . . .	104
3.17	(a) Equilibrium basic states and (b) normalised $\hat{b}_x$ perturbations for the most unstable mode in the cases shown in Figure 3.16, for $\beta_m = 0$ . . . . .	105
3.18	Growth rate $\Re(s)$ as a function of $k_x$ and $k_y$ for various values of $\beta_m$ with $\gamma = 0$ , for $F = 10^{-3}$ . . . . .	106
3.19	(a) Equilibrium basic states and (b) normalised $\hat{b}_x$ perturbations for the most unstable mode in the cases shown in Figure 3.18, for $\gamma = 0$ . . . . .	107
3.20	Growth rate $\Re(s)$ as a function of $k_x$ and $k_y$ for various values of $\gamma_m$ with $\beta = 10\gamma$ , for $F = 10^{-3}$ . . . . .	109
3.21	(a) Equilibrium basic states and (b) normalised $\hat{b}_x$ perturbations for the most unstable mode in the cases shown in Figure 3.20, for $\beta_m = 10\gamma_m$ . . . . .	110
3.22	(a) Equilibrium basic states and (b) normalised $\hat{b}_x$ perturbations for the most unstable mode in the cases shown in Figure 3.23, for $\beta_m = 0.1\gamma_m$ . . . . .	110
3.23	Growth rate $\Re(s)$ as a function of $k_x$ and $k_y$ for various values of $\gamma_m$ with $\beta = 0.1\gamma$ , for $F = 10^{-3}$ . . . . .	111
3.24	Gradients of the basic states for $\beta = 0.1\gamma$ . . . . .	113
4.1	Growth rate of the most unstable mode when $\gamma$ and $\beta$ are applied only to the basic state, $F = 10^{-1}, 10^{-2}, 10^{-3}, 10^{-4}, 10^{-5}$ . . . . .	118

## LIST OF FIGURES

---

4.2	Normalised difference in the growth rate of the most unstable mode when $\gamma$ and $\beta$ are applied to all scales versus applied only to the basic state, for (a) $F = 10^{-1}, 10^{-2}, 10^{-3}$ , and (b) $F = 10^{-4}, 10^{-5}$ . Note that the division of these results into two plots is in part to differentiate the two $F$ regimes discussed in Section 3.5, which also exist in this case, and in part for convenience as the value of the quantity defined by Equation (4.1) is of a different order of magnitude in the two regimes, especially in the case of $F = 10^{-5}$ .	119
4.3	Contour plots for $F = 10^{-3}$ and various values of $\gamma_m$ , with $\gamma = \beta$ applied only to the basic state; cf. Figure 3.3.	120
4.4	Contour plots for $F = 10^{-5}$ and various values of $\gamma_m$ , with $\gamma = \beta$ applied only to the basic state; cf. Figure 3.9.	122
4.5	Contour plots for $F = 10^{-3}$ for various values of $\gamma_m$ , with $\gamma = \beta$ applied to the basic state according to (2.4), (2.5) and to the perturbations according to (4.2).	124
4.6	Growth rate of the most unstable mode when $\gamma$ and $\beta$ are applied to the perturbations according to (4.2), for $F = 10^{-1}, 10^{-2}, 10^{-3}, 10^{-4}, 10^{-5}$ .	125
4.7	Fractional variation of the growth rate of the most unstable mode when $\gamma$ and $\beta$ are applied to the perturbations according to (4.2), compared to equal application to all scales, for (a) $F = 10^{-1}, 10^{-2}, 10^{-3}$ , and (b) $F = 10^{-4}, 10^{-5}$ .	125
4.8	Growth rate $\Re(s)$ as a function of $k_x$ and $k_y$ for various values of $\gamma_m$ , for $F = 10^{-3}$ , with prescribed basic state $\bar{B} = 2z$ .	127
4.9	Normalised $\hat{b}_x$ perturbations for the case of $\bar{B} = 2z$ , for the most unstable modes in the cases shown in Figure 4.8.	128
4.10	Growth rate of the most unstable mode for prescribed basic state $\bar{B} = 2z$ .	128
4.11	Horizontal scales (a) $k_x$ and (b) $k_y$ of the most unstable mode for prescribed basic state $\bar{B} = 2z$ , with $\gamma_m = 0$ values plotted on the vertical axis. Note the lack of transition to interchange modes at higher $\gamma_m$ .	129
4.12	The top hat field given by Equation (4.3), with $B_o = 0.5$ , $a_B = 30$ , $z_1 = 0.6$ and $z_2 = 0.8$ .	131

**LIST OF FIGURES**

---

4.13	Growth rate contour plots for various values of $\gamma_m$ , for the case $F = 10^{-3}$ , with prescribed “top hat” basic state. Note the global maxima (marked with a cross) are interchange modes for $\gamma_m = 0$ and $\gamma_m = 0.001$ only. For higher $\gamma_m$ the interchange maximum is a local one, and the fastest growing mode is 2D undular, with $k_y = 0$ . <a href="#">132</a>
4.14	Comparison of (a) interchange ( $k_x = 0$ ) and (b) 2D undular ( $k_y = 0$ ) instability maxima for a prescribed top hat basic state, with various values of $\gamma_m$ and for $F = 10^{-3}$ . . . . . <a href="#">133</a>
5.1	$\lambda(\epsilon)$ , the numerically calculated solution to $\tan(\lambda) = \epsilon\lambda$ for initial guess $\lambda_o = \pi$ . . . . . <a href="#">149</a>
5.2	The composite solution $y_c$ , given by (5.77), in the regime of (a) small $\epsilon$ in which it holds, and (b) in the regime of $\epsilon \rightarrow O(1)$ in which it breaks down. . . . . <a href="#">150</a>
5.3	“Error” in the $\epsilon \rightarrow 0$ solution, given by (5.78) multiplied by a factor of $1/\epsilon$ . . . . . <a href="#">150</a>
5.4	Numerical solutions to Equation (5.61), for (a) small $\epsilon$ , and (b) $\epsilon = O(1)$ . Compare with asymptotic approximation (5.77), plotted in Figure 5.2. . . . . <a href="#">152</a>
5.5	Numerically calculated eigenvalues $\lambda$ for Equation (5.61), using initial guess $\lambda_o = \pi$ . Compare with the solution to $\tan(\lambda) = \epsilon\lambda$ , shown in Figure 5.1. . . . . <a href="#">152</a>
5.6	Comparison of the numerical solution shown in Figure 5.4 (blue) with the analytically constructed solution in the asymptotic limit $\epsilon \rightarrow 0$ (maroon, dashed). Both solutions have been normalised to show more easily their convergence as $\epsilon \rightarrow 0$ . . . . . <a href="#">153</a>
5.7	Difference in eigenvalues between the numerical and asymptotic cases (blue), with $\epsilon^2$ dependence overplotted (orange, dashed). . . <a href="#">153</a>
5.8	Numerical solution to Equation (5.61) with boundary conditions $y(0) = 0, y(1) = 0, y'(1) = 0$ , for (a) small $\epsilon$ and (b) $\epsilon = O(1)$ . . . <a href="#">155</a>
5.9	$\lambda^2$ eigenvalues corresponding to the solutions shown in Figure 5.8. <a href="#">155</a>
5.10	Numerical solutions to Equation (5.80), for (a) $\gamma = 10^{-2}$ , (b) $\gamma = 10^{-3}$ , (c) $\gamma = 10^{-4}$ , and (d) $\gamma = 10^{-5}$ . . . . . <a href="#">160</a>

## LIST OF FIGURES

---

- 5.11 Eigenvalues  $\sigma(\gamma)$  corresponding to the numerical solutions plotted in Figure 5.10. Note that the plots of (a)  $k = 1$  and (b)  $k > 1$  are separated due to the difference in scale of the values of  $\sigma$ . . . . . 161
- 5.12 Eigenvalues  $\sigma(0, k)$  for  $\gamma = 0$ , corresponding to the eigenvalues of the parabolic cylinder equation, i.e. the outer equation (cf. Figure 5.13). . . . . 161
- 5.13 The variation of  $\sigma(\gamma, k) - \sigma(0, k)$  as a function of  $k$  and  $\gamma$ , showing the deviation from the parabolic cylinder function eigenvalues due to non-zero  $\gamma$ . . . . . 163
- 5.14  $\sigma(\gamma, k) - \sigma(0, k)$  as a function of  $\ln(k)$  and  $\ln(\gamma)$ , with arbitrary colour values assigned to constant values of  $\sigma(\gamma, k) - \sigma_o(k)$ . Dashed lines correspond to constant  $\gamma k$ , and dotted lines to constant  $\gamma/k^2$ , showing the approximate dependence for high and low  $k$ , respectively. 164

# Chapter 1

## Introduction

### 1.1 The Sun

Throughout human history, we have been looking up at the Sun and making observations of it. Even before the advent of the modern scientific method, we have made informal observations of its position and the changes it may undergo; after all, the Sun has always been vital to human existence, providing the energy required by all life on earth. As technology advanced, however, multiple civilisations began to formalise their observations. The Babylonians regularly recorded the incidence of solar eclipses in the 8th century BC, though their very first eclipse observations go back several centuries earlier.

However, at around the same time, Chinese astronomers were able to measure a more ephemeral solar phenomenon: the first recorded observations of sunspots date from around 800BC. Sunspots appear as darkened patches on the solar disc, usually appearing in pairs or other more complex groupings. They are visible to the naked eye or through a filter or a solar telescope, though historically, they would have first been viewed through smoke or fog, or on an image of the solar disc projected through a lens onto a screen. Sunspots are dynamic features with a lifetime that can vary from the order of days to months. Over this timescale, they are observed to move across the surface of the solar disc in a west-to-east direction, travelling with the Sun's rotation.

## 1. INTRODUCTION

---

Although we have ancient and medieval records of sunspots, the earliest measurements we have that are relatively regular and accurate by modern standards date from around the early 17th century, when the telescope was invented and came into greater use. Telescope observations of sunspots were first taken in 1611, by Thomas Harriot and independently by Johannes and David Fabricius, as well as by Galileo Galilei and Christoph Scheiner. However, probably the best-known early sunspot observations are those of Galileo, who made meticulous drawings of sunspots over their lifetimes, from which it was easily possible to see their motion across the solar disc.

Over the following centuries, sunspot observations became even more systematic, and several observational laws were developed to describe how and where they formed. One thing that quickly became apparent over decades of sunspot measurements was the fact that their incidence is subject to a cycle: over the timescale of approximately eleven years, the number of sunspots can be seen to peak and then fall, only to begin the cycle again. Over the course of this cycle, the average location of sunspots is observed to move from higher latitudes to lower, as the cycle moves towards solar maximum. We also observe that sunspots often come in pairs, orientated at a characteristic angle, relative to the equator, which varies over the course of the solar cycle. These observations are key to our modern understanding of how the solar magnetic field is created and maintained.

It was [Hale \(1908\)](#) who first suggested that sunspots are inherently associated with magnetic field, and may be used as indicators of variation in the Sun's large-scale field over the course of the solar cycle. Sunspots appear at locations where tubes of strong magnetic flux pierce the solar surface, inhibiting convection in a localised area. They appear darker than the surrounding material because these regions are cooler, producing lower levels of emission than the surrounding material. This understanding of sunspots also explains why they tend to occur in pairs, or sometimes more complex configurations: a sunspot pair corresponds with the two “footpoints” of a loop of magnetic field, emerging partially from beneath the solar surface. This is a product of the fact that magnetic fields are divergence free ( $\nabla \cdot \mathbf{B} = 0$ ), and so the field lines cannot have “ends”, but

must rather be connected back to the Sun's field itself. However, although more accurate observations across the electromagnetic spectrum have given us an ever-increasing level of detail in our observations of the magnetic structure that exists on the surface of the Sun, there remain the questions of what actually drives this cycle, and what processes set the timescale over which it operates. This leads to the more fundamental question of the origin of the Sun's magnetic field itself, and how it is maintained over time. This is the problem of the solar dynamo, and it is one that may be addressed both theoretically and computationally, in order to compare with observations.

As well as being theoretically and mathematically rich and challenging, the study of the solar dynamo is also potentially of great practical importance. Today, we know that the solar cycle and variations in the solar magnetic field associated with it give rise to what is referred to as “space weather”: changes in the magnetic field of the solar wind due to material that is expelled from solar active regions, which are both more common, and more prone to eruptive events such as flares and coronal mass ejections, at times of high solar activity.

Such events have the potential to have a large effect on our lives, in the modern world especially, as they can disrupt the communications technologies and power grids upon which we all rely. Thus, it is now more important than ever to study the solar magnetic field, its origins, and its behaviour, not only as a matter of pure scientific interest but as a way to help us understand and mitigate against the possible danger posed by living close to the star that sustains and facilitates life and civilisation as we know it.

## 1.2 The Solar Cycle

The phrase “solar cycle” is often conflated with the sunspot cycle, though the two are distinct: the sunspot cycle measures simply the incidence of sunspots and their number, and lasts approximately eleven years. However, following the realisation that sunspots are magnetic in origin, it has been shown that the full solar cycle itself lasts twice this long, as after each sunspot cycle the magnetic

## 1. INTRODUCTION

---

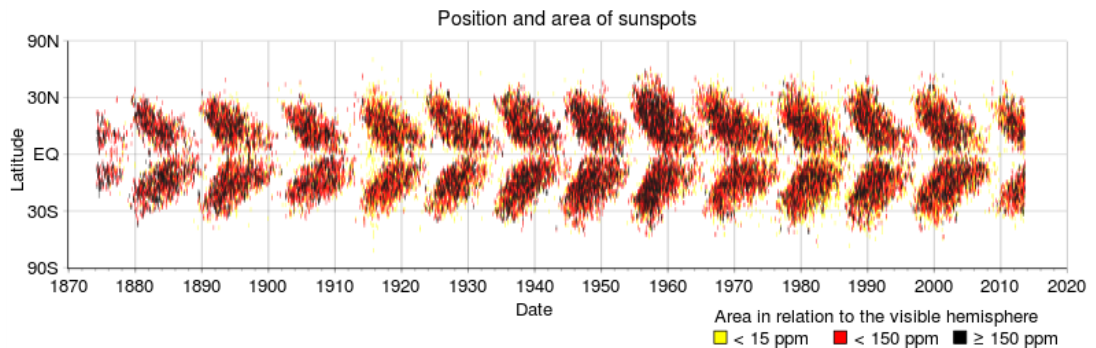


Figure 1.1: Sunspot butterfly diagram (Royal Observatory Greenwich/NOAA), showing the change in the average latitude of sunspots over the course of the solar cycle. Note that the magnetic field switches polarity with each sunspot cycle, giving rise to the full twenty-two year magnetic cycle.

field of the Sun reverses, so a “full” solar cycle lasts approximately twenty-two years.

The cycle is most clearly visualised by plotting the incidence of sunspots by latitude as a function of time. By this metric, we may see the number of sunspots increase and their average latitude decrease approaching sunspot maximum. This type of plot is known as a “butterfly diagram”, shown in Figure 1.1 for data covering the twentieth century. To understand this variation, we must consider the internal structure and rotation profile of the Sun.

### 1.2.1 Solar Structure and the Effects of Differential Rotation

We will briefly summarise the structure of the Sun, and then discuss the issues that motivate the work presented here. We are able to use both theoretical and observational approaches in combination to better understand the internal regions of the Sun. With the advent of helioseismology, it has become possible to study the solar interior all the more easily. Helioseismology uses measured oscillations of the Sun to infer its internal structure and motion, and has been invaluable in providing data to motivate and support theoretical work.

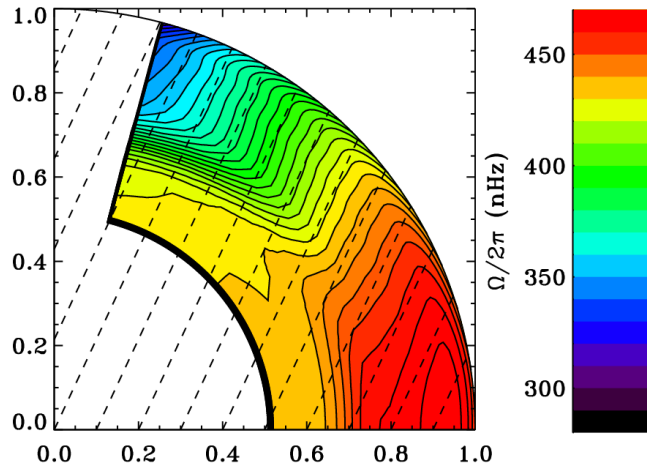


Figure 1.2: Observed differential rotation velocity of the solar convection zone, from helioseismological measurements averaged over the period 1995-2009 (NSO/GONG, 2009).

The Sun has a convective envelope that accounts for the outer 28.7% of its radius (Christensen-Dalsgaard *et al.*, 1991), surrounding the non-convecting radiation zone below. Within the radiation zone is the core, where fusion reactions produce heating in the Sun. However, it is primarily the outer convective envelope and just below it that we shall concern ourselves with here, rather than the deep interior of the Sun. In the convection zone, turbulent convection is present, as well as differential rotation.

The convective motion is the source of the magnetic structure we see emerging over the course of the solar cycle. The convection zone undergoes differential rotation, with a rotation period of approximately 24.5 days at the equator, compared with approximately 36 days at the poles; see Figure 1.2 for the associated rotation frequency profile, showing the difference between high and low latitudes.

Between the radiation and the convection zones, there is an interface layer that

## 1. INTRODUCTION

---

is known as the tachocline, and it is the region of this boundary that we shall mainly focus on in this work. The existence of an outer convection zone region separated from the radiative interior is not, in itself, a consequence of rotation; rather, the temperature gradient in the outer regions of Sun-like stars makes this region susceptible to convective instability according to the Schwarzschild criterion that predicts the onset of such an instability.

However, as discussed by Spiegel (1972), due to the coupling of the magnetic field in the convection zone to that of the outflowing solar wind and its escaping flux, it is expected that some external layer of the Sun be spun down by this process. This led to the idea of a region where convective motion acts to spin down the rotation, giving rise to a departure from solid body rotation in a specific upper region with a defined boundary near the base of the convection zone.

The existence of such a boundary was confirmed via helioseismological measurements in the following decades, showing a sharp change in azimuthal velocity as a function of depth. Its position, rotation, and other properties were constrained by observational work such as that of Duvall *et al.* (1984), Brown (1985), Duvall *et al.* (1986), Brown & Morrow (1987), Kosovichev (1988), Brown (1989), Dziembowski (1989), Basu *et al.* (1994), and Charbonneau *et al.* (1999). In describing the structure and evolution of this region, Spiegel & Zahn (1992) were the first to apply the name “tachocline” — in analogue to the concept of an oceanic thermocline, over which temperature changes abruptly — denoting a narrow region of high velocity gradient.

Because of the abrupt change in velocity, the tachocline is a layer of strong velocity shear. For this reason, it is thought to be the location of the solar dynamo process, which requires strong velocity shear in order to “wind up” poloidal field (field in the radial and meridional directions) to toroidal field (in the azimuthal direction, for an axisymmetric field; see Section 1.4.3 for further discussion and definitions) over the course of the solar cycle. The link between the base of the convection zone and the dynamo process had been noted for some time (for example in the work of Spiegel & Weiss (1980), Golub *et al.* (1981), and Gilman

*et al.* (1989)). As a result of this conclusion, Parker (1993) developed a model of a dynamo process that operated at this interface.

To understand the link between strong velocity shear and the dynamo, imagine a simple model of the solar magnetic field where all of the field lines are poloidal. In a fluid with very high electrical conductivity — which is generally the case in astrophysical systems — magnetic flux is what is known as “frozen in” to the flow, meaning that the field lines move with the flow of the material they penetrate. In fact, both radial and latitudinal shear is present in the tachocline region, and both are able to generate toroidal field from poloidal. Thus, under the effect of differential rotation such as that shown in Figure 1.2, the velocity shear results in a conversion of poloidal to toroidal field.

However, this “winding up” of toroidal field — known as the  $\omega$ -effect — ultimately produces a toroidal field of sufficient strength that it becomes unstable. As the toroidal field rises through the convection zone, it becomes susceptible to instabilities, a process which is responsible for the structures that we see emerging from the solar surface, that also result in the formation of sunspots.

Such a model lacks much of the complexity that we observe in the Sun, but it is useful for illustrative purposes, as it goes some way towards explaining the variation that we see over the course of the solar cycle. The number and complexity of active regions (typically associated with sunspot pairs or groups) on the solar surface increases approaching solar maximum, as velocity shear increasingly destabilises the underlying field. Furthermore, the average orientation of the line connecting sunspot pairs — which becomes more parallel to the equator, i.e. more toroidal, over the course of the cycle — is also consistent with this picture, because as the field is sheared it becomes increasingly toroidal, as previously stated.

This model is of course extremely limited; for a start, it does not include the effects of convective motion that we observe occurring in the convection zone, nor does it fully explain the driving mechanism of this process, and how it is maintained, and the physical origin of the time and spatial scales involved.

## 1. INTRODUCTION

---

It also highlights another important question facing any model that hopes to explain the solar dynamo process. Differential rotation acts as a source of toroidal field, converted from poloidal field; however, in order to have a closed, cyclical process the poloidal field must somehow be regenerated from toroidal field. This fundamental question will be discussed in more detail in Section [1.4.2](#).

These issues all fall under the larger question of the operation of the solar dynamo. We will discuss dynamo theory and modelling approaches later. However, we may first ask an associated question based on observation of the field that the dynamo produces: how can we explain the magnetic structure that we are able to observe as emerging over the course of the solar cycle, given the motion present in the convection zone? We are able to observe flux rising, but we aim to explain and characterise this rise and its physical mechanisms. We can further break this down into two separate questions: firstly, how does the field initially escape, and secondly, how does it rise through the convection zone. This work is motivated by the first of these questions. Fortunately, we have a strong candidate for the mechanism of the escape of field from the base of the convection zone: the effect of magnetic buoyancy. In the main body of this work, we consider the effect of turbulent convection on the linear stability to magnetic buoyancy of a layer of field at the base of the convection zone. However, we will first consider the physical effect of magnetic buoyancy itself, and the instability of an equilibrium field to which it gives rise.

### 1.3 Magnetic Buoyancy

Within astrophysics, there are several usages of the term magnetic buoyancy, which refer to slightly different physical mechanisms. For our purposes, we will consider the magnetic buoyancy instability resulting from the stratification of the magnetic field and the density under gravity.

Note that sometimes the term magnetic buoyancy is also used to refer to a related physical effect, that is, the lack of equilibrium of an isolated tube of flux in

a non-magnetic atmosphere, described by [Parker \(1955a\)](#). “Magnetic buoyancy”, in this sense, is a result of the pressure balance on a flux tube creating a lack of mechanical equilibrium. For an isolated flux tube permeated by a field  $B$ , the field gives rise to an additional magnetic pressure within the tube. Thus, total pressure within the tube is the sum of the thermal and the magnetic pressure. Outside the tube, where there is no field, the total pressure is given only by the thermal pressure. If we assume the system is in pressure equilibrium, however, the pressure within the tube is required to be equal to that outside, giving a higher thermal pressure outside than inside, and therefore a decreased density within the tube under isothermal conditions. This difference in density means that the tube is subject to an additional upwards buoyancy force as a result of the field.

This effect, however, is more accurately referred to as a lack of equilibrium than an instability, as an instability is typically the effect of a perturbation to an equilibrium state. The magnetic buoyancy instability, as it is usually referred to, occurs in an atmosphere containing not isolated flux tubes but a vertically-stratified, horizontal field, that is horizontally homogeneous.

Below, we consider the criteria for the instability of such a stratified layer in magnetohydrostatic equilibrium. The magnetic buoyancy instability is in many ways analogous to the non-magnetic case, for a parcel of gas within a stratified atmosphere; here, the stability is determined by a buoyancy frequency, derived using a parcel argument, and we can make an equivalent argument for the magnetic case.

### 1.3.1 Linear Magnetic Buoyancy Instability

We shall consider the magnetic buoyancy instability in a layer of stratified field in equilibrium; see the review by [Hughes \(2007\)](#) for further discussion. The linear stability of such a system can be quantified using an argument based on fluid parcels. Initially, we make the assumptions that there is no diffusion within the

## 1. INTRODUCTION

---

system, and that the field lines do not bend. Consider an atmosphere in equilibrium, in a Cartesian coordinate system  $(x, y, z)$ , under vertical gravity  $\mathbf{g} = -g\mathbf{e}_z$ . If we take a fluid parcel permeated by a horizontal magnetic field  $\mathbf{B} = B(z)\mathbf{e}_x$ , then raise it from height  $z$  to  $z + \delta z$ , we will see changes in the pressure, density and field within the parcel given by  $p \mapsto p + \delta p$ ,  $\rho \mapsto \rho + \delta\rho$ , and  $B \mapsto B + \delta B$ , where the notation  $\delta A$  represents the change in quantity  $A$ . Assuming the parcel moves adiabatically (Acheson, 1979), the motion is subject to

$$\frac{\delta p}{p} = \gamma \frac{\delta \rho}{\rho}, \quad (1.1)$$

where  $\gamma$  denotes the ratio of the specific heats. Also, by conservation of mass and magnetic flux,

$$\frac{\delta B}{B} = \frac{\delta \rho}{\rho}. \quad (1.2)$$

In addition, we assume that the motion is slow in comparison to the adiabatic sound speed, such that pressure balance is maintained and the parcel is always in mechanical equilibrium with its surroundings. Thus, pressure balance gives:

$$\delta p + \frac{B\delta B}{\mu_0} = dp + \frac{BdB}{\mu_0}, \quad (1.3)$$

where  $\mu_0$  is the magnetic permeability, and the notation  $dA$  represents the change in quantity  $A$  of the surrounding background state, external to the moving parcel. For instability, we require  $\delta\rho < d\rho$ . From this, we can derive the following criterion for instability:

$$-\frac{gv_A^2}{c^2} \frac{d}{dz} \ln\left(\frac{B}{\rho}\right) > N^2. \quad (1.4)$$

Here,  $v_A$  is the Alfvén speed and  $c$  is the adiabatic sound speed. The quantity  $N$  is the Brunt-Väisälä frequency, given by

$$N^2 = \frac{g}{\gamma} \frac{d}{dz} \ln(p\rho^{-\gamma}). \quad (1.5)$$

Equation (1.4) is analogous to the Schwarzschild criterion for instability in a non-magnetised fluid layer, though in this case the initial assumption of hydrostatic equilibrium takes into account the magnetic field and the additional pressure it creates. Note that in the non-magnetic case,  $\mathbf{B} = 0$ , (1.4) reduces to

the Schwarzschild criterion for convective instability,  $N^2 < 0$ . However, criterion (1.4) tells us an important feature of the magnetic buoyancy instability; that in the magnetic case, a stratified layer with  $N^2 > 0$  can be unstable, in contrast to when  $\mathbf{B} = 0$ .

We may also derive a similar criterion for the 3D instability. We seek to find the stability of horizontally periodic modes whose scale is defined by horizontal wavenumbers  $k_x$  and  $k_y$ . The criterion given by (1.4) is specific to the instability of so-called interchange modes, with  $k_x = 0$ . In the interchange instability the field lines do not bend but are carried with a fluid parcel as it moves. However, there is also an analogous criterion for 3D modes, originally derived by [Newcomb \(1961\)](#), and written in the following form by [Thomas & Nye \(1975\)](#):

$$-\frac{gv_A^2}{c^2} \frac{d}{dz} \ln(B) > N^2. \quad (1.6)$$

If we compare (1.4) and (1.6), we can see that 3D modes are more easily destabilised than interchange modes; that is to say, owing to the presence of the  $\frac{d}{dz} \ln\left(\frac{B}{\rho}\right)$  term in (1.4), the instability of interchange modes places a requirement on the gradients of both density and magnetic field. However, the instability of 3D modes depends only on  $\frac{d}{dz} \ln(B)$ , i.e. only on the field gradient. Thus there is a less restrictive requirement for 3D modes to be destabilised. It is for this reason that we may expect parameter regimes in which the only modes that are unstable are 3D. Furthermore, [Newcomb \(1961\)](#) showed that the most unstable 3D modes are those in the limit  $k_x \rightarrow 0$ . This is significant as the limiting case for  $k_x \rightarrow 0$  is not equal to the interchange mode case, with  $k_x = 0$ , but has large-scale variation in the  $x$ -direction (see [Hughes & Cattaneo \(1987\)](#) for further discussion of the physical arguments underlying the preference for 3D modes).

### 1.3.2 Diffusive Case

The previous discussion of magnetic buoyancy has neglected any diffusive effects. However, if we consider a local analysis of the instability of a vertically stratified field, with horizontally periodic perturbations defined by wavenumbers  $k_x$  and  $k_y$ , it is also possible to include diffusive effects in the analysis. [Gilman \(1970\)](#),

## 1. INTRODUCTION

---

and [Acheson \(1979\)](#) used a local approximation and extended the stability criterion in the case of small  $k_x$ , i.e., 3D modes with long wavelength in the direction of the field lines. However, the criterion for their stability is not equal to that of the case of interchange modes. The criterion for the interchange instability (analogous to (1.4)) is:

$$-\frac{g}{c^2} \frac{d}{dz} \ln \left( \frac{B}{\rho} \right) > \frac{\eta}{\kappa} \frac{\gamma N^2}{v_A^2}, \quad (1.7)$$

where  $\eta$  is the magnetic and  $\kappa$  the thermal diffusivity. For 3D modes, the criterion, analogous to (1.6), is:

$$-\frac{g}{c^2} \frac{d}{dz} \ln(B) > k_x^2 \left( 1 + \frac{k_z^2}{k_y^2} \right) \frac{\eta}{\kappa} \frac{\gamma N^2}{v_A^2}. \quad (1.8)$$

These criteria are based on a local approximation, which assumes the background state varies over a long spatial scale in comparison to the scales defined by  $k_x$ ,  $k_y$ , and  $k_z$ . Note that in the diffusive case of 3D modes, instability depends on the scale of the modes in  $x$ ,  $y$ , and  $z$ .

### 1.3.3 Linear magnetic buoyancy instability: previous work

We shall now briefly discuss some of the existing literature on the linear magnetic buoyancy instability, especially work that places it in a solar context. For a literature review that is more extensive and broader in scope, however, refer to [Hughes \(2007\)](#).

[Kruskal & Schwarzschild \(1954\)](#) proposed a mechanism for the instability of a layer of field with a discontinuous field strength in the vertical direction, and following this, [Newcomb \(1961\)](#) described the instability of a stratified atmosphere and considered the criteria for linear stability to magnetic buoyancy. Newcomb showed that in the absence of diffusion or rotation, 3D modes of the instability are more easily destabilised than 2D interchange modes, despite the bending of the field lines required — as opposed to simple translation of the field lines in the perpendicular direction — to produce the 3D instability. Later, [Thomas & Nye \(1975\)](#) extended this analysis, writing the stability criteria in the form in which

we commonly refer to them, that of (1.6).

[Gilman \(1970\)](#) considered the diffusionless case of the instability in the asymptotic limit of small horizontal scale, deriving stability criteria and other relations for this system. [Tayler \(1973\)](#) considered stability of perturbations to a toroidal field in a star. [Parker \(1975\)](#) considered magnetic buoyancy as a mechanism for the rise of large-scale flux in the context of a dynamo process, in order to infer the location of dynamo action in an astrophysical body comparable to the Sun.

[Acheson \(1979\)](#) considered the effects of both stratification and rapid rotation on the instability, finding that stratification is expected to have a strongly stabilising effect in the parameter regime of the Sun's radiative zone, while in the upper part of the convection zone, rapid rotation is expected to suppress the magnetic buoyancy instability.

[Hughes \(1985\)](#) considered the linear stability of the magneto-Boussinesq equations in a plane layer, identifying a new mode of the instability previously thought stable: he showed that instability was possible for  $\frac{d}{dz} \ln\left(\frac{B}{\rho}\right) > 0$ , allowing instability of fields that increased with height. [Hughes & Cattaneo \(1987\)](#) considered linear stability to the interchange versus undular instabilities, offering a physical explanation for the preference for 3D modes. They showed that, since for interchange modes, the density fluctuations depend on the total pressure (the sum of the gas and magnetic pressure) whereas for undular modes they depend only on the gas pressure, this allows for circumstances where the interchange instability is more stable than the undular, even though the undular instability requires work to be done against magnetic tension while the interchange does not. [Mizerski \*et al.\* \(2013\)](#) considered the diffusionless problem studied by [Gilman \(1970\)](#), seeking to understand the broader context for Gilman's small-scale results, and their relation to the more general magnetic buoyancy instability problem.

## 1. INTRODUCTION

---

### 1.3.4 Nonlinear simulation

As well as the work on the linear regime detailed above, there have also been a number of studies of the nonlinear evolution of the instability, by way of numerical simulation. [Cattaneo & Hughes \(1988\)](#) numerically simulated the nonlinear interchange instability in a layer of field in a convectively stable atmosphere, with both static and rotating basic states. The numerical simulations of [Matthews \*et al.\* \(1995\)](#) showed the initial linear development of the instability in a layer of field to be largely 2D, and that the onset of the 3D instability was associated with the transition to nonlinear behaviour. They also showed that this transition to a 3D instability did not occur for isolated rising flux tubes, and that therefore the 3D instability onsets as a result of nonlinear interaction between adjacent flux tubes in such a system. Similarly, [Wissink \*et al.\* \(2000\)](#) numerically simulated the nonlinear evolution of the magnetic buoyancy instability in a layer of field, and found that the development of the nonlinear instability is such that the structure produced grows increasingly 3D with time. The 3D problem was also addressed by [Kersalé \*et al.\* \(2007\)](#), who considered the nonlinear instability of a linearly stratified layer. They found that coherent magnetic structures may be formed in their configuration by an inherently nonlinear mechanism, driven by the boundary conditions imposed on the system.

In an effort to better understand the instability in a solar context, [Vasil & Brummell \(2008\)](#) considered the nonlinear magnetic buoyancy instability in a layer of toroidal field, created by applying shear to a weaker poloidal field, in order to model the way that the  $\omega$ -effect acts on the solar poloidal magnetic field and how this may affect the buoyant rising flux. In this configuration, they found the system to be less susceptible to magnetic buoyancy instability than in other work that did not use such a velocity shear.

[Barker \*et al.\* \(2012\)](#) combined simulation of the magnetic buoyancy instability, of both a plain slab of magnetic field and a shear-generated layer, with the  $\gamma$  turbulent pumping velocity that results from mean field dynamo theory: see Section 1.4.4 for a fuller discussion of the  $\gamma$  effect and its origin. Following this

work, we will include this effect in our study of the linear regime, along with the additional turbulent diffusivity that goes with it. We will justify the inclusion of these effects, and discuss how they emerge from dynamo theory and the idea of mean field turbulence, in Section 1.4.4.

### 1.3.5 Rising flux tubes in the convection zone

When he first proposed the idea of magnetic buoyancy as a mechanism for rising flux, Parker (1955a) suggested that it could provide a plausible mechanism for the formation of sunspots from the solar toroidal field, providing explanations of all the features of sunspot occurrence that we see over the course of the solar cycle in terms of this effect. Indeed, the emergence of magnetic flux ropes from the surface of the Sun as the “loop” structures that we observe appears suggestively similar to an instability of the underlying flux tubes, causing them to rise in a spatially periodic way, with a given horizontal scale. However, there is a problem to do with the region of turbulent convection through which the large-scale magnetic structure must pass: the turbulent motion in the convection zone has a much smaller spatial scale than that of the rising magnetic structures, prompting the question of how the field maintains this larger scale of variation, without being subject to a turbulent “shredding” effect that would produce smaller-scale variation from the larger.

Magnetic buoyancy instability theory does not, in itself, provide any kind of “threshold” field for the instability, however, we require that the rising field be strong enough to withstand this turbulent shredding effect. Therefore, it seems probable that there is some other effect playing a role in destabilising sufficiently strong field. One candidate for this is the turbulent pumping effect of mean field dynamo theory. In an effort to motivate this, we shall now discuss mean field theory and the solar dynamo problem in greater depth.

### 1.4 Mean Field Dynamo Theory

#### 1.4.1 Motivation: the Solar Dynamo Problem

One argument for the existence of a dynamo process involves timescales, namely the comparison between the age of the object and its characteristic Ohmic decay time,  $\tau_\eta \sim L^2/\eta$ , where  $L$  is a characteristic length scale of the system and  $\eta$  is the magnetic diffusivity. This corresponds to the timescale over which an object's magnetic field would decay if not regenerated in some way. If the age of an object is longer than this decay time, and it has an observed magnetic field, then it follows that this field cannot be a “fossil” field, left behind from its formation but in the process of dying away, and must have some mechanism to regenerate itself. This would require some kind of dynamo process, i.e. a flow of material within the body that acts to produce and maintain its own self-consistent magnetic field.

For the Earth, for example, the Ohmic decay timescale is of the order  $\tau_\eta \sim 10^4$  years. This is much shorter than the length of time for which Earth is known to have had a magnetic field, which is of the order  $\sim 10^9$  years. This implies that if the Earth's magnetic field were not being regenerated in some way, then it would have decayed away very early in the planet's lifetime. This implies that some process must be maintaining the field, necessitating the existence of a dynamo.

Interestingly, in the Sun we cannot make such an argument by timescales of age alone; both the Ohmic decay timescale of the Sun and its age are of the order  $\sim 10^9 - 10^{10}$  years. So, from an argument of timescales alone, the Sun could potentially have a fossil field. However, as discussed, the Sun has an observed magnetic cycle, involving the reversal of its global magnetic field that occurs approximately every eleven years. This is much less than the Ohmic decay timescale, and so we may assume that this cycle is a product of a dynamo process that maintains the Sun's magnetic field, as it is very difficult to reconcile such cyclical variation with the slow Ohmic decay of a fossil field. Such an argument tells us that the much shorter-time variation seen in the form of the solar cycle is an important

consequence of how the solar dynamo operates, and any dynamo process we may postulate must be able to explain it.

### 1.4.2 The Kinematic Dynamo Problem

If a given flow of magnetised fluid is able to induce its own magnetic field, such that it does not decay at large time, then it is said to act as a dynamo. Specifically, the condition for dynamo action is that over long timescales, the total magnetic energy of the system is bounded below by a positive number; in a flow that acts as what is known as a “dynamic” dynamo, the velocity flow is fully self-consistent in allowing this.

Although the dynamic dynamo problem may be simply stated in this way, it is, both numerically and analytically, extremely difficult to solve. For this reason, theorists have invoked a simpler variation on this full problem, in which the flow velocity field is prescribed, as opposed to emerging self-consistently from the magnetic field solution. This is known as the “kinematic” dynamo problem, and it is in solving this problem that most effort has been concentrated in the area. Essentially, it considers the MHD induction equation:

$$\frac{\partial \mathbf{B}}{\partial t} = \nabla \times (\mathbf{u} \times \mathbf{B}) - \nabla \times (\eta \nabla \times \mathbf{B}), \quad (1.9)$$

and seeks to find a velocity field  $\mathbf{u}(\mathbf{x}, t)$  for which  $\mathbf{B}$  does not decay as  $t \rightarrow \infty$ .

Several systems have been shown to act as kinematic dynamos, with a fixed  $\mathbf{u}(\mathbf{x}, t)$  defined as a function of space and time, including several in spherical geometry, which may be used to model astrophysical dynamos. For example, [Choudhuri \*et al.\* \(1995\)](#) proposed a solar dynamo model with meridional circulation, in order to produce simulated butterfly diagrams that could be compared with the real solar cycle. There were also advances in the more general field of dynamo theory; [Glatzmaier & Roberts \(1995\)](#) produced a 3D convective MHD dynamo model, for a geodynamo-like system. However, we will focus on the approach detailed by [Steenbeck \*et al.\* \(1966\)](#), as well as subsequent papers by the same authors (see translation by [Roberts & Stix \(1971\)](#)) and further detailed by [Moffatt \(1978\)](#)

## 1. INTRODUCTION

---

and Moffatt & Dormy (2019); that of a mean field dynamo. (See Krause & Rädler (1980) and Dormy & Soward (2007) for further discussion and examples.) This has allowed several types of kinematic dynamo systems to be developed. However, for our purposes, we will consider the approach to characterising turbulence inherent to this area: the concept of mean field turbulence, and the net effects implied by it as a way to construct a linear model of an otherwise complicated, nonlinear, turbulent system.

### 1.4.3 Implications of differential rotation

It is useful to define the field on the Sun (or any spherical body) in terms of two quantities, the toroidal and poloidal components of the field,  $\mathbf{B}_T$  and  $\mathbf{B}_P$ . We are able to make this decomposition because of the solenoidality of the field,  $\nabla \cdot \mathbf{B} = 0$ . If we write the field as the sum  $\mathbf{B} = \mathbf{B}_T + \mathbf{B}_P$ , we can define  $\mathbf{B}_T$  and  $\mathbf{B}_P$  in terms of two scalar potentials,  $T$  and  $P$ . In terms of the radial vector  $\mathbf{r}$ :

$$\mathbf{B}_T = \nabla \times (\mathbf{r}T(\mathbf{r})), \quad (1.10)$$

$$\mathbf{B}_P = \nabla \times \nabla \times (\mathbf{r}P(\mathbf{r})). \quad (1.11)$$

It follows from this that the toroidal and poloidal field components have the properties

$$\mathbf{r} \cdot \mathbf{B}_T = 0, \quad (1.12)$$

$$\mathbf{r} \cdot \nabla \times \mathbf{B}_P = 0. \quad (1.13)$$

For an axisymmetric field, the toroidal field is equivalent to the azimuthal component, and the poloidal field is essentially all the non-azimuthal field, composed of the radial and meridional components. Using cylindrical polar coordinates  $(s, \phi, z)$ , we can write the toroidal and poloidal field components as follows:

$$\mathbf{B}_T = B_\phi \mathbf{e}_\phi, \quad (1.14)$$

$$\mathbf{B}_P = \nabla \times A \mathbf{e}_\phi, \quad (1.15)$$

where  $A \mathbf{e}_\phi$  a vector potential corresponding to the poloidal component of  $\mathbf{B}$ . Similarly, we may write the velocity as the sum of a poloidal (meridional) component  $\mathbf{u}_m$  and a toroidal component given by the spatially-dependent angular

## 1.4 Mean Field Dynamo Theory

---

velocity resulting from differential rotation:

$$\mathbf{u} = \mathbf{u}_m(s, z) + s\Omega(s, z)\mathbf{e}_\phi. \quad (1.16)$$

Under these assumptions, we may take the toroidal and poloidal components of the induction equation, (1.9), and find that the field and the associated vector potential satisfy:

$$\frac{\partial}{\partial t} \left( \frac{B_\phi}{s} \right) = \mathbf{B}_P \cdot \nabla \Omega - \nabla \cdot \left( \frac{B_\phi}{s} \mathbf{u}_m \right) + \left( \frac{\eta}{s} \right) \left( \nabla^2 - \frac{1}{s^2} \right) B_\phi, \quad (1.17)$$

$$\frac{\partial}{\partial t} (sA) = -\mathbf{u}_m \cdot \nabla (sA) + s\eta \left( \nabla^2 - \frac{1}{s^2} \right) A. \quad (1.18)$$

Note also that we have assumed constant magnetic diffusivity  $\eta$  here, and will continue to make this assumption from now on. The first of these equations quantifies the idea of the toroidal field being geometrically “wound up” from poloidal field, with a source term for toroidal field proportional to  $\mathbf{B}_P$ . However, there is no such source term for the poloidal field, suggesting that under these assumptions the poloidal component decays to zero at large  $t$ . The idea that the field of the Sun is all toroidal is not consistent with observations. Furthermore, given the solenoidal condition on the field, the limiting case of a fully toroidal field with no poloidal field at large time would be axisymmetric. Such a field would not be able to sustain the dynamo process, by Cowling’s theorem (Cowling, 1933), which states that an axisymmetric field cannot be maintained by dynamo action given an axisymmetric flow.

It is for all of these reasons that we require some other effect that acts as a source term for poloidal field in order to produce a system that can act as a dynamo. The requirement for a poloidal source term motivates the mean field approach. Although Parker (1955b) had detailed a similar concept several years earlier, the groundwork for this approach was laid when Steenbeck *et al.* (1966) proposed a way of characterising the turbulent motion of an electrically conducting fluid permeated by a magnetic field, approximating the net effects of turbulence using a mean electromotive force (EMF) quantity, an idea upon which they expanded in subsequent papers. Moffatt (1978) proposed the idea of a mean-field dynamo

## 1. INTRODUCTION

---

in the sense and the notation that we use here. [Golub \*et al.\* \(1981\)](#) referred to models of the emergence of small- and large-scale flux structure, and how it could be reconciled with observational evidence of variation over the course of the solar cycle.

We will now consider the mean field approximation to characterise the turbulence. We will also discuss the argument for the existence of the  $\alpha$  effect, in order to provide a poloidal source term in Equation (1.18).

### 1.4.4 Mean Field Turbulence: Mathematical Formulation

The mean field approach is based on the assumption that the flow is separated into large- and small-scale variations in field and velocity, where the small-scale variations average to zero over the length scale of the larger ones. With this assumption, we may then take averages of quantities over an intermediate scale. The total field and velocity  $\mathbf{B}(\mathbf{x}, t)$  and  $\mathbf{U}(\mathbf{x}, t)$  are written as:

$$\mathbf{B}(\mathbf{x}, t) = \mathbf{B}_0(\mathbf{x}, t) + \mathbf{b}(\mathbf{x}, t), \quad (1.19)$$

$$\mathbf{U}(\mathbf{x}, t) = \mathbf{U}_0(\mathbf{x}, t) + \mathbf{u}(\mathbf{x}, t), \quad (1.20)$$

where  $\mathbf{B}_0(\mathbf{x}, t)$  and  $\mathbf{U}_0(\mathbf{x}, t)$  are the large-scale field and velocity as functions of position and time, and  $\mathbf{b}(\mathbf{x}, t)$  and  $\mathbf{u}(\mathbf{x}, t)$  are the small-scale fluctuations.

This means that the induction equation, too, can be separated into two parts, one for the mean field  $\mathbf{B}_0$  and one for the fluctuating field  $\mathbf{b}$  ([Moffatt, 1978](#)).

$$\frac{\partial \mathbf{B}_0}{\partial t} = \nabla \times (\mathbf{U}_0 \times \mathbf{B}_0) + \nabla \times \mathcal{E} + \eta \nabla^2 \mathbf{B}_0, \quad (1.21)$$

$$\frac{\partial \mathbf{b}}{\partial t} = \nabla \times (\mathbf{U}_0 \times \mathbf{b}) + \nabla \times (\mathbf{u} \times \mathbf{B}_0) + \nabla \times \mathbf{G} + \eta \nabla^2 \mathbf{b}, \quad (1.22)$$

where  $\mathcal{E} = \langle \mathbf{u} \times \mathbf{b} \rangle$ , and  $\mathbf{G} = \mathbf{u} \times \mathbf{b} - \langle \mathbf{u} \times \mathbf{b} \rangle$ , with the notation  $\langle Q \rangle$  indicating the spatial average of quantity  $Q$ . The quantity  $\nabla \times \mathcal{E}$  is a new addition to the induction equation for the mean field (Equation (1.21)) due to the interaction of the fluctuating velocity and magnetic field, representing an additional EMF

## 1.4 Mean Field Dynamo Theory

---

(electromotive force). We assume separation of scales, and we neglect small-scale dynamo action, both for simplicity, and because there is no well-established theory about what form this contribution should take. (In addition, it seems likely that small-scale dynamo action is not a prevalent effect within the stably stratified region upon which we focus; see [Cattaneo & Hughes \(2009\)](#) as well as the review by [Hughes \(2018\)](#), however, for further discussion of the topic.) Neglecting small-scale dynamo action, we note that the mean EMF is linear in the mean field. Due to the large scale of the mean field, we assume that successive derivatives decrease with increasing order. With these assumptions, we can write  $\mathcal{E}$  in terms of the mean field and its derivatives as follows:

$$\mathcal{E}_i = \alpha_{ij} B_j + \beta_{ijk} \frac{\partial B_j}{\partial x_k} + \dots \quad (1.23)$$

If we now assume, for the sake of simplicity, that the turbulence is homogeneous and isotropic, then the tensor quantities  $\alpha_{ij}$  and  $\beta_{ijk}$  take the form  $\alpha_{ij} = \alpha \delta_{ij}$  and  $\beta_{ijk} = \beta \epsilon_{ijk}$ . We may isolate the antisymmetric part of  $\alpha_{ij}$ , writing it as  $\gamma_j \epsilon_{ijk}$ , and allowing us to write:

$$\mathcal{E}_i = \alpha \delta_{ij} B_j + \gamma_j \epsilon_{ijk} B_k + \beta \epsilon_{ijk} \frac{\partial B_j}{\partial x_k} + \dots \quad (1.24)$$

We may then rewrite the induction equation for the mean field in terms of these newly-defined quantities, as follows:

$$\frac{\partial \mathbf{B}_0}{\partial t} = \nabla \times (\alpha \mathbf{B}_0) + \nabla \times ((\mathbf{U}_0 + \boldsymbol{\gamma}) \times \mathbf{B}_0) - \nabla \times ((\eta + \beta) \nabla \times \mathbf{B}_0). \quad (1.25)$$

See [Moffatt & Dormy \(2019\)](#) for further mathematical details and discussion of this expansion. Crucially, this form does not explicitly depend on the turbulent quantities  $\mathbf{b}(\mathbf{x}, t)$  and  $\mathbf{u}(\mathbf{x}, t)$ , and therefore we may consider the net effect of the turbulence on the mean field without having to explicitly simulate the full turbulent motion of the system. In this form of the induction equation, there are three new quantities compared to (1.9), namely  $\alpha$ ,  $\beta$ , and  $\boldsymbol{\gamma}$ .

The quantity  $\alpha$  is a pseudo-scalar, and therefore is required to change sign under a parity transformation, such as that from a right- to left-handed reference frame,

## 1. INTRODUCTION

---

or vice-versa. However,  $\alpha$  is also a statistical property of the turbulent, fluctuating velocity field  $\mathbf{u}$ , therefore must also be invariant under a transformation of  $\mathbf{u}$ . Let us consider, specifically, the parity transform of mirror reflection, for which  $\mathbf{u}' = -\mathbf{u}$ . If  $\mathbf{u}$  is mirror symmetric, then all of its statistical properties must be invariant under this transformation, including  $\alpha$ . Therefore, we require  $\alpha = 0$  if  $\mathbf{u}$  has mirror symmetry.

$\beta$  takes the form of an additional diffusivity, the “turbulent diffusivity” that is a net effect of the turbulence on the mean field. The quantity  $\boldsymbol{\gamma}$  is a vector with the form of an additional advection velocity acting on the mean field, and is known as the turbulent pumping velocity. It is the  $\gamma$  and  $\beta$  effects upon which we will primarily focus in the work presented here.

### 1.4.5 Past work on mean field turbulent effects

There have been a number of studies that have considered the turbulent transport effects we have just described in relation to the solar dynamo. [Drobyshevski & Yuferev \(1974\)](#) proposed the related effect of topological pumping, whereby magnetic flux in a convecting layer is subject to a non-zero net transport effect due to asymmetry between upwards and downwards flows in convection cells. After initially characterising them some years prior ([Moffatt, 1978](#)), [Moffatt \(1983\)](#) calculated the strength of mean transport effects with specific consideration for the role of helicity, focusing on calculating  $\alpha$  and  $\beta$  in the astrophysical regime of large magnetic Reynolds number. [Cattaneo \*et al.\* \(1988\)](#) discussed this effect and how scalar and vector magnetic fields can be subject to different effective velocities under the effect of convection. [Ossendrijver \*et al.\* \(2002\)](#) quantified the turbulent pumping effect on the mean field, as a function of various physical parameters and effects. [Plunian & Rädler \(2002\)](#) found expressions for components of the  $\alpha$  tensor in the case of the Roberts dynamo flow ([Roberts, 1970](#)), in terms of the magnetic Reynolds number and the length scales of the system.

[Cattaneo & Hughes \(2006\)](#) considered magneto-Boussinesq convection in a rotating layer, in order to understand the effect of rotation on convection in such

## 1.4 Mean Field Dynamo Theory

---

a regime, in relation to dynamo processes, and calculated the strength of the resulting  $\alpha$  effect. [Mason \*et al.\* \(2008\)](#) considered the effect of  $\gamma$  in two different kinematic dynamo models for the base of the solar convection zone, while [Hughes & Proctor \(2010\)](#) focused on the  $\beta$  turbulent diffusivity effect, specifically acting on a time-dependent mean field. [Davies & Hughes \(2011\)](#) calculated the mean field EMF resulting from magnetic buoyancy as the mechanism behind the rise of the large scale field, under a variety of conditions.

This mean field kinematic dynamo approach is not, however, without its difficulties, highlighted in greater detail by the review of [Hughes \(2018\)](#). Writing the mean field induction equation in the form (1.25) requires that the term in Equation (1.22) containing  $\mathbf{G}$  be neglected, and the circumstances in which this is possible do not necessarily reflect physical reality in the systems to which the approximation is applied. A common assumption is the so-called first order smoothing approximation, which holds in the case of magnetic Reynolds number  $Rm \sim UL/\eta \ll 1$ , in which case it may be assumed that  $\mathbf{G} = O(Rm)$ , and thus this term may be neglected in comparison to the diffusive term. However, in the solar convection zone, this does not hold as we expect  $Rm \sim 10^6 - 10^{10}$ . (See [Ossendrijver \(2003\)](#) and [Hood & Hughes \(2011\)](#) for further discussion of dimensionless parameters and estimates of their values in the solar convection zone.) Indeed,  $Rm \gg 1$  is generally typical of astrophysical systems.

Alternatively, one could also eliminate the  $\mathbf{G}$  term by assuming that the correlation between  $\mathbf{u}$  and  $\mathbf{b}$  is only on a short timescale: this is known as the “short sudden” approximation, and it is valid if the dimensionless quantity  $S = U\tau_c/L$  is small. However, we expect  $S \sim O(1)$  in the region under consideration.

Furthermore, as [Hughes & Cattaneo \(2008\)](#) pointed out, the scale of the system (and thus the computational domain of simulations) is of critical importance to the calculated strength of the  $\alpha$  effect in numerical simulations of convection in a rotating layer. They found that larger domains require a shorter time-average in order to arrive at a constant strength of the  $\alpha$  effect, implying that the choice of simulation geometry is a major determining factor in the results.

## 1. INTRODUCTION

---

Nevertheless, with all these difficulties in mind, we consider the magnetic buoyancy instability under the effect of mean field turbulence. As previously discussed with regard to work on magnetic buoyancy, [Barker \*et al.\* \(2012\)](#) applied a  $\gamma$  effect to numerical simulations of the nonlinear magnetic buoyancy instability in a layer modelling the region of the base of the solar convection zone, using a downwards advection velocity. We will use a similar approach for the  $\gamma$  effect as applied to the linear stability problem. In the numerical simulations of [Tobias \*et al.\* \(1998a\)](#), the effect of convection was found to give a net downwards transport of flux and magnetic energy, when applied to a horizontal layer of uniform field. Thus, for our purposes we consider the turbulent pumping velocity to be directed downwards. This is opposite to the direction of the rise of flux via the magnetic buoyancy instability, producing an arrangement where the two effects act directionally counter to one another in the region that we consider. The picture is also further complicated by the addition of the turbulent diffusivity  $\beta$ , which, while not directional, is spatially dependent due to the spatial variation of the turbulence.

We do not include  $\alpha$  in the present work, as this is an additional layer of complexity. Furthermore, as previously discussed,  $\alpha$  is an effect that can be non-zero only in a rotating system, and the model system we consider does not include rotation. However, in the solar convection zone in reality, rotation is expected to be of importance. Thus, there are certainly grounds for the inclusion of  $\alpha$  in future extensions to this analysis.

In our set-up of the problem, we consider the linear stability to magnetic buoyancy of a layer of field acted upon in an upper region by a turbulent diffusivity and a downwards turbulent pumping velocity. Both  $\gamma$  and  $\beta$  are applied according to a step-like profile in order to model the abrupt decline of turbulence outside of the convection zone. Such a system has not been studied before, except in the numerical simulations of [Barker \*et al.\* \(2012\)](#), who added the turbulent pumping effect  $\gamma$  to the nonlinear magnetic buoyancy problem, beginning with a slab of

## 1.4 Mean Field Dynamo Theory

---

field acted upon from above by the turbulent pumping effect. They then numerically simulated the time evolution of this configuration by magnetic buoyancy, subject to the  $\gamma$  effect. By contrast, in this work, we concentrate on the linear evolution of the instability, under the effects of both  $\gamma$  and  $\beta$ , with a basic state that represents an equilibrium under these effects.

We will first solve for an equilibrium field under given vertical profiles of  $\gamma$  and  $\beta$  and subject to a variety of boundary conditions, in order to discern the effect of  $\gamma$  and  $\beta$  on the basic state. We will also discuss the physical relevance of various basic states considered. From this, we choose an equilibrium state that will be used as the basis for stability analysis. As an additional consideration, we show that for a given basic state, while  $\gamma$  and  $\beta$  that support it as an equilibrium state of the system can, formally, be found as a function of  $z$ , they do not necessarily model the region of the solar convection zone well, and thus we justify our choice of prescribing  $\gamma$  and  $\beta$  and letting the equilibrium field depend on their spatial variation.

Following our analysis of the basic states, we introduce linear perturbations, with horizontally periodic variation. We solve the system for the most unstable mode, including its growth rate, horizontal scale, and vertical dependence, and we consider how this depends on the strengths of the  $\gamma$  and  $\beta$  effects, including their relative strengths. We also consider the effect on the instability of varying the field strength parameter in the system. In addition to this, in order to better understand the question of scale dependence of the instability and validity of the mean field approximation, we also consider the application of  $\gamma$  and  $\beta$  on a basis that is dependent on scale. This is to try to understand to what extent the role of  $\gamma$  and  $\beta$  in determining the equilibrium basic state is primarily responsible for the change in stability we see, compared to the direct effect of  $\gamma$  and  $\beta$  on the perturbed quantities.

We also consider, analytically, a special case of the instability; the diffusionless, isothermal case. We derive analogous expressions to those of [Gilman \(1970\)](#)

## 1. INTRODUCTION

---

and [Mizerski \*et al.\* \(2013\)](#), in terms of the growth rate and horizontal wavenumbers, the vertical velocity profile, and the basic states, given the turbulent pumping effect. Given the complexity of the resulting third order system in the latter case, we discuss two simpler third order model problems, finding numerical and analytical solutions in the asymptotic limit  $\gamma \rightarrow 0$ . We also apply a local analysis approach following that of [Acheson \(1979\)](#), in order to derive local dispersion relations for the interchange system under both isothermal and adiabatic conditions.

First, however, we lay out the mathematical basis for the following analysis, including notation and the full equations of the system.

### 1.5 Mathematical Formulation

#### 1.5.1 Coordinate system

We will work in a Cartesian box defined by  $(x, y, z)$  with  $-z$  corresponding to the radial direction, i.e. with the top of the layer located at  $z = 0$ .  $x$  is in the meridional direction and  $y$  is azimuthal. We will consider a layer of height  $d$ , such that the base of the layer is at  $z = d$ . (Note that this is opposite to the direction of  $z$  as discussed in Section 1.3.1 and as detailed in the work of, for example, [Acheson \(1979\)](#), who used  $z$  as height; we will instead follow the convention of [Cattaneo & Hughes \(1988\)](#) and use  $z$  as depth from now on.) Thus,  $\mathbf{g} = g\mathbf{e}_z$ , and the initial magnetic field points in the  $x$ -direction and is vertically stratified.

#### 1.5.2 MHD Equations

We consider first the MHD equations in their dimensional form. These are the induction equation (note the addition of the turbulent pumping and turbulent diffusion effects), the momentum equation, the energy equation, mass conservation,

and the gas law.

$$\frac{\partial \mathbf{B}}{\partial t} = \nabla \times ((\mathbf{u} + \boldsymbol{\gamma}) \times \mathbf{B}) - \nabla \times ((\eta + \beta)\nabla \times \mathbf{B}), \quad (1.26)$$

$$\rho \frac{D\mathbf{u}}{Dt} = -\nabla p + \frac{1}{\mu_0}(\nabla \times \mathbf{B}) \times \mathbf{B} + \mu \nabla \cdot \boldsymbol{\tau} + \rho \mathbf{g}, \quad (1.27)$$

$$c_v \rho \frac{DT}{Dt} = -p \nabla \cdot \mathbf{u} + k \nabla^2 T + \mu \frac{\partial u_i}{\partial x_j} \tau_{ij} + \frac{\eta}{\mu_0} (\nabla \times \mathbf{B})^2, \quad (1.28)$$

$$\frac{\partial \rho}{\partial t} = -\nabla \cdot (\rho \mathbf{u}), \quad (1.29)$$

$$p = R\rho T. \quad (1.30)$$

Here, the quantity  $\boldsymbol{\tau}$  refers to the viscous stress tensor, given by:

$$\tau_{ij} = \frac{\partial u_i}{\partial x_j} + \frac{\partial u_j}{\partial x_i} - \frac{2}{3} \delta_{ij} \frac{\partial u_k}{\partial x_k}. \quad (1.31)$$

In addition to this, the parameter  $k$  is the thermal conductivity,  $c_v$  the heat capacity at constant volume,  $\mu$  is the shear viscosity,  $\eta$  is the magnetic diffusivity,  $g$  is the gravitational field strength,  $R$  is the gas constant, and  $\mu_0$  the magnetic permeability constant.

### 1.5.3 Dimensionless Form

We scale the temperature, density, pressure, and magnetic field with their values at the top of the layer,  $T_o$ ,  $\rho_o$ ,  $p_o$  and  $B_o$ , distances with the layer depth  $d$ , and times with the sound travel time  $d/\sqrt{RT_o}$ .

## 1. INTRODUCTION

---

This gives the following system of nonlinear, dimensionless equations:

$$\frac{\partial \mathbf{B}}{\partial t} = \nabla \times ((\mathbf{u} + \boldsymbol{\gamma}) \times \mathbf{B}) - \nabla \times ((\zeta_o C_k + \beta) \nabla \times \mathbf{B}), \quad (1.32)$$

$$\begin{aligned} \frac{\partial}{\partial t}(\rho \mathbf{u}) &= -\nabla \left( p + \frac{F}{2} |\mathbf{B}|^2 \right) + \nabla \cdot (F \mathbf{B} \mathbf{B} - \rho \mathbf{u} \mathbf{u} + \sigma C_k \boldsymbol{\tau}) \\ &+ \theta(m+1) \rho \mathbf{e}_z, \end{aligned} \quad (1.33)$$

$$\begin{aligned} \frac{\partial T}{\partial t} &= -\mathbf{u} \cdot \nabla T - (\Gamma - 1) T \nabla \cdot \mathbf{u} + \frac{\Gamma C_k}{\rho} \nabla^2 T \\ &+ \frac{C_k(\Gamma - 1)}{\rho} \left( \frac{\sigma}{2} \|\boldsymbol{\tau}\|^2 + F \zeta_o |\nabla \times \mathbf{B}|^2 \right), \end{aligned} \quad (1.34)$$

$$\frac{\partial \rho}{\partial t} = -\nabla \cdot (\rho \mathbf{u}), \quad (1.35)$$

$$p = \rho T. \quad (1.36)$$

Note that here we use the notation  $\Gamma = c_p/c_v$  for the heat capacity ratio (also known as the adiabatic index), as we use  $\gamma$  to represent the turbulent pumping effect. The quantity  $\theta$  represents the equilibrium temperature gradient in the absence of a magnetic field, and  $m$  is the polytropic index, given in terms of the adiabatic index by  $m = \frac{1}{\Gamma-1}$ . This leaves the system with seven dimensionless parameters, defined in terms of quantities taken at the top of the layer, as well as a new thermal conductivity quantity  $\kappa$ , given by  $\kappa = k/\rho_o c_p$ , the shear viscosity  $\mu$ , and the magnetic diffusivity  $\eta$ . The dimensionless parameters are, Prandtl number  $\sigma$ :

$$\sigma = \frac{\mu c_p}{\kappa}, \quad (1.37)$$

ratio of the magnetic to thermal diffusivity at the top of the layer  $\zeta_o$ :

$$\zeta_o = \frac{\eta \rho_o c_p}{\kappa}, \quad (1.38)$$

dimensionless thermal diffusivity  $C_k$ :

$$C_k = \frac{\kappa}{\rho_o c_p d \sqrt{RT_o}}, \quad (1.39)$$

and dimensionless field strength  $F$  (related to the plasma  $\beta_p$  at the top of the layer by  $F = 2/\beta_p$ ):

$$F = \frac{B_o^2}{RT_o \rho_o \mu_o}. \quad (1.40)$$

## 1.5 Mathematical Formulation

---

Note that here we follow the notation of [Barker \*et al.\* \(2012\)](#), however, this scaling has been used previously by [Cattaneo & Hughes \(1988\)](#) and [Matthews \*et al.\* \(1995\)](#).

## 1. INTRODUCTION

---

# Chapter 2

## Equilibrium Basic State

### 2.1 Equilibrium States of the System

In this Chapter, we consider the equilibrium magnetic field of the system, in order to select a basic state field to which we will later apply linear perturbations. Given that, as we have discussed, we intend to consider the linear stability to magnetic buoyancy subject to the effects of turbulent pumping and turbulent diffusion, we shall begin from a basic state that is an equilibrium under these effects. This is in contrast with previous work on the linear magnetic buoyancy instability that does not include  $\gamma$  and  $\beta$ , in which the basic state field has been prescribed directly; for example, [Kersalé \*et al.\* \(2007\)](#) used a linearly stratified magnetic field as the basis for linear stability analysis, and [Matthews \*et al.\* \(1995\)](#) used a slab of constant field embedded in a non-magnetic atmosphere. Both of these are equilibria over the timescale of the problem; the former indefinitely, and the latter having a diffusion timescale much less than the growth rate of the linear instability, making its decay negligible over the course of the time considered in the problem. However, given the presence of  $\gamma$  and  $\beta$  in the induction equation in our system, we will take a slightly different approach.

In order to find a vertically-stratified equilibrium field consistent with  $\gamma$  and  $\beta$ , we will prescribe only the parameters and the vertical variation of the  $\gamma$  and  $\beta$  effects, which we choose to model the variation in turbulent motion at the base of the convection zone. We will then solve the induction equation (1.32) for the

## 2. EQUILIBRIUM BASIC STATE

---

equilibrium field with  $\frac{\partial \bar{B}}{\partial t} = 0$ , under conditions of zero flow velocity,  $\bar{\mathbf{u}} = 0$ . (Note that throughout this work we will denote the basic state of the system with an overbar, i.e.  $\bar{B}$ ,  $\bar{\mathbf{u}}$ , and therefore we will also use this notation to refer to the equilibrium quantities discussed in this Chapter.) From this, we can solve the energy equation (1.34) at equilibrium for the basic state temperature  $\bar{T}$ . We may then eliminate  $\bar{p}$  by the gas law (1.36), and then, from magnetohydrostatic pressure balance (the  $z$ -component of Equation (1.33), for equilibrium) we may find the corresponding density  $\bar{\rho}$ .

To produce a self-consistent equilibrium basic state field, we consider the dimensionless induction equation (1.32) under equilibrium conditions, i.e.  $\frac{\partial \bar{B}}{\partial t} = 0$  and  $\mathbf{u} = 0$ , given by

$$\nabla \times (\boldsymbol{\gamma} \times \bar{\mathbf{B}}) - \nabla \times ((\zeta_o C_k + \beta) \nabla \times \bar{\mathbf{B}}) = 0. \quad (2.1)$$

As previously discussed, we choose a vertically stratified field in the  $x$ -direction,  $\bar{\mathbf{B}} = \bar{B}(z) \mathbf{e}_x$ , as well as  $\boldsymbol{\gamma} = \gamma(z) \mathbf{e}_z$ ,  $\beta = \beta(z)$ . Equation (2.1) then becomes:

$$(\zeta_o C_k + \beta) \frac{d^2 \bar{B}}{dz^2} + \left( \frac{d\beta}{dz} - \gamma \right) \frac{d\bar{B}}{dz} - \frac{d\gamma}{dz} \bar{B} = 0. \quad (2.2)$$

This is a second order ODE, allowing us to solve for  $\bar{B}(z)$  given  $\gamma(z)$ ,  $\beta(z)$ , and the parameters  $\zeta_o$  and  $C_k$ . It also allows a choice of two boundary conditions, which will be discussed in detail later in this Chapter.

Note that we may also write down the ‘‘uncurled’’ form of Equation (2.1), which is equivalent to the integral of Equation (2.2) and is given by

$$(\zeta_o C_k + \beta) \frac{d\bar{B}}{dz} - \gamma \bar{B} = c, \quad (2.3)$$

where  $c$  is a constant, free to be determined by the boundary conditions. The usefulness of this form will become apparent in Section 2.6.1.

## 2.2 Choice of $\gamma(z)$ and $\beta(z)$ profiles

### 2.2.1 Standard “step” functional form of $\gamma$ and $\beta$

As discussed in Chapter 1, we apply the turbulent pumping  $\gamma$  and the turbulent diffusivity  $\beta$  in order to model the mean effects of turbulence resulting from turbulent convection. We choose the profiles of  $\gamma$  and  $\beta$  in order to model the distribution of turbulent motion at the base of the solar convection zone, spanning the region of the tachocline and into the non-convecting region below. Let us first consider the  $\gamma$  effect. For reasons also described in Chapter 1, we will take  $\gamma$  as a downwards velocity, i.e. in the positive  $z$ -direction. As for the  $z$ -dependence, we aim to model the incidence of turbulence across a region spanning the base of the convection zone. Therefore, we consider a horizontal layer with effectively constant turbulence in some upper region, dropping off abruptly below with the decrease in turbulent convection. To model this, we choose the following profile:

$$\gamma(z) = \frac{\gamma_m}{2}(1 + \tanh(a(z_i - z))), \quad (2.4)$$

following [Barker \*et al.\* \(2012\)](#), pictured in Figure 2.1. Note that the shape of this profile is controlled by three parameters,  $\gamma_m$ ,  $a$  and  $z_i$ .  $\gamma_m$  is equivalent to the magnitude of the turbulent pumping effect, in relation to the sound speed used to scale the MHD equations, and  $\gamma(0) = \gamma_m$ .  $a$  is effectively the “gradient” in the narrow region over which  $\gamma \rightarrow 0$ . It controls the width of the transition region between the turbulent and non-turbulent regions. (Note that the  $a \rightarrow \infty$  limit of this profile corresponds to a step function.) The final parameter,  $z_i$ , gives the position at which the transition is located, with  $0 \leq z_i \leq 1$ . We will assume  $\beta(z)$ , the turbulent diffusion effect, to have the same functional form as  $\gamma(z)$ , and unless otherwise stated, to be proportional to  $\gamma(z)$  according to

$$\beta(z) = \frac{\beta_m}{2}(1 + \tanh(a(z_i - z))). \quad (2.5)$$

We make this choice because  $\gamma$  and  $\beta$  are both the result of assuming mean field turbulence as detailed in Chapter 1, and we aim to model both effects as spatially coincident with the turbulent region at the top of the layer, and thus with each other. Additionally, for the purposes of this Chapter it may be assumed that

## 2. EQUILIBRIUM BASIC STATE

---

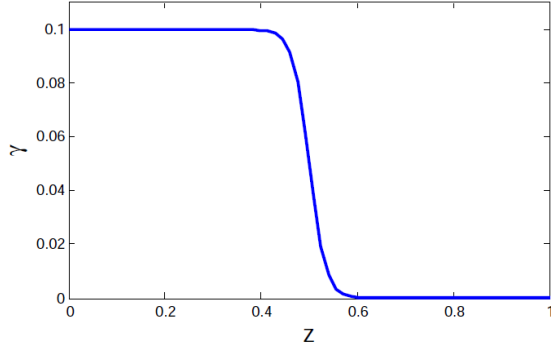


Figure 2.1: The vertical  $\gamma(z)$  profile given by (2.4), with  $\gamma_m = 0.1$ ,  $a = 30$ , and  $z_i = 0.5$ .

$\beta_m = \gamma_m$ . Initially, we will also assume that  $\gamma$  and  $\beta$  have the same value of  $z_i$ ; however in Section 2.10, for the sake of comparison, we will also consider the two effects as extending over different distances into the layer.

### 2.2.2 “Top hat” functional form of $\gamma(z)$ and $\beta(z)$

At this point, we introduce an additional functional form for  $\gamma$  and  $\beta$ , which we will refer to as a “top hat” profile, in contrast to the “step” profile give in Section 2.2. These are given by

$$\gamma(z) = \frac{\gamma_m}{2}(\tanh(a(z - z_{i1})) - \tanh(a(z - z_{i2}))), \quad (2.6)$$

and

$$\beta(z) = \frac{\beta_m}{2}(\tanh(a(z - z_{i1})) - \tanh(a(z - z_{i2}))). \quad (2.7)$$

The top hat form of  $\gamma$  is shown in Figure 2.2. The use and importance of these forms of  $\gamma$  and  $\beta$  will become clear in Section 2.4, and we will discuss their physical relevance to the problem there. However, for now we will use the step forms of  $\gamma$  and  $\beta$  unless stated otherwise.

## 2.3 Choice of Boundary Conditions

Besides freedom in the choice of  $\gamma$  and  $\beta$ , there is also a freedom of choice in the boundary conditions when solving Equation (2.2) for the basic state. It is

## 2.3 Choice of Boundary Conditions

---

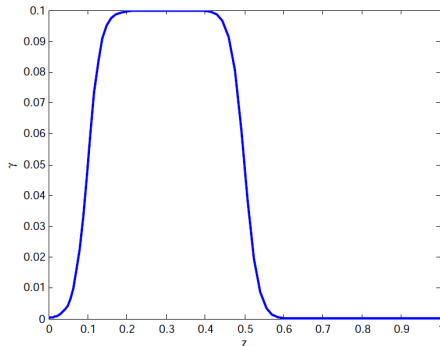


Figure 2.2: The modified form of  $\gamma$  given by (2.6), with  $\gamma_m = 0.1$ ,  $a = 30$ ,  $z_{i1} = 0.1$ , and  $z_{i2} = 0.5$ .

necessary to consider which boundary conditions are most physically realistic if the goal is to model a region at the base of the convection zone.

One possible choice may be to fix the flux of the field within the layer, restricting it to some set value, for which we choose 1. We define the flux  $\phi(z)$  according to

$$\phi(z) = \int_0^z \bar{B}(z') dz', \quad (2.8)$$

and take the boundary condition  $\phi(1) = 1$  in order to fix the flux in the layer. Note that this type of integral boundary condition may be implemented in a standard numerical BVP solver (such as MATLAB's `bvp4c` solver, which we have used throughout our consideration of the basic states) by writing Equation (2.2) as a third order boundary value problem in  $\phi$  rather than  $\bar{B}$ , and then applying  $\phi(0) = 0$ ,  $\phi(1) = 1$ , and one additional boundary condition. Subsequently, however, we will discuss the numerical solutions in terms of  $\bar{B}(z)$  rather than  $\phi(z)$ .

This type of integral boundary condition prevents the field from growing excessively in magnitude, limiting how much field the  $\gamma$  pumping effect at the top of the layer can “draw down” from above and outside the domain. (This effect, whereby a large amount of field is drawn into the layer, is discussed alongside the results presented in Section 2.4.) However, fixing the flux still leaves a free choice of one other boundary condition. We will consider various other choices for this

## 2. EQUILIBRIUM BASIC STATE

---

final boundary condition, including Dirichlet and Neumann conditions, as well as considering the effect of applying the boundary conditions at the top versus the bottom of the layer. We will then discuss which sets of boundary conditions produce results that best reflect the physical reality we plan to model.

We will begin, however, by choosing boundary conditions that do not include the requirement of constant flux, in order to demonstrate the physical motivation for using such a condition.

### 2.4 $\bar{B}'(0) = 1, \bar{B}(0) = 0$

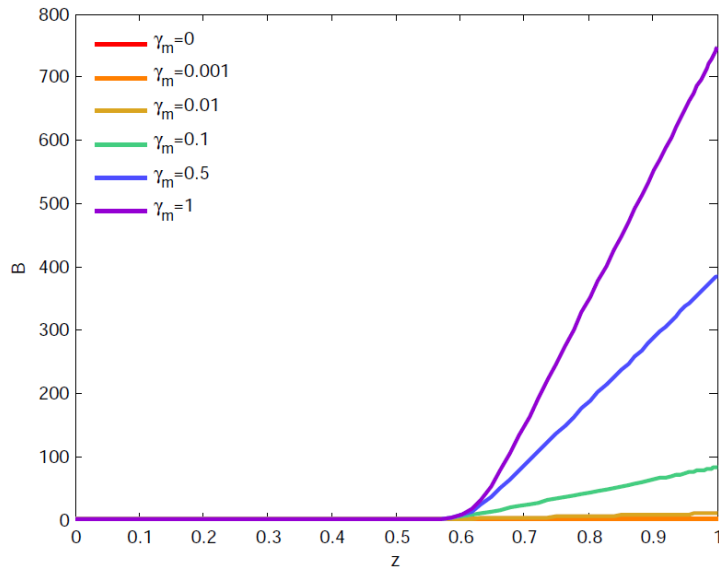


Figure 2.3: Variation of equilibrium field for  $\bar{B}'(0) = 1$  and  $\bar{B}(0) = 0$ ,  $\gamma = \beta$  with varying amplitude given by (2.4) and (2.5).

First we consider a case which does not involve constant flux, but merely fixes the value of the field as zero, and its gradient as some fixed value  $\lambda$ , at the top of the layer. Here we have chosen  $\lambda = 1$  for the gradient. We assume the “step function-like”  $\gamma$  and  $\beta$  profiles given by (2.4) and (2.5), with  $z_i = 0.5$  and  $a = 30$ .

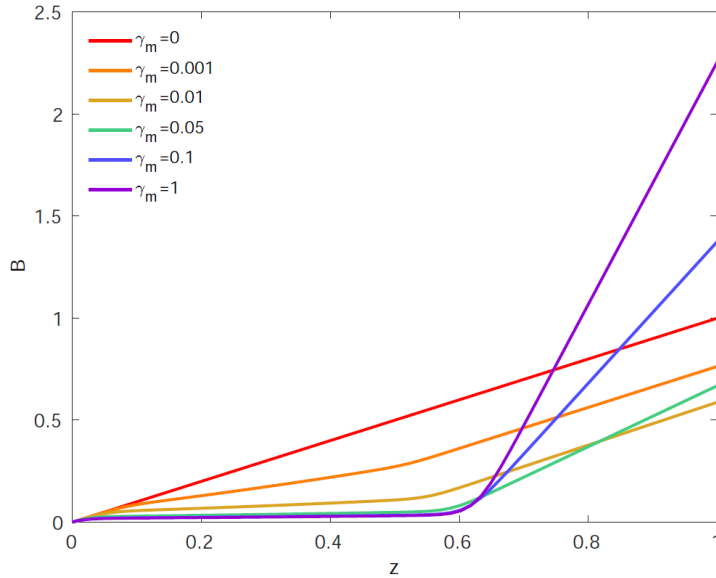


Figure 2.4: Variation of equilibrium field for  $\bar{B}'(0) = 1$  and  $\bar{B}(0) = 0$ ,  $\gamma = \beta$  with varying amplitude given by (2.6) and (2.7), with  $z_{i1} = 0.1$  and  $z_{i2} = 0.5$ .

It can be seen that here, the choice of the form of  $\gamma$  and  $\beta$  makes a large difference to the gradient of the field at the base of the layer, if not its functional form. The gradient and the size of the field increase greatly as the pumping and turbulent diffusion strength  $\gamma_m$  is increased. This is due to the presence of pumping at the very top of the layer, which for these boundary conditions is able to “draw in” an effectively unlimited amount of field if it acts at the boundary, as no limit is placed on the total flux in the layer.

It is this effect that motivates us to consider the top hat profiles for  $\gamma$  and  $\beta$ , discussed in Section 2.2.2. Let us now apply  $\gamma$  and  $\beta$  according to (2.6) and (2.7) with  $z_{i1} = 0.1$  and  $z_{i2} = 0.5$ , such that there is a small gap between the top of the layer and the point at which  $\gamma$  and  $\beta$  become significant. Note that we still set  $\beta_m = \gamma_m$  here. Compare the magnitude of the field at the bottom of the layer in Figures 2.3 and 2.4; the step profile  $\gamma$  and  $\beta$  give a maximum value of  $\bar{B}$  (Figure 2.3) that is of the order  $10^2$  larger than that in the case of the top hat profile (Figure 2.4), due to field being brought into this layer. When  $\gamma$  and  $\beta$  are

## 2. EQUILIBRIUM BASIC STATE

---

absent in a small region at the very top of the layer as in the case of the top hat profiles, we do not see the same scale of increase with  $\gamma_m$  and  $\beta_m$ .

The effect of such a “drawing in” of field is to increase the total field gradient dramatically, especially in the lower section of the layer where  $\gamma$  and  $\beta$  are effectively absent. If used as a basic state for linear stability analysis, this could result in the instability being extremely sensitive to small changes in the size of the  $\gamma$  and  $\beta$  effects in this region. This would arguably constitute an unphysical situation as the instability is not expected to depend so strongly on effects present in the small region surrounding the upper boundary.

Removing the pumping and turbulent diffusion effects from the top of the layer as in the case of the top hat  $\gamma$  and  $\beta$ , however, ensures that the large increase in the field gradient with  $\gamma_m$  does not occur to the same extent; the gradient and value of the field at the bottom of the layer do increase overall, but remain of the same order of magnitude as when  $\gamma = \beta = 0$ .

Physically speaking, if a boundary condition set such as this is chosen, it would be beneficial to use a pumping of the top hat form that “cuts off” just below the top of the layer. This would ensure that the field gradient is not overly sensitive to the strength of the pumping, as in this example. However, as we will see, we may also make use of a boundary condition that constrains the flux in the layer in order to prevent such a problem entirely.

### 2.5 $\bar{B}'(0) = 1, \phi(1) = 1$

As a variation on the previous case, we may consider the case where the gradient of the field is still fixed at the top of the layer, but instead of fixing the field at zero, we assume the total flux in the layer, given by (2.8), is constant; we set  $\phi(1) = 1$ . This prevents the value of the field at the base of the layer from increasing without limit as more field is pumped in from the upper boundary.

It can be seen that such a choice makes a marked difference, for both the step and

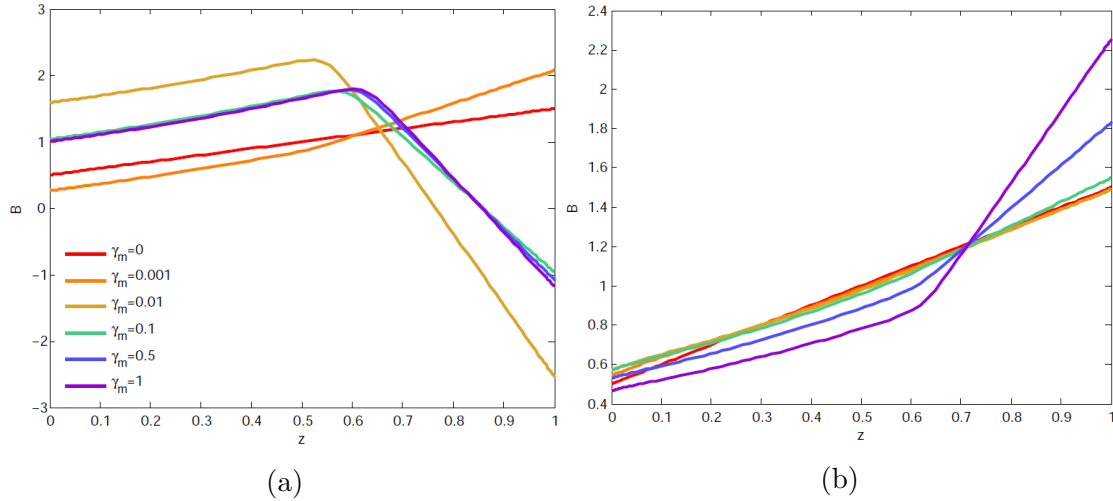


Figure 2.5: Variation of equilibrium field for  $\bar{B}'(0) = 1$  and constant flux,  $\gamma = \beta$  with varying amplitude, for (a) step profile and (b) top hat profile with  $z_{i1} = 0.1$  and  $z_{i2} = 0.5$ .

top hat  $\gamma$  profiles (see Figure 2.5). In the case of the step profile, the gradient at the bottom of the layer changes sign for some value of  $\gamma_m$ , which depends on the other parameters of the problem (see Section 2.6.1 for further explanation of this change in field direction). This does not occur, however, for the top hat field. Thus the top hat field for this boundary condition set may represent a more physically appropriate basic state field. (That is to say, a state that does not display any behaviour inconsistent with what we know of the mean field in the solar convection zone. See Section 2.14 for further discussion.) We can see from Figure 2.5b that top hat  $\gamma$  and  $\beta$  do not give reversals of sign or large changes in gradient resulting from small changes in  $\gamma_m$ , and that the form of the resulting field is not completely determined by conditions at the top of the layer, which, in the real system, represents some arbitrary point within the convection zone.

## 2.6 $\bar{B}'(0) = 0, \phi(1) = 1$

We consider a similar case to the previous one, however we now fix the field gradient at zero at the top of the layer. In Figure 2.6a, for the step  $\gamma$  and  $\beta$  effects, the change in the sign of the gradient still occurs, though it occurs at a lower value

## 2. EQUILIBRIUM BASIC STATE

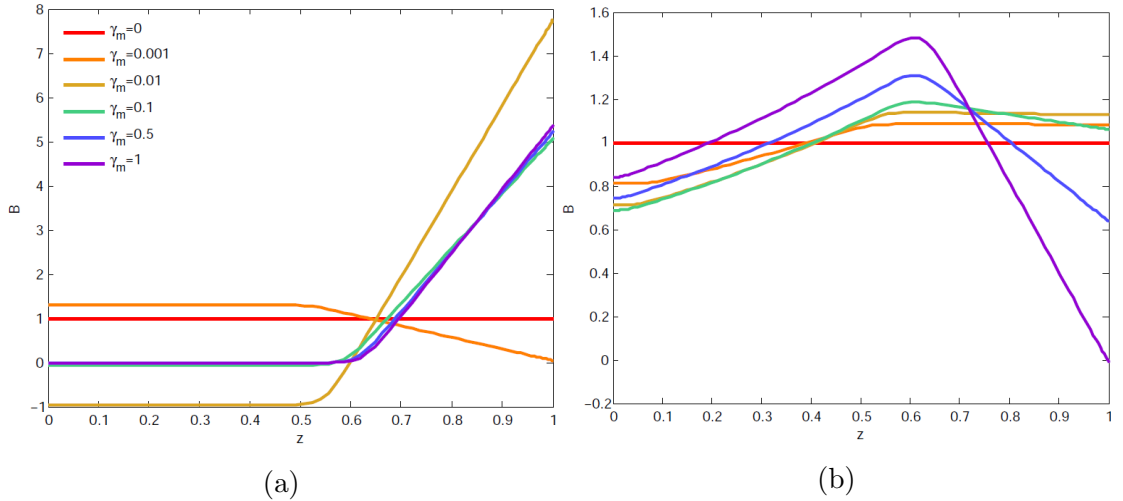


Figure 2.6: Variation of equilibrium field for  $\bar{B}'(0) = 0$  and constant flux,  $\gamma = \beta$  with varying amplitude, for (a) step profile and (b) top hat profile with  $z_{i1} = 0.1$  and  $z_{i2} = 0.5$ .

of  $\gamma_m$  for the same parameters. In addition, the gradient in the upper half of the layer — where the step pumping effect acts — is zero, and the field is simply a constant that depends on the pumping strength.

However, for the top hat  $\gamma$  and  $\beta$  case, introducing a small region of no pumping and turbulent diffusion at the top of the layer allows the field to have a gradient in the pumping region. It also changes the gradient at the lower boundary, including a change in its sign for larger values of  $\gamma_m$ , with respect to the equivalent case for a step  $\gamma$ .

In the case of the solar convection zone, this dependence on  $\gamma_m$  would mean that there would be a complete reversal of the direction of the mean field at some radius, as the strength of the pumping effect varies. However, physically speaking, we do not want to consider a mean field that contains large-scale reversals of sign with radius. This would constitute an unphysical scenario for the solar case, because it is improbable that dynamo action would result from a field effectively containing “shells” of different sign of mean field. Thus, we seek a basic state for our linear stability analysis that does not exhibit such dependence.

In the limit of large  $a$ , we may also use an analytic approach to try to understand why fixing the gradient gives rise to this behaviour.

### 2.6.1 Analytic solution for step functions $\gamma = \beta, \bar{B}'(0) = 0, \phi(1) = 1$

We will also give some consideration to an analytic solution in the limit  $a \rightarrow \infty$ , to compare with the numerical solution. In the limit of large gradient  $a$ , the form of  $\gamma$  and  $\beta$  given by Equation (2.4) becomes a true step function. With this assumption, it is possible to approximate the function  $\gamma$  as a constant value of  $\gamma_m$  in the range  $0 \leq z < z_i$  and zero in  $z_i < z \leq 1$ . Using this approximation, it is possible to obtain an analytic solution to Equation (2.2), for the regions on each side of  $z_i$ . We require that the solution is continuous at this boundary, so that the induction equation can be solved. This acts as a matching condition for the solutions on either side of  $z_i$ .

Additionally, we may use the induction equation in the integrated form given by (2.3) to obtain a second jump condition. From the induction equation at equilibrium in the form (2.3), we find that the quantity  $(\zeta_o C_k + \beta)\bar{B}' - \gamma\bar{B}$  must be constant everywhere, including at the interface. The jump conditions are, therefore:

$$[\bar{B}]_{z_i} = 0, \tag{2.9}$$

$$[(\zeta_o C_k + \beta)\bar{B}' - \gamma\bar{B}]_{z_i} = 0. \tag{2.10}$$

We may use these two conditions at  $z_i$ , along with the two chosen boundary conditions, to match the solutions at the interface and obtain a continuous, analytic estimate for the field.

Let us consider the case of constant flux and  $\bar{B}'(0) = 0$  boundary conditions; a similar argument is possible for the more general  $\bar{B}'(0) = \lambda$  case, but is more mathematically involved, so for the sake of example, in the coming analysis we

## 2. EQUILIBRIUM BASIC STATE

---

will consider  $\lambda = 0$ . The equivalent result for  $\lambda \neq 0$ , however, is given in Appendix A.

For equilibrium:

$$(\zeta_o C_k + \beta)\bar{B}'' + (\beta' - \gamma)\bar{B}' - \gamma'\bar{B} = 0.$$

Also, take:

$$\beta = \gamma = \begin{cases} \gamma_m = \text{constant} & 0 \leq z < z_i \\ 0 & z_i < z \leq 1 \end{cases}.$$

At  $z = z_i$ , the jump conditions given by Equations (2.9) and (2.10) apply. In addition, we select boundary conditions:

$$\phi(1) = \int_0^1 \bar{B}(z) dz = 1, \quad (2.11)$$

$$\bar{B}'(0) = 0. \quad (2.12)$$

Initially, we solve for the two regions separately.

Firstly, for  $0 \leq z < z_i$ :

$$(\zeta_o C_k + \gamma_m)\bar{B}'' - \gamma_m\bar{B}' = 0,$$

so that

$$\bar{B} = P + Q \exp\left(\frac{\gamma_m z}{\zeta_o C_k + \gamma_m}\right).$$

Applying the boundary condition  $\bar{B}'(0) = 0$  gives  $Q = 0$ , and here

$$\bar{B} = P = \text{constant}.$$

Secondly, for  $z_i < z \leq 1$ :

$$\bar{B}'' = 0,$$

$$\bar{B} = R + Sz.$$

Then, applying condition (2.9), i.e. continuity of the field at  $z_i$ , gives:

$$P - R - Sz_i = 0. \quad (2.13)$$

The other jump condition, (2.10), allows us to obtain:

$$\gamma_m P + \zeta_o C_k S = 0. \quad (2.14)$$

Finally the constant flux condition gives:

$$\int_0^{z_i} P dz + \int_{z_i}^1 R + S z dz = 1,$$

i.e.

$$P z_i + R(1 - z_i) + \frac{S}{2}(1 - z_i^2) = 1. \quad (2.15)$$

Here, (2.14) gives  $P = -\frac{\zeta_o C_k}{\gamma_m} S$ , and (2.13) gives  $R = -\left(\frac{\zeta_o C_k}{\gamma_m} + z_i\right) S$ .

Therefore Equation (2.15) becomes

$$\left(-\frac{\zeta_o C_k z_i}{\gamma_m} - \left(\frac{\zeta_o C_k}{\gamma_m} + z_i\right)(1 - z_i) + \frac{1}{2} - \frac{z_i^2}{2}\right) S = 1,$$

giving, finally,

$$S = \left(-\frac{\zeta_o C_k}{\gamma_m} + \frac{(1 - z_i)^2}{2}\right)^{-1}. \quad (2.16)$$

Similarly, from equations (2.14) and (2.13):

$$P = -\frac{\zeta_o C_k}{\gamma_m} \left(-\frac{\zeta_o C_k}{\gamma_m} + \frac{(1 - z_i)^2}{2}\right)^{-1}, \quad (2.17)$$

$$R = -\left(\frac{\zeta_o C_k}{\gamma_m} + z_i\right) \left(-\frac{\zeta_o C_k}{\gamma_m} + \frac{(1 - z_i)^2}{2}\right)^{-1}. \quad (2.18)$$

From this analysis, we can see that this set of boundary conditions gives rise to a constant equilibrium field in the region where pumping is present, and a linearly varying field where it is absent. Note the form of the coefficient  $S$ , the gradient of the linear section of the field, in the lower part of the layer; with fixed values of  $\zeta_o$ ,  $C_k$ , and  $z_i$ ,  $S \rightarrow \infty$  for a value of  $\gamma_m$  given by:

$$\gamma_m = \frac{2\zeta_o C_k}{(1 - z_i)^2}. \quad (2.19)$$

Approaching this value of the pumping strength, the gradient at the bottom of the layer approaches infinity, and changes sign. This can be seen in the numerical

## 2. EQUILIBRIUM BASIC STATE

---

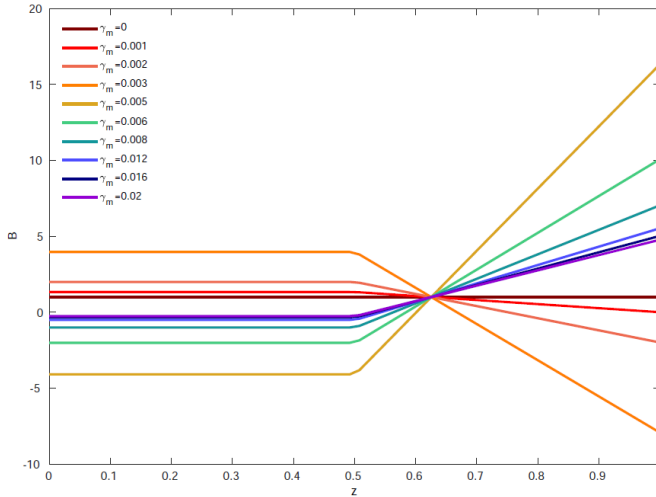


Figure 2.7: The variation of the equilibrium field, calculated numerically for  $\bar{B}'(0) = 0$  and constant flux boundary conditions, and pumping and turbulent diffusion  $\gamma = \beta$  given by Equation (2.4), with parameters  $z_i = 0.5$  and  $a = 1000$ . Compare with the numerical result for a step-like  $\gamma$  and  $\beta$  for the same boundary conditions, presented in Figure 2.6a.

results by plotting the basic state for varying values of  $\gamma_m$ .

Taking a much larger value of  $a$  allows us to compare with the analytic approximation, as the limit of large  $a$  is effectively a step function. We plot the numerical solution for  $a = 1000$  in Figure 2.7, allowing us to see that the gradient at the lower end of the layer changes sign. Equation (2.19) allows us to calculate the approximate value at which this occurs, taking parameter values of  $z_i = 0.5$ ,  $\zeta_o = 0.05$  and  $C_k = 0.01$ . We obtain a value of  $\gamma_m = 0.004$ , which is also seen in the numerical profiles shown in Figure 2.7. In addition, the sign of the constant value in the upper half of the layer changes in accordance with that of the gradient in the lower half, as the analytic approximation also predicts.

We may also carry out a similar analysis for the top hat profiles for  $\gamma$  and  $\beta$ . In the top hat case, the analysis is similar but the matching conditions are applied at both interfaces. This gives a system of six linear equations to solve (which

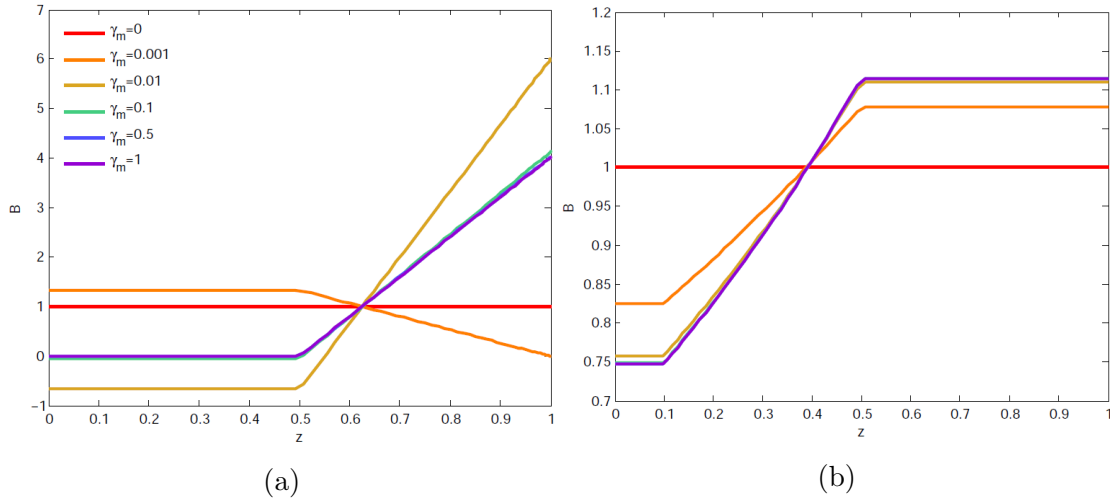


Figure 2.8: Semi-analytic field profiles for  $\bar{B}'(0) = 0$ , constant flux boundary conditions, with  $\gamma = \beta$  given by (a) step function and (b) top hat function between  $z_{i1} = 0.1$  and  $z_{i2} = 0.5$ .

maintain the two jump conditions at each interface, as well as the constant flux boundary condition and one additional boundary condition) as opposed to four in the case of the step profile. In order to simplify the analysis in this case, we solve this system numerically, giving rise to what we will call the “semi-analytic” approximation to the solution in the limit  $a \rightarrow \infty$ , shown in Figure 2.8.

This shows the variation of the semi-analytic solution for infinitely steep step and top hat profiles of  $\gamma$  and  $\beta$ . This may be compared with the numerical calculation of the equilibrium field for both of these forms of  $\gamma$  and  $\beta$ , shown in Figure 2.6. We can see that the case of the equilibrium field for the step  $\gamma$ , the analytically predicted form matches the numerical form well, showing a similar constant value in the pumping region at the top of the layer, and linear variation outside it. The change in the sign of the gradient that we noted before is still present, and occurs at approximately the same pumping strength  $\gamma_m$ .

In the case of the top hat  $\gamma$  and  $\beta$  profiles, however, the form is qualitatively different as compared to the numerical results for  $a = 30$  in Figure 2.6b, specifically for larger  $\gamma_m$ . Analytical considerations predict a constant value of the field

## 2. EQUILIBRIUM BASIC STATE

---

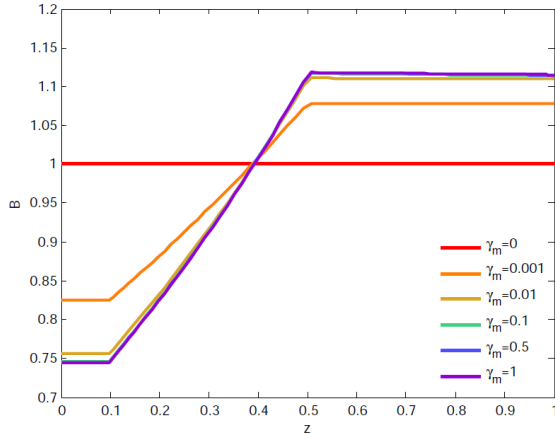


Figure 2.9: Numerically calculated profiles for  $\bar{B}'(0) = 0$ , constant flux, and top hat  $\gamma$ , with  $a = 1000$ .

below the “top hat” pumping region, however, in the numerical plot we see a negative gradient, which becomes quite significant as  $\gamma_m$  increases.

This deviation from the analytical form is a product of the fact that the analytic approximation assumes that — in terms of  $\gamma$  given by (2.4) as used in the numerical calculation — the quantity  $a$ , which quantifies the gradient with which the field drops to zero at the edges of the pumping region, is infinite. This, however, is not the case in the original numerical case, for which we take a value of  $a = 30$ . We may find a numerical profile that approaches the analytical one by taking a larger value of  $a = 1000$ , shown in Figure 2.9. Here, the only thing that has been changed compared to Figure 2.6b is that  $a$  has been changed from 30 to 1000. The effect, however, is significant; the numerically calculated field in this case is effectively constant at the bottom of the layer, as predicted by the analytic approximation. This demonstrates that the validity of the numerical solution can in some cases depend strongly on the value of  $a$ . In many cases — indeed, in the case of the step pumping for this boundary condition — the value of  $a$  makes little difference to the general form of the equilibrium field apart from the change in the “sharpness” with which the switch from one field regime to the other occurs. However, in the top hat case, the effect is significant in both a qualitative and a

quantitative sense. This sensitivity to  $a$  in the resulting field gradient must be taken into account when considering this boundary condition for use in the calculation of the basic state for the stability problem. The instability is driven by field gradient, and so using such a boundary condition may potentially result in positive or negative changes in stability driven by changing the effective “width” of the transition region.

Moreover, the change in the direction of the field with  $\gamma_m$  also poses problems with using this field to represent the basic state of the physical system. A large change in direction of the field for some value of  $\gamma_m$  means that physically, such a boundary condition may not be a suitable choice. In the context of the solar magnetic field, it seems improbable that dynamo action would give rise to a large-scale reversal in direction of the background field over radius, which would be the physical analogue for such a dependence on the strength of the turbulent pumping effect. Nevertheless, this case provides an example of the method by which an analytical comparison can be made.

## 2.7 $\bar{B}(0) = 0, \phi(1) = 1$

Here we consider a Dirichlet condition, namely, zero field at the top of the layer. We also fix the total flux as in Sections 2.5 and 2.6. The numerically calculated equilibrium fields are shown in Figure 2.10.

In both the step and top hat cases, these boundary conditions produce a positive gradient in every part of the layer, which is larger where pumping and turbulent diffusion are not present. This case also gives the most similar behaviour for step and top hat profiles, as the field is fixed at the top of the layer, so having a small region with low  $\gamma$  and  $\beta$  surrounding this fixed  $\bar{B}$  point makes little difference to the final profile.

Such a boundary condition may be the best choice to minimise the dependence of the equilibrium field on the condition at the top of the layer, while still allowing sensitivity to the pumping strength.

## 2. EQUILIBRIUM BASIC STATE

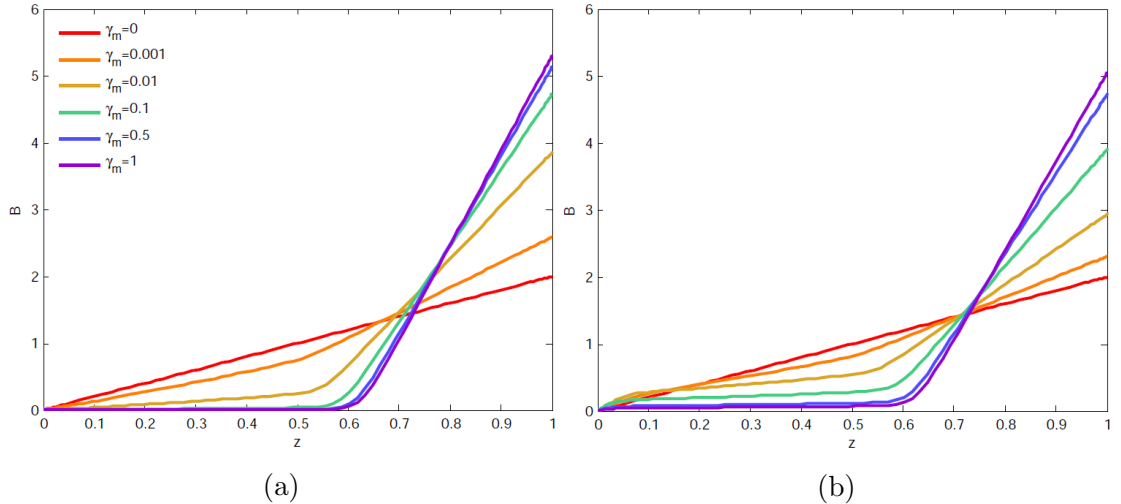


Figure 2.10: Variation of equilibrium field for  $\bar{B}(0) = 0$  and constant flux,  $\gamma = \beta$  with varying amplitude, for (a) step profile and (b) top hat profile with  $z_{i1} = 0.1$  and  $z_{i2} = 0.5$ .

### 2.7.1 Semi-analytic comparison for $\bar{B}(0) = 0$ , $\phi(1) = 1$

In this Section, we will once more apply the semi-analytic approach to the calculation of the basic state, which corresponds to the  $a \rightarrow \infty$  limit of the numerical calculation.

In the case of  $\bar{B}(0) = 0$  and constant flux, the semi-analytic field profiles (Figure 2.11) are qualitatively similar in form to the numerically calculated versions shown in Figure 2.10. The main difference is that the overall change in field across the layer (i.e. the field at the bottom of the layer) is larger in the numerical case. In consequence, in the case of the numerically calculated field, the gradient in the upper part of the layer is lower, in order to maintain the constant flux condition.

Again, this change in the field gradient has implications for the behaviour of the instability, as it affects the variation of the field gradient as a function of  $z$ . However, unlike in the case of  $\bar{B}'(0) = \lambda$  as considered previously, the gradient at the bottom of the layer increases monotonically with  $\gamma$ , as opposed to changing sign as in cases such as  $\bar{B}'(0) = 0, 1$ .

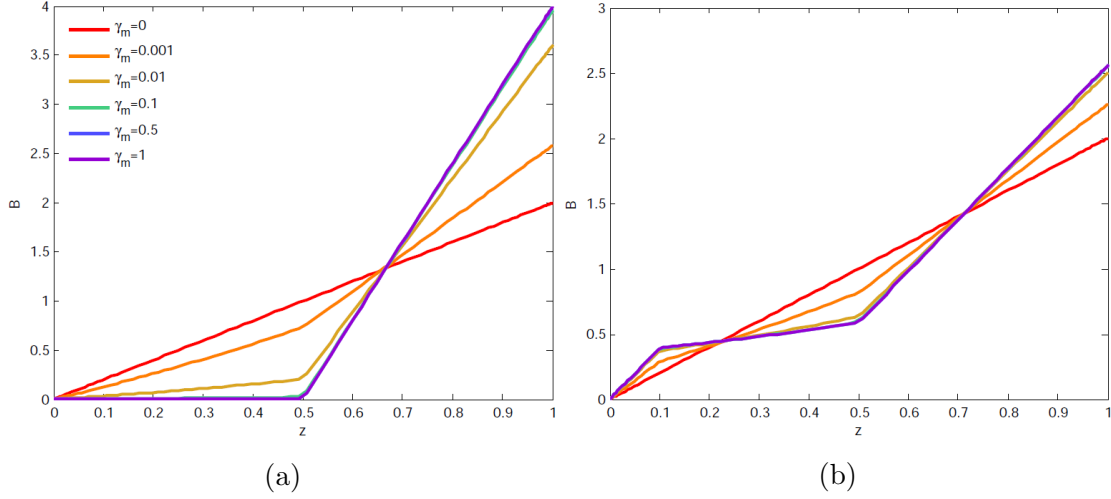


Figure 2.11: Semi-analytic field profiles for  $\bar{B}(0) = 0$ , constant flux boundary conditions, with  $\gamma = \beta$  given by (a) step function and (b) top hat function between  $z_{i1} = 0.1$  and  $z_{i2} = 0.5$ .

### 2.7.2 Analytic form of the equilibrium field for $\bar{B}(0) = 0$ , $\phi(1) = 1$

To understand the variation in the field gradient as a function of  $\gamma_m$  and why it differs from the Neumann condition case, let us use a similar analytic approach to that described in Section 2.6.1. Using the same notation as in Section 2.6.1 for the general form of the equilibrium field in the case of step functions  $\gamma$  and  $\beta$ , we have:

$$\bar{B} = \begin{cases} P + Q \exp\left(\frac{\gamma_m z}{\zeta_0 C_k + \gamma_m}\right) & 0 \leq z < z_i, \\ R + Sz & z_i < z \leq 1. \end{cases}$$

We can then once more apply the matching conditions and the boundary conditions of constant flux and  $\bar{B}(0) = 0$ , to obtain analytic expressions for the

## 2. EQUILIBRIUM BASIC STATE

---

coefficients  $P$ ,  $Q$ ,  $R$ , and  $S$ :

$$P = \left( \left( 2 + \frac{\zeta_o C_k}{\gamma_m} \right) - \frac{\gamma_m}{2\zeta_o C_k} (z_i - 1)^2 - \left( 2 + \frac{\zeta_o C_k}{\gamma_m} - z_i \right) \exp \left( \frac{\gamma z_i}{\zeta_o C_k + \gamma_m} \right) \right)^{-1}, \quad (2.20)$$

$$Q = - \left( \left( 2 + \frac{\zeta_o C_k}{\gamma_m} \right) - \frac{\gamma_m}{2\zeta_o C_k} (z_i - 1)^2 - \left( 2 + \frac{\zeta_o C_k}{\gamma_m} - z_i \right) \exp \left( \frac{\gamma z_i}{\zeta_o C_k + \gamma_m} \right) \right)^{-1}, \quad (2.21)$$

$$R = \left( 1 - \exp \left( \frac{\gamma z_i}{\zeta_o C_k + \gamma_m} \right) + \frac{\gamma_m z_i}{\zeta_o C_k} \right) \left( \left( 2 + \frac{\zeta_o C_k}{\gamma_m} \right) - \frac{\gamma_m}{2\zeta_o C_k} (z_i - 1)^2 - \left( 2 + \frac{\zeta_o C_k}{\gamma_m} - z_i \right) \exp \left( \frac{\gamma z_i}{\zeta_o C_k + \gamma_m} \right) \right)^{-1}, \quad (2.22)$$

$$S = - \frac{\gamma_m}{\zeta_o C_k} \left( \left( 2 + \frac{\zeta_o C_k}{\gamma_m} \right) - \frac{\gamma_m}{2\zeta_o C_k} (z_i - 1)^2 - \left( 2 + \frac{\zeta_o C_k}{\gamma_m} - z_i \right) \exp \left( \frac{\gamma z_i}{\zeta_o C_k + \gamma_m} \right) \right)^{-1}. \quad (2.23)$$

We seek to understand the  $\gamma_m$  dependence of these coefficients. Plotting (2.20) – (2.23) as a function of  $\gamma_m$  (see Figure 2.12), for example parameter values of  $\zeta_o = 0.05$  and  $C_k = 0.01$ , we can see that each of the coefficients varies monotonically with  $\gamma_m$ , which is also consistent with the variation we see when we calculate the equilibrium state numerically (see Figure 2.10). However, they also appear to diverge as  $\gamma_m \rightarrow 0$ . This raises a question about the convergence of the full solution in this limit, which we may address with an asymptotic analysis.

First, however, consider the case of  $\gamma = \beta = 0$ , corresponding to  $\gamma_m = 0$  here. In this case, (2.2) reduces to  $\bar{B}'' = 0$ . Solving this and applying the boundary conditions, we expect a solution  $\bar{B} = 2z$  when  $\gamma_m = 0$ . However, naively, it is not immediately clear how the coefficients  $P$ ,  $Q$ ,  $S$ , and  $R$ , which appear divergent in this limit, produce this simple linear solution in the limit  $\gamma_m \rightarrow 0$ . In the event though, they do produce a convergent linear solution in this limit, and we shall show this via asymptotic analysis.

Let us approximate the coefficients  $P$ ,  $Q$ ,  $R$ , and  $S$  in the limit  $\gamma_m \rightarrow 0$ . We must take a second order approximation for the exponential term in this instance, i.e.:

$$\exp \left( \frac{\gamma_m z_i}{\zeta_o C_k + \gamma_m} \right) = 1 + \frac{\gamma_m z_i}{\zeta_o C_k + \gamma_m} + \frac{\gamma_m^2 z_i^2}{2!(\zeta_o C_k + \gamma_m)^2} + o(\gamma_m^2). \quad (2.24)$$

Substituting into the expression for the coefficients  $P, Q, R,$  and  $S,$  we rearrange and find that, to leading order:

$$P \rightarrow -\frac{2\zeta_o C_k}{\gamma_m}, \quad (2.25)$$

$$Q \rightarrow \frac{2\zeta_o C_k}{\gamma_m}, \quad (2.26)$$

$$R \rightarrow -\frac{(2 - z_i)z_i\gamma_m}{\zeta_o C_k}, \quad (2.27)$$

$$S \rightarrow 2, \text{ as } \gamma_m \rightarrow 0. \quad (2.28)$$

Thus, we can immediately see that for the solution for  $z_i < z \leq 1$  (in the region of  $\gamma = \beta = 0$ ):

$$\lim_{\gamma_m \rightarrow 0} \bar{B}_{right} = \lim_{\gamma_m \rightarrow 0} \left( 2z - \frac{(2 - z_i)z_i\gamma_m}{\zeta_o C_k} \right) = 2z. \quad (2.29)$$

For  $0 \leq z < z_i,$  we may also make the same second order approximation to the exponential to allow us to find the behaviour as  $\gamma_m \rightarrow 0$ :

$$\begin{aligned} \lim_{\gamma_m \rightarrow 0} \bar{B}_{left} &= \lim_{\gamma_m \rightarrow 0} \left( -\frac{2\zeta_o C_k}{\gamma_m} + \frac{2\zeta_o C_k}{\gamma_m} \exp\left(\frac{\gamma_m z}{\zeta_o C_k + \gamma_m}\right) \right) \quad (2.30) \\ &= \lim_{\gamma_m \rightarrow 0} \left( -\frac{2\zeta_o C_k}{\gamma_m} + \frac{2\zeta_o C_k}{\gamma_m} \left( 1 + \frac{\gamma_m z}{\zeta_o C_k + \gamma_m} + \frac{\gamma_m^2 z^2}{2!(\zeta_o C_k + \gamma_m)^2} + o(\gamma_m^2) \right) \right) \\ &= \lim_{\gamma_m \rightarrow 0} \left( \frac{2\zeta_o C_k z}{\zeta_o C_k + \gamma_m} + \frac{\zeta_o C_k \gamma_m z^2}{(\zeta_o C_k + \gamma_m)^2} + o(\gamma_m) \right) \\ &= 2z. \end{aligned}$$

Here we can see that even though the individual coefficients  $P$  and  $Q$  diverge in the limit  $\gamma_m \rightarrow 0,$  the solution does not, but goes to  $\bar{B} = 2z$  as expected. In Figure 2.13 we compare the approximate forms (2.25) – (2.28) as  $\gamma_m \rightarrow 0$  with the full forms of coefficients (2.20) – (2.23).

Thus, we have shown that the boundary conditions  $\bar{B}(0) = 0$  and constant flux produce a solution that does not diverge for any value of  $\gamma_m,$  nor does it depend strongly on the effect of  $\gamma$  and  $\beta$  at the very top of the layer. Both these properties make this type of equilibrium state a strong contender for use as a basic state in the linear stability problem. However, so far we have only considered the application of Dirichlet and Neumann conditions at the top of the layer. Now, we will consider the results of applying them at the bottom.

## 2. EQUILIBRIUM BASIC STATE

---

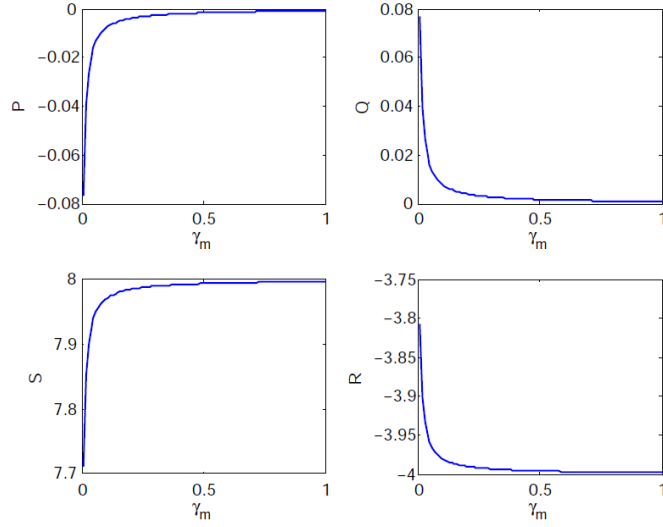


Figure 2.12: Coefficients  $P$ ,  $Q$ ,  $R$ , and  $S$  as a function of  $\gamma_m$  in the case of constant flux and  $\bar{B}(0) = 0$  boundary conditions, assuming a step function form for  $\gamma = \beta$ , with  $\zeta_o = 0.01$  and  $C_k = 0.01$ .

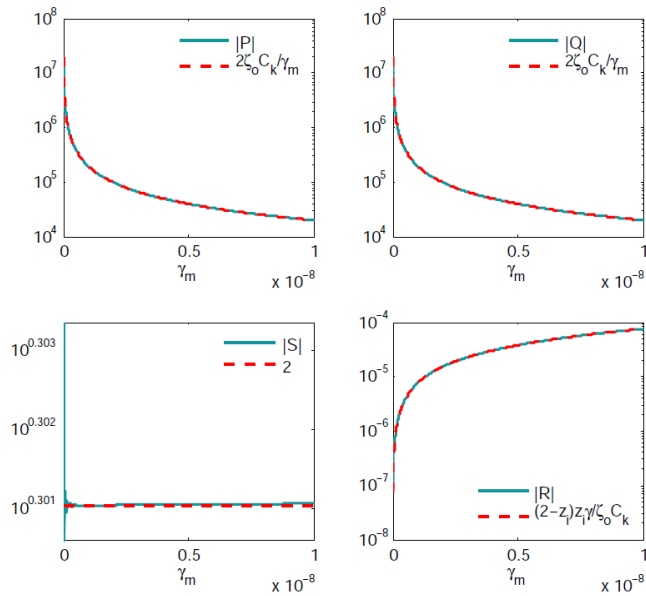


Figure 2.13: Absolute values of coefficients  $P$ ,  $Q$ ,  $S$ , and  $R$  as a function of small  $\gamma_m$ , compared with their full analytic forms, (2.20) – (2.23), in the limit  $\gamma_m \rightarrow 0$ .

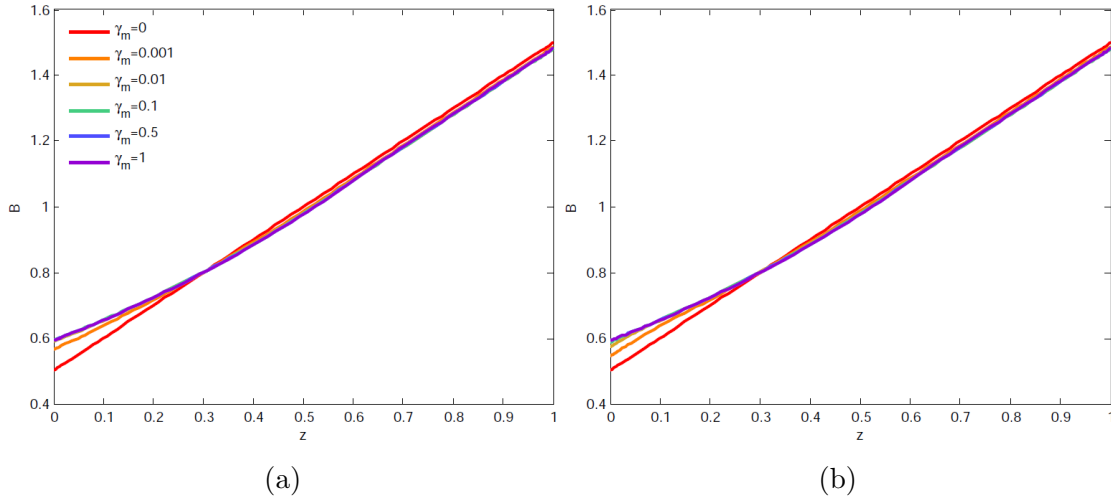
2.8  $\bar{B}'(1) = 1, \phi(1) = 1$ 

Figure 2.14: Variation of equilibrium field for  $\bar{B}'(1) = 1$  and constant flux,  $\gamma = \beta$  with varying amplitude, for (a) step profile and (b) top hat profile with  $z_{i1} = 0.1$  and  $z_{i2} = 0.5$ .

So far, all the scenarios considered have fixed the additional boundary condition at the top of the layer, leaving only the constant flux condition to determine what occurs at the bottom. But for comparison, we may also consider a case where the gradient is fixed at the bottom of the layer, as we have plotted in Figure 2.14.

In such a scenario, sensitivity of the equilibrium field to the pumping and turbulent diffusion effects is decreased in general, with the field never varying far from the linear form it takes when no pumping or turbulent diffusion are present. For this reason, it also makes very little difference whether we use a step or top hat profile in this case, and the field is always close to linear for  $\gamma_m = O(1)$ .

### 2.8.1 Semi-analytic comparison for $\bar{B}'(1) = 1, \phi(1) = 1$

In the case of  $\bar{B}'(1) = 1$  and constant flux, the field depends little on whether  $\gamma$  and  $\beta$  are present at the very top of the layer (and therefore on whether the step or top hat profile is used for  $\gamma$  and  $\beta$ ), or on their amplitude  $\gamma_m$  within the range

## 2. EQUILIBRIUM BASIC STATE

---

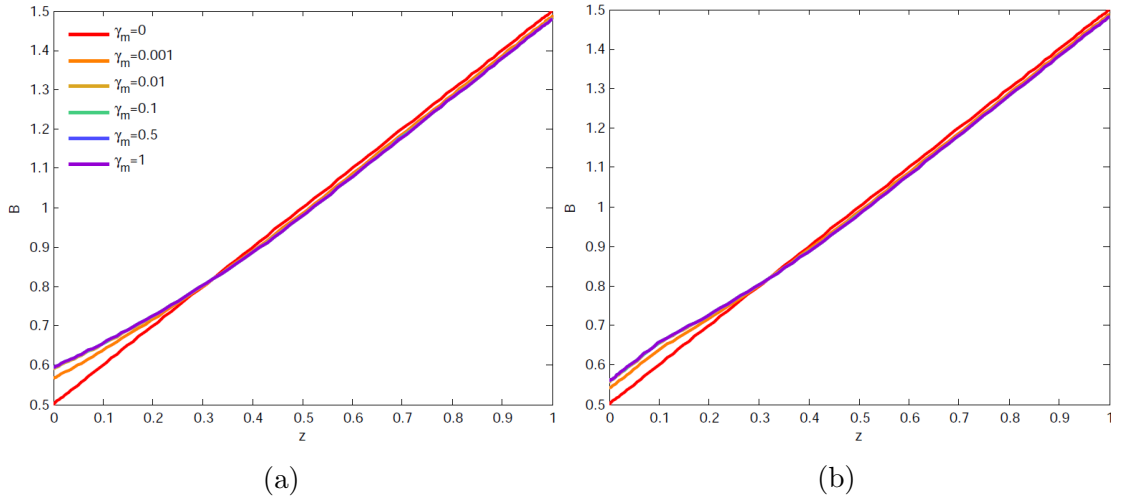


Figure 2.15: Semi-analytic field profiles for  $\bar{B}'(1) = 1$ , constant flux boundary conditions, with  $\gamma = \beta$  given by (a) step function and (b) top hat function between  $z_{i1} = 0.1$  and  $z_{i2} = 0.5$ .

considered. Indeed, this is also true of the numerically calculated profiles; in this case the equilibrium field has very little sensitivity to  $\gamma$  and  $\beta$ , and the analytic consideration confirms this (see Figure 2.15).

Furthermore, as  $\gamma_m$  increases, the equilibrium field seems to approach a limiting profile, with the higher few values of  $\gamma_m$  giving almost identical equilibria.

This lack of sensitivity to the  $\gamma$  and  $\beta$  may result from the fact that the location, close to the top of the layer, where the  $\gamma$  and  $\beta$  effects are present is not where the boundary condition is applied. Thus the field is able to assume a form that is not too dissimilar to the linear form, with non-zero gradient, that it would take were  $\gamma$  and  $\beta$  absent. However, so far we have only considered a non-zero gradient for this field. We will now consider how this changes when we fix the gradient to be zero at the bottom of the layer.

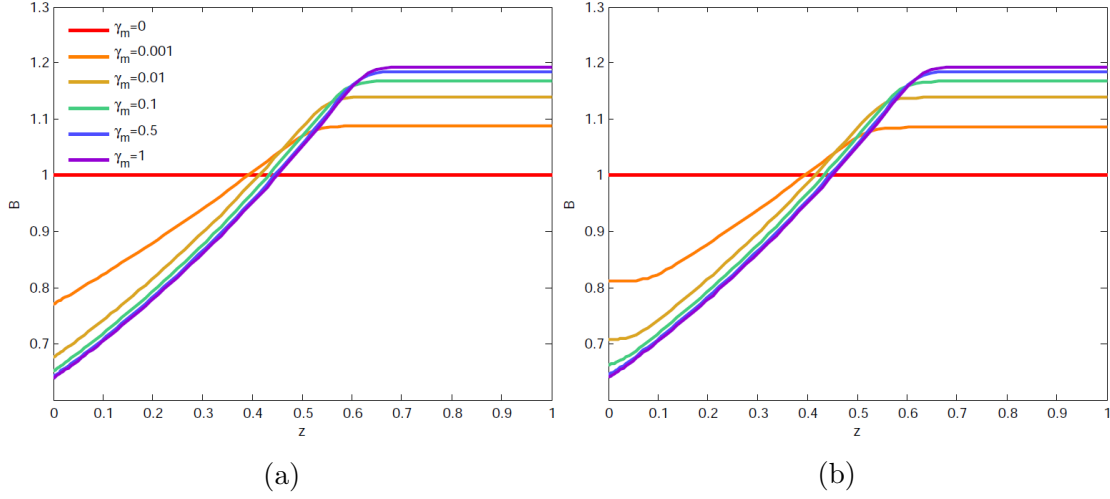


Figure 2.16: Variation of equilibrium field for  $\bar{B}'(1) = 0$  and constant flux,  $\gamma = \beta$  with varying amplitude, for (a) step profile and (b) top hat profile with  $z_{i1} = 0.1$  and  $z_{i2} = 0.5$ .

## 2.9 $\bar{B}'(1) = 0, \phi(1) = 1$

In this case, the results for step and top hat profiles of  $\gamma$  and  $\beta$  are broadly similar to each other (see Figure 2.16), as the boundary condition does not act at the top of the layer, which is where the two forms differ.

The effect of setting the gradient to zero at the bottom of the layer is to force the field to assume a constant value in the lower region of the layer where neither  $\gamma$  nor  $\beta$  are present. It also increases the sensitivity of the magnitude of the field to  $\gamma_m$  once more, making this case potentially of more interest than that of fixing the field gradient at the bottom to some non-zero value.

### 2.9.1 Semi-analytic comparison for $\bar{B}'(1) = 0, \phi(1) = 1$

In this case, the analytically calculated profiles (Figure 2.17) for this boundary condition are fairly consistent with the numerical estimate (Figure 2.16) both qualitatively and quantitatively. The resulting field gradient and magnitude do not depend strongly on how “sharply” the step or top hat profiles vary. Furthermore, in all cases the field is necessarily fixed at a constant value at the bottom

## 2. EQUILIBRIUM BASIC STATE

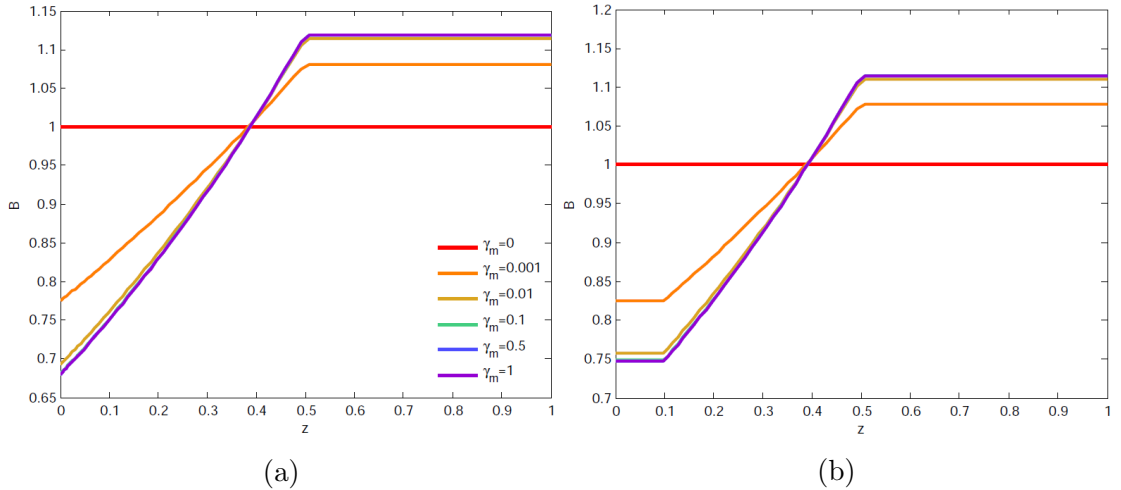


Figure 2.17: Semi-analytic field profiles for  $\bar{B}'(1) = 0$ , constant flux boundary conditions, with  $\gamma = \beta$  given by (a) step function and (b) top hat function between  $z_{i1} = 0.1$  and  $z_{i2} = 0.5$ .

of the layer, since this is required by the boundary condition. The solution also shows more “sensitivity” in the gradient and value of the field at the base of the layer than the case of  $\bar{B}'(1) = 1$  discussed in Section 2.8. As far as fixing the gradient at the bottom of the layer is concerned, this choice of boundary conditions does not exhibit unphysical behaviour for any limiting value of  $\gamma_m$ , while still being sensitive to the strength of the  $\gamma$  and  $\beta$  effects. Thus, it can also be considered as a potentially useful basic state for the linear stability problem.

We have studied the equilibrium field under several different choices of boundary condition, for  $\gamma = \beta$  present in the upper part of the layer. Now, we seek a better understanding of each effect as it acts individually on  $\bar{B}$ .

### 2.10 Shifting the interfaces of $\gamma$ and $\beta$ in the $z$ -direction

We have considered so far the effect of varying the strength of the pumping and the turbulent diffusion effects, and whether they are present at the top of the

---

## 2.10 Shifting the interfaces of $\gamma$ and $\beta$ in the $z$ -direction

layer. However, throughout this analysis, we have maintained the condition that  $\gamma$  and  $\beta$  are proportional to one another. Physically, this is a reasonable assumption for the base of the solar convection zone, as both  $\gamma$  and  $\beta$  are products of turbulence, and may therefore be expected to coincide in spatial location. However, the  $\gamma$  and  $\beta$  effects result from different aspects of turbulent convection, and their spatial coincidence is not inherent to their derivation from the mean field induction equation (Section 1.4.4) but is rather a simplifying assumption that we have made for the purposes of this work. For these reasons, it is also worth giving consideration to cases in which they do not exactly coincide. Thus, we will consider the effects of having  $\gamma$  and  $\beta$  “cut off” at different points in the layer, to better understand the individual effects that each has on the equilibrium field.

We will use a step  $\gamma$  and  $\beta$ , and we will consider the effect of shifting the values of  $z_i$  in Equations (2.4) and (2.5). We still assume  $\gamma$  and  $\beta$  have the same amplitude  $\gamma_m$ , but now we define a value of  $z_{i\gamma}$  and  $z_{i\beta}$ , so that this “cut-off point” of each profile can be varied individually in  $z$ . Therefore,  $\gamma$  and  $\beta$  are given by

$$\gamma(z) = \frac{\gamma_m}{2}(1 - \tanh(a(z - z_{i\gamma}))), \quad (2.31)$$

$$\beta(z) = \frac{\beta_m}{2}(1 - \tanh(a(z - z_{i\beta}))), \quad (2.32)$$

where  $\beta_m = \gamma_m$ . Assuming these forms of the pumping and turbulent diffusion effects, we will consider the effect of varying  $z_{i\gamma}$  and  $z_{i\beta}$ , and once again solve numerically for various choices of boundary conditions. Note that throughout this Section, we take  $\gamma_m = \beta_m = 0.1$ .

### 2.10.1 $\bar{B}'(0) = 0$ , $\phi(1) = 1$

We begin with the case where the field gradient is fixed at the top of the layer, with the flux held constant. We take a value of  $z_{i\gamma}$  (not necessarily equal to 0.5, as before) and shift the value of  $z_{i\beta}$  across the  $z$  domain. As an example, we first consider the case of  $z_{i\gamma} = 0.25$  (see Figure 2.18).

The case here of  $z_{i\beta} = 0$  approximates the case where there is no  $\beta$  effect present in the layer. This means that in a region of constant  $\gamma$  the field would be expected

## 2. EQUILIBRIUM BASIC STATE

---

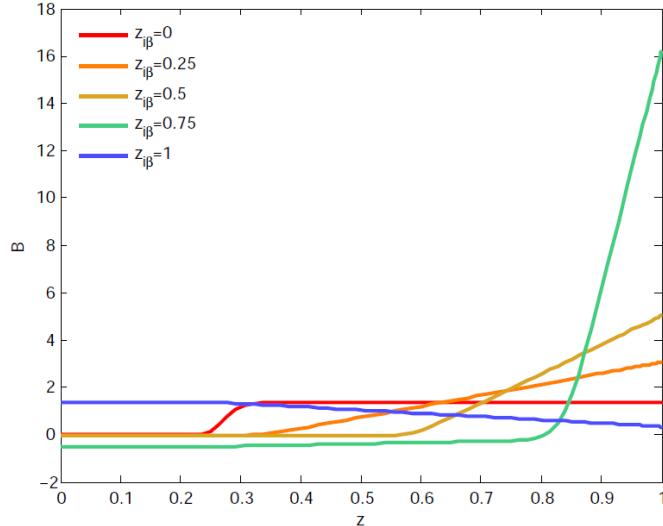


Figure 2.18: Numerically calculated equilibrium fields for  $z_{i\gamma} = 0.25$ , with constant flux and  $\bar{B}'(0) = 0$  boundary conditions.

to obey  $\bar{B}' = 0$ , or in other words to be constant. This is indeed what we see for the case of  $z_{i\beta} = 0$  in 2.18; the constant value of the field takes a different value in the regions where  $\gamma$  is zero compared to non-zero, with a step at the interface.

In fact, we may explain this in terms of the induction equation (2.2). We may take  $\beta = \beta' = 0$  and obtain

$$\zeta_o C_k \bar{B}'' - \gamma \bar{B}' - \gamma' \bar{B} = 0, \quad (2.33)$$

which, for small diffusivity  $\zeta_o C_k$ , we can approximate to first order as  $\frac{d}{dz}(\gamma \bar{B}) = 0$ , giving  $\gamma \bar{B} = \text{constant}$ . (Note that we may discount the possibility of a boundary layer solution to (2.33) in this instance. Due to the opposite signs of the first two terms, any such boundary layer would be located at  $z = 1$ . In the region of the base of the layer, however, for the cases we consider here we have  $\gamma \sim 0$ , and, indeed,  $\gamma \ll \zeta_o C_k$ , which means that Equation (2.33) does not become singular.) This implies that the field should, to first order, appear as the inverse of the step function  $\gamma$ , i.e. it should appear as a smoothed step function itself. This is in fact what we see in the numerically calculated profiles, shown in Figure 2.18.

## 2.10 Shifting the interfaces of $\gamma$ and $\beta$ in the $z$ -direction

---

For  $z_{i\beta} = 0.25$ , the problem is essentially equivalent to one that we have already considered; the case where  $\gamma$  and  $\beta$  are equal, for arbitrary  $z_i$ . (See Section 2.6.1.) In this case we see an exponential profile in the region where both are present and a linear profile where both are absent. Because of the boundary condition, the coefficient multiplying exponential term in the left hand side solution would be zero for this case. This, however, is also consistent with the analytic considerations put forward in Section 2.6.1.

In the case of  $z_{i\beta} = 0.5$ , there is a region where only the  $\beta$  effect is present. However, since  $\beta$  is constant there, the field still obeys  $\bar{B}'' = 0$  in this region, and because there is constant field in the upper part of the layer (with both  $\gamma$  and  $\beta$  effects) the field is effectively constant in the region with only  $\beta$  too. Again, in Figure 2.18 we see that the field is linear with non-zero gradient in the region where neither  $\gamma$  nor  $\beta$  are present.

For  $z_{i\beta} = 0.75$ , the situation is similar, though there is a small non-zero gradient in the region between where the  $\gamma$  and  $\beta$  effects fall off to zero. The gradient at the base of the layer is also higher, to maintain the constant flux boundary condition. Physically, we can consider this as turbulent diffusion acting to confine the majority of the field in the section of the layer where the pumping effect does not act, so that the field does not “see” the effect of  $\gamma$ .

We see a similar effect in the case of  $z_{i\beta} = 1$ . This case is somewhat equivalent to having a constant diffusion effect throughout the layer, and, as expected, gives rise to a constant field in the region where  $\gamma$  is present, and a linearly varying one elsewhere. However, the gradient at the base of the layer (i.e. close to  $z = 1$ ) has now changed sign; this is also a consequence of the constant flux boundary condition.

These results, for  $z_{i\gamma} = 0.25$  and variable  $z_{i\beta}$ , are representative of the kind of equilibrium field profiles we obtain for cases with  $z_{i\gamma} \neq z_{i\beta}$ . We may also consider the example case with  $z_{i\gamma} = 0.75$ , shown in Figure 2.19. It is worth noting that for the case of  $z_{i\gamma} = 0.75$ ,  $z_{i\beta} = 0$ , the solution does not converge

## 2. EQUILIBRIUM BASIC STATE

---

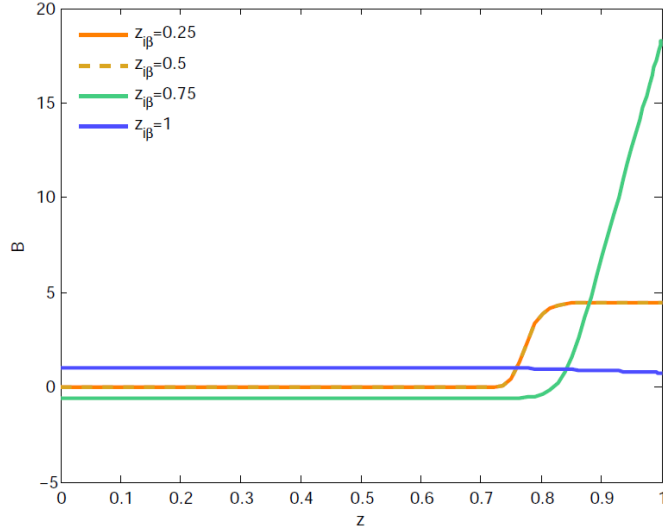


Figure 2.19: Numerically calculated equilibrium fields for  $z_{i\gamma} = 0.75$ , with constant flux and  $\bar{B}'(0) = 0$  boundary conditions.

for this set of boundary conditions. This is true for cases with  $z_{i\gamma}$  greater than  $z_{i\beta}$ , with a difference larger than approximately 0.5. Numerically, this is due to the constant flux boundary condition giving rise to a large gradient at the point where  $\gamma \rightarrow 0$ , which the numerical scheme struggles to resolve. Furthermore, such cases correspond to a potentially unphysical situation; one in which there is a large region where only the turbulent pumping acts, with no turbulent diffusion. Since the turbulence that gives rise to the pumping effect also creates the turbulent diffusion, this situation is unphysical, therefore we may discount it in this analysis, even though it is still theoretically a valid solution to the induction equation for equilibrium.

Another effect that is evident for  $z_{i\gamma} = 0.75$  that was not as clear for the case of  $z_{i\gamma} = 0.25$  is the behaviour of the field for  $z_{i\beta} < z_{i\gamma}$ . It can be seen from the results shown in Figure 2.19 that the profiles for  $z_{i\beta} = 0.25$  and  $z_{i\beta} = 0.5$  overlap each other; the equilibrium field does not change between the two. In general, if there is a significant (here, greater than about 0.25) separation between the two, with  $\beta$  only present within the region where  $\gamma$  acts, then the value of  $z_{i\beta}$  does

## 2.10 Shifting the interfaces of $\gamma$ and $\beta$ in the $z$ -direction

---

not have a significant effect on the equilibrium field. Physically, this corresponds to a situation where the pumping acts to confine most of the flux in a smaller region in the lower part of the layer, where it cannot interact with the turbulent diffusion effect. Thus the position where  $\beta$  is cut off has no significant effect on the field, so long as it is not present outside the pumping region.

### 2.10.2 $\bar{B}'(1) = 1, \phi(1) = 1$

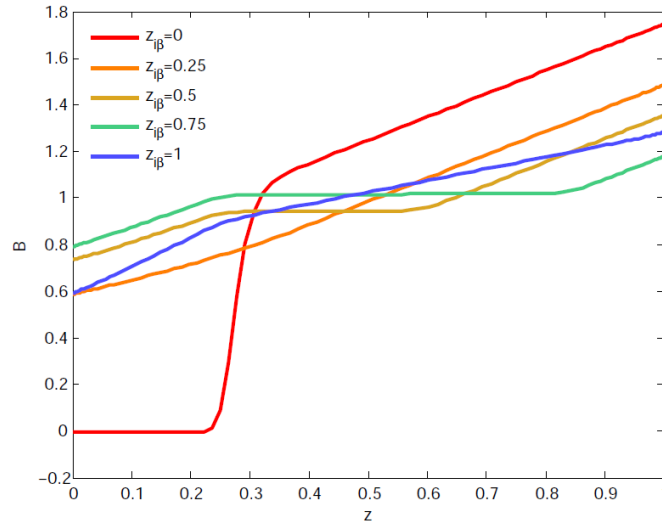


Figure 2.20: Numerically calculated equilibrium fields for  $z_{i\gamma} = 0.25$ , with constant flux and  $\bar{B}'(1) = 1$  boundary conditions.

We may also consider a case where the gradient of the field is fixed not at the top of the layer but at the bottom. We will vary  $z_{i\gamma}$  and  $z_{i\beta}$  in the same way as in Section 2.10.1, and again we will consider the cases of  $z_{i\gamma} = 0.25$  and  $z_{i\gamma} = 0.75$  as illustrative examples. (See Figures 2.20 and 2.21.)

In the case of  $z_{i\gamma} = 0.25$  (Figure 2.20), we see a step-like field for  $z_{i\beta} = 0$ , though — unlike the equivalent case for  $\bar{B}'(0) = 0$  — now the field is linear with a gradient of 1 in the region where neither effect is present, as specified by the boundary condition.

## 2. EQUILIBRIUM BASIC STATE

---

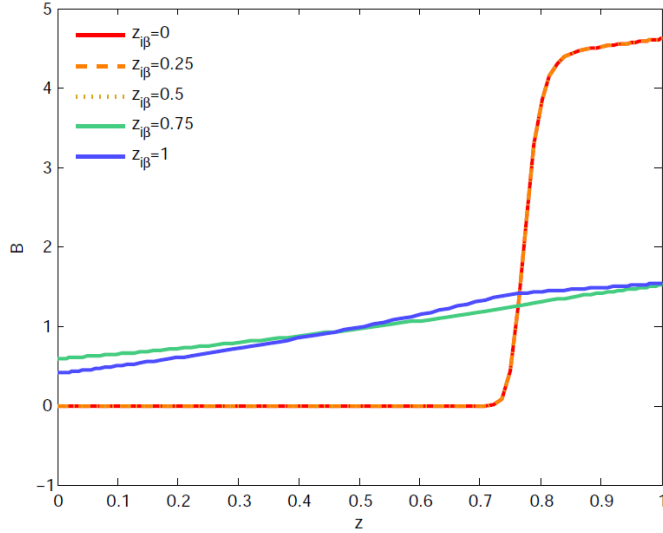


Figure 2.21: Numerically calculated equilibrium fields for  $z_{i\gamma} = 0.75$ , with constant flux and  $\bar{B}'(1) = 1$  boundary conditions.

Furthermore, with a fixed gradient in the lower part of the layer, the gradient cannot increase as the turbulent diffusion is present in a larger upper region of the layer, allowing the sharp transition to be diffusively “smoothed”. Thus, to maintain the required flux, the gradient of the fields varies less between the different regions in the layer than before.

In the case of  $z_{i\gamma} = 0.75$  (Figure 2.21), we see again that the cases with  $z_{i\beta} < z_{i\gamma}$  show no variation with  $z_{i\beta}$ , being all simply a step-like function, though with the gradient fixed according to the boundary condition at the base of the layer. This is consistent with the idea that if there is no turbulent diffusion present in the region where there is no turbulent pumping, the field does not “see” the  $\beta$  effect at all because  $\gamma$  has confined it to the bottom of the layer outside of where  $\beta$  is present. The cases of  $z_{i\beta} \gtrsim z_{i\gamma}$  (see the cases of  $z_{i\beta} = 0.75, 1$  in Figure 2.21) are much closer to linear, as  $\beta$  is able to smooth the gradient of the field.

## 2.11 Constant $\beta$ : numerical and analytical results

We may also consider the case where  $\beta$  is constant across the layer. This is also the limit, as  $a \rightarrow \infty$ , of the case of  $z_{i\beta} = 1$  in the above considerations. However, it is also a valuable problem to study in itself, as it allows once again for an analytic approach to determine the effect on the equilibrium field of varying the location of the  $\gamma$  effect. We will consider  $\gamma$  to be given by (2.31), with constant  $\beta = \gamma_m$ , taking  $\gamma_m = 0.1$ .

### 2.11.1 Constant $\beta = \gamma_m$ with $\bar{B}'(0) = 0$ , $\phi(1) = 1$

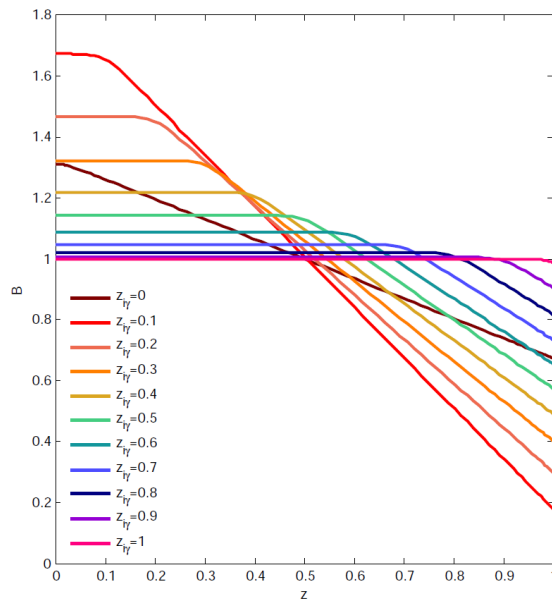


Figure 2.22: Numerically calculated equilibrium fields for constant  $\beta = \gamma_m = 0.1$ , with variable  $z_{i\gamma}$ , and  $\bar{B}'(0) = 0$  and constant flux boundary conditions.

In the case of the boundary conditions  $B'(0) = 0$  and constant flux, the analytic estimate of the equilibrium field — assuming infinite  $\gamma$  gradient at the interface between turbulent and non-turbulent regions, or  $a \rightarrow \infty$  — may be found using the matching conditions (2.9) and (2.10). By solving on either side of the

## 2. EQUILIBRIUM BASIC STATE

---

boundary, we again obtain:

$$\bar{B} = \begin{cases} P + Q \exp\left(\frac{\gamma_m z}{\zeta_o C_k + \gamma_m}\right) & 0 \leq z < z_{i\gamma}, \\ R + Sz & z_{i\gamma} < z \leq 1. \end{cases}$$

Applying the boundary and jump conditions in an equivalent way to that described in Section 2.6.1, we can find analytic expressions for the constants  $P$ ,  $Q$ ,  $R$  and  $S$ . By analogy with the case of  $\beta = \gamma$ , we obtain:

$$P = \frac{-\left(\frac{\zeta_o C_k}{\gamma_m} + 1\right)}{-\left(\frac{\zeta_o C_k}{\gamma_m} + 1\right) + \frac{1}{2}(1 - z_{i\gamma})^2}, \quad (2.34)$$

$$Q = 0, \quad (2.35)$$

$$R = \frac{-\left(\frac{\zeta_o C_k}{\gamma_m} + 1 + z_{i\gamma}\right)}{-\left(\frac{\zeta_o C_k}{\gamma_m} + 1\right) + \frac{1}{2}(1 - z_{i\gamma})^2}, \quad (2.36)$$

$$S = \frac{1}{-\left(\frac{\zeta_o C_k}{\gamma_m} + 1\right) + \frac{1}{2}(1 - z_{i\gamma})^2}. \quad (2.37)$$

These analytic expressions help in explaining the forms of the numerically calculated equilibrium fields shown in Figure 2.22. Most clearly, we see that the field is in each case constant in the region where  $\gamma$  is present; this is required by the boundary condition  $\bar{B}'(0) = 0$ , which sets  $Q = 0$  and thus removes the exponential term from the solution in this region. It is also possible to see the dependence of the value of this constant field in this part of the layer (i.e.  $P$ , given by (2.34)) on the value of  $z_{i\gamma}$ . Note also the dependence of the gradient  $S$  at  $z > z_{i\gamma}$ .

The case of  $z_{i\gamma} = 0$  in Figure 2.22 appears to be the exception to this variation; the field is effectively linear, as we expect, but its gradient is of lower magnitude than we expect given the monotonic variation with  $z_{i\gamma}$  of analytic coefficients (2.34) – (2.37). These coefficients, however, only apply in the limit  $a \rightarrow \infty$ , and indeed, the assumption that the field can be matched using (2.9) and (2.10) only holds if there are two distinct regions of the domain with, effectively, constant non-zero and zero  $\gamma$  respectively. However, in the case of  $z_{i\gamma} = 0$  and finite  $a$  (for this numerical case we have used  $a = 30$ ) the only region of  $\gamma$  is the small transition region near the top of the layer, with large negative  $\gamma'$ .

## 2.11 Constant $\beta$ : numerical and analytical results

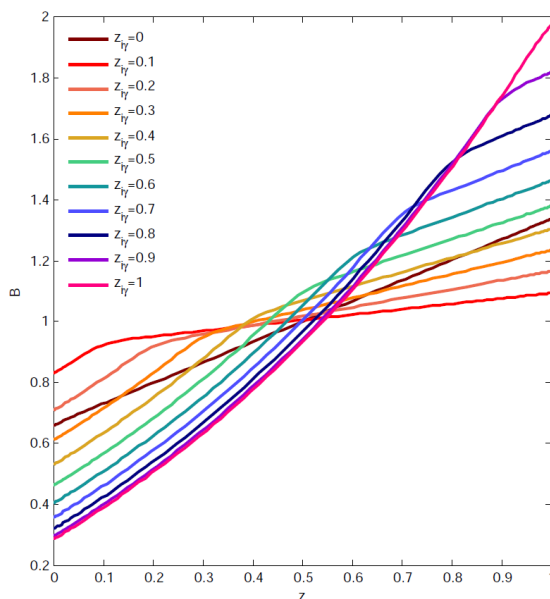


Figure 2.23: Numerically calculated equilibrium fields for constant  $\beta = \gamma_m = 0.1$ , with variable  $z_{i\gamma}$ , and  $\bar{B}'(0) = 1$  and constant flux boundary conditions.

This is not the assumption under which coefficients (2.34) – (2.37) are derived, which may account for the non-monotonic change in the gradient in this case as compared with the others displayed in Figure 2.22.

### 2.11.2 Constant $\beta$ , $\bar{B}'(0) = 1$ , $\phi(1) = 1$

Let us now consider fixing the gradient at the top of the layer as a non-zero value. In the numerical results for this case, (Figure 2.23) we may once again see that the field varies exponentially in the region where both  $\gamma$  and  $\beta$  are present and linearly where there is only diffusion, as there is no requirement that sets  $Q = 0$ . However, the boundary condition  $\bar{B}'(0) = 1$  ensures that the field gradient is positive and the field is maximised at the bottom of the layer. The gradient is largest for  $z_{i\gamma} = 1$ , i.e. the case when both  $\gamma$  and  $\beta$  are effectively constant across the layer.

## 2. EQUILIBRIUM BASIC STATE

---

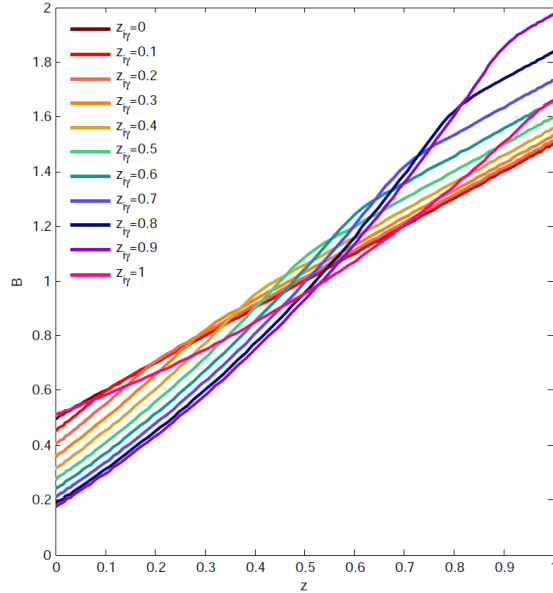


Figure 2.24: Equilibrium fields for constant  $\beta = \gamma_m = 0.1$ , with variable  $z_{i\gamma}$ , and  $\bar{B}'(1) = 1$  and constant flux boundary conditions.

### 2.11.3 Constant $\beta$ , $\bar{B}'(1) = 1$ , $\phi(1) = 1$

We may also fix the gradient at the bottom of the layer, for constant  $\beta$  (Figure 2.24). From the results we see that this makes the gradient at the top of the layer, and the value of the field at either end, less dependent on  $z_{i\gamma}$ . This behaviour is similar to the case of  $\bar{B}'(1) = 1$  (Figure 2.14) for proportional  $\gamma$  and  $\beta$ ; this boundary condition in general reduces the sensitivity of the equilibrium field to the pumping and turbulent diffusion effects, so varying  $z_{i\gamma}$  has less effect in general.

## 2.12 Finding $\gamma$ required to produce a given field, given $\beta$

So far, we have calculated the equilibrium magnetic field resulting from prescribed  $\gamma(z)$  and  $\beta(z)$ . However, using the equilibrium form of the induction equation given by (2.2), the reverse process may also be carried out; (2.2) may be rear-

## 2.12 Finding $\gamma$ required to produce a given field, given $\beta$

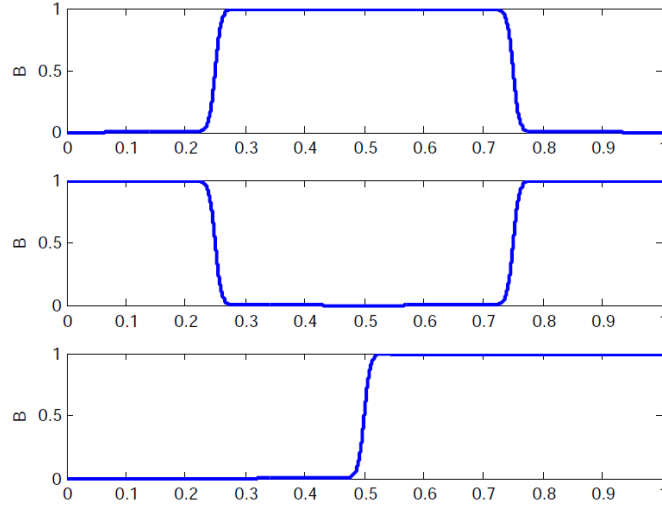


Figure 2.25: The three forms of  $\bar{B}$  involved in the inverse analysis. Upper: top hat profile, middle: step profile, lower: sandwich profile.

ranged to give  $\gamma$  (or, alternatively,  $\beta$ ) for a given equilibrium field, as long as  $\beta$  (or  $\gamma$ ) is specified. This means that a given  $\bar{B}(z)$  profile could be specified, and the  $\gamma$  (or  $\beta$ ) required to produce this profile may then be determined.

The motivation for addressing this problem is that other work that incorporates  $\gamma$  and  $\beta$  into such a system has not started from an equilibrium state that takes their effect into account. Instead, other work (for example, [Barker \*et al.\* \(2012\)](#)), in which a prescribed slab of field is acted upon by a step-like  $\gamma$  acting from above it) has used prescribed forms for the basic state  $\bar{B}$ . These states, however, do not constitute an equilibrium under the turbulent effects  $\gamma$  and  $\beta$ . We will consider such prescribed states, and whether they may feasibly be generated by the action of some form of  $\gamma$  and  $\beta$ . It is common for other work on magnetic buoyancy instabilities to use a top hat field, so we will consider the form of  $\gamma$  required to create one, given various functional forms of  $\beta$ . For the sake of comparison, we will also consider two other functional forms of the field, and find  $\gamma$  required to ensure that they represent equilibria. These are step function field, and a “sandwich” field, pictured in [Figure 2.25](#).

Making no assumption about the proportionality of  $\gamma$  and  $\beta$  now, we consider the

## 2. EQUILIBRIUM BASIC STATE

---

induction equation for equilibrium, specifically in the form given by (2.3). We may set  $c = 0$ ; in this problem, this acts as a statement of a boundary condition by fixing the relationship between  $\bar{B}$  and  $\bar{B}'$ , thus allowing  $\gamma$  to be found. With this choice, we may rearrange to give the relation

$$\frac{d}{dz}(\ln \bar{B}) = \frac{\gamma}{\beta + \zeta_o C_k}. \quad (2.38)$$

This allows a given  $\bar{B}$  profile to be used to produce an estimate for either  $\gamma$  or  $\beta$ , provided the other is known. Here we solve for  $\gamma$ , using several types of  $\beta$  profile. These are:

- $\beta$  given by the same step-like tanh function as we have previously considered (Equation (2.5)), with  $\beta_m = 0.1$ ,  $a = 30$  and  $z_i = 0.5$ .
- Linear:  $\beta = \beta_m(1 - z)$ .
- Exponential:  $\beta = \beta_m e^{-z}$ .

Each of these are applied to the “top hat”, “sandwich” and “step” profiles of  $\bar{B}$ , i.e.

- Top hat profile:  $\bar{B} = B_o(\tanh(a(z - z_o)) - \tanh(a(z - z_i)))$ .
- Sandwich profile:  $\bar{B} = -B_o(\tanh(a(z - z_o)) - \tanh(a(z - z_i)) - 2)$ .
- Step profile:  $\bar{B} = B_o(\tanh(a(z - z_s)) + 1)$ .

In these cases, the parameters are taken to have values of  $B_o = 0.5$ ,  $a = 100$ ,  $z_o = 0.25$ ,  $z_s = 0.5$ ,  $z_i = 0.75$ , giving the profiles for  $\bar{B}$  shown in Figure 2.25.

In order to calculate  $\gamma$ , it is necessary to find  $\frac{d}{dz}(\ln \bar{B})$ , equivalent to  $\bar{B}'/\bar{B}$ . This may be calculated analytically.

For the top hat and step profiles, the limit of  $\bar{B}'/\bar{B}$  is, numerically, convergent everywhere. In the case of the sandwich profile however, the quantity  $\bar{B}'/\bar{B}$  creates a numerical problem in the region  $z_o < z < z_i$ . As both  $\bar{B}$  and  $\bar{B}'$  approach zero within this region, the quantity  $\bar{B}'/\bar{B}$  is subject to a large numerical error

## 2.12 Finding $\gamma$ required to produce a given field, given $\beta$

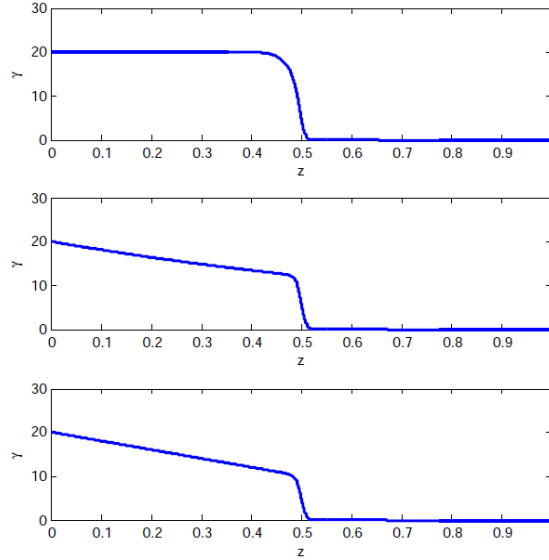


Figure 2.26:  $\gamma$  required to produce a step field, given various forms of  $\beta$ . From top to bottom: with tanh, exponential, linear  $\beta$ .

and causes the solution to diverge if we define this quantity explicitly as the ratio of  $\bar{B}$  and  $\bar{B}'$ , as for the top hat and step profiles. Thus, we approximate the quantity  $\frac{d}{dz}(\ln \bar{B}) = \bar{B}'/\bar{B}$  for small  $\bar{B}$ , defined by  $\bar{B} < \epsilon$ ,  $\epsilon = 10^{-12}$ . We use the approximation

$$\frac{d}{dz}(\ln \bar{B}) \approx -2a + 4a \frac{\exp(2a(2z - z_o - z_i))}{1 + \exp(2a(2z - z_o - z_i))}, \quad (2.39)$$

which can be found by expanding the stated form of the sandwich  $\bar{B}$  profile in a region where  $\exp(-a(z - z_o))$ ,  $\exp(-a(z - z_i)) \ll 1$ , which holds true in a region that contains the  $\bar{B} < \epsilon$  region where we apply the approximation.

By applying each of the  $\beta$  profiles to the fields described above, with  $\zeta_o C_k = 10^{-5}$ ,  $\gamma$  may be calculated for each combination of  $\bar{B}$  and  $\beta$ . The results are shown in Figures 2.26, 2.27, and 2.28.

In general, we find that positive  $\gamma$  is necessary above the required position of the field. Because  $\gamma$  acts downwards, and the diffusion effects of  $\beta$  and  $\zeta_o C_k$  have no preferred direction, in cases where the field must be pumped upwards (i.e. a

## 2. EQUILIBRIUM BASIC STATE

---

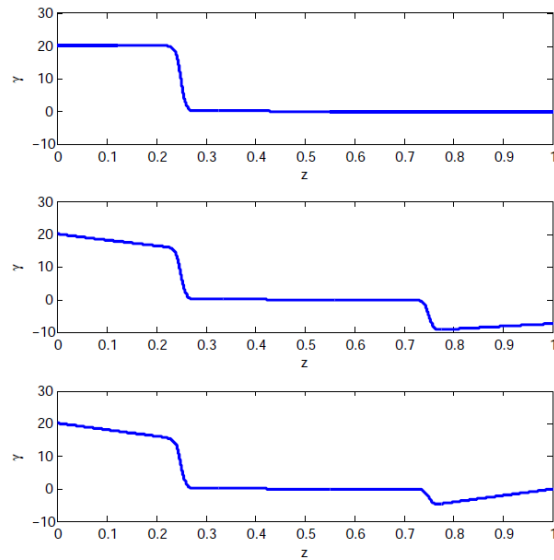


Figure 2.27:  $\gamma$  required to produce a top hat field, given various forms of  $\beta$ . From top to bottom: with tanh, exponential, linear  $\beta$ .

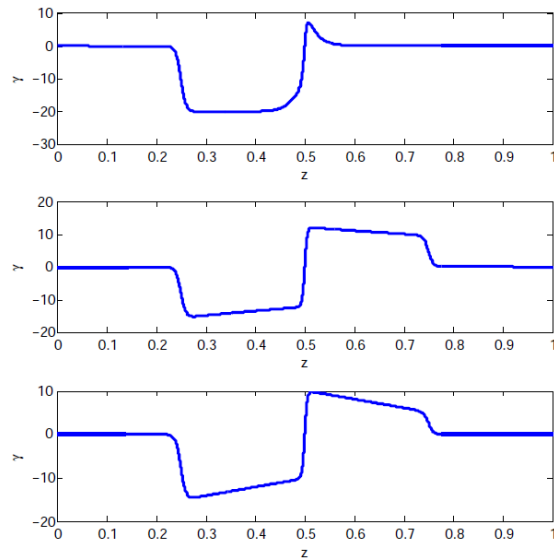


Figure 2.28:  $\gamma$  required to produce a sandwich field, given various forms of  $\beta$ . From top to bottom: with tanh, exponential, linear  $\beta$ .

## 2.12 Finding $\gamma$ required to produce a given field, given $\beta$

---

region of no field must be maintained below a region where field is present) we require  $\gamma < 0$ , i.e. an upwards pumping effect.

Let us first consider the case where we produce a step function-like  $\bar{B}$ , with the required  $\gamma$  shown in Figure 2.26. To maintain this field as an equilibrium, we require non-zero  $\gamma$  to be present in the upper part of the layer. This corresponds to a positive, downwards advection velocity in the section of the domain where we require the effectively constant, non-zero part of the field to exist. In this case, the effect of  $\beta$  is to vary the required functional form of the  $\gamma$  effect in the region where  $\gamma$  is present.

Now let us consider the case of the top hat field, with the resulting  $\gamma$  shown in Figure 2.27. To produce a top hat profile between two points in the domain (in this case  $z_o = 0.25$  and  $z_i = 0.75$ ) we still require a non-zero  $\gamma$  effect above the location of the top hat. The functional form of  $\gamma$  in this region is modulated by the form of  $\beta$ . However, once the field has been pumped down by  $\gamma$  into the region within the top hat field layer, it must be maintained within that region; given the presence of  $\beta$  (and the much lesser  $\zeta_o C_k$  diffusivity effect) the field could still feasibly diffuse out of this region. Thus, the presence of a secondary region of non-zero  $\gamma$  is required, which is in this case a negative velocity. This corresponds to an upwards advection in this region, whose functional form corresponds to that of  $\beta$  for each individual case. Note that this is also true in the case of the tanh form of  $\beta$  shown in the top plot of Figure 2.27; though it is not evident on the scale shown, there is a region of approximately constant  $\gamma \sim -0.2$  required for  $z \gtrsim 0.75$ , i.e. outside of the top hat region. In this case, however, a lower magnitude of pumping is required in this position to maintain the top hat  $\bar{B}$  profile than for exponential or linear  $\beta$ .

Similarly, in the case of the sandwich field (see Figure 2.28), we also see a region of  $\gamma < 0$  just below the top boundary of the central region where the field must be zero. This is necessary to keep the upper part of the field from diffusing back into the gap. However, we also require there to be a step-like portion of the field at the bottom of the layer, which requires an additional region of positive

## 2. EQUILIBRIUM BASIC STATE

---

(downwards)  $\gamma$  just above this boundary.

In all of these cases, the general effect of  $\beta$  is to modulate the magnitude of  $\gamma$  required. If we return to Equation (2.38), this is more intuitively clear; since the molecular diffusivity is small in magnitude in comparison to  $\beta$ , the quantity  $\bar{B}'/\bar{B}$  is essentially proportional to  $\gamma/\beta$ . We have shown that it is generally possible to construct a pumping profile in  $z$  that will give rise to a variety of different forms of field at equilibrium, given a prescribed form for the turbulent diffusivity  $\beta$ . However, not all of the scenarios considered in this reversal of the equilibrium problem are equally physically relevant to the region of the base of the solar convection zone. In particular, those required to produce the sandwich-type field all require regions of both positive and negative  $\gamma$ , a scenario that would imply several layers in which the mean field is pumped variously upwards and downwards. This scenario in particular is not consistent with the action of turbulence, as it would imply not only a turbulent region in the centre of the layer surrounded by stably stratified regions, but one with the pumping effect changing sign somewhere within it.

The  $\gamma$  profiles required to produce a top hat equilibrium field are more physically plausible given this picture, in that they are maximised at the same point as the respective  $\beta$  profiles used to produce them. However, in these cases, we still obtain a change of sign of  $\gamma$  in two cases, those of linearly and exponentially varying  $\gamma$ , as well as two distinct “regions” of non-zero  $\gamma$ , this time at both the top and the bottom of the layer. This would also imply a region of turbulent motion at the bottom of the layer, which again is not the physical scenario we aim to model. In the case of top hat field and step  $\beta$ , the situation is closer to being physically realistic; we have a turbulent  $\gamma$  and  $\beta$  both present at the top of the layer but not in the lower part. In this case, however, while  $\beta$  is cut off at a point within the layer that is defined by the prescribed form, the cut-off point of the required  $\gamma$  depends on where the specified top hat field is non-zero, which results in a region where  $\beta$  is present but  $\gamma$  is not. This is not consistent with there being a region of turbulent motion which gives rise to both effects.

---

## 2.13 Other Basic States of the System

The case of the step field, which drops to zero at the same point as the  $\beta$  effect, is closer still to the scenario that we aim to model; namely, that of a layer of turbulence characterised by effectively constant  $\gamma$  and  $\beta$  above a transition region where the turbulent motion falls rapidly to zero, characterised by a lack of  $\gamma$  and  $\beta$  effect. The step field case results in  $\gamma$  effects that are confined to the upper part of the layer, coincident with the maximum value of  $\beta$ . In addition, the calculated field, assuming step  $\beta$ , also gives a constant  $\gamma$  in the region where the  $\gamma$  effect is non-zero, which is most representative of a region of effectively constant turbulent motion, which had been our assumption when addressing the equilibrium problem directly.

This implies that of the scenarios considered in this “reverse” analysis of equilibrium, the most physically useful is the scenario of step  $\beta$  giving rise to step  $\bar{B}$ , i.e. an equilibrium field that is present and effectively constant in the region where the turbulent effects are not present.

In this inverse problem treatment, the action of  $\beta$  is at a different spatial location to  $\gamma$ , since in all the cases we have considered,  $\beta$  is maximised at the top of the layer. This is not consistent with the physical picture of  $\gamma$  and  $\beta$  being spatially coincident, as we assume for the majority of this work. However, as a modelling approach in itself it is at least internally consistent. The results of this analysis, however, while not directly relevant to the scenario we wish to consider in the larger linear stability problem, serve to demonstrate that it is in general possible to find a  $\gamma$  that gives rise to a given  $\bar{B}$  (such as those prescribed in other, similar work, as discussed in Section 2.1), with some prescribed form of  $\beta$ .

## 2.13 Other Basic States of the System

The solution to Equation (2.1) gives an equilibrium state of the magnetic field, subject to the effects of  $\gamma$  and  $\beta$ . This solution has been the primary focus of this Chapter; however, in order to make use of  $\bar{B}$  as the basic state for the linear stability problem, we must also find the corresponding basic states for the other properties of the system, namely, velocity, pressure, temperature, and density.

## 2. EQUILIBRIUM BASIC STATE

---

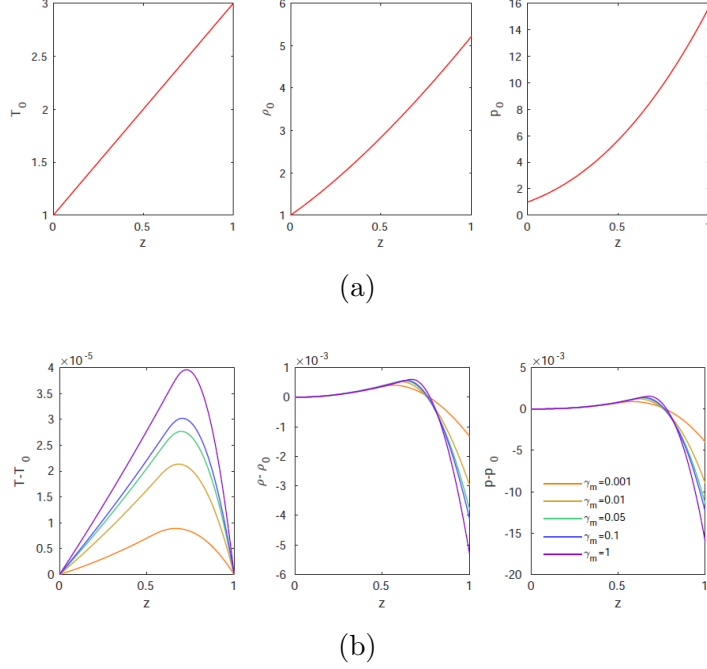


Figure 2.29: (a) Temperature, density and pressure equilibrium states for  $\gamma_m = 0$ , and (b) difference in equilibrium states for non-zero  $\gamma = \beta$ , for  $F = 0.001$ .

We have already assumed that for the initial equilibrium,  $\bar{\mathbf{u}} = 0$ , and we may eliminate the pressure  $\bar{p}(z)$  by means of the gas law (1.36). Then, in order to find  $\bar{T}(z)$  and  $\bar{\rho}(z)$  we may return to the full equations of the system and use the assumption of magnetohydrostatic equilibrium to find the remaining basic states.

### 2.13.1 Temperature Equilibrium State

We consider the time-independent energy equation (Equation (1.34), with  $\frac{\partial \bar{T}}{\partial t} = 0$ ) and set  $\bar{\mathbf{u}} = 0$ . With this assumption, the temperature equilibrium state  $\bar{T}(z)$  is fixed by the Ohmic heating term, such that:

$$\nabla^2 \bar{T} + \frac{(\Gamma - 1)}{\Gamma} F \zeta_o |(\nabla \times \bar{B})|^2 = 0. \quad (2.40)$$

## 2.13 Other Basic States of the System

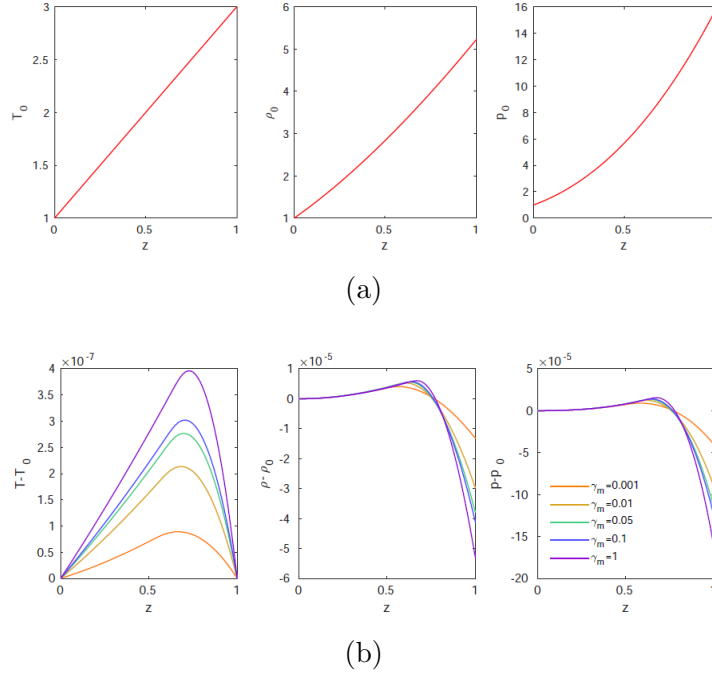


Figure 2.30: (a) Temperature, density and pressure equilibrium states for  $\gamma_m = 0$ , and (b) difference in equilibrium states for non-zero  $\gamma = \beta$ , for  $F = 0.00001$ .

With our assumptions about the form of the equilibrium states, however, this equation takes the form of a simple second order ODE for  $\bar{T}$ :

$$\frac{d^2\bar{T}}{dz^2} = -\frac{(\Gamma - 1)}{\Gamma} F \zeta_o \left( \frac{d\bar{B}}{dz} \right)^2. \quad (2.41)$$

This may be solved numerically given the form of  $\bar{B}(z)$ , and two boundary conditions for  $\bar{T}$ . Following [Barker \*et al.\* \(2012\)](#), we choose boundary conditions  $\bar{T}(0) = 1$  and  $\bar{T}(1) = 1 + \theta$ .

Note that for a linear field — which is an equilibrium field in the absence of the turbulent  $\gamma$  and  $\beta$  effects — the temperature equilibrium state is simply quadratic in  $z$ .

## 2. EQUILIBRIUM BASIC STATE

---

### 2.13.2 Density Equilibrium State

Similarly, we find the  $z$ -dependence of the density  $\bar{\rho}(z)$  given magnetohydrostatic equilibrium. Under this condition, the vertical component of the momentum equation (Equation (1.33)) gives:

$$-\nabla \left( \bar{p} + \frac{F}{2} |\bar{B}|^2 \right) + \theta(m+1)\bar{\rho} = 0. \quad (2.42)$$

Assuming a perfect gas and  $z$ -dependent equilibrium states, we obtain:

$$\bar{T} \frac{d\bar{\rho}}{dz} + \bar{\rho} \left( \frac{d\bar{T}}{dz} - \theta(m+1) \right) = -F\bar{B} \frac{d\bar{B}}{dz}. \quad (2.43)$$

If  $\bar{B}$  and  $\bar{T}$  are known, the first order ODE (2.43) may be solved for  $\bar{\rho}$ ; however, we require a boundary condition, for which we choose  $\bar{\rho}(0) = 1$ . (Note that another possible choice would have been to fix the total mass in the layer, rather than the total magnetic flux. This alternative scenario may give different results, but it is not obvious, without carrying out the full linear stability analysis, how it would affect the stability problem. This, however, represents a possible area of further study.)

Note that the calculation of  $\bar{T}$  and  $\bar{\rho}$  is not very sensitive to  $\gamma_m$  for the chosen parameters and boundary conditions. In Figure 2.29, the basic states for  $\bar{T}_0$ ,  $\bar{\rho}_0$  and  $\bar{p}_0$  (as calculated from the  $\bar{B}$  states shown in Figure 2.10a) for  $\gamma_m = 0$ , and then for  $\gamma_m > 0$  the difference from these  $\gamma = \beta = 0$  values is shown. The equivalent results for  $F = 10^{-5}$  are shown in Figure 2.30; the significance of these parameter values will be further discussed in Chapter 3. The calculation of the temperature and density equilibrium states, however, is predicated on our knowledge of  $\bar{B}$ , and so as we conclude our consideration of the equilibrium states of the system, we will summarise and offer some further discussion of the most appropriate  $\bar{B}$  to use in the linear stability problem.

## 2.14 Summary and Conclusions

We have considered the mean field induction equation under the assumption of equilibrium under the action of turbulent pumping and turbulent diffusion effects,

and solved for an equilibrium field with a view to finding a viable basic state field for linear stability analysis. We have considered various boundary conditions, and varied the form and strength of the turbulent effects, in order to gain an understanding of how these factors shape the equilibrium field. Where possible, we have considered analytic approximations, in order to compare with the numerical solution to the second order linear ODE.

As an aside, we have also considered the inverse problem, and found that it is possible to generate  $\gamma(z)$  that will produce a given field, under various assumptions for the form of  $\beta(z)$ .

All of this, however, is motivated by the desire to better understand the possible equilibrium states for a layer of field, in order to choose a suitable basic state for the linear analysis of stability to magnetic buoyancy. We require that the basic state exhibit no unphysical behaviour, assuming that the layer we aim to model is situated at the base of the solar convection zone, with the pumping and turbulent diffusion effects acting from above. We therefore exclude cases in which the direction of the field gradient changes sign or goes to infinity for some value of the pumping strength.

We also reject as unphysical, cases where the pumping at the top of the layer is able to draw in an effectively unlimited amount of field from above; numerically, this issue may be solved either by leaving a small region with no pumping at the very top of the layer (which may also be an unphysical assumption in itself, given the fact that pumping is due to turbulent motion in the convection zone above) or fixing the total flux within the layer using an integral boundary condition.

Finally, for the purposes of finding how the turbulent effects interact with magnetic buoyancy in the perturbed equilibrium state, we require that the field is sensitive to the parameters of the  $\gamma$  and  $\beta$  profiles, at least to an extent. However, choosing a case in which the field is extremely sensitive to the parameters (in the sense that it becomes qualitatively different in form due to small changes, or a

## 2. EQUILIBRIUM BASIC STATE

---

variation in one specific point in the layer) is likely not a desirable scenario either.

In light of these considerations, it seems that the use of a constant flux boundary condition, along with either a  $\bar{B}(0) = 0$  or  $\bar{B}'(1) = 0$  boundary condition, is the best choice. The constant flux condition places a limit on the integral of the field, ensuring that the pumping effect does not act to draw a large amount of field into the layer. Additionally, in both of these cases the form of the field does not depend on whether there is a small layer around  $z = 0$  where there are no turbulent effects.

This last point is of interest because, ideally, we would like to avoid having to rely on there being a thin, non-turbulent region at the top of the layer; physically speaking, there is no reason for a configuration resembling the top hat  $\gamma$  profile to be present in the region of the base of the convection zone, as this would imply a thin layer within the convection zone in which there is no turbulent convection, which is less physically representative of the situation we want to consider than having the pumping and turbulent diffusion effects extend to the top of the layer.

Thus, we may narrow the choice down to the cases of  $\bar{B}(0) = 0$  or  $\bar{B}'(1) = 0$ , each combined with a constant flux boundary condition. Of these two sets of boundary conditions, we may then choose between setting the value of the field at the top of the layer, or its gradient at the lower end. In terms of which of these options should be used as a basic state in the linear stability analysis, the former ( $\bar{B}(0) = 0$ , constant flux) is likely to be the better option. This is because stability to magnetic buoyancy depends on the field gradient. In the  $\bar{B}(0) = 0$  case where we fix the value of the field rather than its gradient, the gradient of the field is everywhere a function of the strength of the turbulent effects,  $\gamma$ . However, if we fix the gradient at the bottom of the layer (the case  $\bar{B}'(1) = 0$ ), owing to the form of the induction equation in the region without the turbulent effects we find a field with a constant (in this case zero) gradient in this region. This field is not a function of the strength of the turbulent effects. Since the goal is to look at the effect of the turbulent pumping and turbulent diffusion on the stability of the layer, then using a case where the gradient is set by the boundary

## 2.14 Summary and Conclusions

---

condition at the outset in a large section of the layer may not be the best case to consider. Thus, for the purpose of the linear stability analysis, we shall consider the stability of a layer with boundary conditions  $\bar{B}(0) = 0$  and  $\phi(1) = 1$ . (Note that an equivalent study could be carried out using  $\bar{B}'(1) = 0$  and  $\phi(1) = 1$ . For the sake of simplicity, however, we shall consider only one set of boundary conditions for the basic state, i.e.  $\bar{B}(0) = 0$  and  $\phi(1) = 1$ .)

With the resulting form of  $\bar{B}(z)$ , and the  $\bar{T}(z)$  and  $\bar{\rho}(z)$  profiles that follow from it (with the implicit  $\bar{p}(z)$ , and  $\bar{\mathbf{u}} = 0$ ) we will, in the following Chapters, examine the linear stability of the system to magnetic buoyancy.

## **2. EQUILIBRIUM BASIC STATE**

---

# Chapter 3

## Linear Stability of Equilibrium Basic States

### 3.1 Linear Stability Analysis

As discussed in Chapter 2, we shall consider an equilibrium magnetic field under the effects of  $\gamma$  and  $\beta$ , subject to linear perturbations. We solve for the basic state  $\bar{B}$  choosing the boundary conditions  $\bar{B}(0) = 0$  and  $\phi(1) = 1$  (see Section 2.7, Figure 2.10a, as well as Section 2.14 for discussion) where  $\phi(z)$ , the total integrated magnetic flux, is given by (2.8). We solve the induction equation under equilibrium conditions for  $\bar{B}(z)$ , subject to the effects of  $\gamma(z)$  and  $\beta(z)$  given by (2.4) and (2.5). We may then solve for the temperature and density basic states  $\bar{T}(z)$  and  $\bar{\rho}(z)$ , eliminating the pressure  $\bar{p}(z)$  by means of the gas law, as described in Section 2.13.

With the equilibrium states  $\bar{B}(z)$ ,  $\bar{T}(z)$ , and  $\bar{\rho}(z)$ , we may perturb the system and find its linear stability. We perturb the three components of the field and velocity, as well as the temperature and density, according to:

$$\mathbf{B} = \bar{\mathbf{B}} + \tilde{\mathbf{b}} = (\bar{B} + \tilde{b}_x)\mathbf{e}_x + \tilde{b}_y\mathbf{e}_y + \tilde{b}_z\mathbf{e}_z, \quad (3.1)$$

$$\mathbf{u} = \mathbf{0} + \tilde{\mathbf{u}}\mathbf{e}_x + \tilde{\mathbf{v}}\mathbf{e}_y + \tilde{\mathbf{w}}\mathbf{e}_z, \quad (3.2)$$

$$T = \bar{T} + \tilde{T}, \quad (3.3)$$

$$\rho = \bar{\rho} + \tilde{\rho}. \quad (3.4)$$

### 3. LINEAR STABILITY OF EQUILIBRIUM BASIC STATES

---

We consider perturbations of the general form:

$$\tilde{\xi} = \hat{\xi}(z)e^{st+ik_x x+ik_y y}. \quad (3.5)$$

The perturbations are horizontally periodic, with horizontal scales in the  $x$ - and  $y$ -directions defined by the inverse of the wavenumbers  $k_x$  and  $k_y$ . The vertical dependence of the perturbations is captured by the functions  $\hat{\xi}(z)$ , which are to be determined. The time dependence is exponential, and characterised by growth rate  $s$ . For instability,  $\Re(s) > 0$ , allowing exponential growth; modes with  $\Re(s) < 0$  are stable. We aim to find the most unstable mode, which is that with the largest positive value of  $\Re(s)$ , as this is the mode that will come to dominate the system at large  $t$ .

Note that for the purposes of this Chapter, we will apply  $\gamma$  and  $\beta$  independently of the scale of perturbations, i.e. with the same magnitude for all  $k_x$  and  $k_y$ , as well as to the basic states. It may be argued, due to the nature of  $\gamma$  and  $\beta$  as mean field effects (see Section 1.4.4), that they should strictly be applied only to the largest scales of variation in the system: this corresponds to the basic state and potentially also the larger scales of the perturbations as defined by near-zero  $k_x$  and  $k_y$ . Therefore, it may be the case that applying  $\gamma$  and  $\beta$  to perturbations of all scales as well as to the basic states misrepresents their effect on the system. Scale-dependent treatment of the effects of  $\gamma$  and  $\beta$ , however, will be the focus of Chapter 4; for now, we will consider  $\gamma$  and  $\beta$  as scale-independent effects in order to gain a broad understanding of their effect on the linear stability of the equilibrium states of the system.

With this in mind, we recall that the system we will solve is given by the linearised forms of Equations (1.32) – (1.36). For the purposes of our system, the real and imaginary parts become decoupled from one another under the assumption that the perturbations have the form (3.5), giving two equivalent systems with the same solution. In order to avoid the additional numerical cost of essentially solving the system twice, we simply choose one of these two decoupled systems to

### 3.1 Linear Stability Analysis

---

solve, which is equivalent to solving with the following perturbations:

$$\tilde{b}_x = \hat{b}_x(z) \cos(k_x x) \sin(k_y y) e^{st}, \quad (3.6)$$

$$\tilde{b}_y = \hat{b}_y(z) \sin(k_x x) \cos(k_y y) e^{st}, \quad (3.7)$$

$$\tilde{b}_z = \hat{b}_z(z) \sin(k_x x) \sin(k_y y) e^{st}, \quad (3.8)$$

$$\tilde{u} = \hat{u}(z) \sin(k_x x) \sin(k_y y) e^{st}, \quad (3.9)$$

$$\tilde{v} = \hat{v}(z) \cos(k_x x) \cos(k_y y) e^{st}, \quad (3.10)$$

$$\tilde{w} = \hat{w}(z) \cos(k_x x) \sin(k_y y) e^{st}, \quad (3.11)$$

$$\tilde{T} = \hat{T}(z) \cos(k_x x) \sin(k_y y) e^{st}, \quad (3.12)$$

$$\tilde{\rho} = \hat{\rho}(z) \cos(k_x x) \sin(k_y y) e^{st}. \quad (3.13)$$

Under these assumptions, the stability of a given mode depends on its horizontal scale. Thus, for a given set of parameters we vary the horizontal wavenumbers to find the stability properties as a function of  $k_x$  and  $k_y$ . The global maximum of  $Re(s)$  in  $k_x$ - $k_y$  space sets the scale of the most unstable mode of the system, or the typical horizontal scale of the instability.

#### 3.1.1 Linearised System

With the assumption that the perturbations are small, we linearise in the perturbed quantities, giving eight linear PDEs:

$$\begin{aligned} \partial_t \tilde{b}_x &= ((\zeta_o C_k + \beta)(\partial_x^2 + \partial_y^2 + \partial_z^2) + \beta' \partial_z - \gamma' - \gamma \partial_z) \tilde{b}_x - \beta' \partial_x \tilde{b}_z - \bar{B} \partial_y \tilde{v} \\ &\quad - (\bar{B}' + \bar{B} \partial_z) \tilde{w}, \end{aligned} \quad (3.14)$$

$$\partial_t \tilde{b}_y = ((\zeta_o C_k + \beta)(\partial_x^2 + \partial_y^2 + \partial_z^2) + \beta' \partial_z - \gamma' - \gamma \partial_z) \tilde{b}_y - \beta' \partial_y \tilde{b}_z + \bar{B} \partial_x \tilde{v}, \quad (3.15)$$

$$\partial_t \tilde{b}_z = ((\zeta_o C_k + \beta)(\partial_x^2 + \partial_y^2 + \partial_z^2) - \gamma \partial_z) \tilde{b}_z + \bar{B} \partial_x \tilde{w}, \quad (3.16)$$

$$\begin{aligned} \bar{\rho} \partial_t \tilde{u} &= F \bar{B}' \tilde{b}_z + \sigma C_k \left( \left( \frac{4}{3} \partial_x^2 + \partial_y^2 + \partial_z^2 \right) \tilde{u} + \frac{1}{3} \partial_x \partial_y \tilde{v} + \frac{1}{3} \partial_x \partial_z \tilde{w} \right) \\ &\quad - \bar{\rho} \partial_x \tilde{T} - \bar{T} \partial_x \tilde{\rho}, \end{aligned} \quad (3.17)$$

$$\begin{aligned} \bar{\rho} \partial_t \tilde{v} &= -F \bar{B} \partial_y \tilde{b}_x + F \bar{B} \partial_x \tilde{b}_y + \sigma C_k \left( \frac{1}{3} \partial_x \partial_y \tilde{u} + \left( \partial_x^2 + \frac{4}{3} \partial_y^2 + \partial_z^2 \right) \tilde{v} + \frac{1}{3} \partial_y \partial_z \tilde{w} \right) \\ &\quad - \bar{\rho} \partial_y \tilde{T} - \bar{T} \partial_y \tilde{\rho}, \end{aligned} \quad (3.18)$$

### 3. LINEAR STABILITY OF EQUILIBRIUM BASIC STATES

---

$$\begin{aligned} \bar{\rho}\partial_t\tilde{w} = & -F(\bar{B}' + \bar{B}\partial_z)\tilde{b}_x + F\bar{B}\partial_x\tilde{b}_z + \sigma C_k \left( \frac{1}{3}\partial_x\partial_z\tilde{u} + \frac{1}{3}\partial_y\partial_z\tilde{v} \right. \\ & \left. + \left( \partial_x^2 + \partial_y^2 + \frac{4}{3}\partial_z^2 \right) \tilde{w} \right) - (\bar{\rho}\partial_z + \bar{\rho}')\tilde{T} - (\bar{T}' + \bar{T}\partial_z - \theta(m+1))\bar{\rho}, \end{aligned} \quad (3.19)$$

$$\begin{aligned} \partial_t\tilde{T} = & \frac{2\bar{B}'C_k(\gamma-1)F\zeta_o}{\bar{\rho}}(\partial_z\tilde{b}_x - \partial_x\tilde{b}_z) - (\gamma-1)\bar{T}(\partial_x\tilde{u} + \partial_y\tilde{v} + \partial_z\tilde{w}) - \bar{T}'\tilde{w} \\ & + \frac{\gamma C_k}{\bar{\rho}}(\partial_x^2 + \partial_y^2 + \partial_z^2)\tilde{T}, \end{aligned} \quad (3.20)$$

$$\partial_t\bar{\rho} = -\bar{\rho}\partial_x\tilde{u} - \bar{\rho}\partial_y\tilde{v} - (\bar{\rho}' + \bar{\rho}\partial_z)\tilde{w}. \quad (3.21)$$

Owing to the form of the perturbations, we may reduce the  $x$ -,  $y$ -, and  $t$ -derivatives simply to algebraic terms, leaving us with a system of ODEs in terms of the  $z$ -dependent functions  $\hat{\xi}(z)$ . In this system, the growth rate  $s$  acts as an eigenvalue, and in fact the system takes the form

$$\mathcal{L}\hat{\xi} = s\hat{\xi}, \quad (3.22)$$

where  $\mathcal{L}$  is a linear differential operator,  $s$  is the growth rate, and  $\hat{\xi}$  is a solution vector of the combined  $\hat{\xi}(z)$  of the perturbed quantities.

We may solve the system numerically, subject to appropriate boundary conditions for each  $\hat{\xi}(z)$ . We choose the boundary conditions:

$$\hat{b}_x, \hat{b}_y, \frac{d\hat{b}_z}{dz} = 0, \quad (3.23)$$

$$\frac{d\hat{u}}{dz}, \frac{d\hat{v}}{dz}, \hat{w} = 0, \quad (3.24)$$

$$\hat{T} = 0, \quad (3.25)$$

at  $z = 0, 1$ .

Note that there is some freedom in the choice of boundary conditions, so long as  $\nabla \cdot \hat{\mathbf{b}} = 0$  is satisfied at each boundary. Throughout this work, however, we have chosen those given by (3.23).  $\hat{b}_x(0) = 0$  is consistent with the basic state boundary condition  $\bar{B}(0) = \bar{B}_x(0) = 0$ , and also fixes the boundary conditions for  $\hat{b}_y$  and  $\hat{b}_z$  given  $\nabla \cdot \hat{\mathbf{b}} = 0$  at  $z = 0$  (and we take the same conditions at  $z = 1$  for the sake of convenience). For the velocity, we use stress-free, impermeable boundary conditions. The temperature perturbation is fixed at zero at the boundaries.

Note that the form of the system does not require a boundary condition to be placed on  $\hat{\rho}$ .

We construct the composite linear operator matrix  $\mathcal{L}$  using Chebyshev differentiation matrices, following Trefethen (2000), apply the boundary conditions, and solve the eigenvalue problem on a grid of  $N = 100$  Chebyshev nodes, using MATLAB's inbuilt eigenvalue solver. This uses either a Cholesky factorisation or a QZ algorithm method to solve generalised eigenvalue problems, depending on the properties of the matrices involved. Of the modes we obtain for each eigenvalue solution, we select the mode with the largest  $\Re(s)$ , i.e. the most unstable mode for a given set of parameters and horizontal spatial scale.

In the remainder of this chapter, we will first consider the case of  $\gamma = \beta$  given by (2.4) and (2.5), and, for the sake of convenience, we will characterise the amplitude of both effects as  $\gamma_m$ .

## 3.2 Parameters

Throughout this analysis, we will keep the values of the dimensionless parameters of the system (defined by (1.37) - (1.40), and those of the  $\gamma$  and  $\beta$  profiles) fixed apart from  $\gamma_m$ , for various values of the dimensionless field strength  $F$ . Our chosen parameter values are shown in Table 3.1.

## 3.3 Linear stability for $\gamma = \beta = 0$

Let us first, for the sake of comparison, discuss the case where  $\gamma$  and  $\beta$  are not present. In the standard, non-turbulent case where both effects are zero, we have the equilibrium state as an analytic function, a linear profile given by  $\bar{B} = 2z$  for the boundary conditions  $\bar{B}(0) = 0$ ,  $\phi(1) = 1$ . In general, for this basic state the most unstable mode is 3D, with a growth rate and horizontal scale that depend on the value of the dimensionless field strength  $F$ , as shown in Figure 3.1.

### 3. LINEAR STABILITY OF EQUILIBRIUM BASIC STATES

---

Parameter	Value
$\sigma$	0.005
$\zeta_o$	0.01
$C_k$	0.01
$F$	Variable
$\theta$	2
$m$	1.505
$\Gamma$	$5/3$
$a$	30
$z_i$	0.5
$\gamma_m$	Variable

Table 3.1: Parameter values used in the linear stability analysis, following the values used by [Barker \*et al.\* \(2012\)](#).

The growth rate of the most unstable mode increases with increasing  $F$ , in the range we have considered (see Figure 3.1c). However, the mode of maximum growth rate also changes in horizontal scale, defined by wavenumbers  $k_x$  (Figure 3.1a) and  $k_y$  (Figure 3.1b), with increasing field strength.

For the lowest  $F$  value that we consider here,  $F = 10^{-7}$ , we see that the mode of “maximum growth rate” in the system has  $\Re(s) = 0$  and occurs at  $k_x = k_y = 0$ , which is a reflection of the fact that at such low field strength, all scales of the system are stable. Increasing  $F$  from this value, however, the first onset of the instability is undular, with  $k_y = 0$ . Further increasing the field strength, the least stable mode becomes 3D ( $k_x, k_y \neq 0$ ). Even larger values of  $F$  ( $F \geq 1$ , of the cases studied here) produce an interchange instability, with  $k_x = 0$ .

We may explain this change in the form of the instability by considering the physical requirements for destabilising interchange and undular modes, as well as their structure. Undular modes require bending of the field lines to be destabilised, which requires work to be done against magnetic tension. Interchange modes do not require this, and therefore it may be expected that the interchange

### 3.3 Linear stability for $\gamma = \beta = 0$

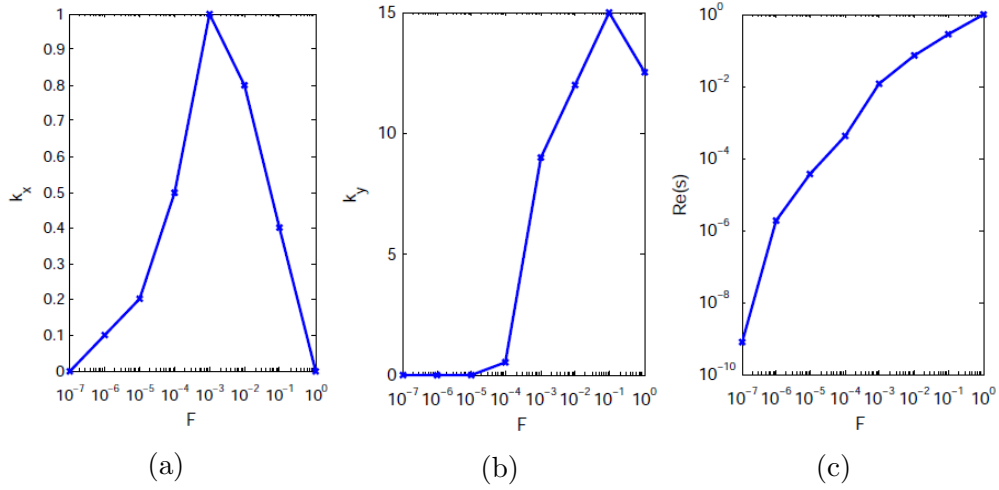


Figure 3.1:  $F$ -dependence of the scale and growth rate of the most unstable mode, when  $\gamma = \beta = 0$ . (a), (b): horizontal wavenumbers  $k_x$  and  $k_y$ , (c): growth rate  $Re(s)$  of the most unstable mode, as a function of  $F$ .

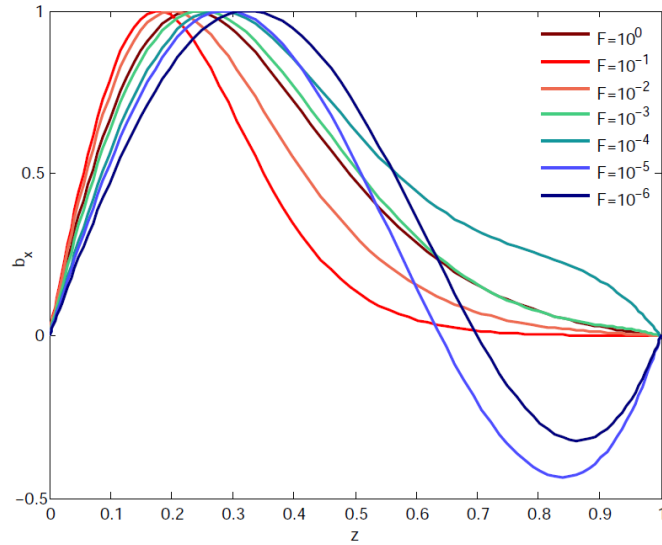


Figure 3.2: Normalised  $\hat{b}_x$  for the most unstable mode, with  $\gamma = \beta = 0$ .

### 3. LINEAR STABILITY OF EQUILIBRIUM BASIC STATES

---

instability should come to dominate over the undular and 3D instabilities when the field strength  $F$ , and therefore the magnetic tension effect, is greater. In other words, the increased field strength is able to suppress the undular instability, and then eventually also the 3D instability. (Note that [Hughes & Cattaneo \(1987\)](#) showed that it is also possible to find parameter regimes where 3D/undular modes are unstable but interchange modes are stable, though our choice of magnetic field basic state does not fall within such regimes and therefore does not give rise to the destabilisation of undular modes in preference to interchange. We will, however, discuss a case for which undular modes are destabilised in [Section 4.4.2](#).)

In addition, the form of the perturbation eigenfunctions of the most unstable mode is dependent on the value of  $F$ . We consider the  $\hat{b}_x$  eigenfunction, and plot its variation in the layer in [Figure 3.2](#). For  $F = 1$ , the  $\hat{b}_x$  eigenfunction peaks in the upper part of the layer, at approximately  $z = 0.25$ . For lower  $F$ , this peak becomes narrower, and slightly higher in the layer for  $F = 0.1$ . If  $F$  is further decreased, however, the peak grows wider again and moves towards the bottom of the layer, a change that corresponds to the change from an interchange maximum when  $F = 1$  to a 3D mode for lower  $F$ . Furthermore, we also see a change in the form of the  $\hat{b}_x$  eigenfunction for the low- $F$  case where the maximum is undular; in this regime, the  $\hat{b}_x$  perturbation reverses and has a local minimum in the lower part of the layer.

#### 3.4 $\gamma = \beta \neq 0$

Having studied the stability of the system with no  $\gamma$  and  $\beta$  effects, we now consider the case of  $\gamma = \beta$  given by [\(2.4\)](#) and [\(2.5\)](#), acting on the basic state and the perturbations as described in [Chapter 1](#). As the value of  $\gamma_m$  is increased (and thus  $\gamma$  and  $\beta$  are applied), we see a change in the horizontal scale of the most unstable mode, as well as a change from 3D to interchange ([Figure 3.1](#)). Once an interchange mode is reached, further increasing  $\gamma_m$  causes the most unstable mode (i.e. the maximum of  $\Re(s)$  as a function of  $k_x$  and  $k_y$ ) to move to larger  $k_y$ , or to smaller scale in  $y$ . We demonstrate this by considering an example case at the parameter value  $F = 10^{-3}$ , which is representative of the higher  $F$

regime within the range we have considered, and then we will consider the case of  $F = 10^{-5}$  as a comparison.

### 3.4.1 $F = 10^{-3}$

The increase in  $\gamma$  and  $\beta$  increases the growth rate of all the unstable modes of the system, and changes the most unstable mode from 3D to interchange, as shown in Figure 3.3. It also affects the form of the eigenfunctions, moving the location of the maximum of  $\hat{b}_x$  towards the bottom of the layer, out of the turbulent region. Note that in the contour plots in Figure 3.3, as well as all subsequent plots of this type, the position of the most unstable mode is marked with a cross,  $\times$ . Note also that although formally, we term  $\Re(s)$  as the “growth rate”, the modes solved for here have purely real  $s$ , barring in some cases a much smaller imaginary component that is the result of numerical error in the eigenvalue solver. This is true for all of the results shown in this Chapter and the next. Physically speaking, this means that the instability has no oscillatory component.

We can explain these changes with  $\gamma_m$  by considering the effect of  $\gamma$  and  $\beta$  on the equilibrium basic state. In the case of larger  $\gamma_m$ , we see an increased field gradient at the bottom of the layer at equilibrium. In our linear analysis, the perturbations are effectively concentrated in, or “confined” to, this high field gradient region when  $\gamma_m \neq 0$ . This suggests that this increased gradient of the basic state is responsible for the change in stability as we increase  $\gamma_m$ . In addition, instability to magnetic buoyancy is known analytically to depend on field gradient; see stability criteria (1.4) – (1.8).

We may also consider the perturbations; we will look at  $\hat{b}_x$ , as its behaviour is indicative of the general effect on the perturbations of adding  $\gamma$  and  $\beta$  (see Figure 3.5). When no  $\gamma$  and  $\beta$  are present, we obtain a  $\hat{b}_x$  perturbation that peaks in the upper part of the layer, however the variation is relatively smooth. Contrast, however, the case of non-zero  $\gamma$  and  $\beta$ ; in this case, the basic state is approximated by a constant (close to zero) value in the region where  $\gamma$  and  $\beta$  are applied, then an effectively linear profile below the point at which they are cut off. This

### 3. LINEAR STABILITY OF EQUILIBRIUM BASIC STATES

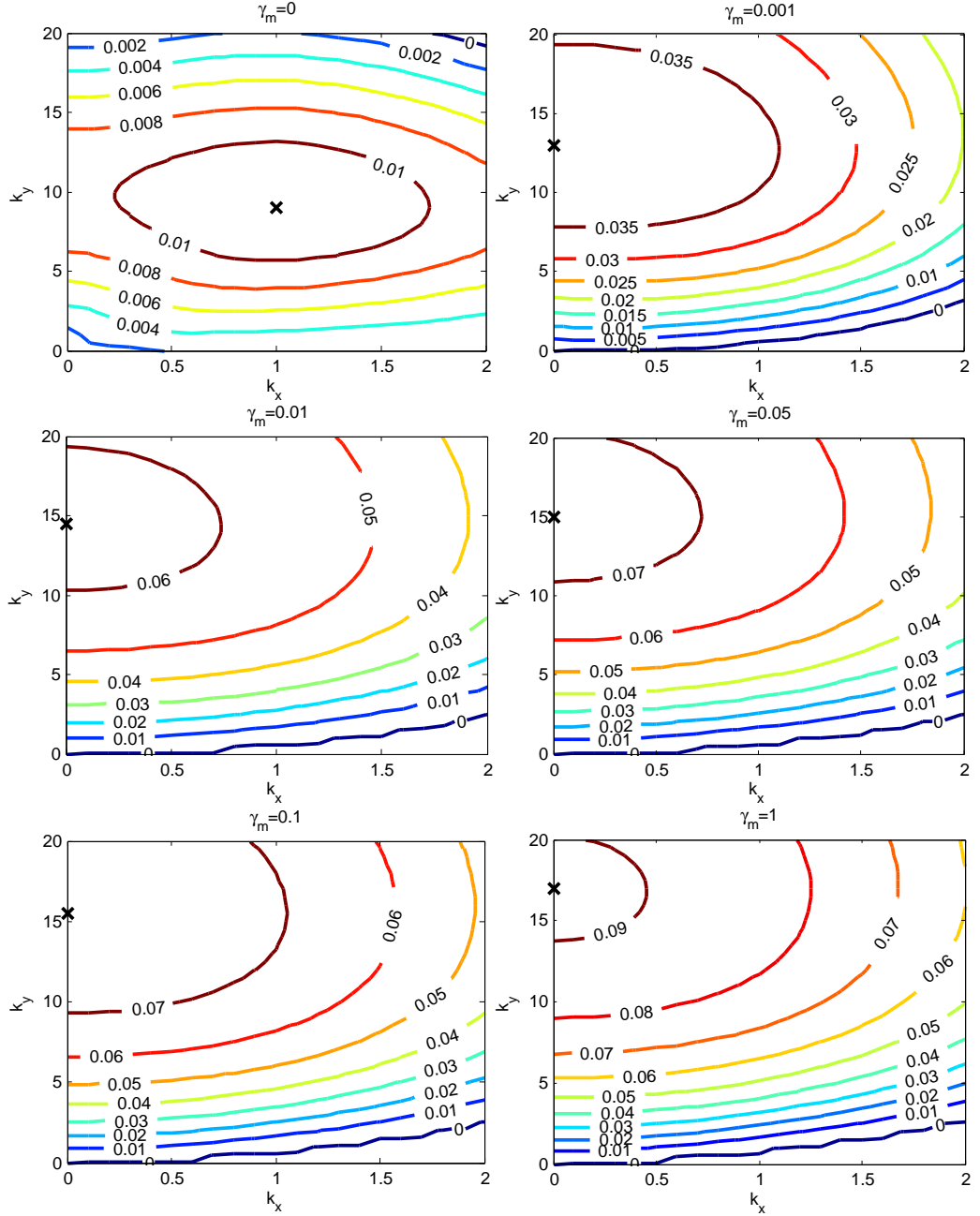


Figure 3.3: Growth rate  $\Re(s)$  as a function of  $k_x$  and  $k_y$  for various values of  $\gamma_m$ , for  $F = 10^{-3}$ , with  $\gamma = \beta$  applied to the basic states and equally to perturbations of all scales.

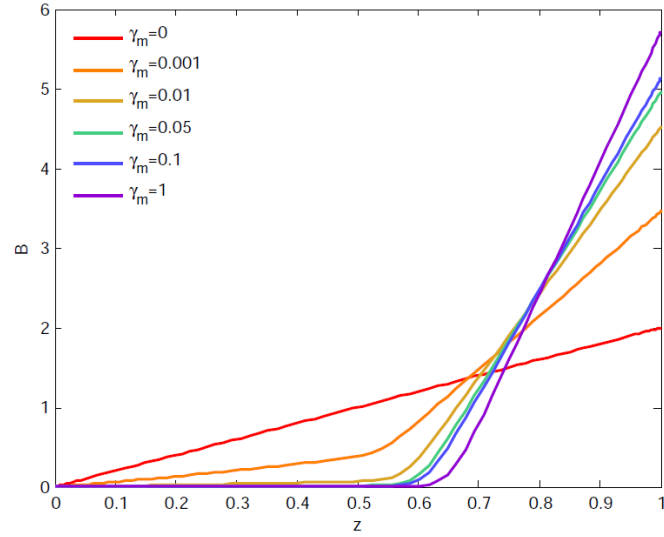


Figure 3.4: Basic states for  $\zeta_o = 0.01$ ,  $C_k = 0.01$ , with  $\gamma = \beta$ .

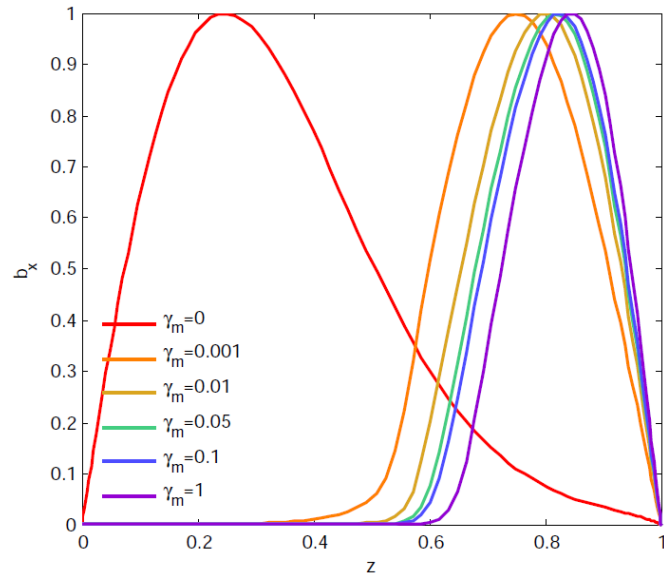


Figure 3.5: Normalised  $\hat{b}_x$  perturbations for the mode of maximum growth rate, for  $F = 10^{-3}$ ,  $\gamma = \beta$  (contour plots shown in Figure 3.3).

### 3. LINEAR STABILITY OF EQUILIBRIUM BASIC STATES

---

suggests that in the region without  $\gamma$  and  $\beta$ , we may see a  $\hat{b}_x$  profile analogous to that across the full layer when  $\gamma = \beta = 0$ , and in the region where they are present we may expect  $\hat{b}_x$  to be small and relatively constant. In other words, for  $\gamma_m \neq 0$  we expect that the perturbation be “concentrated” in the region of larger  $\bar{B}'$ , and this is in fact the result that we do see, especially as  $\gamma_m$  increases. As the  $\gamma$  and  $\beta$  effects are increased in magnitude, we see the perturbations increasingly confined to the area below the level at which  $\gamma$  and  $\beta$  are applied, where there is higher basic state field gradient, and only the molecular diffusion is present.

In addition, from these results, we can see that the change in stability and the change in the form of the eigenfunctions is much more significant for lower values of  $\gamma_m$ . This is especially the case for the larger  $F$  cases studied.

Let us consider again the results shown in Figures 3.3 and 3.5. In both the growth rate contour plots and the vertical variation of  $\hat{b}_x$ , there is a marked difference between the contour plots in  $k_x$  and  $k_y$ , the form of the perturbations, and the growth rate of the most unstable mode, when moving between no  $\gamma$  and  $\beta$  effects ( $\gamma_m = 0$ ) and their lowest value considered, i.e.  $\gamma_m = 10^{-3}$ . This can be ascribed in large part to the change in the basic state with the application of a low level of  $\gamma$  and  $\beta$ .

As discussed in Chapter 2, the greatest effect on the equilibrium state due to the addition of  $\gamma = \beta$  occurs for low  $\gamma_m$ . This is because ordinarily, we choose to take the molecular diffusivity  $\zeta_o C_k = 10^{-4}$  (see Table 3.1) as much less than the maximum value of  $\beta$ , given here by  $\gamma_m$ . However, there is a regime for which  $\gamma_m \sim \zeta_o C_k$ , which occurs here between our two sampled values of  $\gamma_m = 0$  and  $\gamma_m = 10^{-3}$ . It is in this regime that the basic state changes fastest with  $\gamma_m$  (see Figure 3.4, as well as discussion in Section 2.7.2) which is why in this case we see the largest change in stability with application of low levels of  $\gamma$  and  $\beta$ . Furthermore, it suggests that the effect of  $\gamma$  and  $\beta$  on the form of the basic state is critical to understanding the instability, which we will discuss in greater detail in Section 4.1. As an example, compare the basic states (Figure 3.4) used, and note that the difference in the basic state decreases as  $\gamma_m$  is increased. Compare

the perturbed  $\hat{b}_x$  shown in Figure 3.5, which also become more similar to each other for larger  $\gamma_m$ .

The results suggest that the regime of most variation in the instability with  $\gamma_m$  in the  $F = 10^{-3}$  regime is that of low  $\gamma$  and  $\beta$ , which we consider as  $\gamma_m \lesssim \zeta_o C_k$ . We thus consider this regime in greater detail, with the contour plots of growth rate of the instability as a function of horizontal scale shown in Figure 3.6, with the corresponding basic states and  $\hat{b}_x$  perturbations shown in Figures 3.7 and 3.8.

From this we can see that it is for  $\gamma_m \sim \zeta_o C_k$  that the previously discussed change in the form of the instability — from 3D to interchange — occurs. The change in the form of the perturbations  $\hat{b}_x$  also reflects this, with a more gradual transition in the form and position of the peak of the perturbed field, though it is also interesting to note that the greatest “transition” in the shape of the perturbations appears to be between the values  $\gamma_m = 10^{-5}$  and  $10^{-4}$ , rather than between  $\gamma_m = 5 \times 10^{-4}$  and  $10^{-3}$ , which is where the switch to an interchange mode occurs for this parameter set. The key point of interest here, however, is for  $F = 10^{-3}$  this transition in the form of instability occurs for low  $\gamma_m$ ; this, however, is not true for lower  $F$ , as we will see in the next Section.

### 3.4.2 $F = 10^{-5}$

In contrast to the case of  $F = 10^{-3}$ , we now consider the case of low  $F$ , for which we will take  $F = 10^{-5}$  as an example. Note that the basic states do not depend on the value of  $F$ , and so the perturbations are to the same basic states as we considered for  $F = 10^{-3}$ , pictured in Figure 3.4. Note also that, as we saw in the  $\gamma = \beta = 0$  case considered in Section 3.3, for this low  $F$  regime the  $\hat{b}_x$  perturbation takes a slightly different form (see Figure 3.10), changing sign within the layer.

We find, however, that adding  $\gamma$  and  $\beta$  results in  $\hat{b}_x$  similar to those for the higher  $F$  regime, peaking in the lower part of the layer for which the basic state field gradient is large and not showing the same reversal in the perturbed  $\hat{b}_x$ .

### 3. LINEAR STABILITY OF EQUILIBRIUM BASIC STATES

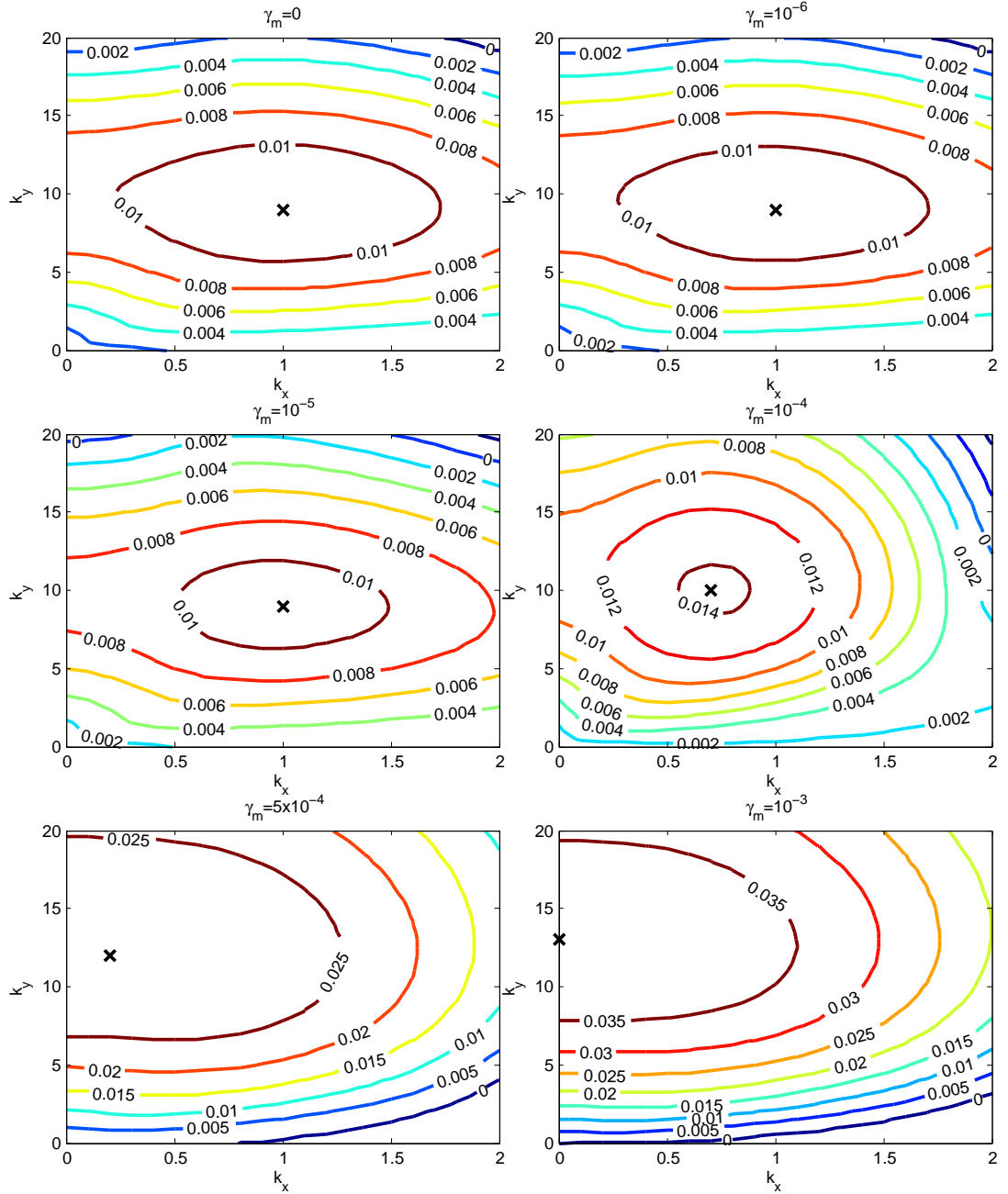


Figure 3.6: Growth rate  $\Re(s)$  as a function of  $k_x$  and  $k_y$  for various values of  $\gamma_m$ , for  $F = 10^{-3}$ , with  $\gamma = \beta$  applied to the basic states and equally to perturbations of all scales, and  $\gamma_m \leq 10^{-3}$ .

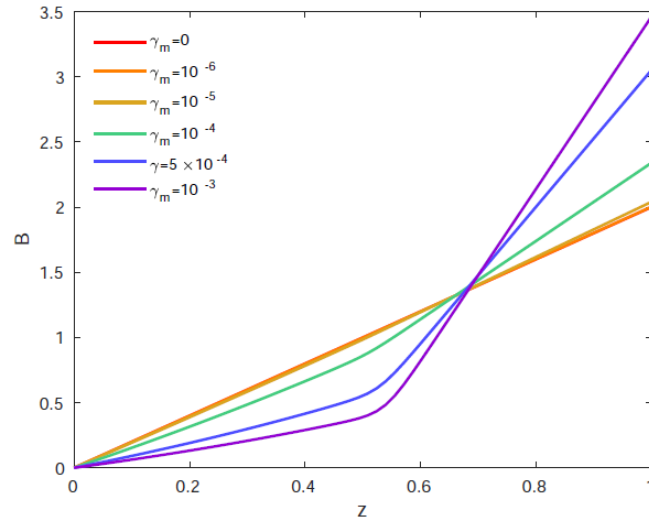


Figure 3.7: Basic states for  $\zeta_o = 0.01$ ,  $C_k = 0.01$ , with  $\gamma = \beta$  and  $\gamma_m \leq 10^{-3}$ .

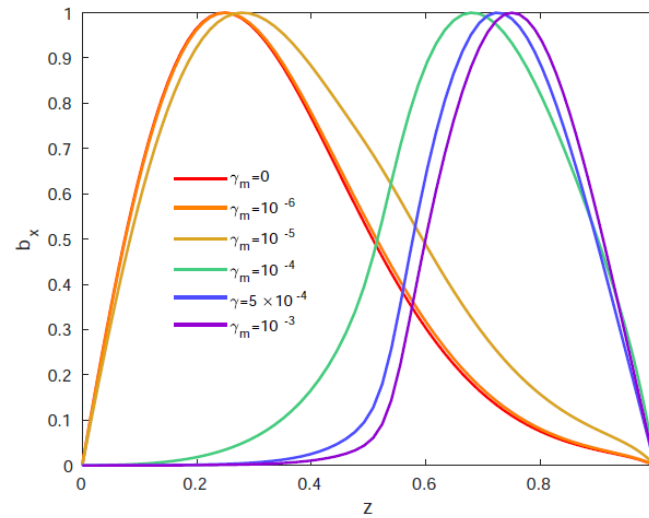


Figure 3.8: Normalised  $\hat{b}_x$  perturbations for the mode of maximum growth rate, for  $F = 10^{-3}$ ,  $\gamma = \beta$ , with  $\gamma_m \leq 10^{-3}$  (contour plots shown in Figure 3.6).

### 3. LINEAR STABILITY OF EQUILIBRIUM BASIC STATES

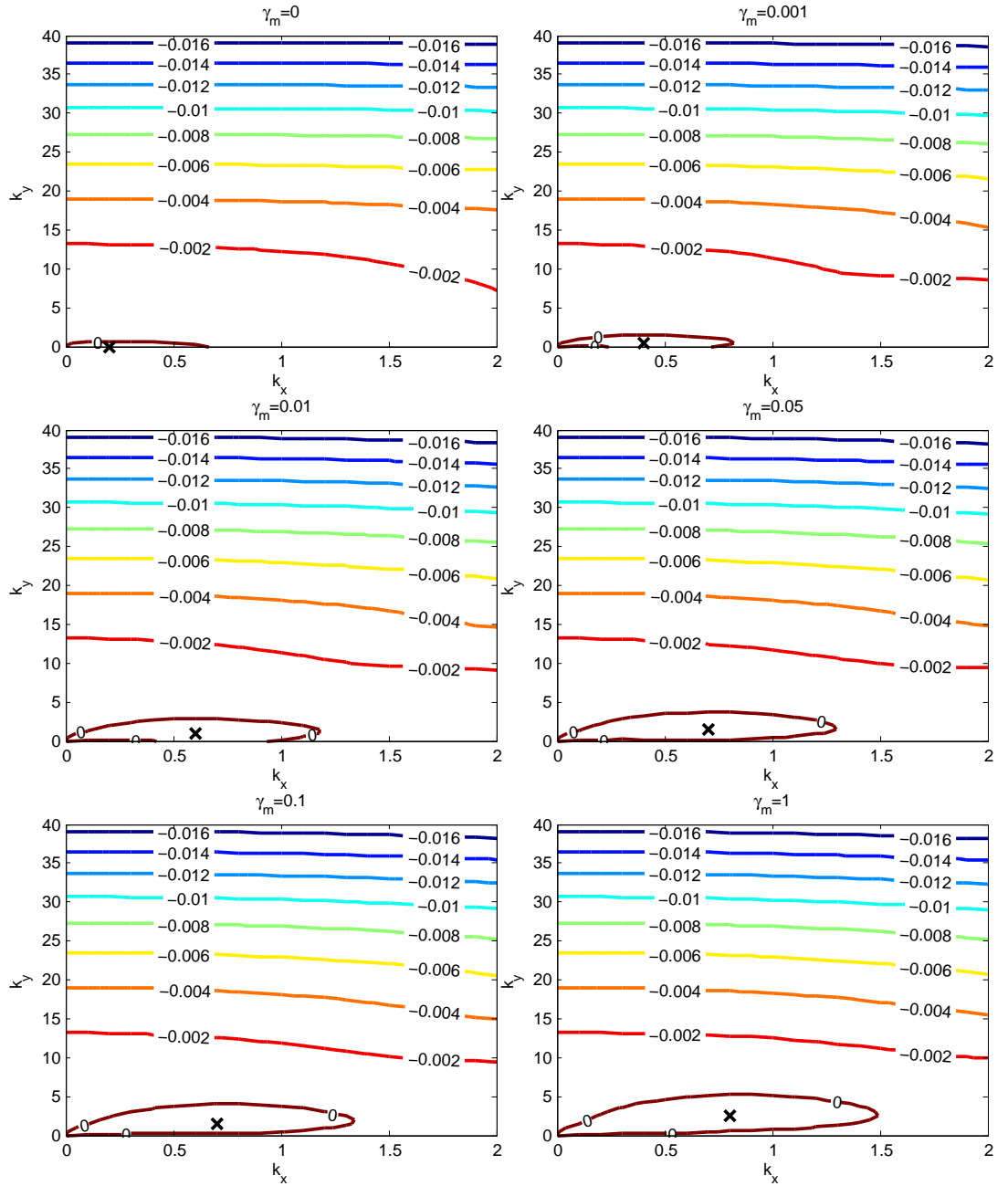


Figure 3.9: Growth rate  $\Re(s)$  as a function of  $k_x$  and  $k_y$  with various values of  $\gamma_m$ , for  $F = 10^{-5}$ , with  $\gamma = \beta$  applied to the basic states and equally to perturbations of all scales.

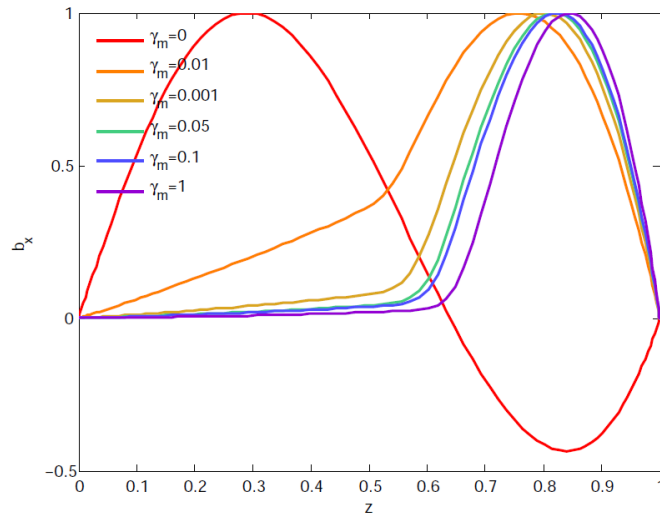


Figure 3.10: Normalised  $\hat{b}_x$  perturbations for the mode of maximum growth rate, for  $F = 10^{-5}$ ,  $\gamma = \beta$ .

Similarly to the case of  $F = 10^{-3}$ , we see an increase in growth rate of the most unstable mode with increasing  $\gamma_m$ , as well as overall lower growth rates than for higher  $F$ ; see Figure 3.13. However, in the contour plots in Figure 3.9, we no longer see the change in the most unstable mode from 3D to interchange; instead we see the position of the most unstable mode increasing slightly in  $k_x$  and  $k_y$  in this regime, with the mode in question remaining 3D.

In general, for this case of  $F = 10^{-5}$ , we see a lower dependence on  $\gamma_m$  in the form and growth rate of the instability. This may seem, initially, counter-intuitive, as the parameter  $F$  does not multiply the  $\gamma$  or  $\beta$  terms in the induction equation (see Equations (3.14) – (3.16)). However, the field strength  $F$  multiplies the basic state magnetic field and its gradient in the momentum and energy equations, (3.17) – (3.20). Given, as we have seen in Section 3.4.1, the fact that the stability depends strongly on the basic state magnetic field and specifically its gradient, the results for lower  $F$  are suggestive of two things; first, that the effect of  $\gamma$  and  $\beta$  on the system is primarily via their effect on the basic state, rather than via their explicit appearance in the perturbation equations, and second,

### 3. LINEAR STABILITY OF EQUILIBRIUM BASIC STATES

---

that the effect of the basic state may be the most important factor affecting the stability of the system.

In the next Section, in order to further understand this we will look more broadly at how the field strength  $F$  affects the interaction of  $\gamma$  and  $\beta$  with the instability, using a range of different  $F$  values.

#### 3.5 Effect of varying $F$

We will consider the variation in the horizontal scale and growth rate of the most unstable mode as a function of  $\gamma_m$ , as it varies with the field strength  $F$ . First, we will seek to understand the effect on the horizontal scale of the instability, as defined by the wavenumbers  $k_x$  and  $k_y$ . For each field strength considered, in Figure 3.11, we plot the  $k_x$  and  $k_y$  value of the most unstable mode — in the same  $k_x$ - $k_y$  space considered in the contour plots 3.3 and 3.9 — for increasing  $\gamma_m$ . From this, we are able to discern a “path” in  $k_x$ - $k_y$  space taken by the most unstable mode as a result of the addition of more  $\gamma$  and  $\beta$ . Comparing the plots in Figure 3.11 reveals the effect of  $F$ .

The “general” path of the most unstable mode with  $\gamma_m$  begins at  $k_x = k_y = 0$ , continues to larger  $k_x$  and  $k_y$ , then begins to decrease in  $k_x$  again, moving towards interchange modes at  $k_x = 0$ , with  $k_y$  still increasing. Once an interchange mode is reached, the only change seen is an increase in  $k_y$ , as in general the 3D instability is not present for  $\gamma_m$  above some maximum value, which depends on  $F$ . The overall effect of  $F$  is to determine, effectively, where on this general curve the most unstable mode “begins” when  $\gamma_m = 0$ , and where it ends up once we reach the maximum value of  $\gamma_m$  under consideration.

Returning, for example, to the results of Sections 3.4.1 and 3.4.2, the instability with  $F = 10^{-3}$  is in the region of the curve where the most unstable mode is 3D with no  $\gamma$  or  $\beta$  present, but has made the transition to interchange by the

### 3.5 Effect of varying $F$

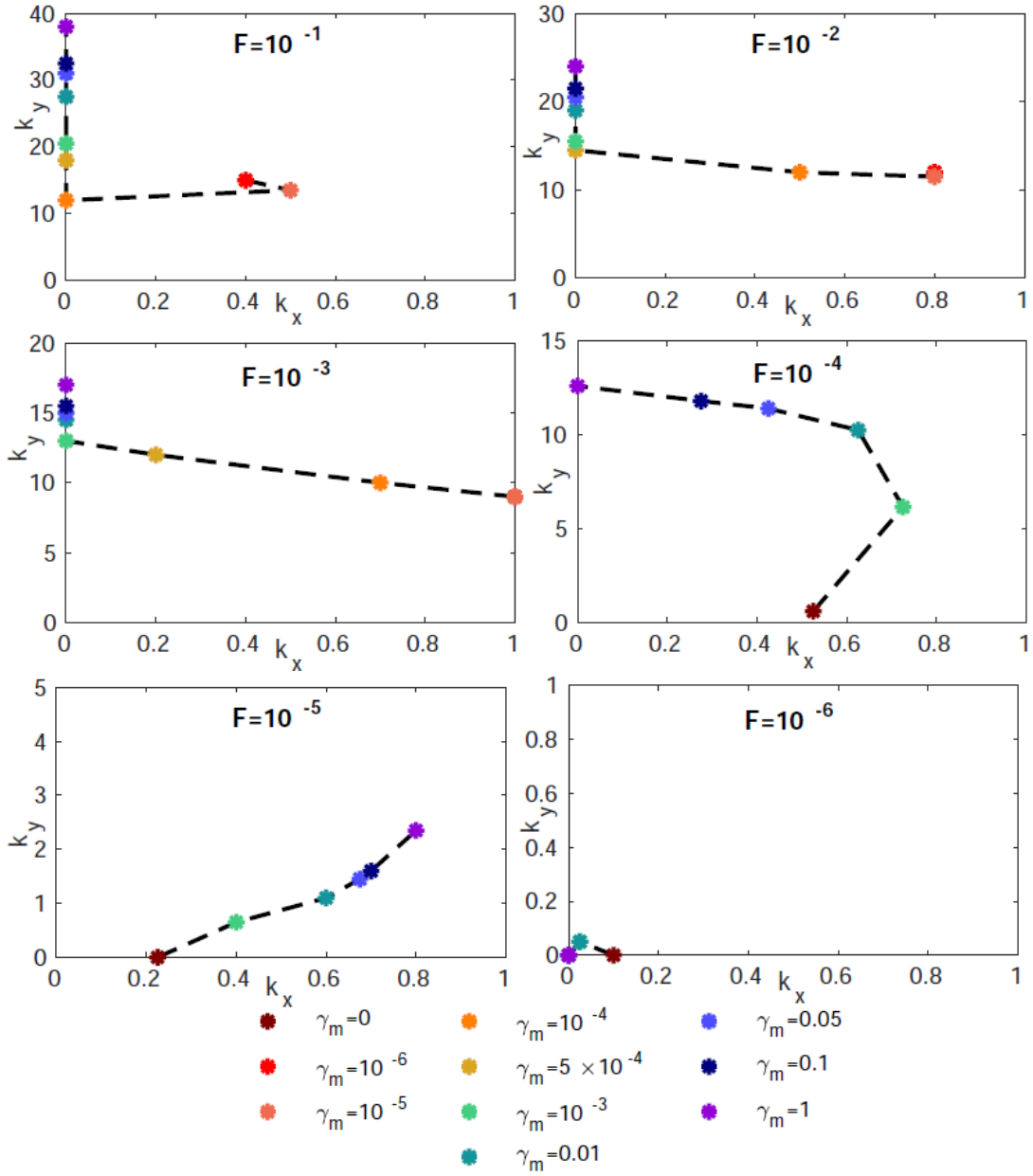


Figure 3.11: Horizontal scale of the most unstable mode for various values of  $F$ , for comparison with equivalent contour plots shown in Figures 3.3 for  $F = 10^{-3}$  and 3.9 for  $F = 10^{-5}$ .

### 3. LINEAR STABILITY OF EQUILIBRIUM BASIC STATES

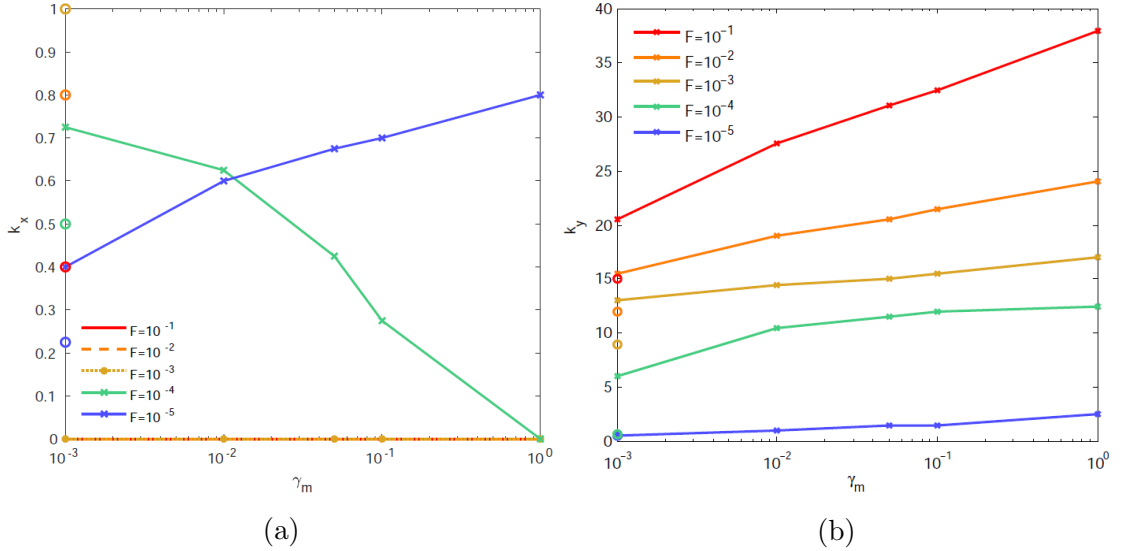


Figure 3.12: (a)  $k_x$  and (b)  $k_y$  of the most unstable mode as a function of  $\gamma_m$ , for various values  $F$ . Note that  $\gamma_m = 0$  values are plotted with circles on the vertical axis. Note also that in (a), the value of  $k_x$  is zero for all  $\gamma_m$  in the cases of  $F = 10^{-1}, 10^{-2}, 10^{-3}$ , as in these cases the most unstable mode is interchange.

time  $\gamma_m = 0.001$  is reached (Figure 3.3 and 3.11, middle left). In the case of  $F = 10^{-5}$ , however, (Figure 3.9 and 3.11, bottom left) we see the most unstable mode simply has an increase in  $k_x$  and  $k_y$ , suggesting that in this regime it has not yet reached the maximum value of  $k_x$  that we have discussed. This implies that if we further increased the value of  $\gamma_m$  in the case of  $F = 10^{-5}$ , we would at some point see a further increase in  $k_x$  and then a decrease, culminating in an interchange instability for some large value of  $\gamma_m$ . Note, however, for  $F \lesssim 10^{-6}$  the instability is suppressed to the extent that all scales are effectively stable (i.e. their growth rate  $\Re(s) \sim 0$ , subject to a small numerical error) thus we do not see this variation. As a summary, we plot the  $k_x$  and  $k_y$  values of these most unstable modes in Figure 3.12.

Note also that in the high field strength case of  $F = 10^{-1}$ , we see a slight deviation from the trend described above for the case of very low  $\gamma_m$ ; in the case of  $\gamma_m \lesssim 10^{-4}$  and  $F = 10^{-1}$  the  $k_x$  and  $k_y$  variation does not follow the same progression with  $\gamma_m$  towards an interchange mode. This may be the result of

### 3.6 Separating the effects of $\gamma$ and $\beta$

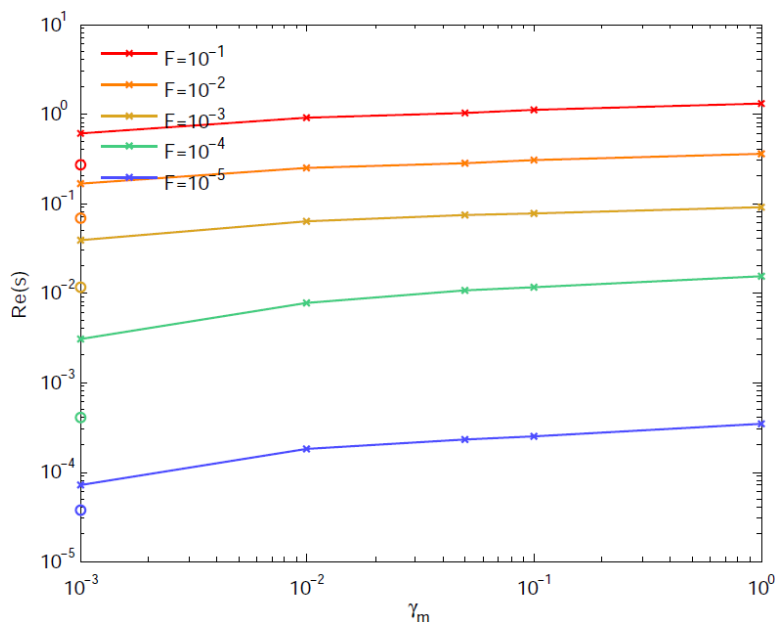


Figure 3.13: Growth rate of the most unstable mode as a function of  $\gamma_m$ . Note that  $\gamma_m = 0$  values are plotted with circles on the vertical axis.

another effect at high field strength, which may warrant further investigation.

We may also plot the growth rate of these most unstable modes of the instability for fixed  $F$ , as a function of  $\gamma_m$  (Figure 3.13). This allows us to see that the functional form of the maximum growth rate  $\Re(s)$  is broadly similar for each value of  $F$ , though the size of the growth rates is larger for higher  $F$  values. This is true despite the variation in the horizontal scale of the instability that we have just discussed.

### 3.6 Separating the effects of $\gamma$ and $\beta$

We will now explore the separate effects of  $\gamma$  and  $\beta$ , in contrast to the previously considered cases for which we always assumed that  $\gamma = \beta$ . We will first consider the extremes, of either only  $\gamma$  or only  $\beta$ . The former of these cases, i.e. that of  $\gamma$  but no  $\beta$ , may be considered unphysical as we expect turbulent pumping to

### 3. LINEAR STABILITY OF EQUILIBRIUM BASIC STATES

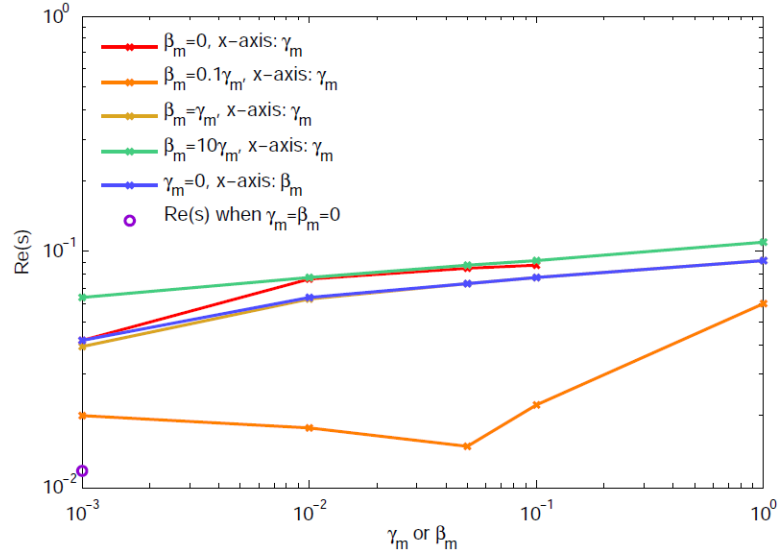


Figure 3.14: Growth rates of the most unstable mode for the case of  $\beta = q\gamma$ , with the additional case of  $\gamma = 0$ , with fixed  $F = 10^{-3}$ .

necessarily give rise to a turbulent diffusion; however, it is important to consider the ratio between the two, and it is informative to be able to separate the two effects.

We consider  $\gamma$  and  $\beta$  given by (2.4) and (2.5); however, we no longer assume that  $\beta_m = \gamma_m$ . Instead we will take  $\beta_m = q\gamma_m$ , for some constant  $q$ , and therefore  $\beta(z) = q\gamma(z)$ . We will consider  $q = 0$  (equivalent to  $\beta_m = 0, \gamma_m \neq 0$ ),  $q = 0.1$ ,  $q = 1$  (i.e. the previously considered  $\beta_m = \gamma_m$  case, as a comparison),  $q = 10$ , and a case where  $\beta_m = 0, \gamma_m \neq 0$ , effectively corresponding to  $q = \infty$ . In Figures 3.14 and 3.15 we plot the growth rates and horizontal wavenumbers of the most unstable mode for these cases, for the sake of comparison between them, before discussing each  $q \neq 1$  case in more detail. Note that throughout the remainder of this Chapter we will consider the higher  $F$  regime as detailed in the previous Sections, taking a fixed value of  $F = 10^{-3}$ , so the results may be compared with those in Section 3.4.1.

### 3.6 Separating the effects of $\gamma$ and $\beta$

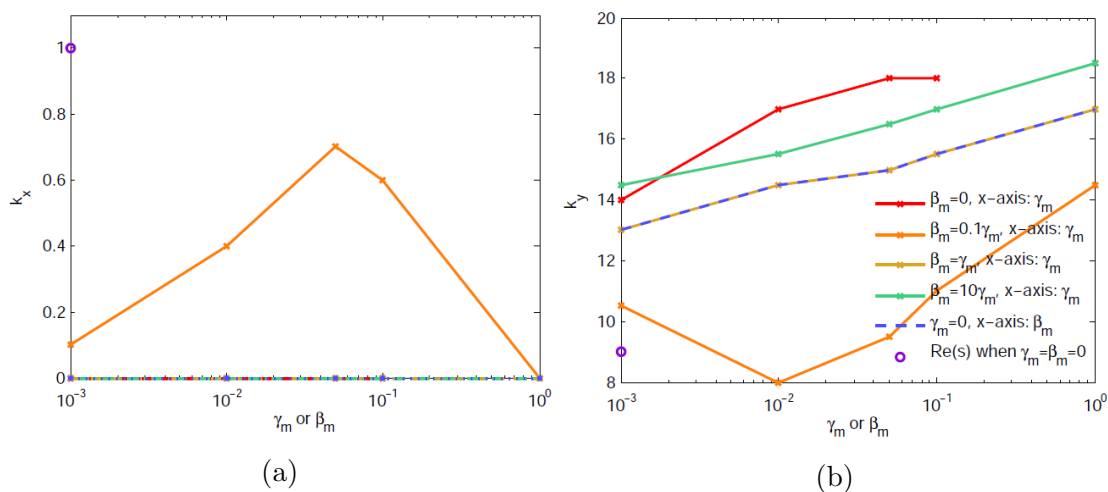


Figure 3.15: (a)  $k_x$  and (b)  $k_y$  for the most unstable mode in the case  $\beta = q\gamma$ , with the additional case of  $\gamma = 0$ , for  $F = 10^{-3}$ .

#### 3.6.1 $\beta = 0$

We consider the case where  $q = 0$ , i.e. when  $\beta = 0$  but  $\gamma$  is still given by (2.4). In Figure 3.16 we show the contours in  $k_x$ - $k_y$  space, as well as the basic states and the  $\hat{b}_x$  perturbations (Figure 3.17) of the most unstable mode in each case. (For growth rate,  $k_x$ , and  $k_y$  of the most unstable modes, see Figures 3.14 and 3.15.) The basic state is given by a “step-like” field, with  $\gamma$  pumping the flux down into the non-turbulent lower half of the layer where the field is effectively constant at equilibrium, as there is no turbulent diffusion. Due to the constant flux boundary condition, the maximum field at the base of the layer is not significantly higher for larger  $\gamma_m$ ; however, the gradient at the cutoff point is much greater.

A high enough gradient at this interface effectively introduces a discontinuity in the basic state magnetic field, when the transition region is on the scale of the numerical grid, and it is for this reason that for  $\gamma_m = 1$  a numerically converged solution to the perturbation equations can no longer be found. We still include the basic state for this case in Figure 3.17a in order to demonstrate this behaviour; note, however, that we do not obtain a solution for  $\gamma_m > 0.1$  in this case. Indeed, we can see the form of  $\hat{b}_x$  becoming increasingly sharply peaked

### 3. LINEAR STABILITY OF EQUILIBRIUM BASIC STATES

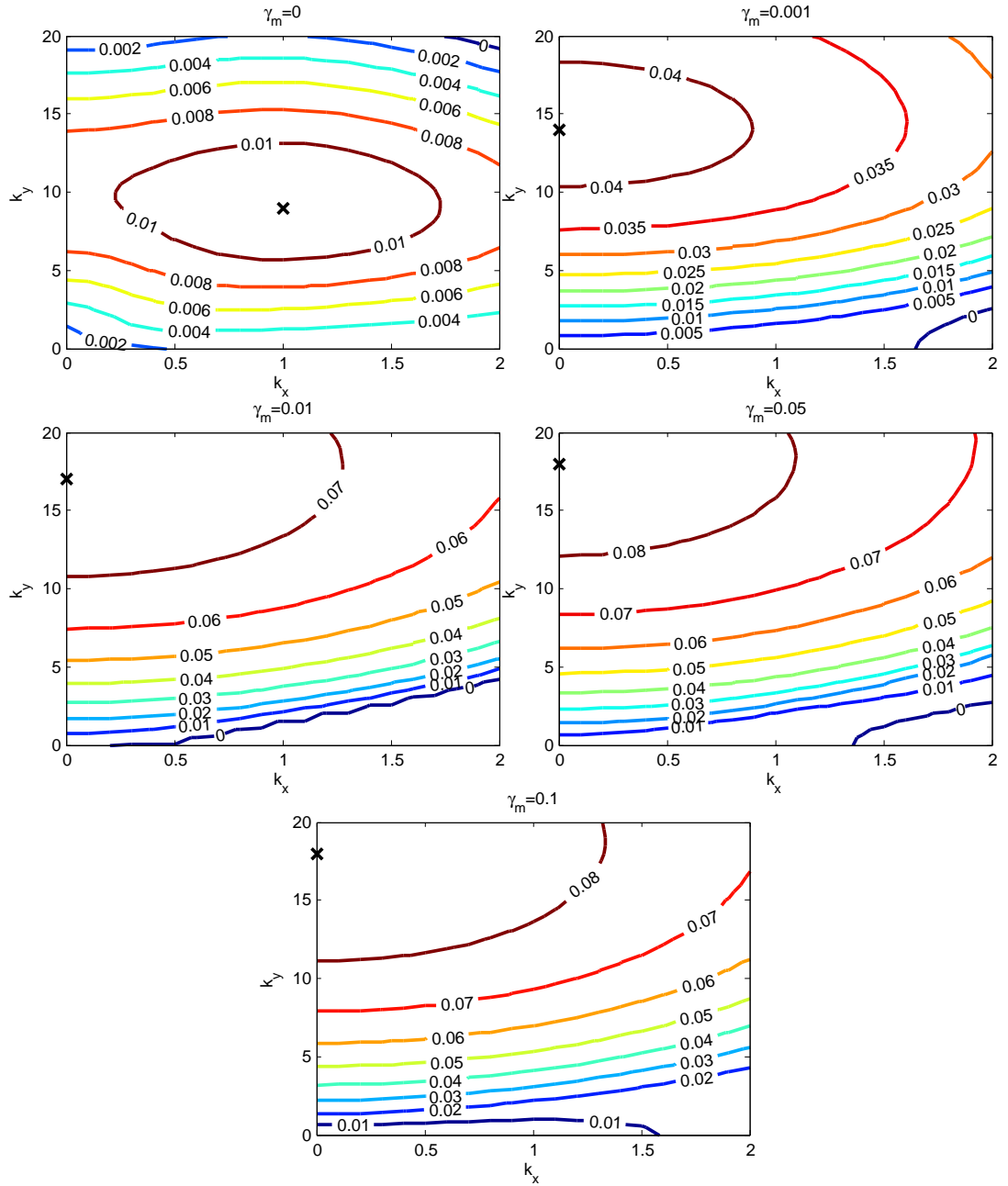


Figure 3.16: Growth rate  $\Re(s)$  as a function of  $k_x$  and  $k_y$  at various values of  $\gamma_m$  with  $\beta = 0$ , for  $F = 10^{-3}$ .

### 3.6 Separating the effects of $\gamma$ and $\beta$

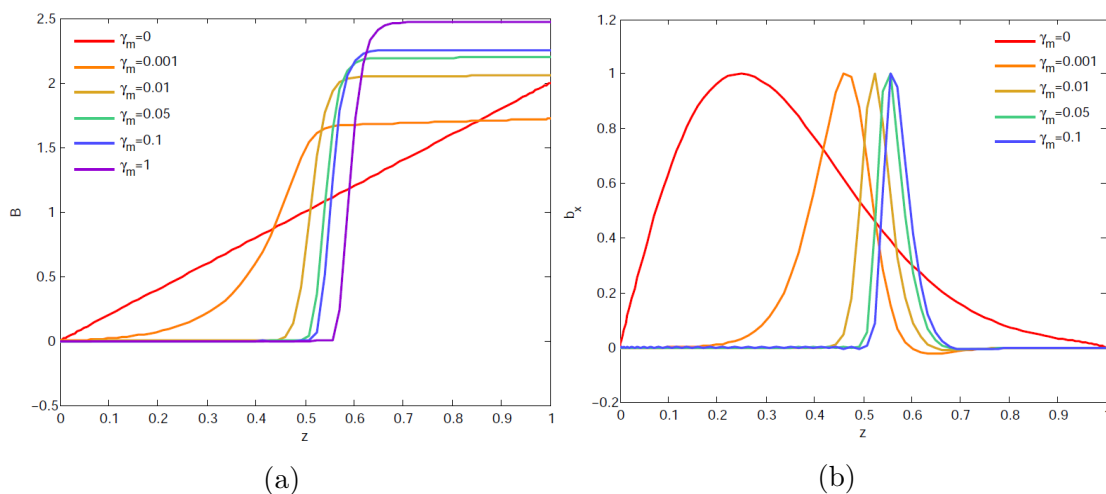


Figure 3.17: (a) Equilibrium basic states and (b) normalised  $\hat{b}_x$  perturbations for the most unstable mode in the cases shown in Figure 3.16, for  $\beta_m = 0$ .

at the point where the field has high gradient. We shall consider a less extreme (and more numerically tractable) case that also demonstrates something of this behaviour in Section 3.6.4.

For lower  $\gamma_m$ , however, the solution is more easily resolved and we can see that, in terms of the growth rate and the horizontal scale of the instability at least, the behaviour of the instability under increasing levels of  $\gamma_m$  is not that different from the case in which we have both  $\gamma$  and  $\beta$ . We still see the change from 3D to interchange as  $\gamma_m$  increases (contour plots shown in Figure 3.16), and the growth rate (Figure 3.14) is somewhat higher, but has a similar functional form. It is mostly in the form of the resulting eigenfunctions that the difference from the case of  $\gamma = \beta$  is noticeable.

#### 3.6.2 $\gamma = 0$

We now consider the case where we have a  $\beta$  effect but no  $\gamma$  effect, equivalent to  $q = \infty$  in the notation described in Section 3.6. We will increase  $\beta_m$  in the same way as we have previously treated  $\gamma_m$ , while this time keeping  $\gamma_m$  fixed at zero. In this situation, we obtain a basic state (Figure 3.19a) which is qual-

### 3. LINEAR STABILITY OF EQUILIBRIUM BASIC STATES

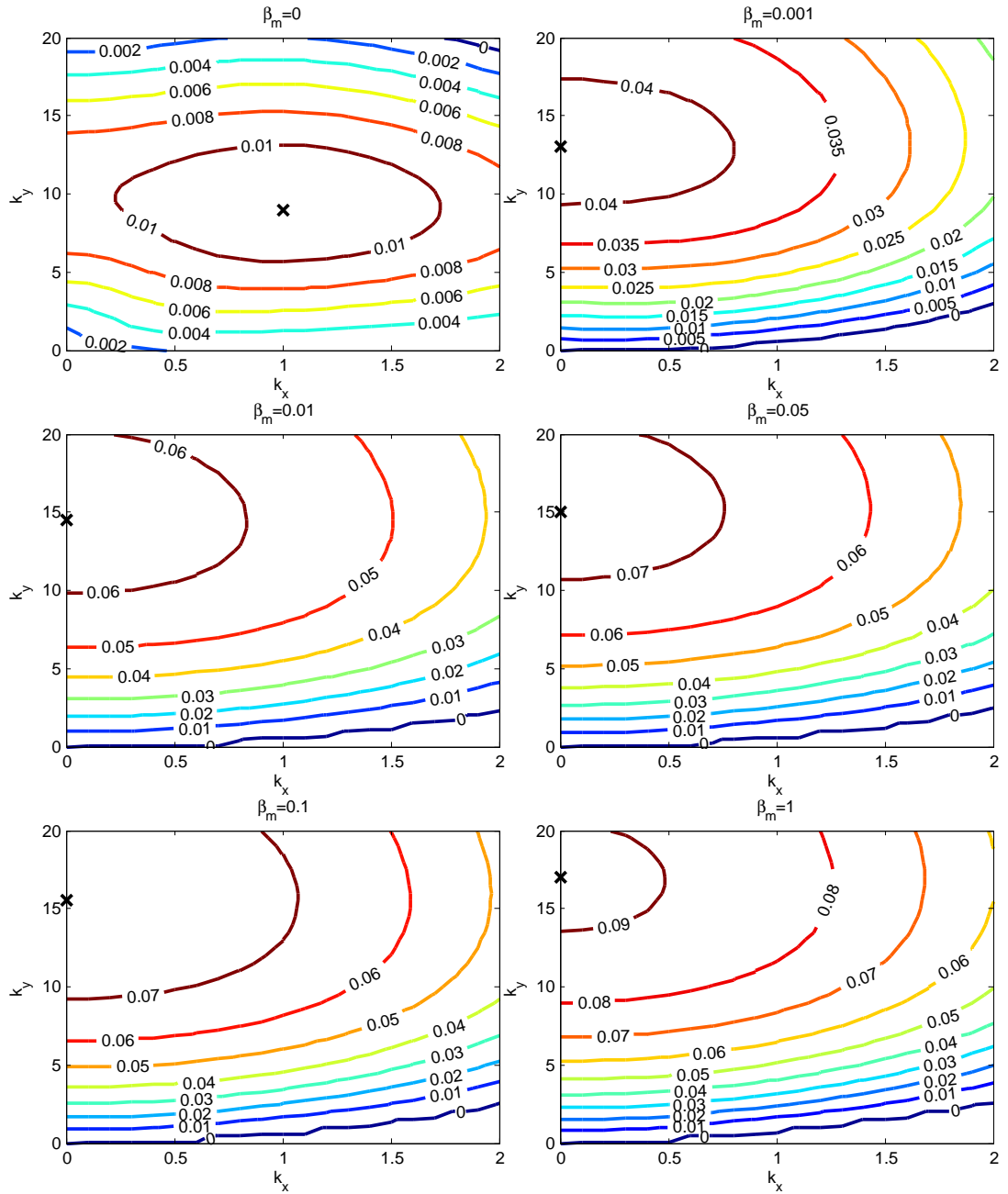


Figure 3.18: Growth rate  $\Re(s)$  as a function of  $k_x$  and  $k_y$  for various values of  $\beta_m$  with  $\gamma = 0$ , for  $F = 10^{-3}$ .

### 3.6 Separating the effects of $\gamma$ and $\beta$

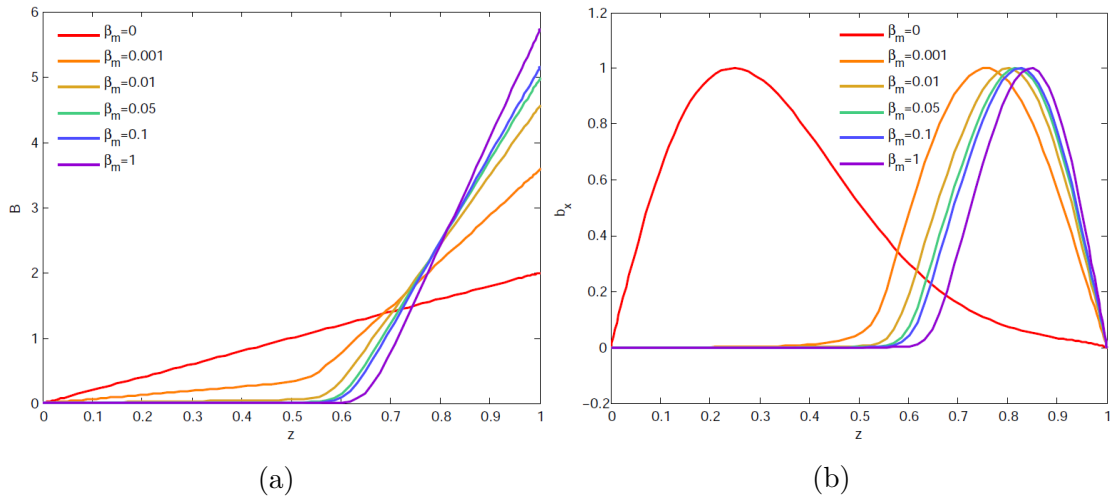


Figure 3.19: (a) Equilibrium basic states and (b) normalised  $\hat{b}_x$  perturbations for the most unstable mode in the cases shown in Figure 3.18, for  $\gamma = 0$ .

itatively similar to the case of equal  $\gamma$  and  $\beta$ , with most of the flux distributed linearly in the lower part of the layer, and with the gradient at the base of the layer increasing as  $\beta_m$  is increased. Also, following the case of  $\gamma = \beta$ , we see the change from 3D to interchange as the most unstable mode occurring between  $\beta_m = 0$  and  $\beta_m = 0.001$  (Figure 3.18). Both the contour plots and the form of the perturbations (Figure 3.19b) are similar to those in the case of  $\gamma = \beta$ . Likewise, the growth rate and horizontal scale of the instability (see Figures 3.14 and 3.15) are similar in this case. This seems to imply that  $\beta$  is the dominant effect in determining the basic state and also its stability in this parameter regime.

This importance of  $\beta$  is not immediately obvious from the form of the equation for the basic state given by (2.2), however, the role of  $\beta$  is more evident when we consider what happens when it is absent. Consider the basic states for  $\gamma = 0$  shown in Figure 3.19a compared to those with  $\beta = 0$  shown in Figure 3.17a, for example. In the case where  $\gamma = 0$ , as discussed in Section 2.10.1, when  $\beta \sim 0$  and  $\gamma$  acts alone apart from a small constant molecular diffusivity, we find that the basic state field is effectively constant where  $\gamma$  is constant, being proportional to  $1/\gamma$ . Furthermore, with boundary condition  $\bar{B}(0) = 0$ , the constant value is fixed at effectively zero at the top of the layer, a dependence borne out by the

### 3. LINEAR STABILITY OF EQUILIBRIUM BASIC STATES

---

basic states shown in Figure 3.17a. However, in the case of non-zero  $\beta$  — with little dependence on the value of  $\gamma_m$  — the magnetic field can have a non-zero gradient and indeed a non-zero value at the top of the layer. This situation, shown in Figure 3.19a as well as being the case for the  $\gamma = \beta$  basic states studied previously, is less sensitive to the value of  $\gamma$ , allowing  $\gamma = 0$  states to have a similar stability to the equivalent cases with non-zero  $\gamma$ .

Having considered the two extreme cases of only  $\gamma$  and only  $\beta$ , we will now discuss some “intermediate” cases and vary the ratio between the two effects. We will still consider  $\beta = q\gamma$ , with proportionality constant  $q$ , for  $q = 10$  and  $q = 0.1$ .

#### 3.6.3 $\beta > \gamma$

The case where  $\beta = 10\gamma$  is similar to several of those that we have already discussed, in the sense that we see a linear profile in the lower half of the layer, with increasing gradient, where molecular diffusion is the dominant effect. In the upper half of the layer,  $\beta$  is the dominant effect. However, the amount of flux here is very small, especially for  $\beta$  much greater than the molecular diffusion. The contour plots for various values of  $\gamma_m$  (with  $\beta_m = q\gamma$ ,  $q = 10$ ) are shown in Figure 3.20, with the corresponding perturbation profiles  $\hat{b}_x$  plotted in Figure 3.21b. We also plot the basic states in Figure 3.21a. These basic states are not greatly different, either qualitatively or quantitatively, from the case where the two effects act equally (Figure 3.4), other than the field gradient being slightly higher for lower values of  $\gamma_m$  when  $\beta(z) = 10\gamma$ . Thus, we do not expect the instability to be very strongly affected, and if we consider the contour plots in  $k_x$ - $k_y$  space, shown in Figure 3.20, we see that this is indeed the case. In fact, in terms of the growth rate (Figure 3.14), both cases are also similar to the case of  $\gamma = 0$ .

We will now compare the case of  $\beta < \gamma$ , using the example case of  $\beta = 0.1\gamma$ .

#### 3.6.4 $\beta < \gamma$

This case provides a clearer insight into the effect of field gradients on the instability. For the basic state (Figure 3.22a) we see that the flux within the region

### 3.6 Separating the effects of $\gamma$ and $\beta$

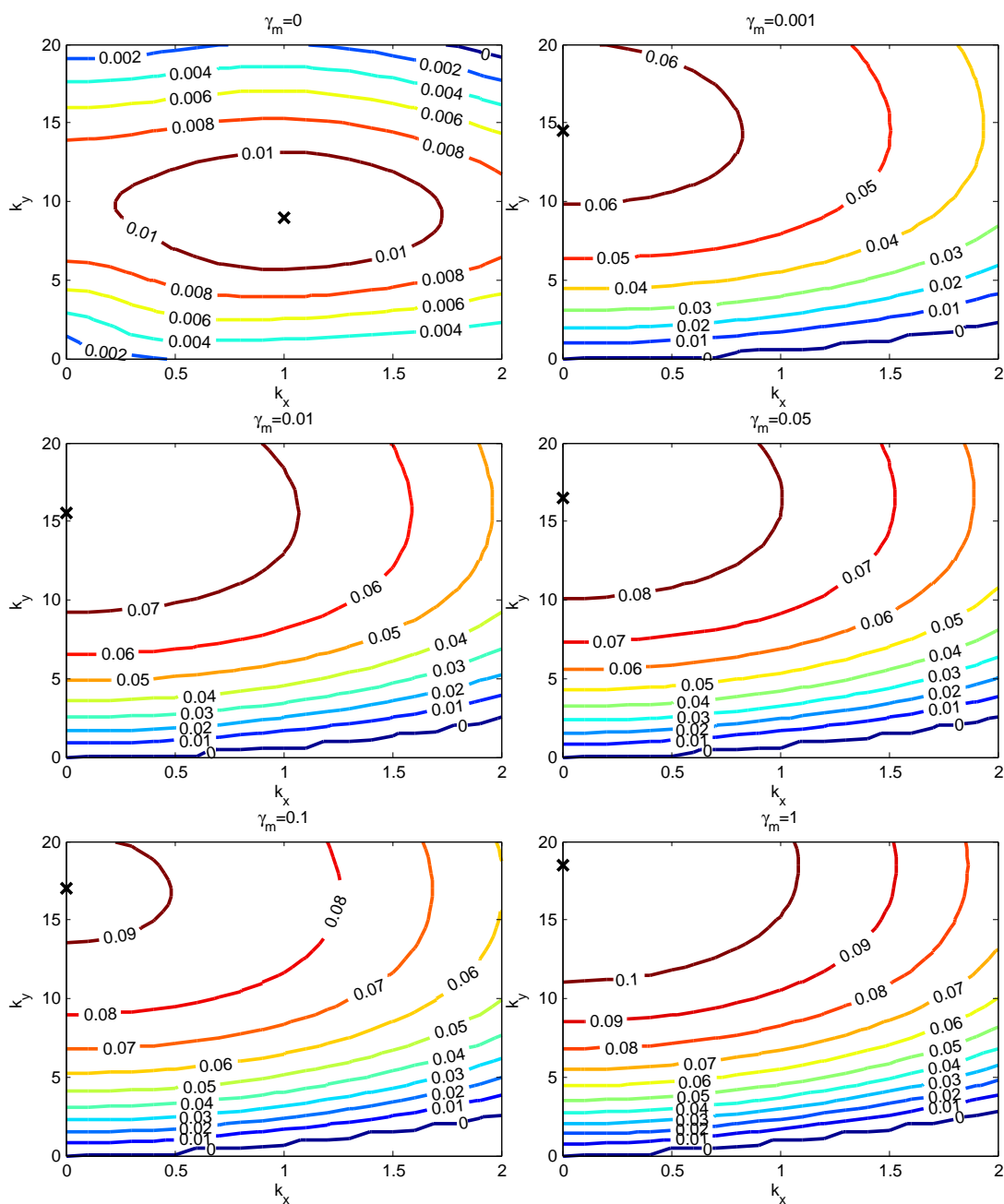


Figure 3.20: Growth rate  $\Re(s)$  as a function of  $k_x$  and  $k_y$  for various values of  $\gamma_m$  with  $\beta = 10\gamma$ , for  $F = 10^{-3}$ .

### 3. LINEAR STABILITY OF EQUILIBRIUM BASIC STATES

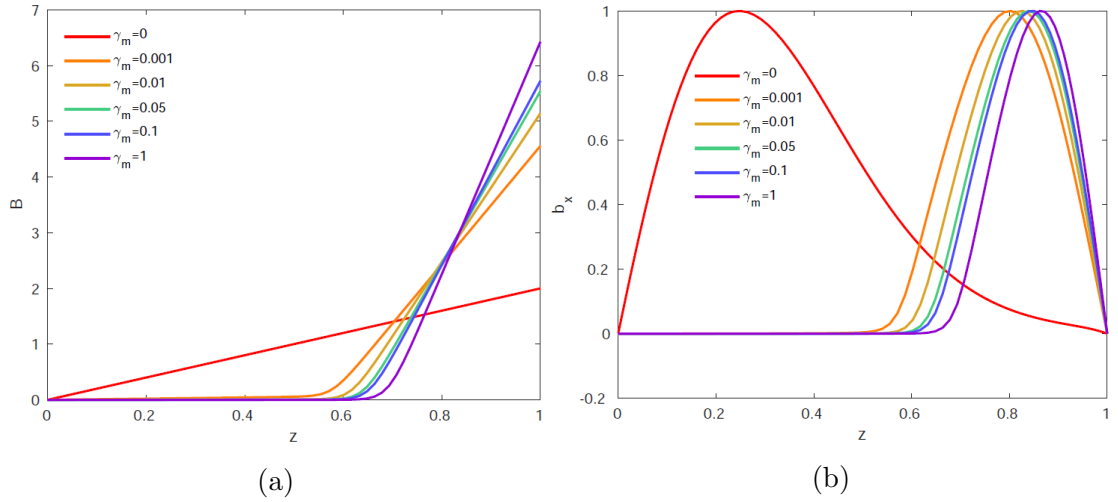


Figure 3.21: (a) Equilibrium basic states and (b) normalised  $\hat{b}_x$  perturbations for the most unstable mode in the cases shown in Figure 3.20, for  $\beta_m = 10\gamma_m$ .

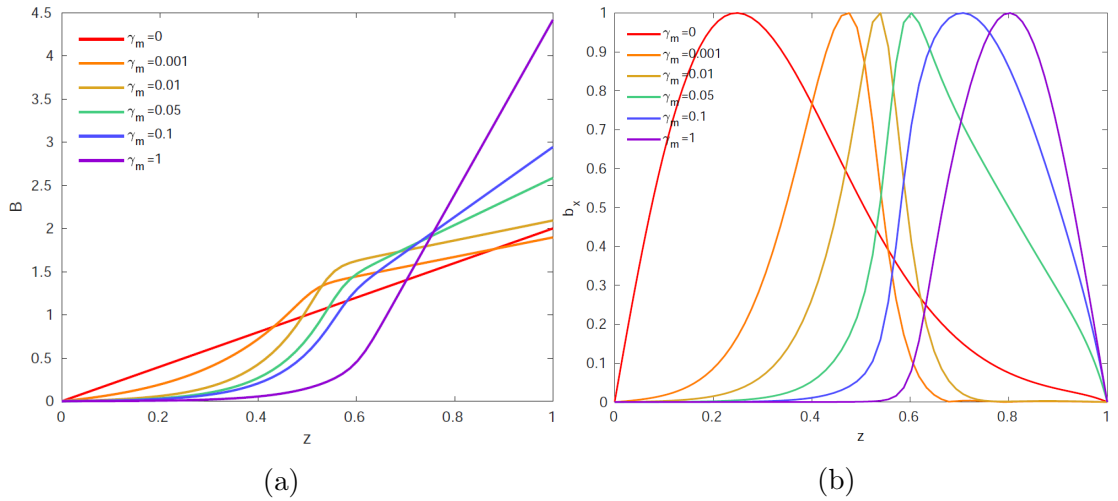


Figure 3.22: (a) Equilibrium basic states and (b) normalised  $\hat{b}_x$  perturbations for the most unstable mode in the cases shown in Figure 3.23, for  $\beta_m = 0.1\gamma_m$ .

### 3.6 Separating the effects of $\gamma$ and $\beta$

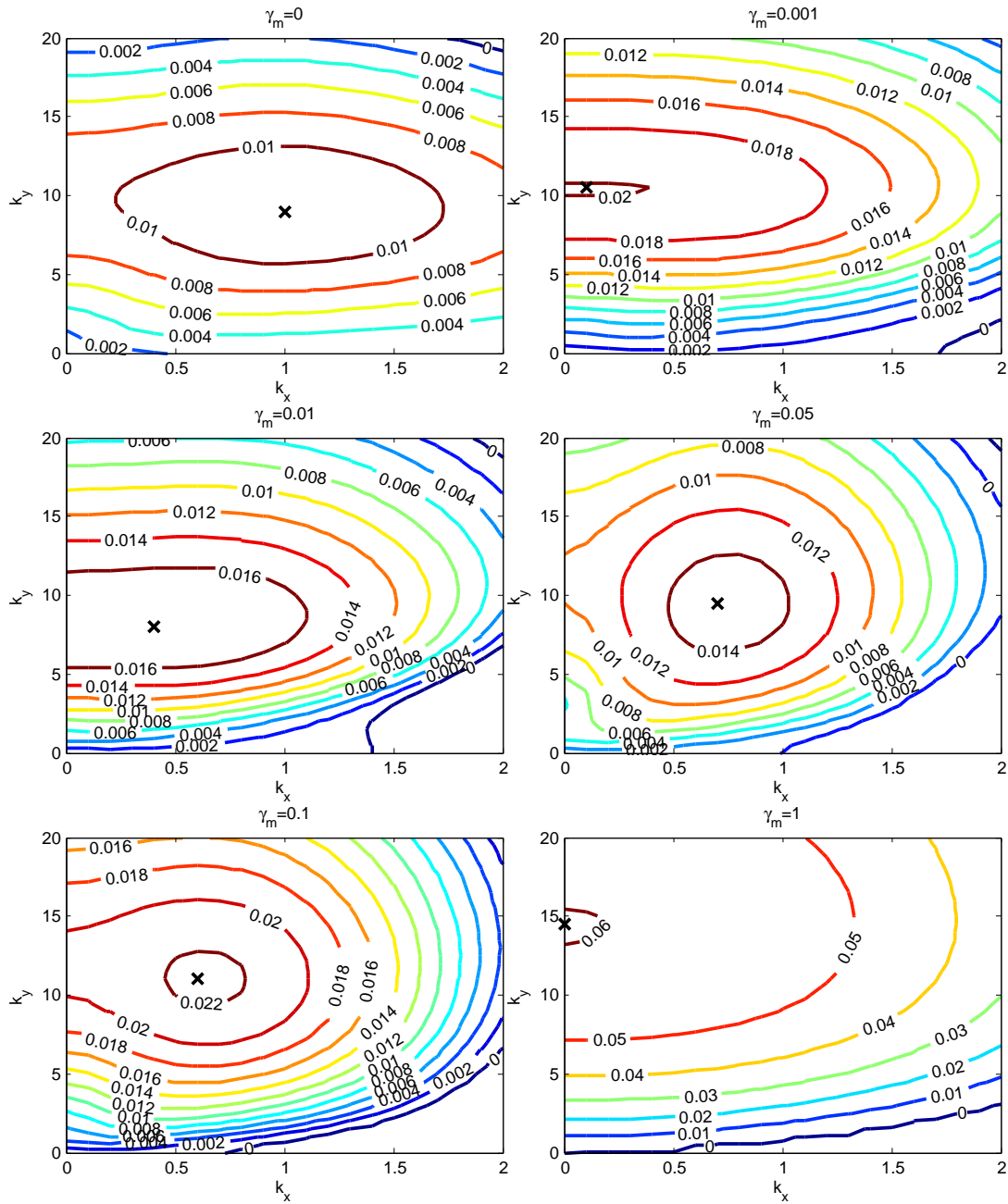


Figure 3.23: Growth rate  $\Re(s)$  as a function of  $k_x$  and  $k_y$  for various values of  $\gamma_m$  with  $\beta = 0.1\gamma$ , for  $F = 10^{-3}$ .

### 3. LINEAR STABILITY OF EQUILIBRIUM BASIC STATES

---

where  $\gamma$  and  $\beta$  are present is distributed in a profile reminiscent of the exponential variation one might expect from analytic considerations in this region (see the discussion on basic states, Chapter 2), and of comparable size to the approximately linear distribution in the lower part of the layer.

This gives rise to a basic state with a high gradient once more in the central region over which  $\gamma$  and  $\beta$  go to zero; see Figure 3.22a. Also, note that in the case of  $\gamma_m = 0.001$  and  $\beta = 0.1\gamma$ ,  $\beta$  is comparable in size to the value of the molecular diffusion,  $\zeta_o C_k = 10^{-4}$ .

With this in mind, we consider the stability. Unlike in the other cases, we do not see the immediate switch from a 3D mode to an interchange mode as  $\gamma$  and  $\beta$  are increased. Rather, the most unstable mode moves towards  $k_x = 0$ , and then back to larger  $k_x$  again, before becoming an interchange mode for  $\gamma_m = 1$ . This last is the result of the fact that for  $\gamma_m = 1$ , we have  $\beta$  of order 0.1 which is now dominant over the molecular diffusion, and so the basic state field looks similar to the cases discussed previously, with minimal curvature of the field in the region where  $\gamma$  and  $\beta$  are present.

We may also consider the form of the perturbation eigenfunctions  $\hat{b}_x$ , shown in Figure 3.22b. The perturbations show a distinct peak concentrated around the point in the layer at which the gradient of the basic state is maximised. In regions of effectively constant  $\bar{B}'$  (for the clearest examples see the linear profile for  $\gamma = \beta = 0$ , as well as the close-to-linear lower portion of the basic state for  $\gamma_m = 1$ ), we see a fairly smooth variation in  $\hat{b}_x$ . In Figure 3.24, we plot the gradient of the basic state  $\bar{B}$  as a function of  $z$ ; note the correspondence in the maxima of these profiles with the location of the perturbation maxima in Figure 3.22b, for which the case of  $\gamma_m = 0.01$  (and, correspondingly,  $\beta_m = 0.1$ ) is a good example. Such a correspondence gives further evidence that the gradient of the basic state is the primary determining factor in the stability and form of the perturbations to the system.

However, it is not necessarily clear why the form of the instability is so different

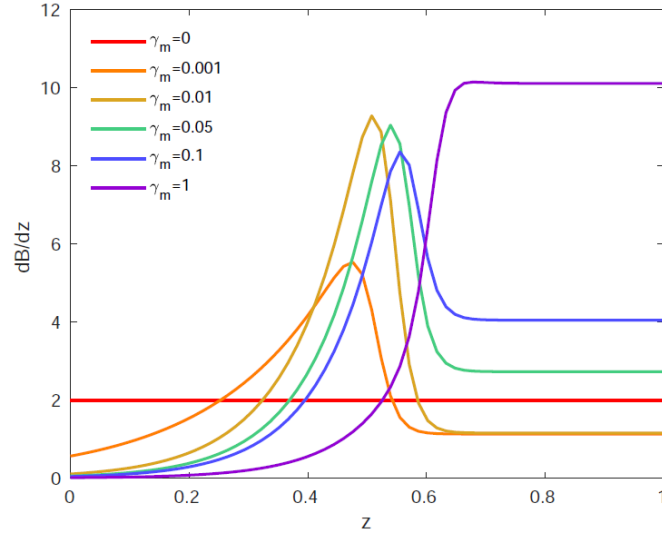


Figure 3.24: Gradients of the basic states for  $\beta = 0.1\gamma$ .

in the case of  $q = 0.1$ ; the basic states and  $\hat{b}_x$  eigenfunctions for  $\beta_m = 0.1\gamma_m$  are at least qualitatively similar to those for  $\beta = 0$  (Figure 3.17), albeit smoother in the case of  $\beta_m = 0.1\gamma_m$ . This suggests that the change from 3D to interchange modes that we observe can be driven — or prevented — by small changes in the gradient around the boundary between the two regions, with a dependence that is not necessarily clear from this analysis alone. Finding a full explanation for this would be a matter for further study.

### 3.7 Summary

In this Chapter, we have considered the linear stability of an equilibrium basic state with boundary conditions  $\bar{B}(0) = 0$  and  $\phi(1) = 1$ , under the turbulent pumping and turbulent diffusion effects characteristic of mean field turbulence in the upper part of a horizontal layer. Broadly, we find that the addition of increased levels of turbulence (given by the “amplitude”,  $\gamma_m$ , of the functional forms of  $\gamma$  and  $\beta$ ) has the effect of changing the most unstable mode of the system from a 3D mode to a 2D,  $k_x = 0$ , interchange mode, as well as increasing the growth rate of the instability overall. This is consistent with the idea that the

### 3. LINEAR STABILITY OF EQUILIBRIUM BASIC STATES

---

stability of the layer is heavily dependent on field gradient, since with increasing  $\gamma_m$ , the gradient of the equilibrium state at the base of the layer is larger. We have considered how this transition from 3D to 2D instability is affected by the field strength  $F$ , as well as the effect of varying the ratio between the strength of  $\gamma$  and  $\beta$ . This has raised questions about to what extent the instability is driven by the action of  $\gamma$  and  $\beta$  on the basic states versus on the perturbations themselves.

We may, however, ask how much of the behaviour we see is due to the effect of  $\gamma$  and  $\beta$  on the perturbations directly, and how much is by way of the use of an equilibrium basic state that depends on  $\gamma$  and  $\beta$ . For that matter, we may also question the assumption that  $\gamma$  and  $\beta$  should be applied equally to all scales of variation in the system; after all, by construction, they are effects that appear in the induction equation for the mean field only. Thus, in the next Chapter, we consider the scale dependence of the effects of  $\gamma$  and  $\beta$  on the instability, and compare the effects of  $\gamma$  and  $\beta$  via the basic state versus on the perturbed quantities directly.

# Chapter 4

## Scale Dependence of the Instability

### 4.1 Effect of $\gamma$ and $\beta$ on the basic state versus the perturbations

As we have discussed in Section 1.4.4, the turbulent pumping and turbulent diffusion effects are derived by making a mean field approximation, and appear in the equation for the large-scale mean field. This means that, physically speaking, they are expected to act on the largest scales of variation of the field only.

In Chapter 3, we made the approximation that the  $\gamma$  and  $\beta$  effects apply at all scales, that is, they act on both the basic states of the system and all scales of the perturbations. This assumption was made as a first approximation, and with the goal of coming to a general understanding of the effects of  $\gamma$  and  $\beta$  on the instability. However, the implicit assumption behind applying  $\gamma$  and  $\beta$  in this way is that all scales of the instability are larger than the scale of the characteristic size of the convection cells in the turbulently convecting region. There is no reason to suppose that this is true, and it is in fact likely not to be the case. Therefore, in this Chapter, we shall consider ways in which we may differentiate between small and large scales of variation in our application of  $\gamma$  and  $\beta$  in the linear stability problem.

#### 4. SCALE DEPENDENCE OF THE INSTABILITY

---

We may, for instance, think of the basic state as corresponding to the mean field, or the largest scale of variation in the system, and the perturbations to the smaller scales. With this assumption, we may model the mean field nature of the  $\gamma$  and  $\beta$  effects by applying them only to the basic state, solving the system of perturbation equations without explicit dependence on  $\gamma$  and  $\beta$ . However, the mean field approximation also contains the assumption that there is a clear separation of scales between the large-scale mean field and the small-scale fluctuations. In our analysis, though, there is less of a division; the perturbations are spread in scale over a large range. This represents an additional departure from the mean field picture inherent in the methodology of Chapter 3. However, since there is not necessarily a large difference between the length scales of the basic state and the largest perturbation scales, we may also consider applying the  $\gamma$  and  $\beta$  effects to the larger scales of the perturbations — effectively considering them as part of the large-scale “mean field” — on a basis that depends on the value of  $k_x$  and  $k_y$ .

Therefore, we will also consider a case in which  $\gamma$  and  $\beta$  are applied to the basic states and also to the larger scale perturbations. This may be considered an “intermediate” approach, between applying  $\gamma$  and  $\beta$  equally to all scales (the case we have considered previously) and the other extreme, which is having only the basic states subject to the  $\gamma$  and  $\beta$  effects. Both of these, however, may be considered refinements to the physical accuracy of the approach we have taken in Chapter 3.

In order to compare the effect of  $\gamma$  and  $\beta$  with regards to the different scale of the problem, we will consider the cases:

1.  $\gamma$  and  $\beta$  act only on the basic state.
2.  $\gamma$  and  $\beta$  act on perturbations on a scale dependent basis, with their effect greatest in magnitude for  $k_x = k_y = 0$ .
3.  $\gamma$  and  $\beta$  act only on the perturbations: an artificial, physically unrealistic comparison case.

---

## 4.2 Applying $\gamma$ and $\beta$ only to the basic state

This will allow us to understand the relative effects of  $\gamma$  and  $\beta$  on the perturbations directly, versus implicitly via the basic state, separating these two effects on the instability that were not necessarily differentiated in the previous analysis. It will also help us to better understand the strong dependence on the basic state seen in results in Chapter 3. Note that for simplicity we will only consider the case of  $\gamma = \beta$ . We will also use the same parameter values as in Chapter 3, which are listed in Table 3.1.

## 4.2 Applying $\gamma$ and $\beta$ only to the basic state

We may argue that formally, the fact that the turbulent pumping and turbulent diffusion effects appear in the mean field induction equation and act on the large-scale mean field implies that to properly model the system, they should only be applied to the largest scale of variation present in the system. Therefore, for the sake of comparison with the simple, all-scales approach of Chapter 3, let us now consider the mean field as corresponding to the basic state  $\bar{B}$ , and apply  $\gamma$  and  $\beta$  only to the equilibrium basic state, leaving them out of the equations for the perturbed system (3.14) – (3.21).

When we carry out this calculation numerically, we produce results that may be compared with those presented in Chapter 3. We find that in fact, the results are, broadly, very similar to those for the case where we apply  $\gamma$  and  $\beta$  to all scales as in Chapter 3. We include, as an example, the contour plots for the cases of  $F = 10^{-3}$  (Figure 4.3) and  $F = 10^{-5}$  (Figure 4.4), for comparison with Figures 3.3 and 3.9 respectively. By comparing the two cases, we can see that the effect on the instability of applying  $\gamma$  and  $\beta$  in this way is small enough to be almost impossible to see by eye on such a diagram, both in terms of growth rates and horizontal scales of the most unstable mode.

In order to better quantify this result we plot the growth rate of the instability at different values of  $F$ , in Figure 4.1. Given the visual similarity of these growth rate results to those of the equivalent case (Figure 3.13) for  $\gamma = \beta$  applied to all scales, we may also plot an “error” quantity, to see more easily the

## 4. SCALE DEPENDENCE OF THE INSTABILITY

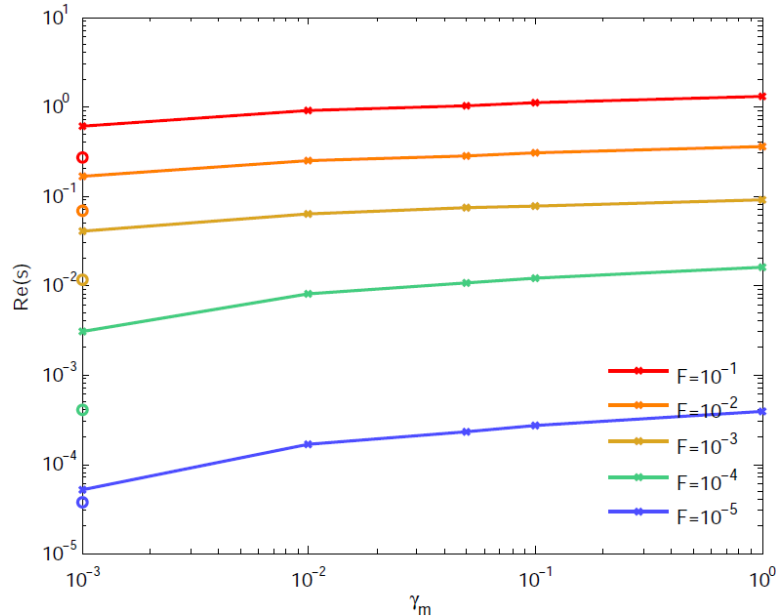


Figure 4.1: Growth rate of the most unstable mode when  $\gamma$  and  $\beta$  are applied only to the basic state,  $F = 10^{-1}, 10^{-2}, 10^{-3}, 10^{-4}, 10^{-5}$ .

difference. We refer to the growth rate of the most unstable mode when  $\gamma$  and  $\beta$  are applied to both the basic state and the perturbations as  $\Re(s_{B+b})$ , and the equivalent growth rate when  $\gamma$  and  $\beta$  are applied only to the basic state (the results plotted in Figure 4.1) as  $\Re(s_B)$ . With this notation, we plot the normalised difference,

$$\text{Difference} = \frac{\Re(s_{B+b}) - \Re(s_B)}{\Re(s_{B+b})}, \quad (4.1)$$

as a function of  $\gamma_m$ , in Figure 4.2. From this we can see that for the ‘‘high  $F$ ’’ cases ( $F \gtrsim 10^{-3}$ , as discussed in the previous Chapter) the behaviour is somewhat different than for the lower  $F$  cases. Thus we consider the two separately.

### 4.2.1 High $F$ Regime

We consider first the cases of  $F = 10^{-1}, 10^{-2}, 10^{-3}$ . We show the contour plots for the case of  $F = 10^{-3}$  in Figure 4.3 as an example. We also show the growth rates of the most unstable modes in Figures 4.1, and the fractional difference from the results when  $\gamma$  and  $\beta$  are applied to all scales in Figure 4.2a. For this

## 4.2 Applying $\gamma$ and $\beta$ only to the basic state

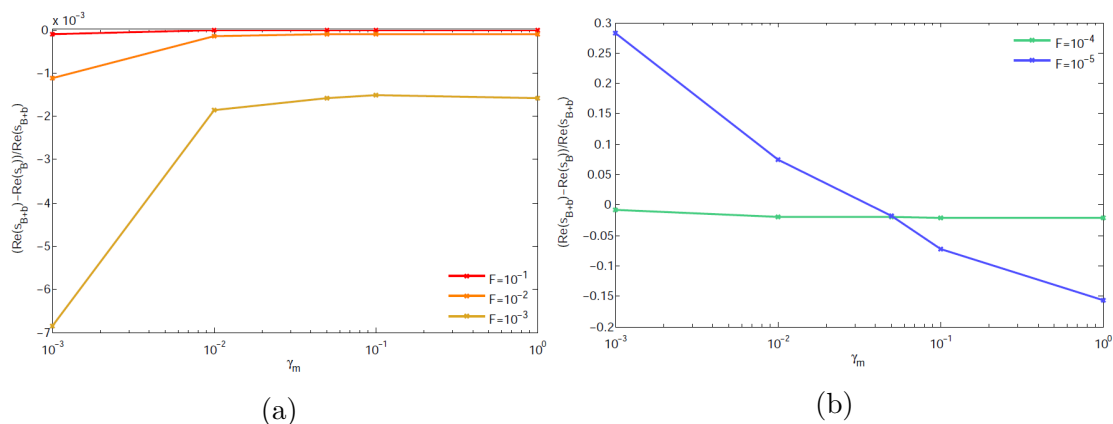


Figure 4.2: Normalised difference in the growth rate of the most unstable mode when  $\gamma$  and  $\beta$  are applied to all scales versus applied only to the basic state, for (a)  $F = 10^{-1}, 10^{-2}, 10^{-3}$ , and (b)  $F = 10^{-4}, 10^{-5}$ . Note that the division of these results into two plots is in part to differentiate the two  $F$  regimes discussed in Section 3.5, which also exist in this case, and in part for convenience as the value of the quantity defined by Equation (4.1) is of a different order of magnitude in the two regimes, especially in the case of  $F = 10^{-5}$ .

high  $F$  regime, the quantity (4.1) is negative, and decreases in magnitude as  $\gamma_m$  increases. Also, the effect of larger  $F$  is to decrease the magnitude of this error. (Note that because we select the most unstable mode such that  $\Re(s_{B+b})$  and  $\Re(s_B)$  are always positive, the sign of (4.1) indicates whether the addition of the  $\gamma$  and  $\beta$  effects to the perturbed quantities is stabilising or not; if (4.1) is positive, the effect of  $\gamma$  and  $\beta$  on the perturbations is destabilising, and if (4.1) is negative,  $\gamma$  and  $\beta$  acting on the perturbations have a stabilising effect.)

This implies that in the case of the interchange maxima, the effect of  $\gamma$  and  $\beta$  on the perturbations is stabilising, though small in comparison to the destabilising effect of  $\gamma$  and  $\beta$  on the basic state. This is consistent with the idea that the predominant factor in destabilising the system is the form of the basic state, as implied by the similarity between the contour plots 4.3 compared to 3.3. Furthermore, it shows that this effect is greater for lower  $F$  in this regime, though this is likely to be a product of the fact that lower  $F$  gives lower growth rates in general.

#### 4. SCALE DEPENDENCE OF THE INSTABILITY

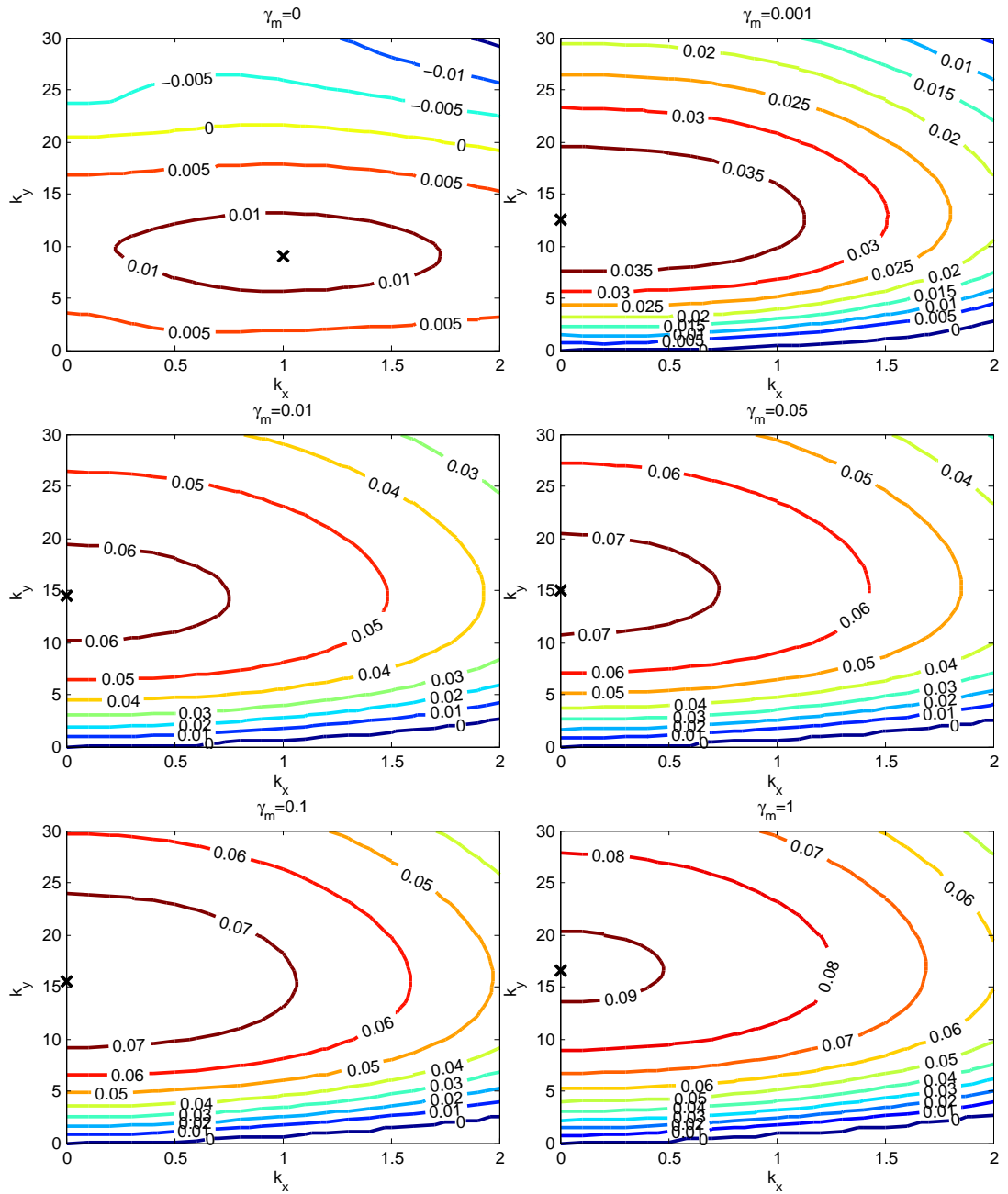


Figure 4.3: Contour plots for  $F = 10^{-3}$  and various values of  $\gamma_m$ , with  $\gamma = \beta$  applied only to the basic state; cf. Figure 3.3.

### 4.2.2 Low $F$ Regime

The regime of lower field strength,  $F = 10^{-4}, 10^{-5}$ , (contour plots shown in Figure 4.4 for the case of  $F = 10^{-5}$ , with growth rates of the most unstable mode and associated fractional difference from application of  $\gamma$  and  $\beta$  to all scales in Figures 4.1 and 4.2b) is characterised by the most unstable mode remaining 3D for higher levels of  $\gamma$  and  $\beta$ . In this case the effect of increasing  $\gamma_m$  is stabilising, as the gradient of (4.1) with respect to  $\gamma_m$  is negative. We consider the two cases shown in Figure 4.2b. For  $F = 10^{-4}$ ,  $\Re(s_{B+b}) - \Re(s_B) < 0$  still, but in this case the effect of additional  $\gamma_m$  further stabilises the system, since the gradient is negative. In the case of  $F = 10^{-5}$ , the gradient is of larger magnitude and remains negative. However, in this case we in fact see it pass through  $\Re(s_{B+b}) - \Re(s_B) = 0$ , i.e. low levels of  $\gamma$  and  $\beta$  on the perturbations are actually destabilising, while higher levels are, as before, stabilising. This, however, may simply be due to the fact that for this value of  $F$  the system is less unstable in general, and the difference is only an order of magnitude or so less than the growth rates themselves.

Overall, this analysis very much supports the idea that the growth rate and horizontal scale of the most unstable mode are much more dependent on the basic state than on the effect of  $\gamma$  and  $\beta$  on the perturbations. Here, we have considered the perturbations as a whole, regardless of scale. However, we may also consider larger-scale perturbations to be part of the “mean field” variation and thus subject to  $\gamma$  and  $\beta$ . In the next section, we apply  $\gamma$  and  $\beta$  on the basis of  $k_x$  and  $k_y$ .

## 4.3 Scale-dependent $\gamma$ and $\beta$

In the mean field approximation, we make the assumption of separation of scales; that is to say, we assume that the largest scale of variation is much larger than the small-scale turbulent motion, such that we may take spatial averages over an intermediate scale that is separated from both the small and the large components. This is the assumption upon which the derivation of the  $\gamma$  and  $\beta$  effects

#### 4. SCALE DEPENDENCE OF THE INSTABILITY

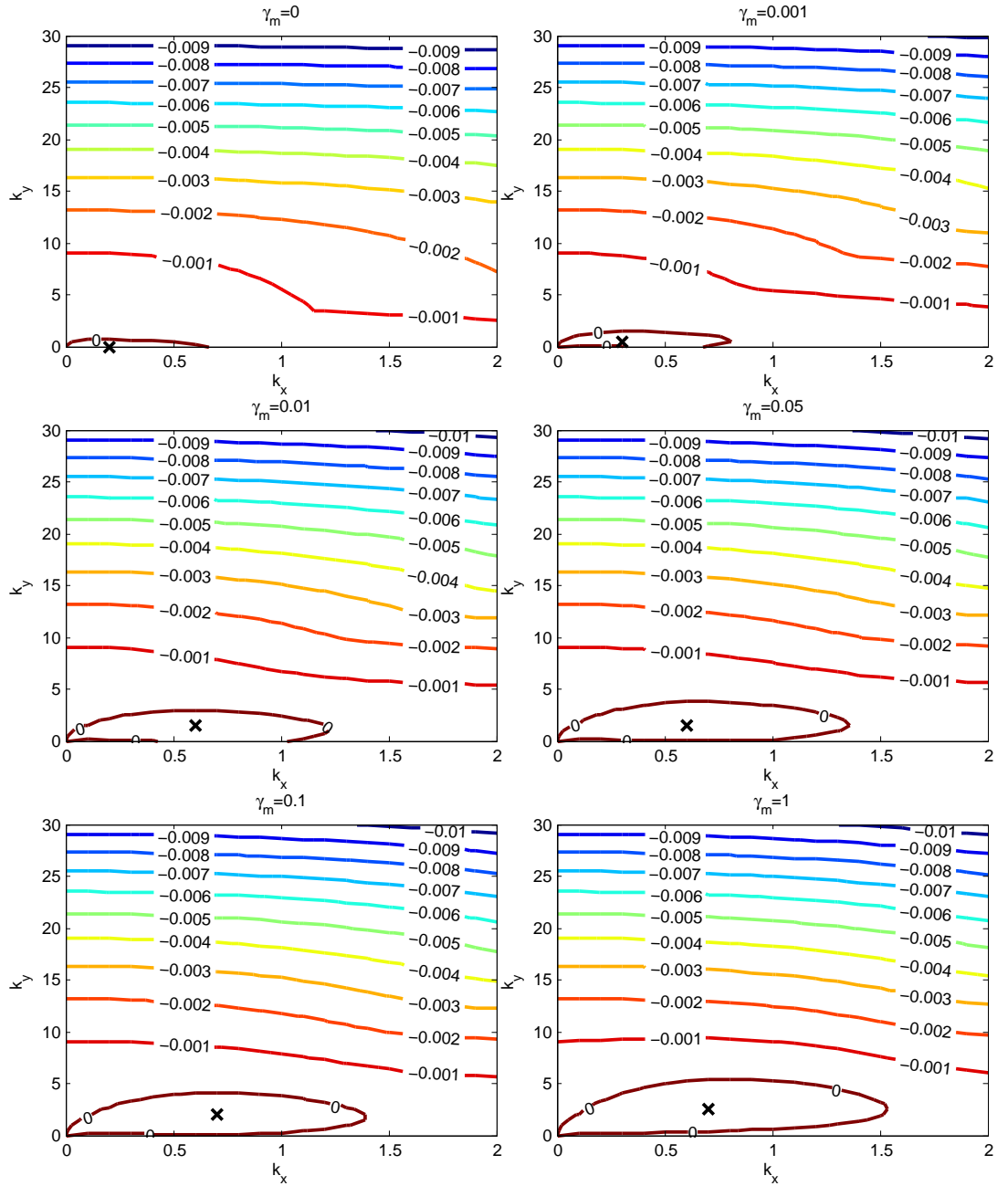


Figure 4.4: Contour plots for  $F = 10^{-5}$  and various values of  $\gamma_m$ , with  $\gamma = \beta$  applied only to the basic state; cf. Figure 3.9.

is based. In a real system, however, we see many scales of variation with no such clear separation of scales. Thus, we consider the case where the basic state is not the only variation that may be considered “large-scale” under the mean field approximation; if it is the case that the turbulence does not, in fact, have a clear separation of scales, it is possible that the larger scales of the perturbations may also be counted as “mean field”, if we are to apply the mean field approximation to such a system.

We shall take account of this possibility by applying  $\gamma$  and  $\beta$  to both the basic state and preferentially to the largest scale perturbations. We multiply  $\gamma$  and  $\beta$  by a function of  $k_x$  and  $k_y$  that peaks at  $k_x = k_y = 0$ , though what form this function takes is a matter of choice. We apply  $\gamma$  and  $\beta$  to the basic state and the perturbations, but when applying to perturbed quantities we multiply by a factor, to obtain  $\gamma_p$ , the  $\gamma$  effect as it applies to the perturbations:

$$\gamma_p = \left( \frac{1}{1 + k_x^2 + k_y^2} \right) \frac{\gamma_m}{2} (1 + \tanh(a(z_i - z))), \quad (4.2)$$

where we assume  $a = 30$  and  $z_i = 0.5$ . Once more, we take  $\beta_p = \gamma_p$  for the  $\beta$  effect acting on the perturbed quantities. With this assumption, we solve the linear system (3.14) – (3.21) as before for all  $F$  previously considered, and show the case of  $F = 10^{-3}$  as an example in Figure 4.5.

We obtain results that, again, look very similar to those of Section 3.4, and, indeed, those of Section 4.2; the scaling of  $\gamma$  and  $\beta$  on the perturbations is not apparent in the contour plots shown in Figure 4.5.

We also consider the growth rate (Figure 4.6) and the difference in the growth rate from the “standard” case considered in the previous chapter, in which  $\gamma$  and  $\beta$  are applied to all scales. We define this fractional difference analogously to (4.1), but instead of  $\Re(s_B)$  we substitute  $\Re(s_{B+b_k})$ , the growth rate for the most unstable mode of the instability with  $\gamma$  and  $\beta$  applied to the perturbations according to (4.2). We plot this quantity in Figure 4.7.

#### 4. SCALE DEPENDENCE OF THE INSTABILITY

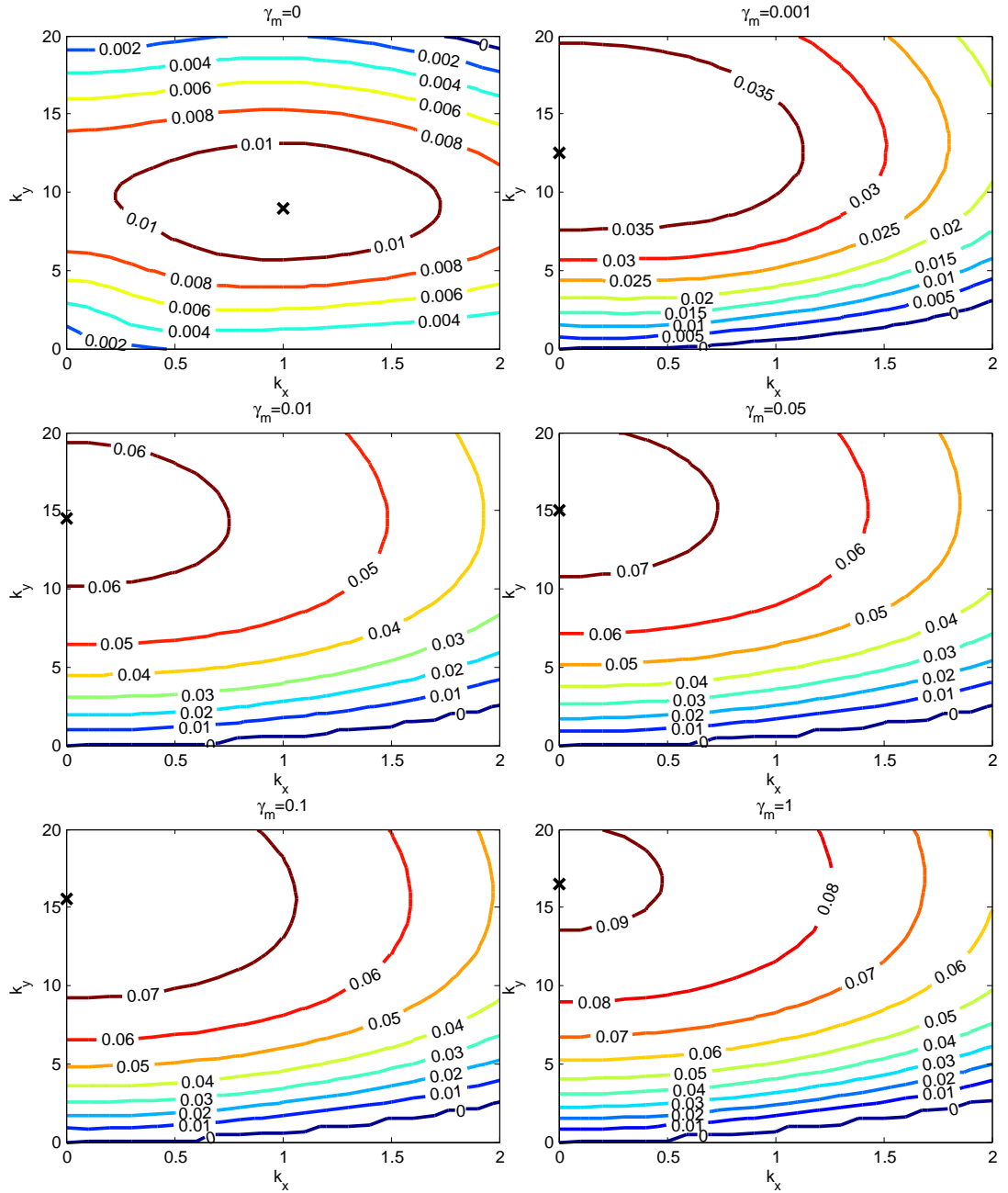


Figure 4.5: Contour plots for  $F = 10^{-3}$  for various values of  $\gamma_m$ , with  $\gamma = \beta$  applied to the basic state according to (2.4), (2.5) and to the perturbations according to (4.2).

### 4.3 Scale-dependent $\gamma$ and $\beta$

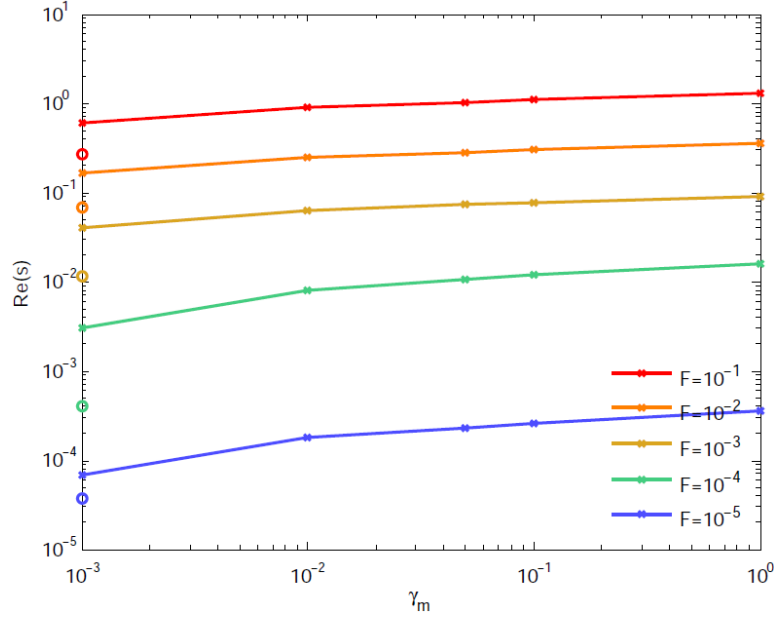


Figure 4.6: Growth rate of the most unstable mode when  $\gamma$  and  $\beta$  are applied to the perturbations according to (4.2), for  $F = 10^{-1}, 10^{-2}, 10^{-3}, 10^{-4}, 10^{-5}$ .

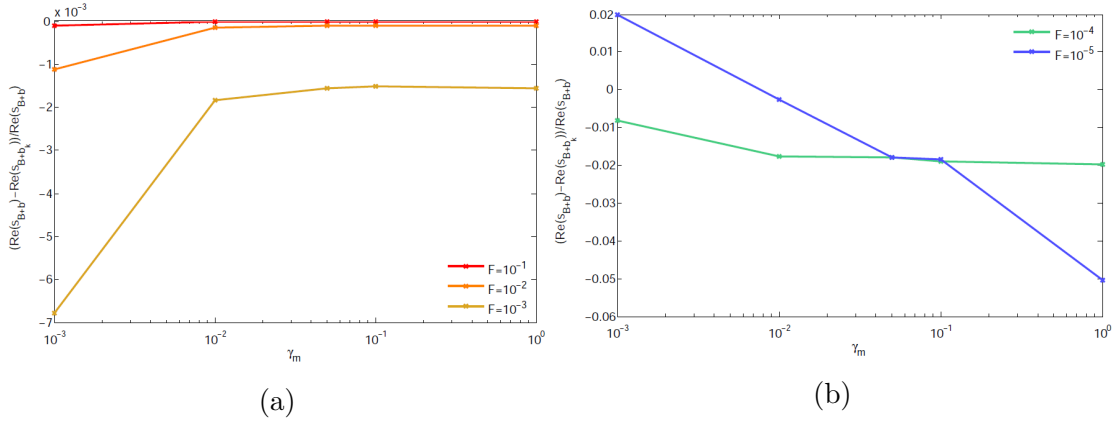


Figure 4.7: Fractional variation of the growth rate of the most unstable mode when  $\gamma$  and  $\beta$  are applied to the perturbations according to (4.2), compared to equal application to all scales, for (a)  $F = 10^{-1}, 10^{-2}, 10^{-3}$ , and (b)  $F = 10^{-4}, 10^{-5}$ .

## 4. SCALE DEPENDENCE OF THE INSTABILITY

---

These results are very similar to those in Section 4.2. This may be expected, as we have already shown that the direct effect of  $\gamma$  and  $\beta$  on the perturbed quantities is very much outweighed by their effect on the instability via the basic state. Therefore, it is natural to assume that the case where we “soften” the effect on the perturbations should be even more marginal than removing it entirely. This is indeed the result we find, and the case of  $\gamma$  and  $\beta$  applied according to (4.2) may be considered an intermediate case between those of Sections 3.4 and 4.2.

We may also characterise the effect of  $\gamma$  and  $\beta$  on the perturbations in a more direct way, by considering the effect of  $\gamma$  and  $\beta$  on the perturbations alone, in isolation from their effect on the basic state. In the next section, we will fix a basic state that is independent of  $\gamma$  and  $\beta$  and consider the action of the turbulent effects on the perturbed quantities alone. This kind of analysis is somewhat artificial with respect to a physical system, however, it serves as a useful comparison case.

### 4.4 Prescribed Basic States

#### 4.4.1 $\bar{B} = 2z$

Previously, we have applied  $\gamma$  and  $\beta$  to all scales of the system, then to only the largest scale, given by the basic state, in order to reflect the mean field nature of these effects. As an intermediate case, we have also applied  $\gamma$  and  $\beta$  to the basic state and preferentially to the largest perturbation scales. We found little difference in the results in these cases (except for a small, generally stabilising, effect of  $\gamma$  and  $\beta$  as they act directly on the perturbations) suggesting that the primary mechanism for the destabilisation of the layer by  $\gamma$  and  $\beta$  is via their effect on the field gradient at equilibrium.

However, we may also test this conclusion by taking an approach that is effectively the opposite extreme: instead of perturbing only the basic state, we shall take a basic state that is an equilibrium when  $\gamma$  and  $\beta$  are absent, and

## 4.4 Prescribed Basic States

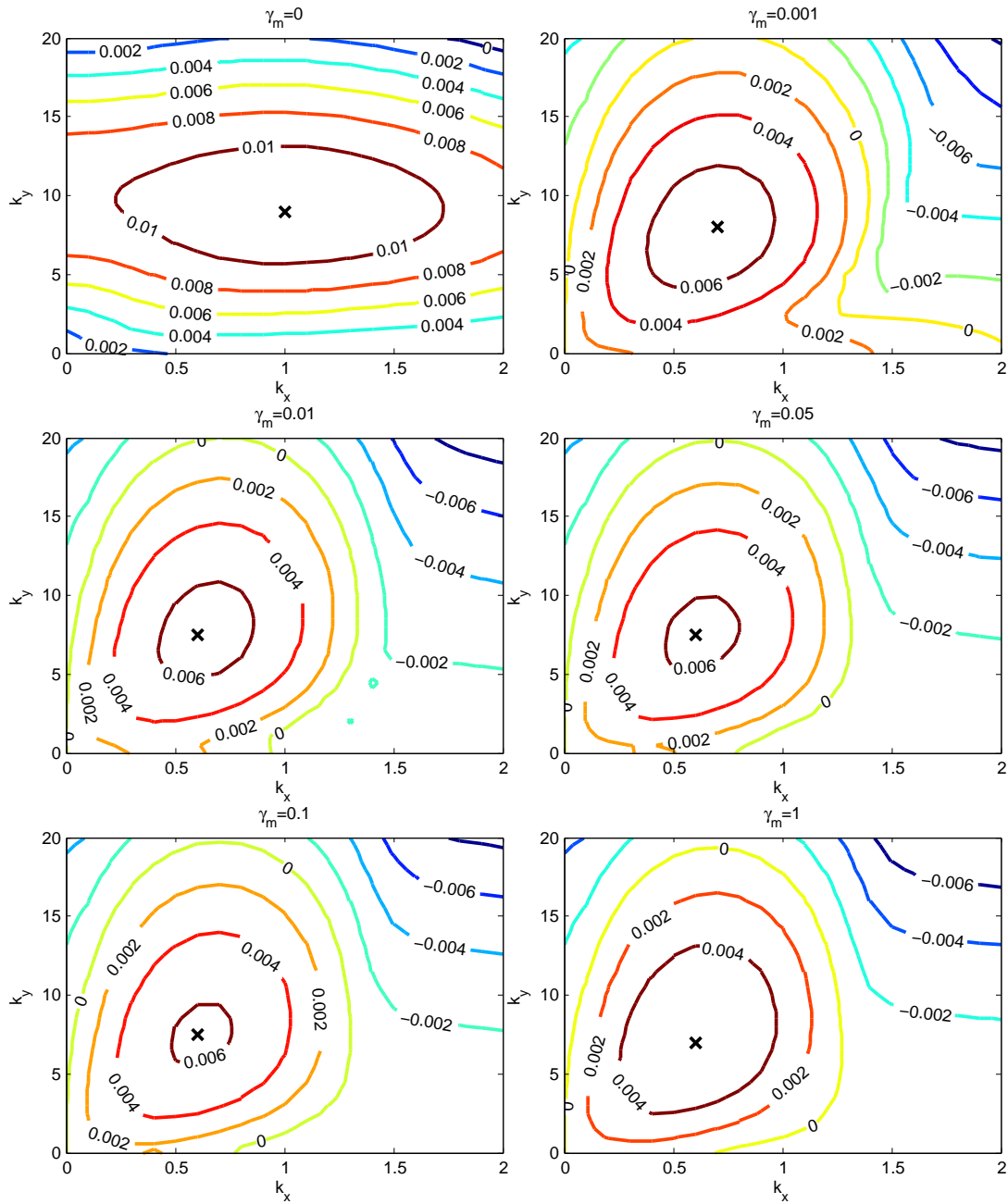


Figure 4.8: Growth rate  $\Re(s)$  as a function of  $k_x$  and  $k_y$  for various values of  $\gamma_m$ , for  $F = 10^{-3}$ , with prescribed basic state  $\bar{B} = 2z$ .

#### 4. SCALE DEPENDENCE OF THE INSTABILITY

---

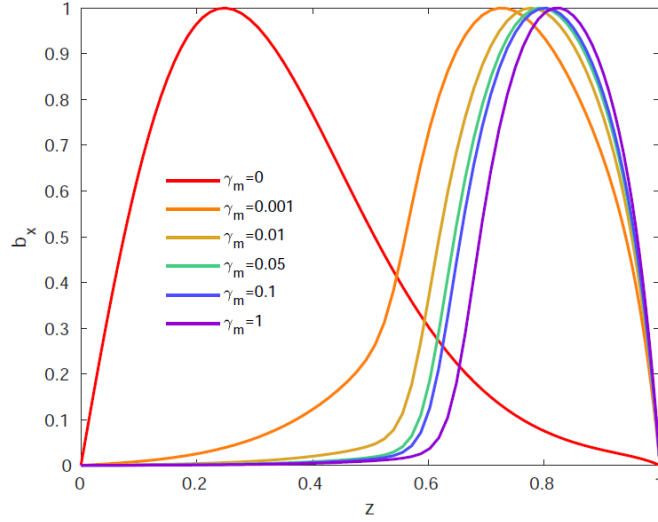


Figure 4.9: Normalised  $\hat{b}_x$  perturbations for the case of  $\bar{B} = 2z$ , for the most unstable modes in the cases shown in Figure 4.8.

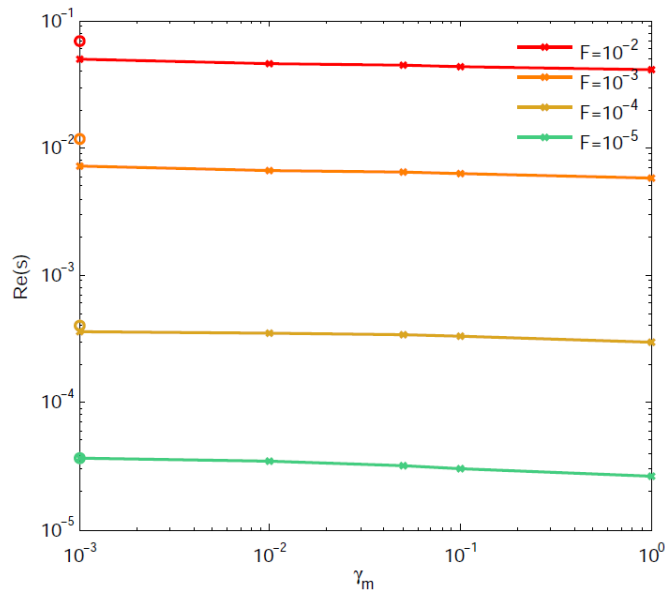


Figure 4.10: Growth rate of the most unstable mode for prescribed basic state  $\bar{B} = 2z$ .

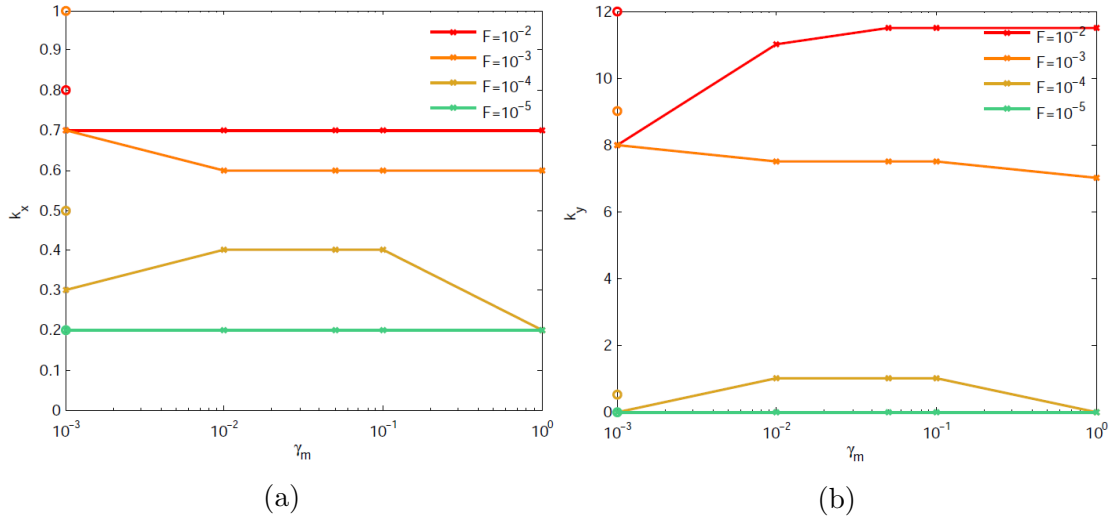


Figure 4.11: Horizontal scales (a)  $k_x$  and (b)  $k_y$  of the most unstable mode for prescribed basic state  $\bar{B} = 2z$ , with  $\gamma_m = 0$  values plotted on the vertical axis. Note the lack of transition to interchange modes at higher  $\gamma_m$ .

apply  $\gamma$  and  $\beta$  only to the perturbations. Although this is an unphysical case, it allows us to separate the much smaller effect of  $\gamma$  and  $\beta$  on the perturbations only.

Thus, we will prescribe a basic state  $\bar{B} = 2z$ , which is an equilibrium in the absence of  $\gamma$  and  $\beta$ , and is subject to the same boundary conditions as the equilibrium basic states we have considered. Artificially introducing this basic state, we will solve perturbation equations (3.14) – (3.21) as before.

The differences are apparent in the contour plots, shown in Figure 4.8, as compared to those in Figures 3.3, i.e. the case where the  $\gamma$  and  $\beta$  effect are applied to both the basic state and the perturbations for otherwise identical parameter values. For the basic state  $\bar{B} = 2z$ , we do not see the same destabilisation resulting from increased  $\gamma$  and  $\beta$  as we do in the case of the self-consistent basic state, nor do we see the change in the most unstable mode from 3D to interchange (see  $k_x$  and  $k_y$  of the most unstable mode, shown in Figure 4.11), as discussed in Chapter 3. Most significantly, when applied to the perturbations only,  $\gamma$  and  $\beta$  have a stabilising effect (see Figure 4.10), for all values of  $F$  considered. In comparison

## 4. SCALE DEPENDENCE OF THE INSTABILITY

---

with the destabilising effect when  $\gamma$  and  $\beta$  act on the basic states, however, this stabilising effect on the perturbations is small, which is why it was not apparent from the results of the analysis with a basic state subject to  $\gamma$  and  $\beta$ . The idea of the effect of  $\gamma$  and  $\beta$  on the perturbations being stabilising when separated from the much larger destabilising effect of  $\gamma$  and  $\beta$  on the basic state, however, is consistent with the results in Sections 4.2 and 4.3. Note, however, that the spatial forms of the  $\hat{b}_x$  perturbations (Figure 4.9) for  $\gamma_m > 0$  do still appear to be governed by the effects of  $\gamma$  and  $\beta$ , being effectively confined to the lower part of the layer as  $\gamma_m$  increases. This effect, however, is not as strong as that seen in the case of varying field gradient, shown in Figure 3.5. It suggests, however, that while the basic state is the main factor in determining the growth rate and horizontal scale of the instability, the vertical location of the perturbation is more directly affected by the terms in the linear system itself.

### 4.4.2 Magnetic slab between $z = 0.6$ and $z = 0.8$

Though it does not use a self-consistent equilibrium basic state, this case is of interest in relation to the magnetic “slab” or top hat field commonly used in numerical simulations of such systems, for example by [Barker \*et al.\* \(2012\)](#). Following this study, we prescribe a basic state of the form:

$$B = B_o(\tanh(a_B(z - z_1)) - \tanh(a_B(z - z_2))) \quad (4.3)$$

where  $B_o = 0.5$ ,  $a_B = 30$ ,  $z_1 = 0.6$  and  $z_2 = 0.8$ . This creates a top hat profile, shown in Figure 4.12, above which  $\gamma$  and  $\beta$  fall to zero. The region of greatest field is  $0.6 \lesssim z \lesssim 0.8$ , which is below the region where the  $\gamma$  and  $\beta$  effects act within the layer ( $0 \leq z \lesssim 0.5$ ), though due to the “gradient” parameters  $a$  and  $a_B$  being non-infinite, there is some overlap present.

In order to make a comparison, we first consider the case of such a top hat field without the effects of  $\gamma$  and  $\beta$ . We find that in this case, the most unstable mode is an interchange mode (see Figure 4.13). However, there is also another local maximum in  $\Re(s)$ ; this occurs for  $k_y = 0$ , i.e. there is another peak in instability for 2D undular modes.

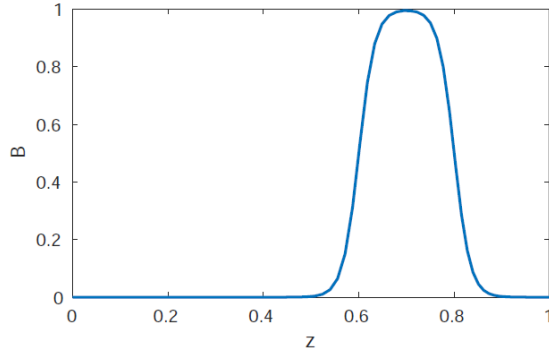


Figure 4.12: The top hat field given by Equation (4.3), with  $B_o = 0.5$ ,  $a_B = 30$ ,  $z_1 = 0.6$  and  $z_2 = 0.8$ .

Furthermore, as we increase  $\gamma$  and  $\beta$ , we find that these 2D undular modes grow more unstable, even as interchange modes become less so. We find that increasing the value of  $\gamma_m$  has several effects: first, it decreases the growth rate of interchange modes, as is the case for the  $\bar{B} = 2z$  prescribed basic state. This is consistent with the idea that the change in the basic state under the action of  $\gamma$  and  $\beta$  is responsible for the large increase in instability we see in the fully-consistent cases. However, in this case, where 2D undular modes are already present in the system, they grow more unstable under the effect of  $\gamma$  and  $\beta$  on the perturbed quantities alone. Furthermore, when large enough  $\gamma$  and  $\beta$  are applied there comes a point at which the undular maximum on the  $k_y = 0$  axis becomes a global maximum, implying that 2D undular modes should come to dominate over interchange modes at some threshold  $\gamma_m$ . This means that applying greater  $\gamma$  and  $\beta$  effects changes the spatial form of the instability under these conditions.

Also, in this case, though we do have unstable 3D modes ( $k_x, k_y \neq 0$ ), they are not the most unstable in the system for any of the cases we have considered. This is the case for both  $F = 10^{-2}$  and  $F = 10^{-3}$ , though the change in the nature of the instability is more sensitive to  $\gamma$  and  $\beta$  (i.e. occurs at a lower  $\gamma_m$ ) for  $F = 10^{-3}$  (shown as an example case in Figure 4.13), as we may expect from

#### 4. SCALE DEPENDENCE OF THE INSTABILITY

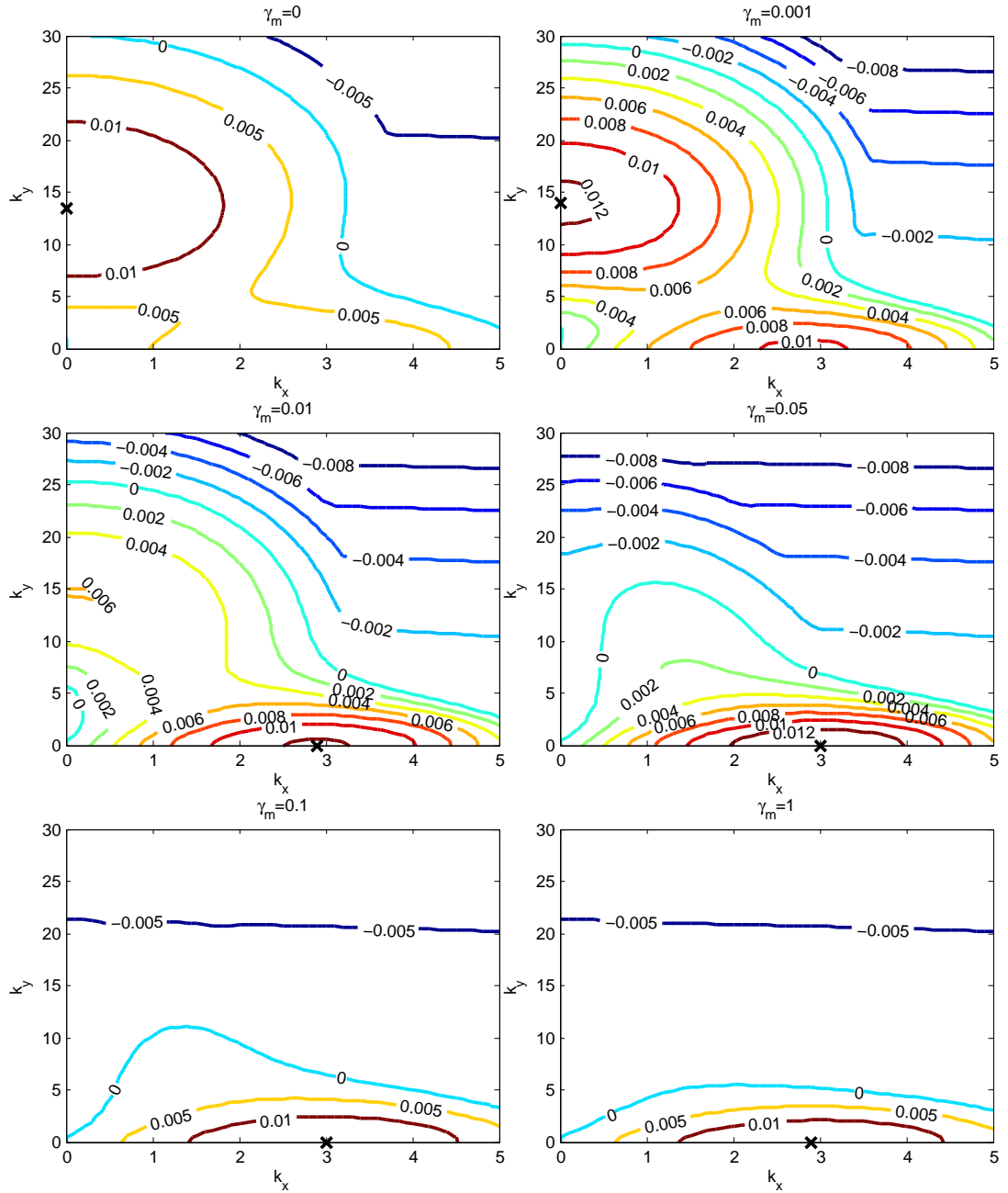


Figure 4.13: Growth rate contour plots for various values of  $\gamma_m$ , for the case  $F = 10^{-3}$ , with prescribed “top hat” basic state. Note the global maxima (marked with a cross) are interchange modes for  $\gamma_m = 0$  and  $\gamma_m = 0.001$  only. For higher  $\gamma_m$  the interchange maximum is a local one, and the fastest growing mode is 2D undular, with  $k_y = 0$ .

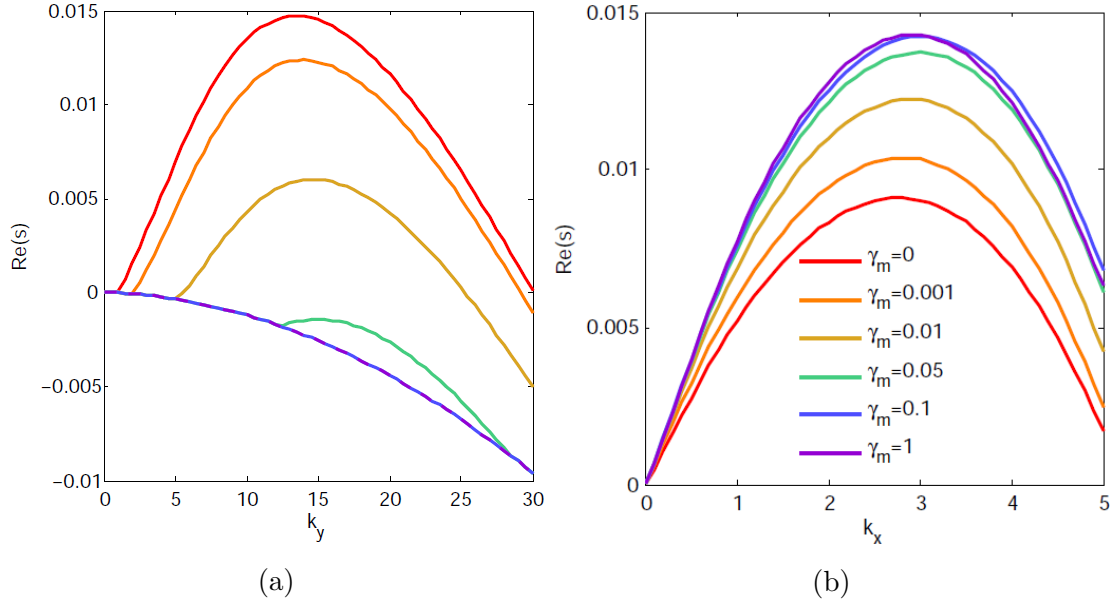


Figure 4.14: Comparison of (a) interchange ( $k_x = 0$ ) and (b) 2D undular ( $k_y = 0$ ) instability maxima for a prescribed top hat basic state, with various values of  $\gamma_m$  and for  $F = 10^{-3}$ .

the discussion of the effect of field strength  $F$  in Chapter 3.

We also notice that the change in stability is not linear in  $\gamma_m$ . Consider Figure 4.14, in which we plot the value of  $\Re(s)$  along both the  $k_y$ - and  $k_x$ -axes of the contour plots in Figure 4.13, corresponding to interchange and 2D undular modes respectively. From this, it becomes clear that there is a “saturation” effect occurring as the strength of the  $\gamma$  and  $\beta$  effects are increased. In the case of interchange modes (Figure 4.14a), as  $\gamma_m$  is increased, the value of the growth rate as a function of  $k_y$  approaches a constant profile with  $\Re(s) < 0$ , i.e. the limit of large  $\gamma_m$  gives stable interchange modes, whose stability is then unchanged as  $\gamma$  and  $\beta$  are further increased. By contrast, for 2D undular modes (Figure 4.14b), we see the stability shift with the application of larger amplitudes of  $\gamma$  and  $\beta$ ; the shape of the profile of  $\Re(s)$  remains approximately the same, however it becomes larger in amplitude, corresponding to the destabilisation of 2D undular modes — and their eventual dominance over the interchange and 3D instabilities — that we have discussed. We still see a limiting  $\Re(s)$  profile (as a function of  $k_x$ ) emerging

## 4. SCALE DEPENDENCE OF THE INSTABILITY

---

for increasing  $\gamma_m$ ; however, there is not such a clear limiting profile for the undular maxima in Figure 4.14b as we see for the interchange maxima in Figure 4.14a.

The destabilisation of 2D undular modes is of note because Hughes & Cattaneo (1987) showed that in general, 2D undular modes of the magnetic buoyancy instability are less easily destabilised than 3D or interchange modes. This conclusion is also borne out by our other linear stability results for a system with  $\gamma$  and  $\beta$  effects present, discussed throughout Chapters 3 and 4, where 3D and interchange modes are preferred over 2D undular modes. In the case of the prescribed top hat basic state field with  $\gamma$  and  $\beta$  effects of sufficient strength, however, we find that 2D undular modes are not only destabilised, but, in fact, preferred over interchange and 3D modes for some threshold level of  $\gamma_m$ . The physical explanation for this is not clear from our analysis alone, but represents grounds for future study in order to come to a fuller understanding of the prevalence of 2D undular modes under such circumstances.

In general, the destabilisation of undular modes for the top hat basic state — in contrast to the other cases with  $\gamma$  and  $\beta$  we have studied — shows that the use of a top hat basic state field, which is artificially imposed and does not represent an equilibrium under the effects of  $\gamma$  and  $\beta$ , is able to significantly change the nature of the instability. Therefore, our results indicate that care should be taken when making use of such top hat fields in other work in the area, lest the choice of basic state introduce additional effects that would not be present in the case of an equilibrium field.

## 4.5 Conclusions

We have considered the  $\gamma$  and  $\beta$  effects as they act on the basic state in comparison to their action on the perturbations, seeking to understand how they affect the linear stability in each case. Building on the results presented in Chapter 3, it is clear that the basic state field — and its gradient — is the most important factor in determining the stability of such a layer to linear perturbations. The effect of  $\gamma$  and  $\beta$  on the basic state is destabilising when such a basic state is

perturbed. The effect on the perturbations themselves, however — though much smaller in magnitude — is stabilising. We have also shown that the change in the most unstable mode from 3D to interchange with the application of increasing  $\gamma$  and  $\beta$  is driven by their effect on the basic state alone. We have considered prescribed fields that are not consistent with equilibrium under  $\gamma$  and  $\beta$ , and found that the stability properties of the system under increasing  $\gamma_m$  differ considerably from the equivalent parameter case with an equilibrium basic state as discussed in Chapter 3.

From a physical point of view, the idea that the action of  $\gamma$  and  $\beta$  on the basic state, and indeed the choice of basic state in general, is critically important in determining the stability is consistent with our assumptions about  $\gamma$  and  $\beta$ ; these effects are derived from the assumption that they act on the large-scale mean field. Therefore, the importance of the effects of  $\gamma$  and  $\beta$  on the basic state lends additional legitimacy to the idea of treating the basic state as analogous to the mean field in the physical system we consider. Furthermore, we have shown that the action of  $\gamma$  and  $\beta$  on the small-scale perturbed quantities is not a dominant effect and can potentially be neglected in future work. Equally, though, this analysis demonstrates that the basic state — although it is not the sole factor at work; see Figure 4.9 — is critical in determining the growth rate and spatial form of the instability, and therefore must be carefully chosen to reflect physical reality.

#### **4. SCALE DEPENDENCE OF THE INSTABILITY**

---

# Chapter 5

## An Analytic Approach to the Diffusionless Instability

We consider the diffusionless case of the magnetic buoyancy instability. The mechanism for the classical, non-oscillating instability (see, for example, [Newcomb, 1961](#)) does not itself rely critically on diffusive effects to function, and so we may remove them in order to simplify the system. In addition, the diffusionless case has been studied in the past, because under the assumption of non-diffusivity it is possible to derive analytic results with much greater ease than for the full problem discussed in Chapters 3 and 4. We aim to add the turbulent pumping  $\gamma$ , to understand its effect on existing analytical relations for the system. We will seek to extend the analytic approaches of [Gilman \(1970\)](#) — for the small-scale limit — and [Mizerski \*et al.\* \(2013\)](#) — for the interchange instability of any scale — to a system that includes the  $\gamma$  turbulent pumping effect. We shall also analyse two model problems to understand the mathematical structure of the third order system that results from the latter case. Additionally, following [Acheson \(1979\)](#), we will perform a local analysis to find a dispersion relation for the diffusionless interchange instability.

### 5.1 Large $k_y$ limit

[Gilman \(1970\)](#) considered the asymptotic limit of large  $k_y$  (i.e. small-scale variation) in the isothermal system and in the absence of magnetic and viscous dif-

## 5. AN ANALYTIC APPROACH TO THE DIFFUSIONLESS INSTABILITY

---

fusion effects. (It should be noted that, given the isothermality of the system, the thermal diffusivity is in fact infinite. However, we refer to this system as diffusionless here for the sake of convenience of discussion.) Taking the dominant balance of terms in the perturbation equations and rearranging the system under this assumption, Gilman obtained an algebraic equation for the growth rate (see Section 5.1.2 for further discussion). This relation depends on the stratified basic states of the system, implying a different dispersion relation at each height, which is both physically unconventional and quite different from the usual form of the system, that of a system of coupled ODEs.

This approach is considerably different from that of finding the solution to a system of perturbation equations, as discussed in Chapters 3 and 4. We will, however, extend such an approach to our system given by (3.14) – (3.21). We consider the diffusionless, isothermal case in the  $k_y \rightarrow \infty$  limit, with the turbulent pumping  $\gamma$  as an additional effect.

### 5.1.1 Diffusionless case, in the limit $k_y \rightarrow \infty$

Consider the perturbed system (3.14) – (3.21). We assume an isothermal system as discussed previously, and remove the magnetic and viscous diffusivity terms, to obtain:

$$s\hat{b}_x = -\frac{d}{dz}(\gamma\hat{b}_x) - \bar{B}ik_y\hat{v} - \frac{d}{dz}(\bar{B}\hat{w}), \quad (5.1)$$

$$s\hat{b}_y = -\frac{d}{dz}(\gamma\hat{b}_y) + \bar{B}ik_x\hat{v}, \quad (5.2)$$

$$s\hat{b}_z = -\gamma\frac{d}{dz}\hat{b}_z + \bar{B}ik_x\hat{w}, \quad (5.3)$$

$$s\bar{\rho}\hat{u} = F\bar{B}'\hat{b}_z - \bar{T}ik_x\hat{\rho}, \quad (5.4)$$

$$s\bar{\rho}\hat{v} = -F\bar{B}ik_y\hat{b}_x + F\hat{B}ik_x\hat{b}_y - \bar{T}ik_y\hat{\rho}, \quad (5.5)$$

$$s\bar{\rho}\hat{w} = -F\frac{d}{dz}(\bar{B}\hat{b}_x) + F\bar{B}ik_x\hat{b}_z - \frac{d}{dz}(\bar{T}\hat{\rho}) + \theta(m+1)\hat{\rho}, \quad (5.6)$$

$$s\hat{\rho} = -\bar{\rho}ik_x\hat{u} - \bar{\rho}ik_y\hat{v} - \frac{d}{dz}(\bar{\rho}\hat{w}). \quad (5.7)$$

Now, following Gilman's analysis, we make the approximation  $k_y \rightarrow \infty$ . In order for the  $\hat{b}_x$  and  $\hat{\rho}$  terms in (5.5) to remain finite, we require:

$$F\bar{B}\hat{b}_x + \bar{T}\hat{\rho} = 0, \quad (5.8)$$

which is a statement of the fact that the perturbation to the total pressure (i.e. the combination of magnetic and thermal pressure perturbations) is zero.

Following from this, (5.6) becomes:

$$s\bar{\rho}\hat{w} = F\bar{B}ik_x\hat{b}_z + \theta(m+1)\hat{\rho}, \quad (5.9)$$

and from (5.1), we require that  $\hat{v} \sim O(k_y^{-1})$ , after which it follows from (5.5) that  $\hat{b}_y \sim O(k_y^{-1})$ . We may eliminate the  $ik_y\hat{v}$  terms in (5.1) and (5.7), to obtain:

$$\bar{\rho} \left( s\hat{b}_x + \frac{d}{dz}(\gamma\hat{b}_x) \right) - \bar{B}\bar{\rho}ik_x\hat{u} + \bar{B}\bar{\rho}\frac{d}{dz} \left( \ln \left( \frac{\bar{B}}{\bar{\rho}} \right) \right) \hat{w} - \bar{B}s\hat{\rho} = 0. \quad (5.10)$$

Equations (5.3), (5.4), (5.8), (5.9), and (5.10) form a closed system of five linear ODEs. The system in the  $k_y \rightarrow \infty$  limit is second order, and may be reduced to two coupled equations in, say,  $\hat{w}$  and  $\hat{b}_z$ :

$$(s\bar{\rho}\hat{w} - F\bar{B}ik_x\hat{b}_z) \left( s^2(F\bar{B}^2 + \bar{T}\bar{\rho}) + s\bar{\rho}\gamma'\bar{T} + F\bar{B}^2\bar{T}k_x^2 - s\gamma\bar{T}\bar{\rho}\frac{d}{dz} \ln \bar{B} \right) \quad (5.11)$$

$$+ s\gamma\bar{T}\bar{\rho} \left( s\frac{d}{dz}(\bar{\rho}\hat{w}) - Fik_x\frac{d}{dz}(\bar{B}\hat{b}_z) \right)$$

$$+ F\bar{B}^2\theta(m+1) \left( F\bar{B}'ik_x\hat{b}_z - s\bar{\rho}\frac{d}{dz} \ln \left( \frac{\bar{B}}{\bar{\rho}} \right) \hat{w} \right) = 0,$$

$$\left( s + \gamma\frac{d}{dz} \right) \hat{b}_z - \bar{B}ik_x\hat{w} = 0. \quad (5.12)$$

These equations are of the form

$$A_1\hat{b}_z + A_2\hat{b}'_z + A_3\hat{w} + A_4\hat{w}' = 0, \quad (5.13)$$

$$A_5\hat{b}_z + A_6\hat{b}'_z + A_7\hat{w} = 0, \quad (5.14)$$

where

$$A_1 = -F\bar{B}ik_x(s^2(F\bar{B}^2 + \bar{T}\bar{\rho}) + s\bar{\rho}\gamma'\bar{T} + F\bar{B}^2\bar{T}k_x^2) - F^2\bar{B}^2\bar{B}'ik_x\theta(m+1), \quad (5.15)$$

$$A_2 = -s\gamma\bar{T}\bar{\rho}Fik_x\bar{B}, \quad (5.16)$$

$$A_3 = s\bar{\rho}(s^2(F\bar{B}^2 + \bar{T}\bar{\rho}) + s\bar{\rho}\gamma'\bar{T} + F\bar{B}^2\bar{T}k_x^2 - s\gamma\bar{T}\bar{\rho}\frac{d}{dz} \ln \bar{B}) \\ + s^2\gamma\bar{T}\bar{\rho}\bar{\rho}' - s\bar{\rho}F\bar{B}^2\theta(m+1)\frac{d}{dz} \ln \left( \frac{\bar{B}}{\bar{\rho}} \right), \quad (5.17)$$

## 5. AN ANALYTIC APPROACH TO THE DIFFUSIONLESS INSTABILITY

---

$$A_4 = s^2 \gamma \bar{T} \bar{\rho}^2, \quad (5.18)$$

$$A_5 = s, \quad (5.19)$$

$$A_6 = \gamma, \quad (5.20)$$

$$A_7 = -\bar{B} i k_x. \quad (5.21)$$

We may then eliminate  $\hat{b}_z$  to obtain a second order ODE of the form:

$$g_2(z) \hat{w}'' + g_1(z) \hat{w}' + g_0(z) \hat{w} = 0, \quad (5.22)$$

with

$$\begin{aligned} g_0 &= (A_6 A_1' - A_2 A_5')(A_6 A_3 - A_2 A_7) \\ &\quad - (A_6(A_1 + A_2') - A_2(A_5 + A_1'))(A_5 A_3 - A_1 A_7) \\ &\quad + (A_2 A_5 - A_6 A_1)(A_6 A_3' - A_2 A_7'), \end{aligned} \quad (5.23)$$

$$\begin{aligned} g_1 &= (A_6 A_1' - A_2 A_5') A_6 A_4 - (A_6(A_1 + A_2') - A_2(A_5 + A_1')) A_5 A_4 \\ &\quad + (A_2 A_5 - A_6 A_1)(A_6(A_3 + A_4') - A_2 A_7), \end{aligned} \quad (5.24)$$

$$g_2 = (A_6 A_1 - A_2 A_5) A_6 A_4. \quad (5.25)$$

From coefficients (5.15) – (5.21),  $A_2$ ,  $A_4$ , and  $A_6$  are proportional to  $\gamma$ , so we can see that  $g_0 = O(\gamma)$ ,  $g_1 = O(\gamma^2)$ , and  $g_2 = O(\gamma^3)$  as  $\gamma \rightarrow 0$ . This explains the reversion to an algebraic problem in this limit. However, when  $k_x = 0$  (i.e. for interchange modes), Equations (5.11) and (5.12) become decoupled and we are left with a first order system given by a single equation in  $\hat{w}$ . We shall now look at each of these cases in more detail.

### 5.1.2 3D system, with $\gamma = 0$ .

This is the case considered by Gilman (1970), which we will briefly summarise. If we take  $\gamma = 0$  in (5.22), the  $z$ -derivatives vanish and the equation becomes simply algebraic. As previously noted in Section 5.1, we may then write a depth-dependent dispersion relation for the instability, given by:

$$\begin{aligned} &\left(\bar{T} + \frac{F \bar{B}^2}{\bar{\rho}}\right) s^4 + \frac{F \bar{B}^2}{\bar{\rho}} \left( \left(2\bar{T} + \frac{F \bar{B}^2}{\bar{\rho}}\right) k_x^2 - \theta(m+1) \frac{d}{dz} \ln \left(\frac{\bar{B}}{\bar{\rho}}\right) \right) s^2 \\ &+ k_x^2 \frac{F^2 \bar{B}^2}{\bar{\rho}^2} \left( k_x^2 \bar{T} - \theta(m+1) \frac{d}{dz} \ln \bar{B} \right) = 0. \end{aligned} \quad (5.26)$$

This is the equation derived by Gilman, and from it come the standard stability criteria for magnetic buoyancy. Gilman showed that, for stationary instability ( $s^2 > 0$ ) of diffusionless 3D modes in the limit  $k_y \rightarrow \infty$ , we require

$$0 < k_x^2 < \frac{\theta(m+1)}{\bar{T}} \frac{d}{dz} \ln \bar{B}. \quad (5.27)$$

In addition to this, for interchange modes ( $k_x = 0$ ), Equation (5.26) tells us that the condition for instability is

$$\frac{F\bar{B}^2\theta(m+1)}{\bar{T}\bar{\rho} + F\bar{B}^2} \frac{d}{dz} \ln \left( \frac{\bar{B}}{\bar{\rho}} \right) > 0. \quad (5.28)$$

This is equivalent to the form of the stability criteria discussed in Section 1.3.1. We shall now consider the case of non-zero  $\gamma$ , our extension of this work on the system.

### 5.1.3 Interchange system with $\gamma \neq 0$

When  $k_x = 0$ , (5.11) and (5.12) become decoupled, and the system may be characterised by a single first order equation when  $\gamma \neq 0$ :

$$s\gamma\bar{T}\bar{\rho} \frac{d\hat{w}}{dz} + \left( s^2(F\bar{B}^2 + \bar{T}\bar{\rho}) + s\gamma\bar{T}\bar{\rho} \frac{d}{dz} \ln \left( \frac{\gamma\bar{\rho}}{\bar{B}} \right) - F\bar{B}^2\theta(m+1) \frac{d}{dz} \ln \left( \frac{\bar{B}}{\bar{\rho}} \right) \right) \hat{w} = 0. \quad (5.29)$$

This has the form of a first order ODE in  $\hat{w}$ . Note that if  $\gamma = 0$ , the criterion for instability (i.e.  $s^2 > 0$ ) reduces once more to (5.28), as expected.

When  $\gamma$  is non-zero, we may solve (5.29) using an integrating factor to obtain:

$$\hat{w} = \hat{w}_o \exp \left( \int \left( \frac{s^2(F\bar{B}^2 + \bar{T}\bar{\rho}) + s\gamma\bar{T}\bar{\rho} \frac{d}{dz} \ln \left( \frac{\gamma\bar{\rho}}{\bar{B}} \right) - F\bar{B}^2\theta(m+1) \frac{d}{dz} \ln \left( \frac{\bar{B}}{\bar{\rho}} \right)}{s\gamma\bar{T}\bar{\rho}} \right) dz \right), \quad (5.30)$$

where  $\hat{w}_o$  is a constant to be determined by the boundary condition on  $\hat{w}$ , and  $s$  is the unknown eigenvalue. Note that the addition of  $\gamma$  necessitates the imposition of boundary conditions on  $\hat{w}$ ; in this case one boundary condition, and in the case of  $k_x \neq 0$  (see Equation (5.22)), two boundary conditions.

## 5. AN ANALYTIC APPROACH TO THE DIFFUSIONLESS INSTABILITY

---

Note also that Equation (5.29) is quadratic in  $s$ :

$$s^2 ((F\bar{B}^2 + \bar{T}\bar{\rho})\hat{w}) + s \left( \gamma \bar{T} \bar{\rho} \hat{w} \frac{d}{dz} \ln \left( \frac{\gamma \bar{\rho} \hat{w}}{\bar{B}} \right) \right) - \left( F\bar{B}^2 \theta(m+1) \frac{d}{dz} \ln \left( \frac{\bar{B}}{\bar{\rho}} \right) \hat{w} \right) = 0, \quad (5.31)$$

and that this relation is also depth-dependent. Given that the eigenfunction  $\hat{w}$  is still unknown, though, we cannot solve for  $s$  in terms of the basic states as before. However, by setting  $s = 0$ , we may find the following criterion for marginal stability:

$$\frac{d}{dz} \ln \left( \frac{\bar{B}}{\bar{\rho}} \right) = 0, \quad (5.32)$$

which is the same as the condition for marginal stability in the diffusionless criterion for interchange instability when  $\gamma = 0$ , (1.4). Thus, the criterion for marginal stability is not affected directly by the action of  $\gamma$ , but by the effect of  $\gamma$  on the basic states  $\bar{B}$  and  $\bar{\rho}$ . This suggests that the action of  $\gamma$  on the basic state — and specifically the increase in field gradient due to the addition of turbulent pumping — is the main factor that determines how  $\gamma$  destabilises the system to magnetic buoyancy. This result is consistent with our linear stability analysis (Chapters 3 and 4), and therefore suggests that this diffusionless system is of value as a simpler model for the diffusive system.

### 5.2 Comparison with the diffusionless interchange system for finite $k_y$

So far, for the diffusionless case we have considered the limit  $k_y \rightarrow \infty$ , and found an analogous result to that of Gilman (1970). However, it is useful to consider how this fits in with the more general interchange instability in the diffusionless limit. Mizerski *et al.* (2013) sought to relate the case studied by Gilman, in which the instability is governed by a depth-dependent dispersion relation, to the solution to the full eigenvalue problem for finite  $k_y$ . We will follow their approach, for the interchange instability with an additional  $\gamma$  effect (without taking the asymptotic limit  $k_y \rightarrow \infty$ ), and discuss two model systems, to try to capture the same behaviour we may see in the more complex problem.

## 5.2 Comparison with the diffusionless interchange system for finite $k_y$

### 5.2.1 Interchange case

Following Mizerski *et al.* (2013), we consider again the diffusionless, isothermal case, according to Equations (5.1) – (5.7). However, we will make no assumption about the size of  $k_y$  at this point.

For simplicity, we consider the interchange case of the linear instability. We have the following linearised system:

$$s\hat{b}_x = -\frac{d}{dz}(\gamma\hat{b}_x) - \bar{B}ik_y\hat{v} - \frac{d}{dz}(\bar{B}\hat{w}), \quad (5.33)$$

$$s\bar{\rho}\hat{v} = -F\bar{B}ik_y\hat{b}_x - \bar{T}ik_y\hat{\rho}, \quad (5.34)$$

$$s\bar{\rho}\hat{w} = -\frac{d}{dz}(F\bar{B}\hat{b}_x + \bar{T}\hat{\rho}) + \theta(m+1)\hat{\rho}, \quad (5.35)$$

$$s\hat{\rho} = -ik_y\bar{\rho}\hat{v} - \frac{d}{dz}(\bar{\rho}\hat{w}). \quad (5.36)$$

We may eliminate  $\hat{v}$  and  $\hat{\rho}$  to derive a system in the form of two coupled equations in  $\hat{b}_x$  and  $\hat{w}$ . This system is third order — rather than second order, as in the  $k_y \rightarrow \infty$  limit — and takes the form of two coupled ODEs of the form:

$$\alpha_1\hat{b}_x + \alpha_2\hat{b}'_x + \alpha_3\hat{w} + \alpha_4\hat{w}' = 0, \quad (5.37)$$

$$\alpha_5\hat{b}_x + \alpha_6\hat{b}'_x + \alpha_7\hat{w} + \alpha_8\hat{w}' + \alpha_9\hat{w}'' = 0, \quad (5.38)$$

with  $z$ -dependent coefficients  $\alpha_1, \dots, \alpha_9$  that depend on the basic states, the parameters of the problem, on  $k_y$  and the growth rate  $s$ . These are given by:

$$\alpha_1 = \bar{\rho}(s^2 + k_y^2T)(s + \gamma') + sF\bar{B}^2k_y^2, \quad (5.39)$$

$$\alpha_2 = \bar{\rho}(s^2 + k_y^2T)\gamma, \quad (5.40)$$

$$\alpha_3 = \bar{\rho}\bar{B}'(s^2 + k_y^2T) - \bar{B}\bar{\rho}'k_y^2\bar{T}, \quad (5.41)$$

$$\alpha_4 = s^2\bar{\rho}\bar{B}, \quad (5.42)$$

$$\alpha_5 = s^2F\bar{B}' + F\bar{B}\theta(m+1)k_y^2, \quad (5.43)$$

$$\alpha_6 = s^2F\bar{B}, \quad (5.44)$$

$$\alpha_7 = s\bar{\rho}(s^2 + k_y^2\bar{T}) + s\bar{\rho}'\theta(m+1) - s\bar{\rho}''\bar{T}, \quad (5.45)$$

$$\alpha_8 = s\bar{\rho}\theta(m+1) - 2s\bar{\rho}'\bar{T}, \quad (5.46)$$

$$\alpha_9 = -s\bar{\rho}\bar{T}. \quad (5.47)$$

## 5. AN ANALYTIC APPROACH TO THE DIFFUSIONLESS INSTABILITY

---

Using this notation we may solve this system numerically. However, we may also write the system as a single third order equation in  $\hat{w}$ . In this arrangement, the coefficient of the highest order derivative  $\hat{w}'''$  is given by:

$$-\alpha_2\alpha_9 = s\bar{T}\bar{\rho}^2(s^2 + k_y^2\bar{T})\gamma. \quad (5.48)$$

This is proportional to  $\gamma$ , so we may see immediately that the problem changes from a third order to a second order problem for  $\gamma = 0$ , as the coefficients of the lower order terms, (5.51) – (5.52), do not become zero when  $\gamma = 0$ . The fact that the addition of a  $\gamma$  effect makes the equation third order is of note because third order systems are unusual, physically; with the additional requirement of a third boundary condition, an additional asymmetry is introduced. There is also the question of what boundary condition we should choose to meet this requirement, which we will address later for the case of a model third order system.

In addition, we may further look at the  $k_y$ –dependence of the coefficients. Motivated by understanding the limit assumed by Gilman, we will find the dominant balance of terms as  $k_y \rightarrow \infty$ , and recover (5.29). First, we note that this system is of the form:

$$f_3(z)\hat{w}''' + f_2(z)\hat{w}'' + f_1(z)\hat{w}' + f_0(z)\hat{w} = 0. \quad (5.49)$$

Using symbolic computation, we may find the forms of the coefficient functions:

$$\begin{aligned} f_0 = \chi & [(\bar{B}F s^2 ((\gamma''\bar{\rho} + \bar{\rho}'(\gamma' + s)) (\bar{T}k_y^2 + s^2) + 2\bar{B}F\bar{B}'k_y^2 s) \quad (5.50) \\ & - \gamma\bar{\rho} (F\bar{B}'\theta(m+1)k_y^2 + F\bar{B}''s^2) (\bar{T}k_y^2 + s^2)) (\bar{B}F s^2 (\bar{B}'\bar{\rho} (\bar{T}k_y^2 + s^2) \\ & - \bar{B}\bar{T}\bar{\rho}'k_y^2) - \gamma\bar{\rho} (\bar{T}k_y^2 + s^2) (\bar{\rho}'s\theta(m+1) - \bar{T}\bar{\rho}''s + \bar{\rho}s (\bar{T}k_y^2 + s^2))) \\ & - ((\bar{B}F\theta(m+1)k_y^2 + F\bar{B}'s^2) (\bar{B}'\bar{\rho} (\bar{T}k_y^2 + s^2) - \bar{B}\bar{T}\bar{\rho}'k_y^2) \\ & - (\bar{\rho}(\gamma' + s) (\bar{T}k_y^2 + s^2) + \bar{B}^2Fk_y^2 s) (\bar{\rho}'s\theta(m+1) - \bar{T}\bar{\rho}''s \\ & + \bar{\rho}s (\bar{T}k_y^2 + s^2))) (\bar{B}F s^2 ((\bar{T}k_y^2 + s^2) (\bar{\rho}'\gamma + \gamma'\bar{\rho}) \\ & + \bar{\rho}(\gamma' + s) (\bar{T}k_y^2 + s^2) + \bar{B}^2Fk_y^2 s) - \gamma\bar{\rho} (\bar{B}F\theta(m+1)k_y^2 \\ & + 2F\bar{B}'s^2) (\bar{T}k_y^2 + s^2)) - (\gamma\bar{\rho} (\bar{B}F\theta(m+1)k_y^2 + F\bar{B}'s^2) (\bar{T}k_y^2 + s^2) \\ & - \bar{B}F s^2 (\bar{\rho}(\gamma' + s) (\bar{T}k_y^2 + s^2) + \bar{B}^2Fk_y^2 s)) (\gamma\bar{\rho} (\bar{T}k_y^2 + s^2) (\bar{\rho}''s\theta(m+1) \\ & - \bar{T}\bar{\rho}'''s + \bar{\rho}'s (\bar{T}k_y^2 + s^2)) - \bar{B}F s^2 ((\bar{T}k_y^2 + s^2) (\bar{B}'\bar{\rho}' + \bar{B}''\bar{\rho}) \\ & - \bar{T}k_y^2 (\bar{B}\bar{\rho}'' + \bar{B}'\bar{\rho}')))] , \end{aligned}$$

## 5.2 Comparison with the diffusionless interchange system for finite $k_y$

$$\begin{aligned}
f_1 = & \chi \left[ (\bar{B}F s^2 ((\gamma''\bar{\rho} + \bar{\rho}'(\gamma' + s)) (\bar{T}k_y^2 + s^2) + 2\bar{B}F\bar{B}'k_y^2 s) \right. \\
& - \gamma\bar{\rho} (F\bar{B}'\theta(m+1)k_y^2 + F\bar{B}''s^2) (\bar{T}k_y^2 + s^2)) (\bar{B}^2 F\bar{\rho}s^4 \\
& + \gamma\bar{\rho} (2\bar{T}\bar{\rho}'s - \bar{\rho}s\theta(m+1)) (\bar{T}k_y^2 + s^2)) - ((\bar{\rho}(\gamma' + s) (\bar{T}k_y^2 + s^2) \\
& + \bar{B}^2 Fk_y^2 s) (2\bar{T}\bar{\rho}'s - \bar{\rho}s\theta(m+1)) + \bar{B}\bar{\rho}s^2 (\bar{B}F\theta(m+1)k_y^2 \\
& + F\bar{B}'s^2)) (\bar{B}F s^2 ((\bar{T}k_y^2 + s^2) (\bar{\rho}'\gamma + \gamma'\bar{\rho}) + \bar{\rho}(\gamma' + s) (\bar{T}k_y^2 + s^2) \\
& + \bar{B}^2 Fk_y^2 s) - \gamma\bar{\rho} (\bar{B}F\theta(m+1)k_y^2 + 2F\bar{B}'s^2) (\bar{T}k_y^2 + s^2)) \\
& - (\gamma\bar{\rho} (\bar{B}F\theta(m+1)k_y^2 + F\bar{B}'s^2) (\bar{T}k_y^2 + s^2) - \bar{B}F s^2 (\bar{\rho}(\gamma' + s) (\bar{T}k_y^2 + s^2) \\
& + \bar{B}^2 Fk_y^2 s)) (\gamma\bar{\rho} (\bar{T}k_y^2 + s^2) (2\bar{\rho}'s\theta(m+1) - 3\bar{T}\bar{\rho}''s + \bar{\rho}s (\bar{T}k_y^2 + s^2)) \\
& \left. - \bar{B}F s^2 (s^2 (\bar{B}\bar{\rho}' + \bar{B}'\bar{\rho}) + \bar{B}'\bar{\rho} (\bar{T}k_y^2 + s^2) - \bar{B}\bar{T}\bar{\rho}'k_y^2)) \right], \tag{5.51}
\end{aligned}$$

$$\begin{aligned}
f_2 = & \chi \left[ (\gamma\bar{\rho} (\bar{B}F\theta(m+1)k_y^2 + F\bar{B}'s^2) (\bar{T}k_y^2 + s^2) - \bar{B}F s^2 (\bar{\rho}(\gamma' + s) (\bar{T}k_y^2 + s^2) \right. \\
& + \bar{B}^2 Fk_y^2 s)) (\bar{B}^2 F\bar{\rho}s^4 + \gamma\bar{\rho} (3\bar{T}\bar{\rho}'s - \bar{\rho}s\theta(m+1)) (\bar{T}k_y^2 + s^2)) \\
& - \bar{T}\bar{\rho}s (\bar{\rho}(\gamma' + s) (\bar{T}k_y^2 + s^2) + \bar{B}^2 Fk_y^2 s) (\bar{B}F s^2 ((\bar{T}k_y^2 + s^2) (\bar{\rho}'\gamma + \gamma'\bar{\rho}) \\
& + \bar{\rho}(\gamma' + s) (\bar{T}k_y^2 + s^2) + \bar{B}^2 Fk_y^2 s) - \gamma\bar{\rho} (\bar{B}F\theta(m+1)k_y^2 + 2F\bar{B}'s^2) (\bar{T}k_y^2 + s^2)) \\
& + \bar{T}\gamma\bar{\rho}^2 s (\bar{B}F s^2 ((\gamma''\bar{\rho} + \bar{\rho}'(\gamma' + s)) (\bar{T}k_y^2 + s^2) + 2\bar{B}F\bar{B}'k_y^2 s) \\
& \left. - \gamma\bar{\rho} (F\bar{B}'\theta(m+1)k_y^2 + F\bar{B}''s^2) (\bar{T}k_y^2 + s^2)) (\bar{T}k_y^2 + s^2) \right], \tag{5.52}
\end{aligned}$$

$$f_3 = \bar{T}\gamma\bar{\rho}^2 s (\bar{T}k_y^2 + s^2), \tag{5.53}$$

where

$$\begin{aligned}
\chi &= \left[ \gamma\bar{\rho} (\bar{B}F\theta(m+1)k_y^2 + F\bar{B}'s^2) (\bar{T}k_y^2 + s^2) \right. \\
& \left. - \bar{B}F s^2 (\bar{\rho}(\gamma' + s) (\bar{T}k_y^2 + s^2) + \bar{B}^2 Fk_y^2 s) \right]^{-1} \\
&= [\alpha_2\alpha_5 - \alpha_1\alpha_6]^{-1}.
\end{aligned} \tag{5.54}$$

In order to find the large  $k_y$  behaviour, we rearrange the coefficients in powers of  $k_y^2$ . To facilitate this computation, we multiply through by  $\chi^{-1}$ , which is biquadratic in  $k_y$ . With this, we are able to obtain the following coefficients:

$$(\alpha_2\alpha_5 - \alpha_1\alpha_6)f_0 = C_{08}(z)k_y^8 + C_{06}(z)k_y^6 + C_{04}(z)k_y^4 + C_{02}(z)k_y^2 + C_{00}(z), \tag{5.55}$$

$$(\alpha_2\alpha_5 - \alpha_1\alpha_6)f_1 = C_{18}(z)k_y^8 + C_{16}(z)k_y^6 + C_{14}(z)k_y^4 + C_{12}(z)k_y^2 + C_{10}(z), \tag{5.56}$$

$$(\alpha_2\alpha_5 - \alpha_1\alpha_6)f_2 = C_{26}(z)k_y^6 + C_{24}(z)k_y^4 + C_{22}(z)k_y^2 + C_{20}(z), \tag{5.57}$$

$$(\alpha_2\alpha_5 - \alpha_1\alpha_6)f_3 = C_{36}(z)k_y^6 + C_{34}(z)k_y^4 + C_{32}(z)k_y^2 + C_{30}(z), \tag{5.58}$$

## 5. AN ANALYTIC APPROACH TO THE DIFFUSIONLESS INSTABILITY

---

where  $C_{ij}$  represents the coefficient of  $k_y^j$  in the  $i$ th order term in Equation (5.49). For the large  $k_y$  limit, the dominant balance is between  $O(k_y^8)$  terms, i.e.

$$\hat{w}' + \frac{C_{08}(z)}{C_{18}(z)}\hat{w} = 0. \quad (5.59)$$

The relevant quantity in this limit is thus  $\frac{C_{08}(z)}{C_{18}(z)}$ . This is given by

$$\frac{C_{08}(z)}{C_{18}(z)} = \frac{s^2(F\bar{B}^2 + \bar{T}\bar{\rho}) + s\bar{T}\bar{\rho}\gamma\frac{d}{dz}\ln\left(\frac{\gamma\bar{\rho}}{\bar{B}}\right) - F\bar{B}^2\theta(m+1)\frac{d}{dz}\ln\left(\frac{\bar{B}}{\bar{\rho}}\right)}{s\bar{T}\bar{\rho}\gamma}, \quad (5.60)$$

which demonstrates that (5.59) is equivalent to (5.29), showing that (5.49) reduces to (5.29) in the limit  $k_y \rightarrow \infty$ , as expected.

We have obtained a full analytic form for the equation governing the diffusionless interchange instability. However, beyond showing that the highest order term is proportional to  $\gamma$  — and therefore that the application of  $\gamma$  changes the order of the problem — the complex dependence of coefficients (5.51) – (5.53) makes it difficult to see the full effect of  $\gamma$  beyond the fact that, presumably, the system has a boundary layer solution in the limit  $\gamma \rightarrow 0$ . However, we may take the approach of Mizerski *et al.* (2013) and seek to understand a simpler model problem that captures some of the behaviour of the full system. In our case, we shall consider the asymptotic limit  $\gamma \rightarrow 0$ , in order to understand the emergence of the boundary layer as a result of a third derivative term proportional to  $\gamma$  in a model system.

### 5.3 Model problem

#### 5.3.1 Simplified third order eigenvalue model problem

Given the complex  $\gamma$ -dependence of the coefficients (5.51) – (5.52), the full system detailed above is not easy to understand fully as  $\gamma \rightarrow 0$ . Therefore, we attempt to find a simpler system that exhibits some of the same behaviour. We seek a third-order eigenvalue problem with a small parameter  $\epsilon$  multiplying the highest

### 5.3 Model problem

---

order term, which will have a boundary layer solution as  $\epsilon \rightarrow 0$ . We consider the ODE

$$\epsilon \frac{d^3 y}{dz^3} + \frac{d^2 y}{dz^2} + \lambda^2 y = 0, \quad (5.61)$$

as  $\epsilon \rightarrow 0$ , with eigenvalue  $\lambda$ . We solve on an interval  $0 \leq z \leq 1$ , and, because of the signs of the first two terms, we expect a boundary layer at the  $z = 0$  end of the domain. Let us, initially, select the boundary conditions:

$$y(0) = 0, \quad (5.62)$$

$$y(1) = 0, \quad (5.63)$$

$$y'(0) = 0. \quad (5.64)$$

First, we may solve for the outer solution, by taking  $\epsilon = 0$ . In this limit, the outer equation is:

$$\frac{d^2 y}{dz^2} + \lambda^2 y = 0, \quad (5.65)$$

with solution

$$y_{out} = \chi_1 \cos(\lambda z) + \chi_2 \sin(\lambda z), \quad (5.66)$$

where  $\chi_1, \chi_2$  are arbitrary constants. Then, by the outer boundary condition  $y_{out}(1) = 0$ , we have  $\chi_1 = -\chi_2 \tan(\lambda)$ . This gives the form of the outer solution as:

$$y_{out} = \chi(\sin(\lambda z) - \tan(\lambda) \cos(\lambda z)), \quad (5.67)$$

where we now have only one arbitrary constant,  $\chi$ . We may find the inner solution by defining a boundary layer coordinate  $s = z/\epsilon$ . With this, we obtain the inner equation

$$\frac{d^3 y}{ds^3} + \frac{d^2 y}{ds^2} = 0, \quad (5.68)$$

the solution to which is given by

$$y_{in} = \beta_1 e^{-\frac{z}{\epsilon}} + \beta_2 \frac{z}{\epsilon} + \beta_3, \quad (5.69)$$

where  $\beta_1, \beta_2, \beta_3$  are arbitrary constants. We apply the inner boundary conditions  $y_{in}(0) = 0$  and  $y'_{in}(0) = 0$  to find

$$y_{in} = \beta \left( e^{-\frac{z}{\epsilon}} + \frac{z}{\epsilon} - 1 \right), \quad (5.70)$$

## 5. AN ANALYTIC APPROACH TO THE DIFFUSIONLESS INSTABILITY

---

with arbitrary constant  $\beta$ . We may now match the inner and outer solutions by introducing a variable of intermediate scale,  $\eta = z/\epsilon^\alpha$ , where  $0 < \alpha < 1$ . Then we take the limit  $\epsilon \rightarrow 0$ , at fixed  $\eta$ . In this limit, the inner and outer solutions become

$$y_{in} \sim \beta(\epsilon^{\alpha-1}\eta - 1), \quad (5.71)$$

$$y_{out} \sim \chi(\lambda\epsilon^\alpha\eta - \tan(\lambda)). \quad (5.72)$$

Matching the  $O(1)$  terms gives us a relation between the constants  $\beta$  and  $\chi$ . Additionally, since (5.71) and (5.72) must hold for all  $\eta$ , we may also match the remaining  $O(\eta)$  terms. By these matchings we obtain two linear relations:

$$-\beta = -\chi \tan(\lambda), \quad (5.73)$$

$$\beta\epsilon^{\alpha-1} = \chi\lambda\epsilon^\alpha, \quad (5.74)$$

from which we may eliminate the unknown constants, giving the relation between  $\epsilon$  and the eigenvalues:

$$\tan(\lambda) = \epsilon\lambda. \quad (5.75)$$

In this case, it is possible to see the effect of  $\epsilon$  on the system; the solutions are perturbations to the solutions of  $\tan(\lambda_o) = 0$  (which are given by  $\lambda_o = n\pi$ , for integer  $n$ ), for small  $\epsilon$ .

We may also construct the composite solution for this system. We have the intermediate solution

$$y_{int} \sim \beta\left(\frac{z}{\epsilon} - 1\right). \quad (5.76)$$

We also know the relation between constants  $\beta$  and  $\chi$ , given by (5.74), so let us choose  $\beta = \tan(\lambda)$ ,  $\chi = 1$ . Therefore, the full composite solution (given by  $y_c = y_{in} + y_{out} - y_{int}$ ) is

$$y_c(z) = \tan(\lambda)(e^{-\frac{z}{\epsilon}} - \cos(\lambda z)) + \sin(\lambda z). \quad (5.77)$$

We may check this approximate solution by solving (5.75) for  $\lambda$  numerically, and then using the result to construct (5.77) as  $\epsilon \rightarrow 0$ , as well as to show that, as we expect, it no longer obeys the boundary conditions in the  $\epsilon = O(1)$  regime.

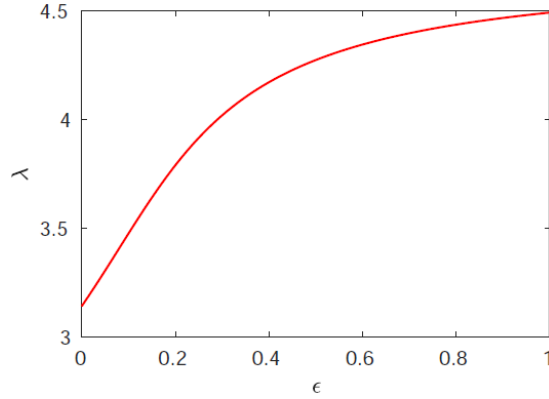


Figure 5.1:  $\lambda(\epsilon)$ , the numerically calculated solution to  $\tan(\lambda) = \epsilon\lambda$  for initial guess  $\lambda_o = \pi$ .

Starting with the initial estimate of  $\lambda_o = \pi$  (the lowest order solution to the unperturbed equation  $\tan(\lambda) = 0$ ) we are able to find  $\lambda$  as a function of  $\epsilon$  numerically, by means of the MATLAB function “fsolve”, which solves systems of nonlinear equations, applying a trust-region dogleg algorithm to systems that may be written in terms of a square matrix. The resulting eigenvalues are shown in Figure 5.1. Using the corresponding values of  $\lambda$  we are then able to construct  $y_c(z)$  (Figure 5.2). We consider the range of  $\epsilon \sim 10^{-2}$  and lower to be “small”  $\epsilon$  as compared to  $\epsilon = O(1)$ , as this distinction makes the difference in whether  $y_c$  obeys the boundary condition visually apparent: see Figure 5.2a compared to Figure 5.2b. Note that when  $\epsilon \rightarrow O(1)$  (Figure 5.2b), the boundary condition  $y(1) = 0$  is no longer satisfied. This is because the fulfilment of this condition requires that the quantity  $e^{-\frac{1}{\epsilon}}$  be transcendently small, which is only the case as  $\epsilon \rightarrow 0$ .

We may also find the “error” in the calculation by substituting the solution back into (5.61). The quantity

$$\epsilon y''' + y'' + \lambda^2 y = \lambda^2 \tan(\lambda) e^{-\frac{z}{\epsilon}} - \epsilon \lambda^3 (\cos(\lambda z) + \tan(\lambda) \sin(\lambda z)) \quad (5.78)$$

should be proportional to  $-\epsilon \cos(\lambda z)$  as  $\epsilon \rightarrow 0$ . In Figure 5.3, we scale this by a factor of  $1/\epsilon$  for the sake of comparison, showing the deviation from the form

## 5. AN ANALYTIC APPROACH TO THE DIFFUSIONLESS INSTABILITY

---

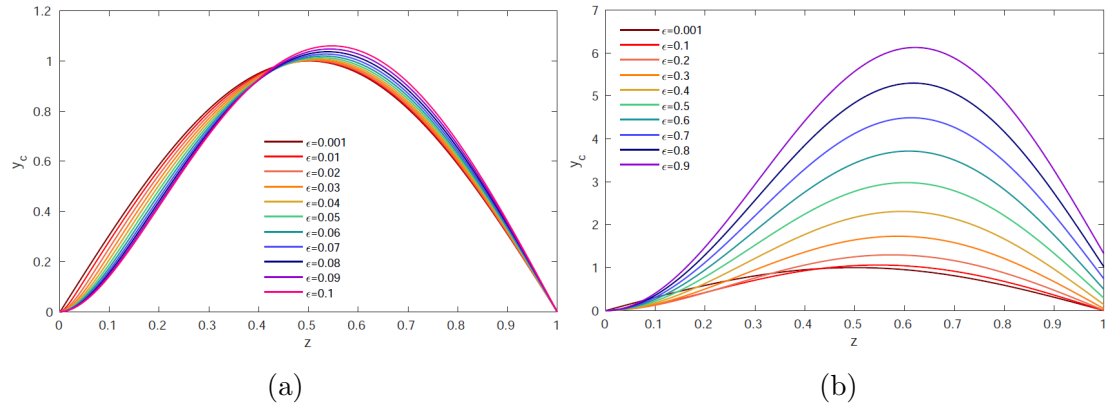


Figure 5.2: The composite solution  $y_c$ , given by (5.77), in the regime of (a) small  $\epsilon$  in which it holds, and (b) in the regime of  $\epsilon \rightarrow O(1)$  in which it breaks down.

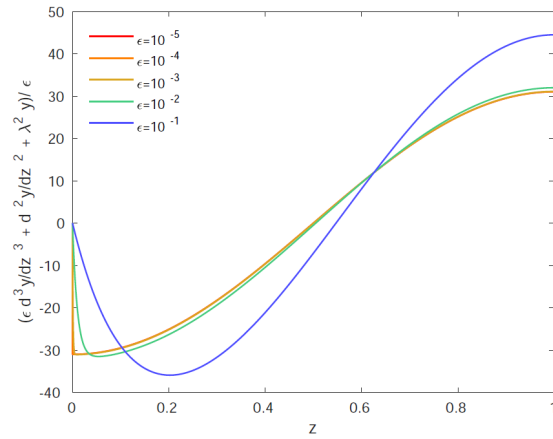


Figure 5.3: “Error” in the  $\epsilon \rightarrow 0$  solution, given by (5.78) multiplied by a factor of  $1/\epsilon$ .

$-\cos(\lambda z)$  outside of the small  $\epsilon$  regime.

Thus, we have constructed the composite solution given by (5.77), showing that it satisfies (5.61) and the boundary conditions (5.62) – (5.64), as we expect, in the limit  $\epsilon \rightarrow 0$ . In the next section we will compare the numerical solution to this approximate form of the solution.

### 5.3.2 Numerical solution to (5.61) for $y'(0) = 0$

We solve Equation (5.61) numerically, with boundary conditions (5.62) – (5.64). We also use a normalisation condition  $y''(0) = 1$  to fix the amplitude of the solutions. The results, for small and  $O(1)$  values of  $\epsilon$ , are shown in Figure 5.4, and the corresponding eigenvalues in Figure 5.5.

The numerical solution necessarily obeys the boundary conditions for all  $\epsilon$ . This is in contrast to the approximate solution  $y_c$  given by (5.77), which only obeys the boundary condition  $y(1) = 0$  in the  $\epsilon \rightarrow 0$  regime. Therefore, we may use the numerical solution as a point of comparison for the solution  $y_c$ , to understand how it breaks down as  $\epsilon \rightarrow O(1)$ .

In the case of  $\epsilon \rightarrow 0$  (Figure 5.4a), the numerical solution takes a similar form to that of the approximation  $y_c$  (Figure 5.2a); its amplitude, however, is different. This is likely due to the normalisation condition used in the numerical solver. Given the linearity of the problem, however, the amplitude is arbitrary. In order to compare the numerical solution more easily with  $y_c$  in the limit  $\epsilon \rightarrow 0$ , we may normalise the solutions and compare for given values of  $\epsilon$ . In Figure 5.6, we compare the asymptotic and numerical solutions (otherwise shown in Figures 5.2 and 5.4 respectively), normalised to 1, in order to see more easily that they become identical as  $\epsilon \rightarrow 0$ .

The eigenvalues (Figure 5.5) also approach the initial guess of  $\lambda_o = \pi$  (which we choose since it is the solution of (5.75) when  $\epsilon = 0$ , i.e.  $\lambda_o = n\pi$  for  $n = 1$ , thus fixing the mode found by the numerical scheme as the lowest order mode) as

## 5. AN ANALYTIC APPROACH TO THE DIFFUSIONLESS INSTABILITY

---

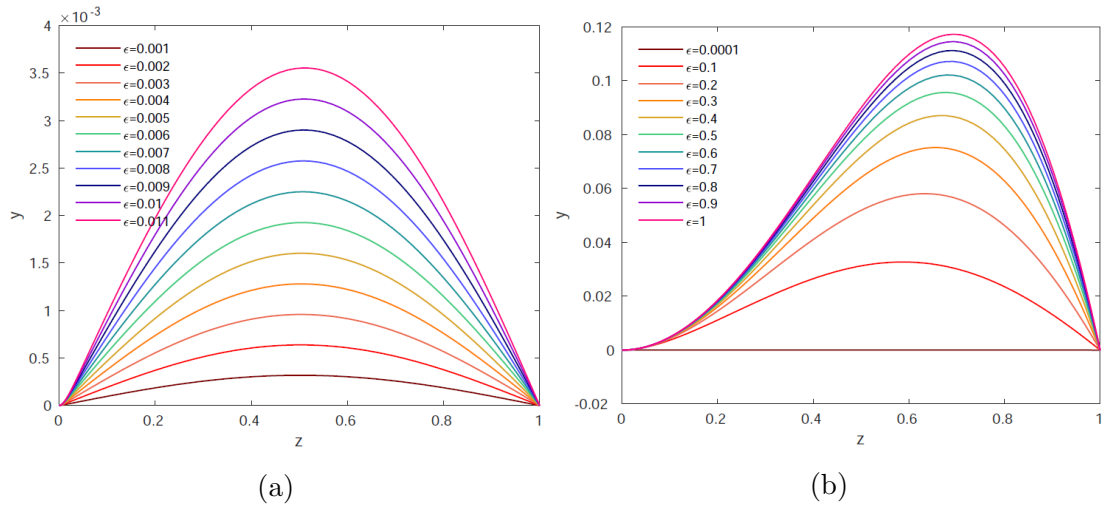


Figure 5.4: Numerical solutions to Equation (5.61), for (a) small  $\epsilon$ , and (b)  $\epsilon = O(1)$ . Compare with asymptotic approximation (5.77), plotted in Figure 5.2.

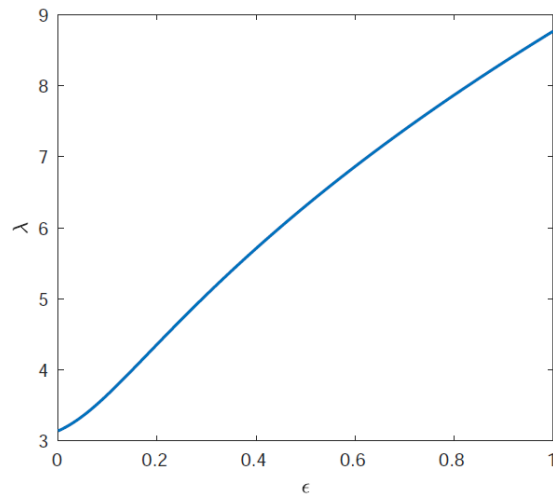


Figure 5.5: Numerically calculated eigenvalues  $\lambda$  for Equation (5.61), using initial guess  $\lambda_o = \pi$ . Compare with the solution to  $\tan(\lambda) = \epsilon\lambda$ , shown in Figure 5.1.

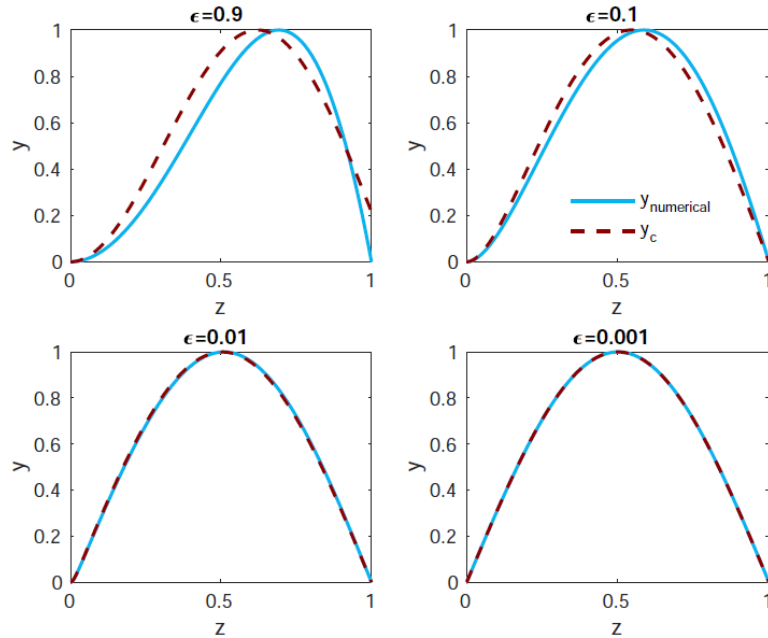


Figure 5.6: Comparison of the numerical solution shown in Figure 5.4 (blue) with the analytically constructed solution in the asymptotic limit  $\epsilon \rightarrow 0$  (maroon, dashed). Both solutions have been normalised to show more easily their convergence as  $\epsilon \rightarrow 0$ .

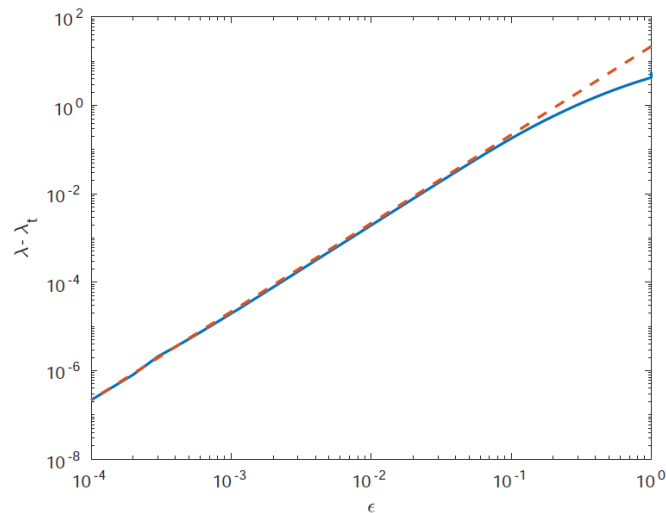


Figure 5.7: Difference in eigenvalues between the numerical and asymptotic cases (blue), with  $\epsilon^2$  dependence overplotted (orange, dashed).

## 5. AN ANALYTIC APPROACH TO THE DIFFUSIONLESS INSTABILITY

---

$\epsilon \rightarrow 0$ . The functional dependence  $\lambda(\epsilon)$ , however, is not the same as that of the solution to  $\tan(\lambda) = \epsilon\lambda$  (Figure 5.1) used to construct  $y_c$  for  $\epsilon \sim O(1)$ . We may, however, plot the difference in the eigenvalues from the asymptotic solution. In Figure 5.7 we plot the difference  $\lambda - \lambda_t$ , where  $\tan \lambda_t = \epsilon\lambda_t$  gives the eigenvalue in the asymptotic limit  $\epsilon \rightarrow 0$ , i.e. the eigenvalues shown in Figure 5.1. We overplot a curve proportional to  $\epsilon^2$ , which has a dependence close to that of  $\lambda - \lambda_t$  as  $\epsilon \rightarrow 0$ .

Of course, in a boundary layer problem such as (5.61), the choice of boundary condition is important in determining the form the solution will take. We will now consider a different choice of boundary condition, solving numerically for the case where the gradient of the solution is fixed at the other end of the domain.

### 5.3.3 Numerical solution to (5.61) for $y'(1) = 0$

We also solve the numerical problem with the boundary condition  $y'(1) = 0$ , in order to understand the effect of fixing the gradient at the opposite boundary of the layer. We find fully numerical solutions for both  $\epsilon \ll 1$  and the  $\epsilon = O(1)$  regime, which are shown in Figure 5.8. Additionally, the associated eigenvalues  $\lambda^2(\epsilon)$  are shown in Figure 5.9.

Although we cannot find an analytical solution using the same asymptotic matching process as in Section 5.3.1, we are able to find a numerical solution, which is quite different — in both functional form and eigenvalues as a function of  $\epsilon$  — from the analytical solution when  $y'(0) = 0$ . The eigenvalues in this case are not real but purely imaginary, as shown in Figure 5.9. The value of  $\lambda^2$  is not monotonically increasing with  $\epsilon$ , but has a maximum of  $\lambda^2 \sim -22.31$  at  $\epsilon \sim 0.1705$ . The solution is also increasingly localised close to  $z = 0$  (i.e. in the boundary layer region) as  $\epsilon \rightarrow 0$ , in contrast to the case of  $y'(0) = 0$ .

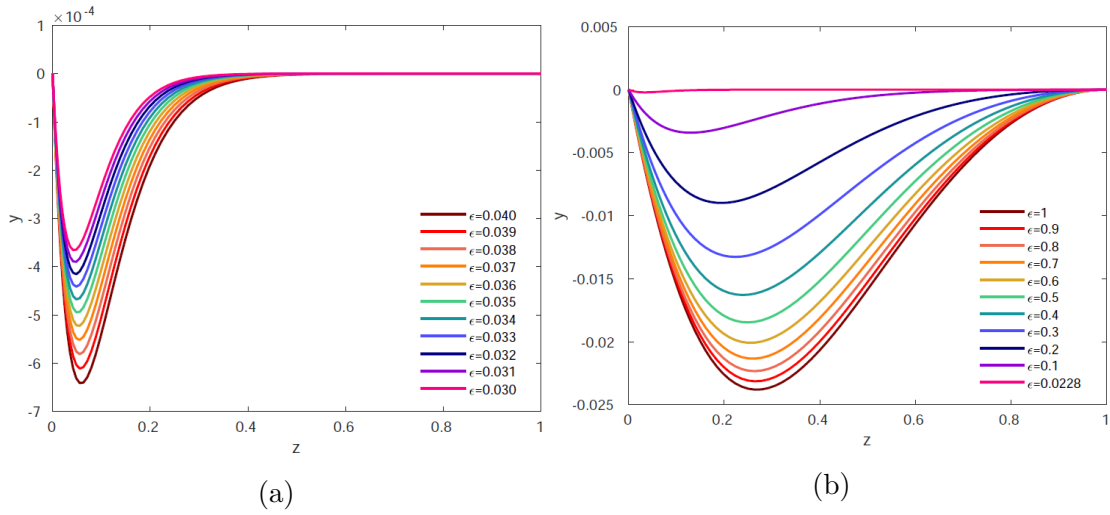


Figure 5.8: Numerical solution to Equation (5.61) with boundary conditions  $y(0) = 0$ ,  $y(1) = 0$ ,  $y'(1) = 0$ , for (a) small  $\epsilon$  and (b)  $\epsilon = O(1)$ .

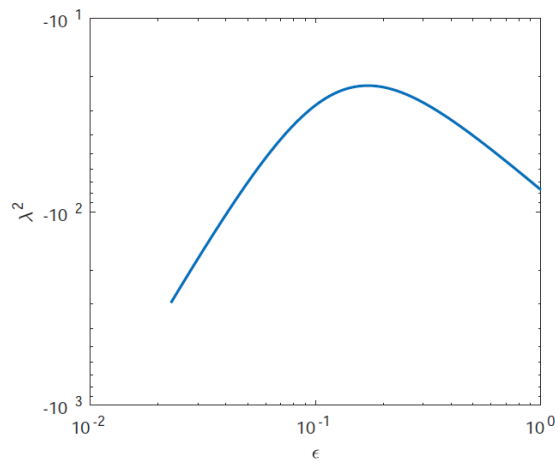


Figure 5.9:  $\lambda^2$  eigenvalues corresponding to the solutions shown in Figure 5.8.

## 5.4 A more complex third order model problem

We may also consider a different third order eigenvalue model problem that is slightly more complex but perhaps more reflective of the full diffusionless interchange system. The problem we choose is equivalent to that presented by [Mizerski \*et al.\* \(2013\)](#), but with two additional terms proportional to  $\gamma$ . As a simplified model for the diffusionless system in the absence of  $\gamma$ , Mizerski *et al.* considered:

$$\frac{d^2 f}{dz^2} - k^2[(\sigma - \sigma_{max}) + (z - z_{max})^2]f = 0, \quad (5.79)$$

where  $\sigma$  is an eigenvalue corresponding to the solution  $f$ , and  $\sigma_{max}$  and  $z_{max}$  are parameters. This form was chosen for several reasons; firstly, because it models the second order problem containing a parameter  $k$  and an unknown eigenvalue  $\sigma$ , which serves as a model for the second order ODE in the case of diffusionless interchange modes with growth rate  $s$ . Secondly, the  $k$ -dependence of Equation (5.79) allowed [Mizerski \*et al.\* \(2013\)](#) to consider the limit  $k \rightarrow \infty$ , in which, in the full problem, the system becomes algebraic as discussed by [Gilman \(1970\)](#). The form of Equation (5.79) also demonstrates this, as well as allowing the meaning of the growth rate  $\sigma$  in this limit to become apparent. Changing variables makes it apparent that (5.79) is in fact a form of the parabolic cylinder equation.

In an effort to understand the effect of  $\gamma$  on such a simplified model problem, we add two new terms proportional to  $\gamma$  to Equation (5.79), one of which contains a third derivative in accordance with the form of (5.49). This results in the following third order problem:

$$\gamma \frac{d^3 f}{dz^3} + \frac{d^2 f}{dz^2} - \gamma k^2 \frac{df}{dz} - k^2[(\sigma - \sigma_{max}) + (z - z_{max})^2]f = 0, \quad (5.80)$$

with the form of the two additional terms chosen for dimensional consistency. Note that unlike in the full problem, we assume  $\gamma$  to be spatially constant, and equivalent to  $\epsilon$  in (5.61). We may apply the same method to solve this as used in Section 5.3.1, in the limit  $\gamma \rightarrow 0$ , with boundary conditions

$$f(0) = 0, \quad (5.81)$$

$$f(1) = 0, \quad (5.82)$$

$$f'(0) = 0. \quad (5.83)$$

## 5.4 A more complex third order model problem

---

Again we solve on an interval  $0 \leq z \leq 1$ , and expect a boundary layer at  $z = 0$ . The equation for the outer solution is:

$$\frac{d^2 f}{dz^2} - k^2[(\sigma - \sigma_{max}) + (z - z_{max})^2]f = 0. \quad (5.84)$$

This is equivalent to the parabolic cylinder equation, which has the general form

$$\frac{d^2 f}{dx^2} - \left(\frac{1}{4}x^2 + a\right)f = 0, \quad (5.85)$$

after change of variables

$$x = \sqrt{2k}(z - z_{max}), \quad (5.86)$$

$$a = \frac{k(\sigma - \sigma_{max})}{2} \quad (5.87)$$

(see [Mizerski \*et al.\*, 2013](#)). The solutions are parabolic cylinder functions, with the form

$$y_1 = \sum_{n=even}^{\infty} A_n \frac{x^n}{n!}, \quad (5.88)$$

$$y_2 = \sum_{n=odd}^{\infty} A_n \frac{x^n}{n!}, \quad (5.89)$$

where the coefficients  $A_n$  are given by

$$A_{n+2} = aA_n + \frac{1}{4}n(n-1)A_{n-2}, \quad (5.90)$$

with  $A_0 = A_1 = 1$ ,  $A_2 = A_3 = a$  ([Abramowitz & Stegun, 1964](#)).

We may write the outer solution as a sum of these parabolic cylinder functions:

$$f_{out} = \chi_1 y_1 + \chi_2 y_2. \quad (5.91)$$

Applying the outer boundary condition (at  $z = 1$ ),  $f_{out}(1) = 0$ , we find that  $\chi_2 = -\frac{y_1(1)}{y_2(1)}\chi_1$ , and therefore we can write:

$$f_{out} = \chi \left( y_1 - \frac{y_1(1)}{y_2(1)} y_2 \right), \quad (5.92)$$

## 5. AN ANALYTIC APPROACH TO THE DIFFUSIONLESS INSTABILITY

---

for arbitrary constant  $\chi$ . Now that we have obtained the outer solution, let us consider the inner solution. Defining the boundary layer coordinate  $s = z/\gamma$  yields the same form of the inner equation as before, i.e. (5.69). This is:

$$\frac{d^3 f}{ds^3} + \frac{d^2 f}{ds^2} = 0, \quad (5.93)$$

which has a solution of the form:

$$f_{in} = \beta_1 e^{-\frac{z}{\gamma}} + \beta_2 \frac{z}{\gamma} + \beta_3. \quad (5.94)$$

Again, as in the previous example, the inner boundary conditions  $f_{in}(0) = 0$  and  $f'_{in}(0) = 0$  allow us, respectively, to fix the constants  $\beta_3 = -\beta_1$  and  $\beta_2 = \beta_1$ . We may then write the inner solution as

$$f_{in} = \beta(e^{-\frac{z}{\gamma}} + \frac{z}{\gamma} - 1). \quad (5.95)$$

We may now match the inner and outer solutions. We introduce the variable of intermediate scale,  $\eta = z/\gamma^\alpha$ , where  $0 < \alpha < 1$ , and take the limit  $\gamma \rightarrow 0$ , at fixed  $\eta$ . In this case, we obtain:

$$f_{in} \sim \beta(\gamma^{\alpha-1}\eta - 1), \quad (5.96)$$

$$\begin{aligned} f_{out} \sim & \chi \left( \left[ \sum_{n=even}^{\infty} \frac{A_n}{n!} (z_{max} \sqrt{2k})^n + \frac{y_1(1)}{y_2(1)} \sum_{n=odd}^{\infty} \frac{A_n}{n!} (z_{max} \sqrt{2k})^n \right] \right. \\ & \left. - \gamma^\alpha \eta \sqrt{2k} \left[ \sum_{n=even}^{\infty} \frac{A_n}{(n-1)!} (z_{max} \sqrt{2k})^{n-1} + \frac{y_1(1)}{y_2(1)} \sum_{n=odd}^{\infty} \frac{A_n}{(n-1)!} (z_{max} \sqrt{2k})^{n-1} \right] \right). \end{aligned} \quad (5.97)$$

Matching  $O(1)$  terms gives the relation:

$$-\beta = \chi \left( \sum_{n=even}^{\infty} \frac{A_n}{n!} (z_{max} \sqrt{2k})^n + \frac{y_1(1)}{y_2(1)} \sum_{n=odd}^{\infty} \frac{A_n}{n!} (z_{max} \sqrt{2k})^n \right), \quad (5.98)$$

while matching  $O(\eta)$  terms gives:

$$\beta \gamma^{\alpha-1} = -\chi \gamma^\alpha \sqrt{2k} \left( \sum_{n=even}^{\infty} \frac{A_n}{(n-1)!} (z_{max} \sqrt{2k})^{n-1} + \frac{y_1(1)}{y_2(1)} \sum_{n=odd}^{\infty} \frac{A_n}{(n-1)!} (z_{max} \sqrt{2k})^{n-1} \right). \quad (5.99)$$

## 5.4 A more complex third order model problem

---

We may then eliminate constants  $\beta$  and  $\chi$  and obtain an implicit equation for the eigenvalues  $\sigma$  in terms of  $A_n$ ,  $\gamma$  and  $k$ :

$$\begin{aligned} & \left[ \sum_{n=even}^{\infty} \frac{A_n}{n!} (z_{max} \sqrt{2k})^n + \frac{y_1(1)}{y_2(1)} \sum_{n=odd}^{\infty} \frac{A_n}{n!} (z_{max} \sqrt{2k})^n \right] \\ & - \gamma \sqrt{2k} \left[ \sum_{n=even}^{\infty} \frac{A_n}{(n-1)!} (z_{max} \sqrt{2k})^{n-1} + \frac{y_1(1)}{y_2(1)} \sum_{n=odd}^{\infty} \frac{A_n}{(n-1)!} (z_{max} \sqrt{2k})^{n-1} \right] = 0. \end{aligned} \quad (5.100)$$

This is the analogue of (5.75), relating the eigenvalues to the small parameter, in this case  $\gamma$ . Also, from the  $O(1)$  matching relation (5.98), we know the proportionality of the coefficients  $\beta$  and  $\chi$ , so we may choose

$$\begin{aligned} \beta &= - \left[ \sum_{n=even}^{\infty} \frac{A_n}{n!} (z_{max} \sqrt{2k})^n + \frac{y_1(1)}{y_2(1)} \sum_{n=odd}^{\infty} \frac{A_n}{n!} (z_{max} \sqrt{2k})^n \right] \\ &= -y_1(0) + \frac{y_1(1)}{y_2(1)} y_2(0), \end{aligned} \quad (5.101)$$

$$\chi = 1. \quad (5.102)$$

Therefore, the composite solution is:

$$f_c(z) = - \left( y_1(0) - \frac{y_1(1)}{y_2(1)} y_2(0) \right) e^{-\frac{z}{\gamma}} + y_1(z) - \frac{y_1(1)}{y_2(1)} y_2(z), \quad (5.103)$$

which obeys the boundary conditions in the limit  $\gamma \rightarrow 0$ , given (5.100). This composite solution may be constructed by solving (5.100) for the eigenvalues  $\sigma$ , and then using these eigenvalues to construct the parabolic cylinder functions  $y_1$  and  $y_2$  using an analogous method to that for the simpler model problem of Section 5.3.1. However, given that this requires a numerical solution in order to find  $\sigma$  that is then used to construct  $f_c$ , it is not a “true” analytical solution, so instead we may just find the numerical solution directly.

### 5.4.1 Numerical solution

We solve (5.80) numerically, for boundary conditions (5.81) – (5.83), along with the normalisation condition  $f''(0) = 1$  in order to fix the amplitude. Starting from the parabolic cylinder function solutions to (5.84), we use a continuation method to find the solution for increasing  $\gamma$ . We plot the normalised solutions in

## 5. AN ANALYTIC APPROACH TO THE DIFFUSIONLESS INSTABILITY

---

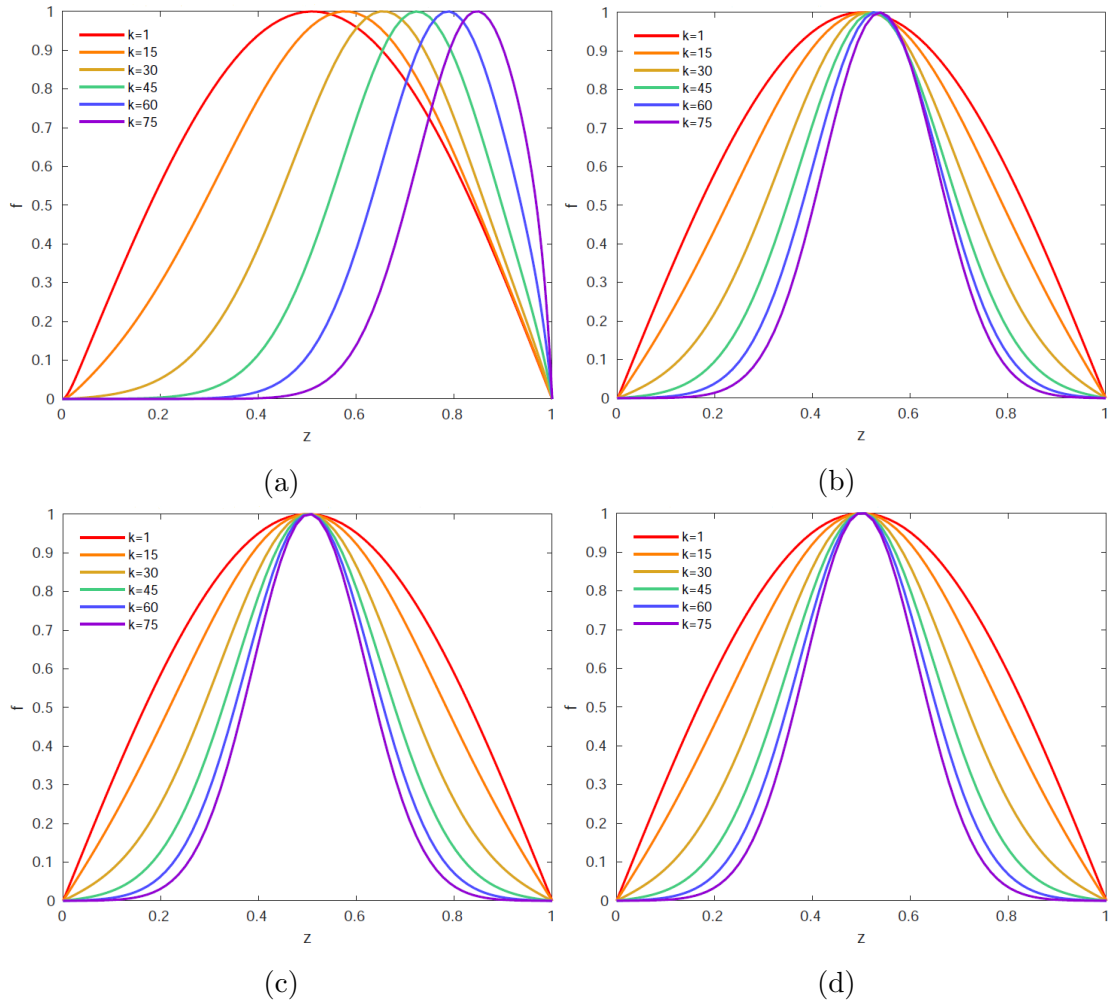


Figure 5.10: Numerical solutions to Equation (5.80), for (a)  $\gamma = 10^{-2}$ , (b)  $\gamma = 10^{-3}$ , (c)  $\gamma = 10^{-4}$ , and (d)  $\gamma = 10^{-5}$ .

## 5.4 A more complex third order model problem

---

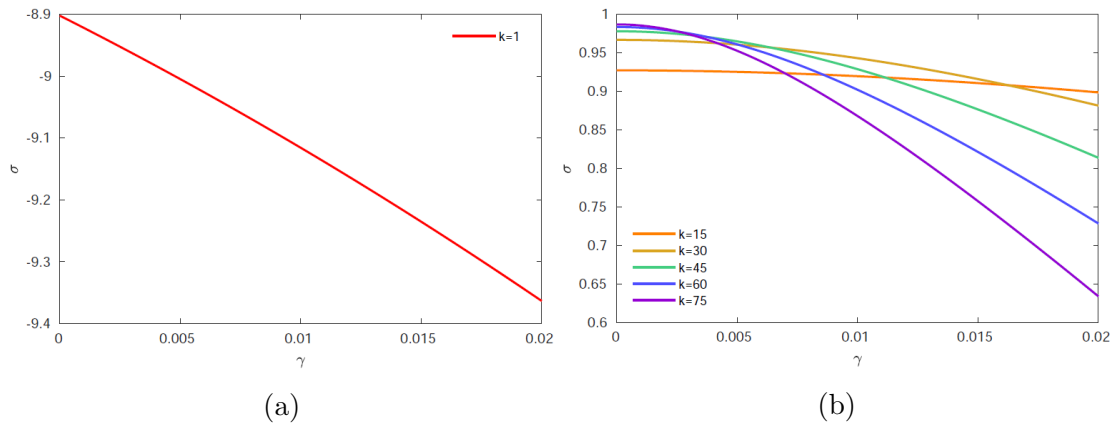


Figure 5.11: Eigenvalues  $\sigma(\gamma)$  corresponding to the numerical solutions plotted in Figure 5.10. Note that the plots of (a)  $k = 1$  and (b)  $k > 1$  are separated due to the difference in scale of the values of  $\sigma$ .

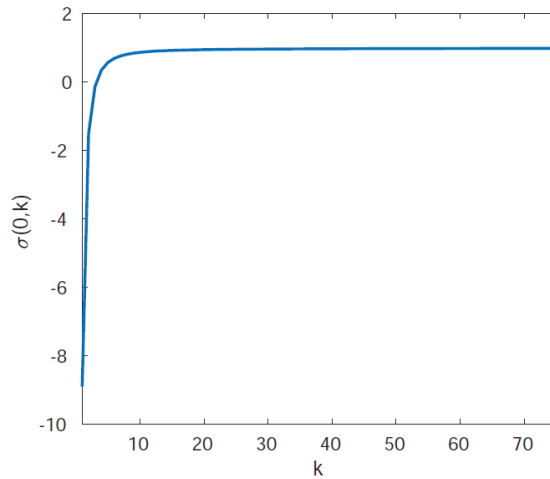


Figure 5.12: Eigenvalues  $\sigma(0, k)$  for  $\gamma = 0$ , corresponding to the eigenvalues of the parabolic cylinder equation, i.e. the outer equation (cf. Figure 5.13).

## 5. AN ANALYTIC APPROACH TO THE DIFFUSIONLESS INSTABILITY

---

Figure 5.10, and the eigenvalues  $\sigma$  in Figure 5.11.

We can see that as  $\gamma \rightarrow 0$ , the solution is more localised close to  $z_{max} = 0.5$ . In other words, larger  $\gamma$  “shifts” the solution to larger  $z$ , an effect that is also larger for higher  $k$ . Greater values of  $k$  give more peaked solutions, as is the case with the general, unperturbed parabolic cylinder functions. However, the boundary layer part of the solution, present in a region with thickness of order  $\sim \gamma$ , is no longer clearly visible once we reach the smaller values of  $\gamma$  shown in Figures 5.10c and 5.10d.

Note that it is not the case that the numerical scheme — in this case a fourth order collocation method — merely fails to resolve a boundary layer structure as  $\gamma \rightarrow 0$ ; with the expected size of the boundary layer region on the order of  $\gamma$ , we have considered grid spacings on the order of  $10^{-3}\gamma$  in the region  $z \sim 0$  where we expect the boundary layer, which should be able to resolve a boundary layer structure similar to that evident in the numerical solutions in Section 5.3.3, if one were present. However, we see no similar large peak in the boundary layer region as  $\gamma \rightarrow 0$  in the numerical solution to (5.80) shown in Figure 5.10.

Let us now consider the eigenvalues of (5.80), shown in Figure 5.11. We can see that these are also dependent on  $k$  and  $\gamma$ ; for one thing, the value of  $\sigma$  when  $\gamma = 0$  tends to  $\sigma_{max} = 1$  for increasing  $k$ . (Note that this is also clear in Figure 5.12, in which the eigenvalues for  $\gamma = 0$  are shown as a function of  $k$ .) For non-zero  $\gamma$ , the curve  $\sigma(\gamma)$  has a negative gradient, which is of greater magnitude for lower  $k$ .

In order to better understand the  $\gamma$ -dependence of the eigenvalues, however, in Figure 5.13, we plot the quantity  $\sigma(\gamma, k) - \sigma(0, k)$ , where we denote the corresponding parabolic cylinder function eigenvalue (i.e. the eigenvalue of the outer solution) by  $\sigma(0, k)$ : these eigenvalues are plotted, for the sake of comparison, in Figure 5.12. Note that  $\sigma(\gamma, k) - \sigma(0, k)$  depends on both  $\gamma$  and  $k$ , according to a power law for larger  $k$ . By plotting this data on logarithmic scales in  $k$  and  $\gamma$ , however (Figure 5.14), we may overplot lines of constant gradient in

## 5.4 A more complex third order model problem

---

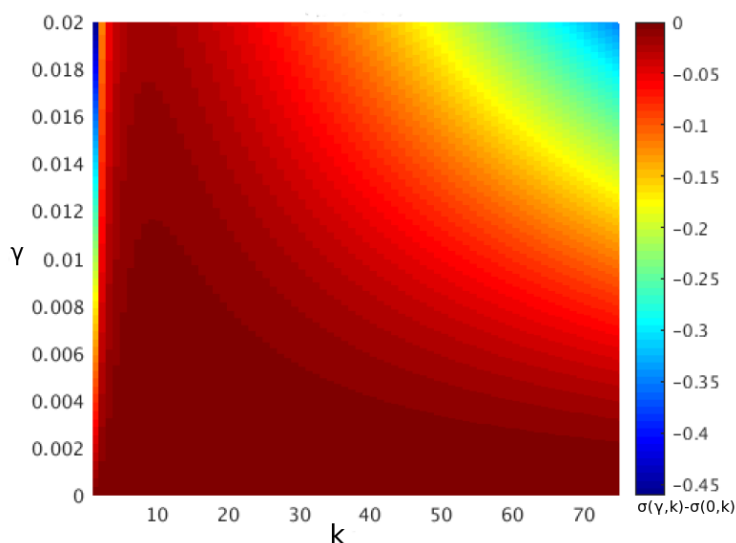


Figure 5.13: The variation of  $\sigma(\gamma, k) - \sigma(0, k)$  as a function of  $k$  and  $\gamma$ , showing the deviation from the parabolic cylinder function eigenvalues due to non-zero  $\gamma$ .

order to show that the quantity  $\sigma(\gamma, k) - \sigma(0, k)$  is approximately constant for  $\gamma$  proportional to  $k^{-1}$ , for large  $k$  (dashed lines). From this, we find that for large  $k$ ,  $\sigma(\gamma, k) - \sigma(0, k)$  is proportional to  $\gamma k$ . It is not clear how this dependence arises from the form of Equation (5.80), or indeed what the dominant balance of terms is that gives rise to it in the large  $k$  regime. Future work on such a model problem, however, could address this issue.

In addition to the dependence of  $\sigma(\gamma, k) - \sigma(0, k)$  for large  $k$ , although it is less apparent on the scale of Figure 5.13, in Figure 5.14 we can see a different power law dependence for small  $k$ . We overplot lines with  $\gamma$  proportional to  $k^2$  (dotted lines), which suggest that there is some dependence on such a power law, with  $\sigma(\gamma, k) - \sigma(0, k)$  proportional to  $\gamma/k^2$  at low  $k$  (with our parameters, for about  $k \lesssim 8$ ). The resolution at low  $k$ , however, is too low to be able to say for certain whether this is a true dependence or the result of a numerical artifact. This, however, constitutes an area for further study.

This type of analysis may also be applied to the full diffusionless interchange

## 5. AN ANALYTIC APPROACH TO THE DIFFUSIONLESS INSTABILITY

---

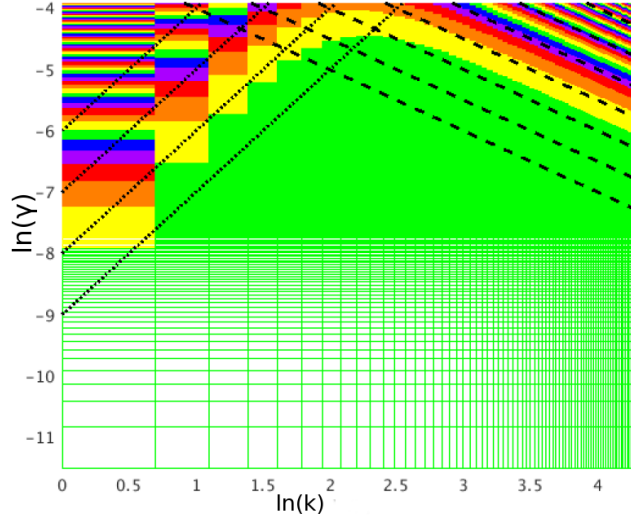


Figure 5.14:  $\sigma(\gamma, k) - \sigma(0, k)$  as a function of  $\ln(k)$  and  $\ln(\gamma)$ , with arbitrary colour values assigned to constant values of  $\sigma(\gamma, k) - \sigma_o(k)$ . Dashed lines correspond to constant  $\gamma k$ , and dotted lines to constant  $\gamma/k^2$ , showing the approximate dependence for high and low  $k$ , respectively.

system given by Equation (5.49). The eigenvalue relation giving the growth rate in terms of  $\gamma$  would be much more complex, but we would see a similar boundary layer type solution forming in the limit  $\gamma \rightarrow 0$ . This, too, is a matter for further work in this area.

We will now return to the full system, and use a local analysis approach to understand the instability.

### 5.5 Local Approximation

Now we take a local approximation, an approach that can allow the derivation of analytic stability criteria (see, for example, the work of [Acheson \(1979\)](#), and [Hughes, 1985](#)), for the linear stability of a small region. Such an approach is valid when the background states vary slowly over the region considered, and in this circumstance, it can allow us to gain insight into the nature of the instability. We

consider perturbations of the general form:

$$\tilde{\xi} = \hat{\xi} \exp(st + ik_x x + ik_y y + ik_z z). \quad (5.104)$$

Note that as opposed to all previous cases, where  $\hat{\xi}$  was a function of  $z$  and encapsulated the vertical dependence (see definition (3.5)), the perturbations are now assumed to be periodic in  $z$ , and therefore  $\hat{\xi}$  is a constant. Allowing perturbations of this form gives a system of algebraic equations, rather than ODEs, which allows a dispersion relation for the system to be derived. This approach is not without its limitations, which we will discuss in greater detail in Section 5.5.4. However, we shall consider two interchange systems, in order to try to understand the effect of adding  $\gamma$  and  $\beta$  to the instability problem.

### 5.5.1 Isothermal, interchange system

In the first instance, for simplicity we will consider interchange modes, as well as removing magnetic and viscous diffusion terms and the temperature perturbation. Note that we refer to this case as “isothermal” even though we assume that the background temperature profile  $\bar{T}$  can have non-zero gradient; the reason for this is on one hand to differentiate it from the adiabatic case discussed in Section 5.5.3, but on the other hand, physically, we may characterise this case as effectively having infinite thermal diffusivity, such that temperature perturbations decay immediately. There may, however, still be a spatially varying background temperature profile that is stably stratified, and therefore we allow a non-zero value of  $\bar{T}'$  to appear in the equations. Thus, this case, like much of the “isothermal” analysis in this Chapter, is not strictly diffusionless; for our purposes, however, we will refer to it as such for the sake of expediency.

These assumptions give the following system of algebraic equations:

$$(s + \beta(k_y^2 + k_z^2) + ik_z(\gamma - \beta') + \gamma')\hat{b}_x + \bar{B}ik_y\hat{v} + (\bar{B}' + ik_z\bar{B})\hat{w} = 0, \quad (5.105)$$

$$ik_y F \bar{B} \hat{b}_x + s\bar{\rho}\hat{v} + ik_y \bar{T} \hat{\rho} = 0, \quad (5.106)$$

$$F(\bar{B}' + ik_z\bar{B})\hat{b}_x + s\bar{\rho}\hat{w} + (\bar{T}' + ik_z\bar{T} - \theta(m+1))\hat{\rho} = 0, \quad (5.107)$$

$$ik_y \bar{\rho} \hat{v} + (\bar{\rho}' + ik_z \bar{\rho}) \hat{w} + s \hat{\rho} = 0. \quad (5.108)$$

## 5. AN ANALYTIC APPROACH TO THE DIFFUSIONLESS INSTABILITY

---

The fact that these equations are algebraic allows us to obtain the dispersion relation analytically. Eliminating the perturbed quantities gives a dispersion relation which is quartic in  $s$ :

$$\begin{aligned} & \bar{\rho}s^4 + \bar{\rho}(\beta(k_y^2 + k_z^2) + ik_z(\gamma - \beta') + \gamma')s^3 + \\ & -((\bar{\rho}' + ik_z\bar{\rho})(\bar{T}' + ik_z\bar{T} - \theta(m+1)) + F(\bar{B}' + ik_z\bar{B})^2 - (F\bar{B}^2 + \bar{T}\bar{\rho})k_y^2)s^2 \\ & -(\beta(k_y^2 + k_z^2) + ik_z(\gamma - \beta') + \gamma')((\bar{\rho}' + ik_z\bar{\rho})(\bar{T}' + ik_z\bar{T} - \theta(m+1)) - k_y^2\bar{T}\bar{\rho})s \\ & -Fk_y^2\bar{B}^2 \frac{d}{dz} \ln\left(\frac{\bar{B}}{\bar{\rho}}\right) \left(\theta(m+1) + \bar{T} \frac{d}{dz} \ln\left(\frac{\bar{B}}{\bar{T}}\right)\right) = 0. \end{aligned} \quad (5.109)$$

Equation (5.109) is of the form

$$f_4s^4 + P_{\gamma,\beta}f_3s^3 + f_2s^2 + P_{\gamma,\beta}f_1s + f_0 = 0, \quad (5.110)$$

where terms of order  $s^3$  and  $s^1$  are multiplied by a factor of

$$P_{\gamma,\beta} \equiv \beta(k_y^2 + k_z^2) + ik_z(\gamma - \beta') + \gamma', \quad (5.111)$$

and the functions  $f_0 - f_4$  are given by

$$f_0 = -Fk_y^2\bar{B}^2 \frac{d}{dz} \ln\left(\frac{\bar{B}}{\bar{\rho}}\right) \left(\theta(m+1) + \bar{T} \frac{d}{dz} \ln\left(\frac{\bar{B}}{\bar{T}}\right)\right), \quad (5.112)$$

$$f_1 = -((\bar{\rho}' + ik_z\bar{\rho})(\bar{T}' + ik_z\bar{T} - \theta(m+1)) - k_y^2\bar{T}\bar{\rho}), \quad (5.113)$$

$$\begin{aligned} f_2 = & -((\bar{\rho}' + ik_z\bar{\rho})(\bar{T}' + ik_z\bar{T} - \theta(m+1)) + F(\bar{B}' + ik_z\bar{B})^2 \\ & - (F\bar{B}^2 + \bar{T}\bar{\rho})k_y^2), \end{aligned} \quad (5.114)$$

$$f_3 = \bar{\rho}, \quad (5.115)$$

$$f_4 = \bar{\rho}. \quad (5.116)$$

From the form of Equation (5.110), we may immediately see that the condition for marginal stability (corresponding to  $s = 0$ ) is given by  $f_0 = 0$ . Note that all of the dependence on  $\gamma$  and  $\beta$  is contained within  $P_{\gamma,\beta}$ . When no  $\gamma$  and  $\beta$  effects are present, in this case, the equation simply becomes biquadratic, i.e. for  $P_{\gamma,\beta} = 0$ :

$$f_4s^4 + f_2s^2 + f_0 = 0. \quad (5.117)$$

We may also note that the condition for instability,  $s^2 > 0$ , is given by  $f_0 < 0$ , i.e.

$$\frac{d}{dz} \ln\left(\frac{\bar{B}}{\bar{\rho}}\right) \left(\theta(m+1) + \bar{T} \frac{d}{dz} \ln\left(\frac{\bar{B}}{\bar{T}}\right)\right) > 0. \quad (5.118)$$

## 5.5 Local Approximation

---

Note the modification to the standard diffusionless criterion for instability in the case of interchange modes (1.4), as well as the isothermal, large  $k_y$  case considered by Gilman (1970), given by (5.28). In criterion (5.118), the stability depends not only on the density and magnetic field gradients, but also on the temperature gradient of the basic state, which is allowed in this case to be non-zero.

We may also find the non-zero solution,  $s_o$ , for  $P_{\gamma,\beta} = 0$ , given by

$$s_o = \pm \sqrt{s_{\pm}^2} = \pm \sqrt{\frac{-f_2 \pm \sqrt{f_2^2 - 4f_4f_0}}{2f_4}}, \quad (5.119)$$

where the four solutions  $s_o$  are two pairs given by  $s_o = \pm s_+, \pm s_-$ .

In the case of  $P_{\gamma,\beta} \neq 0$ , while the condition for marginal stability,  $s = 0$ , is still given by  $f_0 = 0$ , we cannot obtain the solution to the full quartic dispersion relation for a general growth rate. Given solution (5.119), however, we are able to find a perturbative solution to (5.110) for small values of  $|P_{\gamma,\beta}|$ . Let us take small values of  $\gamma$  and  $\beta$  such that

$$P_{\gamma,\beta} = \epsilon \hat{P}, \quad (5.120)$$

for  $\epsilon \ll 1$ , with  $\hat{P}$  a complex,  $O(1)$  function. We may perturb the solutions  $s_o$  given by (5.119), according to

$$s_o \mapsto s_o + \epsilon \hat{P} \hat{s}_o + O(\epsilon^2). \quad (5.121)$$

We substitute this into the dispersion relation (5.110) to obtain

$$\begin{aligned} & f_4(s_o + \epsilon \hat{P} \hat{s}_o + O(\epsilon^2))^4 + \epsilon \hat{P} f_3(s_o + \epsilon \hat{P} \hat{s}_o + O(\epsilon^2))^3 \\ & + f_2(s_o + \epsilon \hat{P} \hat{s}_o + O(\epsilon^2))^2 + \epsilon \hat{P} f_1(s_o + \epsilon \hat{P} \hat{s}_o + O(\epsilon^2)) + f_0 = 0. \end{aligned} \quad (5.122)$$

Taking the balance of  $O(\epsilon^0)$  terms, we obtain

$$f_4 s_o^4 + f_2 s_o^2 + f_0 = 0, \quad (5.123)$$

which simply gives the definition of  $s_o$ , as we expect. If we take the next balance of terms,  $O(\epsilon)$ , we have

$$4f_4 s_o^3 \hat{P} \hat{s}_o + f_3 s_o^3 \hat{P} + 2f_2 s_o \hat{s}_o \hat{P} + f_1 s_o \hat{P} = 0, \quad (5.124)$$

## 5. AN ANALYTIC APPROACH TO THE DIFFUSIONLESS INSTABILITY

---

from which we may obtain an expression for  $\hat{s}_o$ :

$$\hat{s}_o = -\left(\frac{f_3 s_o^2 + f_1}{4f_4 s_o^2 + 2f_2}\right). \quad (5.125)$$

Thus, for  $\gamma, \beta \ll 1$ , we have derived a perturbative solution to Equation (5.110) about the  $P_{\gamma, \beta} = 0$  solution  $s_o$  given by (5.119). Given, however, that  $\hat{s}_o$  is a complex function that depends sensitively on the functions  $f_0 - f_4$ , we may not, in general, say whether the effect of such a perturbation will be stabilising or destabilising, or, indeed, whether oscillatory or growing modes or both will be affected: this depends on the spatial dependence of the basic states chosen.

### 5.5.2 Isothermal 3D system

If we make the same assumptions but no longer specify that  $k_x = 0$ , then in the same way we obtain a set of seven linear algebraic equations:

$$(s + \beta(k_x^2 + k_y^2 + k_z^2) + ik_z(\gamma - \beta') + \gamma')\hat{b}_x + \beta'ik_x\hat{b}_z + \bar{B}ik_y\hat{v} + (\bar{B}' + ik_z\bar{B})\hat{w} = 0, \quad (5.126)$$

$$(s + \beta(k_x^2 + k_y^2 + k_z^2) + ik_z(\gamma - \beta') + \gamma')\hat{b}_y + \beta'ik_y\hat{b}_z - \bar{B}ik_x\hat{v} = 0, \quad (5.127)$$

$$(s + \beta(k_x^2 + k_y^2 + k_z^2) + ik_z\gamma)\hat{b}_z - \bar{B}ik_x\hat{w} = 0, \quad (5.128)$$

$$-F\bar{B}'\hat{b}_z + s\bar{\rho}\hat{u} + \bar{T}ik_x\hat{\rho} = 0, \quad (5.129)$$

$$F\bar{B}ik_y\hat{b}_x - F\bar{B}ik_x\hat{b}_y + s\bar{\rho}\hat{v} + \bar{T}ik_y\hat{\rho} = 0, \quad (5.130)$$

$$F(\bar{B}' + ik_z\bar{B})\hat{b}_x - F\bar{B}ik_x\hat{b}_z + s\bar{\rho}\hat{w} + (\bar{T}' + ik_z\bar{T} - \theta(m+1))\hat{\rho} = 0, \quad (5.131)$$

$$\bar{\rho}ik_x\hat{u} + \bar{\rho}ik_y\hat{v} + (\bar{\rho}' + ik_z\bar{\rho})\hat{w} + s\hat{\rho} = 0. \quad (5.132)$$

Equations (5.126) – (5.132) lead to the following seventh order dispersion relation:

$$g_7 s^7 + g_6 s^6 + g_5 s^5 + g_4 s^4 + g_3 s^3 + g_2 s^2 + g_1 s + g_0 = 0. \quad (5.133)$$

Owing to their length, the coefficients  $g_0 - g_7$  are written out in full in Appendix B, to which the reader may refer. Marginal stability for non-zero  $\gamma$  and  $\beta$  is given by  $g_0 = 0$ . Note also that the coefficients  $g_0, g_2, g_4$  and  $g_6$  of the even power terms depend on  $\gamma$  and  $\beta$  in such a way that they are all zero when  $\gamma, \beta = 0$ . The dependence, however, cannot be characterised in terms of a single factor analogous

to (5.111) as in the interchange case. Nevertheless, in the case of  $\gamma = \beta = 0$ , the dispersion relation becomes cubic in  $s^2$ . While a solution can, formally, be found, and its perturbative modification to the growth rate for  $\gamma, \beta \ll 1$  (analogous to (5.125) for the 3D case) can also be obtained, this would be much more mathematically involved.

Instead, we shall consider another interchange system, based on slightly different physical assumptions.

### 5.5.3 Adiabatic, interchange system

We now include temperature perturbation  $\tilde{T}$  in order to model more closely the full system, although we still exclude diffusive effects apart from  $\beta$ . This introduces an additional equation to satisfy, the energy equation for  $\tilde{T}$ . We consider the following interchange system:

$$\partial_t \tilde{b}_x = (\beta(\partial_y^2 + \partial_z^2) + \beta' \partial_z - \gamma' - \gamma \partial_z) \tilde{b}_x - \bar{B} \partial_y \tilde{v} - (\bar{B}' + \bar{B} \partial_z) \tilde{w}, \quad (5.134)$$

$$\bar{\rho} \partial_t \tilde{v} = -F \bar{B} \partial_y \tilde{b}_x - \bar{\rho} \partial_y \tilde{T} - \bar{T} \partial_y \tilde{\rho}, \quad (5.135)$$

$$\bar{\rho} \partial_t \tilde{w} = -F(\bar{B}' + \bar{B} \partial_z) \tilde{b}_x - (\bar{\rho}' + \bar{\rho} \partial_z) \tilde{T} - (\bar{T}' + \bar{T} \partial_z - \theta(m+1)) \tilde{\rho}, \quad (5.136)$$

$$\partial_t \tilde{T} = -(\Gamma - 1) \bar{T} \partial_y \tilde{v} - ((\Gamma - 1) \bar{T} \partial_z + \bar{T}') \tilde{w}, \quad (5.137)$$

$$\partial_t \tilde{\rho} = -\bar{\rho} \partial_y \tilde{v} - (\bar{\rho}' + \bar{\rho} \partial_z) \tilde{w}. \quad (5.138)$$

Applying interchange perturbations of the form

$$\tilde{\xi} = \hat{\xi} \exp(st + ik_y y + ik_z z), \quad (5.139)$$

leads to the algebraic system:

$$(s + \beta(k_y^2 + k_z^2) + ik_z(\gamma - \beta') + \gamma') \hat{b}_x + \bar{B} ik_y \hat{v} + (\bar{B}' + ik_z \bar{B}) \hat{w} = 0, \quad (5.140)$$

$$ik_y F \bar{B} \hat{b}_x + s \bar{\rho} \hat{v} + ik_y \bar{\rho} \hat{T} + ik_y \bar{T} \hat{\rho} = 0, \quad (5.141)$$

$$F(\bar{B}' + ik_z \bar{B}) \hat{b}_x + s \bar{\rho} \hat{w} + (\bar{\rho}' + ik_z \bar{\rho}) \hat{T} + (\bar{T}' + ik_z \bar{T} - \theta(m+1)) \hat{\rho} = 0, \quad (5.142)$$

$$(\Gamma - 1) \bar{T} ik_y \hat{v} + (\bar{T}' + ik_z(\Gamma - 1) \bar{T}) \hat{w} + s \hat{T} = 0, \quad (5.143)$$

$$ik_y \bar{\rho} \hat{v} + (\bar{\rho}' + ik_z \bar{\rho}) \hat{w} + s \hat{\rho} = 0. \quad (5.144)$$

## 5. AN ANALYTIC APPROACH TO THE DIFFUSIONLESS INSTABILITY

---

Thus we may once more find a dispersion relation, which is in this case quintic in  $s$ .

$$\begin{aligned}
& \bar{\rho}^2 s^5 + \bar{\rho}^2 (\beta(k_y^2 + k_z^2) + ik_z(\gamma - \beta') + \gamma') s^4 \tag{5.145} \\
& + \bar{\rho} (k_y^2 (F\bar{B}^2 + \Gamma\bar{T}\bar{\rho}) - F(\bar{B}' + ik_z\bar{B})^2 - (\bar{\rho}' + ik_z\bar{\rho})(2\bar{T}' + \Gamma ik_z\bar{T} - \theta(m+1))) s^3 \\
& + \bar{\rho} (\beta(k_y^2 + k_z^2) + ik_z(\gamma - \beta') + \gamma') (k_y^2 \Gamma \bar{T} \bar{\rho} - (\bar{\rho}' + ik_z\bar{\rho})(2\bar{T}' + \Gamma ik_z\bar{T} - \theta(m+1))) s^2 \\
& - \bar{\rho} k_y^2 \left( \theta(m+1) (F\bar{B}^2 \frac{d}{dz} \ln \left( \frac{\bar{B}}{\bar{\rho}} \right) + \bar{T}\bar{\rho} \frac{d}{dz} \ln(\bar{T}\bar{\rho}^{1-\Gamma})) \right. \\
& \left. + F\bar{B}^2 \bar{T} \frac{d}{dz} \ln \left( \frac{\bar{B}}{\bar{\rho}} \right) \frac{d}{dz} \ln \left( \frac{\bar{B}^\Gamma}{\bar{T}^2} \right) + \bar{T}^2 \bar{\rho} \frac{d}{dz} \ln \left( \frac{\bar{\rho}}{\bar{T}} \right) \frac{d}{dz} \ln(\bar{T}\bar{\rho}^{1-\Gamma}) \right) s \\
& - k_y^2 \bar{T} \bar{\rho}^2 (\beta(k_y^2 + k_z^2) + ik_z(\gamma - \beta') + \gamma') \left( \bar{T} \frac{d}{dz} \ln \left( \frac{\bar{\rho}}{\bar{T}} \right) + \theta(m+1) \right) \frac{d}{dz} \ln(\bar{T}\bar{\rho}^{1-\Gamma}) = 0.
\end{aligned}$$

Here, we once more notice that the even powers of  $s$  are all multiplied by a factor of

$$P_{\gamma,\beta} \equiv \beta(k_y^2 + k_z^2) + ik_z(\gamma - \beta') + \gamma', \tag{5.146}$$

which is zero when the  $\gamma$  and  $\beta$  effects are not present. Since there is no other dependence on  $\gamma$  or  $\beta$  in this dispersion relation, we may consider two cases:  $P_{\gamma,\beta} = 0$  ( $\gamma = 0$  and  $\beta = 0$ ) and  $P_{\gamma,\beta} \neq 0$  ( $\gamma \neq 0$  and/or  $\beta \neq 0$ ). We shall consider the two cases separately.

Following the same approach as for the isothermal interchange instability, we may write the dispersion relation in the form:

$$\alpha_5 s^5 + \alpha_4 P_{\gamma,\beta} s^4 + \alpha_3 s^3 + \alpha_2 P_{\gamma,\beta} s^2 + \alpha_1 s + \alpha_0 P_{\gamma,\beta} = 0, \tag{5.147}$$

where  $P_{\gamma,\beta}$  is given by (5.146) and, dividing (5.145) through by a factor of  $\bar{\rho}$ ,

$$\alpha_0 = -k_y^2 \bar{T} \bar{\rho} \left( \bar{T} \frac{d}{dz} \ln \left( \frac{\bar{\rho}}{\bar{T}} \right) + \theta(m+1) \right) \frac{d}{dz} \ln(\bar{T}\bar{\rho}^{1-\Gamma}), \tag{5.148}$$

$$\begin{aligned}
\alpha_1 = & -k_y^2 \left( \theta(m+1) \left( F\bar{B}^2 \frac{d}{dz} \ln \left( \frac{\bar{B}}{\bar{\rho}} \right) + \bar{T}\bar{\rho} \frac{d}{dz} \ln(\bar{T}\bar{\rho}^{1-\Gamma}) \right) \right. \\
& \left. + F\bar{B}^2 \bar{T} \frac{d}{dz} \ln \left( \frac{\bar{B}}{\bar{\rho}} \right) \frac{d}{dz} \ln \left( \frac{\bar{B}^\Gamma}{\bar{T}^2} \right) + \bar{T}^2 \bar{\rho} \frac{d}{dz} \ln \left( \frac{\bar{\rho}}{\bar{T}} \right) \frac{d}{dz} \ln(\bar{T}\bar{\rho}^{1-\Gamma}) \right), \tag{5.149}
\end{aligned}$$

$$\alpha_2 = (k_y^2 \Gamma \bar{T} \bar{\rho} - (\bar{\rho}' + ik_z \bar{\rho})(2\bar{T}' + \Gamma ik_z \bar{T} - \theta(m+1))), \tag{5.150}$$

## 5.5 Local Approximation

---

$$\begin{aligned}\alpha_3 &= (k_y^2(F\bar{B}^2 + \Gamma\bar{T}\bar{\rho}) - F(\bar{B}' + ik_z\bar{B})^2 \\ &\quad - (\bar{\rho}' + ik_z\bar{\rho})(2\bar{T}' + \Gamma ik_z\bar{T} - \theta(m+1))),\end{aligned}\quad (5.151)$$

$$\alpha_4 = \bar{\rho}, \quad (5.152)$$

$$\alpha_5 = \bar{\rho}. \quad (5.153)$$

We shall now consider separately the cases of  $P_{\gamma,\beta} = 0$  and  $P_{\gamma,\beta} \neq 0$ , in order to discern the effect of  $\gamma$  and  $\beta$  on the instability. In the case of  $\gamma, \beta = 0$ , implying that  $P_{\gamma,\beta} = 0$ , the dispersion relation given by (5.147) becomes:

$$\alpha_5 s^5 + \alpha_3 s^3 + \alpha_1 s = 0. \quad (5.154)$$

This has one root given by  $s = 0$ , corresponding to marginal stability. The other solutions are given by a biquadratic equation in  $s^2$ :

$$\alpha_5 s^4 + \alpha_3 s^2 + \alpha_1 = 0, \quad (5.155)$$

where  $\alpha_3$  is complex, while  $\alpha_5$  and  $\alpha_1$  are real. Note that the dispersion relation (5.155) is not of the same form as the dispersion relation for instability in the magneto-Boussinesq system found by Hughes (1985), which is quadratic in  $s$ . However, it is likely the difference is due to the presence of additional modes in our system that are not evident under the Boussinesq approximation. Likewise, we may compare (5.155) to the results of Acheson (1979), who found a quadratic dispersion relation under the assumption that the scales of perturbation quantities, as defined by the wavenumbers, are much larger than the variation of the basic state, allowing the perturbation  $\tilde{\rho}$  to be neglected in the mass conservation equation. We, however, make no such assumption about the size of  $k_y$  and  $k_z$ , explaining the difference in the form of the dispersion relation (5.155) from Acheson's (see also Acheson (1978) for further discussion of comparative scales).

We may find the solutions to (5.155) by making use of the fact that it is biquadratic. Using the quadratic formula, we obtain, for  $\gamma = \beta = 0$ , solutions:

$$s_o = \pm \sqrt{s_{\pm}^2} = \pm \sqrt{\frac{-\alpha_3 \pm \sqrt{\alpha_3^2 - 4\alpha_5\alpha_1}}{2\alpha_5}}. \quad (5.156)$$

## 5. AN ANALYTIC APPROACH TO THE DIFFUSIONLESS INSTABILITY

---

As in the isothermal case, the roots are given by two pairs with  $s_o = \pm s_+, \pm s_-$ . Note that for  $\alpha_1 = 0$ , we obtain either an additional  $s_o = 0$  solution (marginal stability), or a solution  $s_o = \pm\sqrt{-\alpha_3/\alpha_5}$ , and therefore we cannot say that the criterion  $\alpha_1 = 0$  guarantees marginal stability. Indeed, in excluding the  $s = 0$  solution to the dispersion relation in the form (5.154), and by dividing by  $s$  in order to obtain the biquadratic form (5.155), we have already implicitly made the assumption that  $s$  is non-zero; it is for this reason that we are unable to apply a similar method to that applied by Hughes (1985) to the magneto-Boussinesq equations, in order to find an analogous stability criterion in this instance. Note also that  $s_o$  may be complex, implying an oscillatory instability for some choices of basic state.

Let us choose  $\alpha_1 \neq 0$  such that  $s \neq 0$ ; this may correspond to a stable or unstable state, which may also have an oscillatory component. We will now consider the effect of a small increase in  $\gamma$  and/or  $\beta$  from zero on such a case. We now consider the case of  $P_{\gamma,\beta} \neq 0$ , in which the dispersion relation is given by (5.147). Marginal stability is given by  $\alpha_0 = 0$ , i.e.

$$\left( \theta(m+1) + \bar{T} \frac{d}{dz} \ln \left( \frac{\bar{\rho}}{\bar{T}} \right) \right) \frac{d}{dz} \ln(\bar{T} \bar{\rho}^{1-\Gamma}) = 0. \quad (5.157)$$

Note that although this form of the condition may lack explicit dependence on  $\bar{B}$ , the marginal stability may be affected by the magnetic field via its effect on the equilibrium basic states  $\bar{T}$  and  $\bar{\rho}$ . Indeed, given the forms of the basic states  $\bar{T}$  and  $\bar{\rho}$  discussed in Section 2.13 and their derivation from  $\bar{B}$  for magnetohydrostatic equilibrium, the condition (5.157) may also be written to show explicit dependence on  $\bar{B}$ . Using the gas law (1.36) to eliminate  $\bar{T}$ , as well as the assumption of magnetohydrostatic equilibrium (2.42) originally used to derive the density basic state, we may write the condition for marginal stability (5.157) in the form

$$\left( 2\bar{\rho} \frac{d}{dz} \ln \bar{\rho} + F \bar{B}^2 \frac{d}{dz} \ln \bar{B} \right) \frac{d}{dz} \ln(\bar{\rho} \bar{\rho}^{-\Gamma}) = 0. \quad (5.158)$$

From (5.158), we can see that the criterion for marginal stability does indeed depend on  $\bar{B}$ , with implicit dependence on  $\gamma$  and  $\beta$  via their effect on the equilibrium basic state. Equally though, this criterion for marginal stability is also

## 5.5 Local Approximation

---

reliant on  $\gamma$  and  $\beta$  in the sense that it only applies at all if  $\gamma$  and  $\beta$  are non-zero, by the form of the dispersion relation (5.147); if  $\gamma, \beta = 0$ , (5.158) does not give marginal stability, as we revert to the  $P_{\gamma, \beta} = 0$  case discussed previously, characterised by the dispersion relation (5.154). As soon as  $\gamma$  and/or  $\beta$  become non-zero, however, the criterion (5.158) applies.

We now return to considering Equation (5.147). The full quintic dispersion relation cannot be solved analytically for a general growth rate, as Equation (5.155) can. Given the solution (5.156), however, we are able to find a perturbative solution to (5.147) for small values of  $|P_{\gamma, \beta}|$ , using the same method as in Section 5.5.1. Let us take small values of  $\gamma$  and  $\beta$  such that

$$P_{\gamma, \beta} = \epsilon \hat{P}, \quad (5.159)$$

for  $\epsilon \ll 1$ , with  $\hat{P}$  the complex form of  $P_{\gamma, \beta}$  involving  $\gamma$  and  $\beta$ . We may perturb the solutions  $s_o$  given by (5.156), according to

$$s_o \mapsto s_o + \epsilon \hat{P} \hat{s}_o + O(\epsilon^2). \quad (5.160)$$

We substitute this into the dispersion relation (5.147) to obtain

$$\begin{aligned} & \alpha_5(s_o + \epsilon \hat{P} \hat{s}_o + O(\epsilon^2))^5 + \alpha_4 \epsilon \hat{P} (s_o + \epsilon \hat{P} \hat{s}_o + O(\epsilon^2))^4 + \alpha_3 (s_o + \epsilon \hat{P} \hat{s}_o + O(\epsilon^2))^3 \\ & + \alpha_2 \epsilon \hat{P} (s_o + \epsilon \hat{P} \hat{s}_o + O(\epsilon^2))^2 + \alpha_1 (s_o + \epsilon \hat{P} \hat{s}_o + O(\epsilon^2)) + \alpha_0 \epsilon \hat{P} = 0. \end{aligned} \quad (5.161)$$

Note that the  $O(1)$  balance of terms gives

$$\alpha_5 s_o^5 + \alpha_3 s_o^3 + \alpha_1 s_o = 0, \quad (5.162)$$

which is equivalent to Equation (5.154). Taking the next balance, of  $O(\epsilon)$  terms, gives:

$$5\alpha_5 s_o^4 \hat{s}_o + \alpha_4 s_o^4 + 3\alpha_3 s_o^2 \hat{s}_o + \alpha_2 s_o^2 + \alpha_1 \hat{s}_o + \alpha_0 = 0, \quad (5.163)$$

which allows us to find  $\hat{s}_o$ :

$$\hat{s}_o = - \left( \frac{\alpha_4 s_o^4 + \alpha_2 s_o^2 + \alpha_0}{5\alpha_5 s_o^4 + 3\alpha_3 s_o^2 + \alpha_1} \right), \quad (5.164)$$

giving the form of the first order perturbation to the solution when  $\gamma, \beta \neq 0$  and  $\ll 1$ . Given the dependence of coefficients (5.148) – (5.153), it is not immediately

## 5. AN ANALYTIC APPROACH TO THE DIFFUSIONLESS INSTABILITY

---

clear whether such a perturbation is stabilising or destabilising; as in the isothermal case, the sign of  $P_{\gamma,\beta}\hat{s}_o$  depends on the form and gradients of the basic states in a sensitive way, as well as the scale of the instability given by  $k_y$  and  $k_z$ , and the parameters chosen. It should, however, be possible to construct a set of basic states for which the real part of  $P_{\gamma,\beta}\hat{s}_o$  is a positive perturbation to the solutions  $s_o$ , and thus  $\gamma$  and  $\beta$  further destabilise the system to stationary instability.

In addition to this, given that  $P_{\gamma,\beta}$ ,  $\alpha_2$  and  $\alpha_3$  are complex functions, it is also possible that the addition of  $\gamma$  and  $\beta$  amplifies oscillatory modes, or, if we restrict  $s_o$  to real values, destabilises them. This would be a potential area for future extensions of this work. However, any such future analysis should take into account the limitations of the local approach as we have applied it, as we shall now discuss.

### 5.5.4 Applicability of the Local Approximation

A local analysis such as that presented here is applicable only in a given set of circumstances. First of all, we require the background states to vary slowly in the system, which is not inconsistent with the systems we consider here. More pertinent, however, is the addition of a directional velocity  $\gamma$  to the system. In the linearised system we have considered, the addition of  $\gamma$ , a downwards-directed velocity, breaks the reflectional symmetry in the vertical direction. However, in cases where the reflectional symmetry is broken in a finite domain, a local analysis only yields correct results if the criterion for absolute instability is considered. This is as opposed to convective instability, which onsets before absolute instability. An early proponent of this distinction was [Briggs \(1964\)](#) (see the review of [Huerre & Monkewitz \(1990\)](#) for further discussion). Convective instability is associated with systems where the group velocity of disturbances is non-zero. This means that, at a given point, the instability structure may be seen to grow although it is only moving past that point, and will decay once again. Absolute instability, on the other hand, requires that there is a growing instability at every point in the domain, and is a more restrictive criterion than convective instability.

In terms of a system akin to that stated above, the criterion for absolute instability requires that the dispersion relation have a double root, which is found in terms of the wavenumber  $k$  (in the case of our analysis, where the local approximation is taken in the vertical direction, this corresponds to  $k_z$ ). However, meeting this condition for a double root means that we must allow the wavenumber to be complex in order to satisfy this double root criterion for absolute instability. (Refer to the works cited above as well as Soward & Jones (1983), Couairon & Chomaz (1997), Meunier *et al.* (1997), and Tobias *et al.* (1998b), for further details and examples of the use of convective and absolute instability to determine global instability in a finite domain.)

In a system such as above, owing to symmetry breaking by the addition of  $\gamma$ , the local approximation is only accurate for a finite domain when we consider the full absolute instability. Thus, the fact that we have not allowed  $k_z$  to be complex represents a major limitation to our approach.

## 5.6 Conclusions

In this chapter we have considered the diffusionless case of the instability. We have sought to understand several previously-studied systems with the inclusion of  $\gamma$ , in order to find how this additional effect changes the form of the analytical relations governing the system.

We have extended the asymptotic analysis of Gilman (1970), to include an additional  $\gamma$  effect present in the induction equation. We have shown that in the case of the 3D instability with  $\gamma \neq 0$ , we obtain a second-order ODE rather than the algebraic equation that emerges when  $\gamma = 0$ , as in Gilman's original work. We also show that for interchange modes, the equation becomes a first order ODE in terms of the perturbed quantities, which is also an eigenvalue problem in the growth rate  $s$ . The criterion for marginal stability, however, still has the same dependence on the gradient of the density and magnetic field basic states, offering support to the idea that the primary way that the  $\gamma$  effect destabilises the system to magnetic buoyancy is via its effect on the initial equilibrium.

## 5. AN ANALYTIC APPROACH TO THE DIFFUSIONLESS INSTABILITY

---

In an effort to bridge the gap between this small-scale case and the more general diffusionless system, we then consider the interchange instability — following Mizerski *et al.* (2013) — with an additional  $\gamma$  effect. We find that the equation for the perturbation velocity  $\hat{w}$  becomes a third order ODE in this case, with a highest order coefficient proportional to  $\gamma$ . This suggests a boundary layer eigenvalue problem as  $\gamma \rightarrow 0$ .

We consider two model third order eigenvalue problems, finding that by using asymptotic matching at the boundary layer, we may find a relation that gives the eigenvalues in terms of the value of  $\gamma$ , an approach that would also work for the full system. This analysis also shows that the boundary conditions must be carefully chosen, as in the case of a boundary layer solution, fixing the gradient (for example) at the opposite end of the domain can completely change the form of the solution obtained.

Finally, we have taken a local approximation to the form of the instability, provided our domain is confined to a region in which the spatial variation of the background states is small compared to the size of the region under consideration. With this assumption, we are able to derive dispersion relations for the instability. We consider several cases: an isothermal case, for both interchange and 3D modes, and an adiabatic interchange case.

In the first of these cases, that of the isothermal interchange instability, we show that the dispersion relation is quartic in  $s$  for  $\gamma \neq 0$  and/or  $\beta \neq 0$ , and that the  $\gamma$  and  $\beta$  effects appear in a factor of the form  $P_{\gamma,\beta} = \beta(k_y^2 + k_z^2) + ik_z(\gamma - \beta') + \gamma'$  that multiplies the  $s^1$  and  $s^3$  terms, thus reducing the system to biquadratic when  $\gamma = \beta = 0$ . In addition, we find that the dispersion relation for 3D modes in this case is a seventh order polynomial, which becomes cubic in  $s^2$  for  $\gamma = \beta = 0$ .

We also consider the case of interchange modes in the adiabatic system. In this case, we obtain a quintic dispersion relation, in which the even power terms are multiplied by  $P_{\gamma,\beta}$ . Therefore, once again we obtain a biquadratic dispersion

relation when  $\gamma = \beta = 0$ . We solve this, and then find the perturbed form of the roots when  $\gamma, \beta \sim \epsilon \ll 1$ , in terms of the coefficients of the initial quintic dispersion relation.

The main limitation of such an approach as regards the system with  $\gamma$ , is the broken symmetry introduced by the directional turbulent pumping effect. As discussed in Section 5.5.4, a local analysis such as that we consider here is only able to produce correct stability criteria in a system with broken reflectional symmetry in a finite domain if a full analysis of the absolute instability is carried out, for which we would require an additional criterion; that the dispersion relation has a double root. To be fully consistent, such an analysis would require a complex vertical wavenumber. Therefore, this approach should be treated with caution as a method for deriving stability criteria. It is, however, still demonstrative of the effect of  $\gamma$  and  $\beta$  on the system, and the full consideration of the absolute instability of such a system represents grounds for future work.

This consideration of the magnetic buoyancy instability of a diffusionless system has been motivated by extant mathematically interesting results under the non-diffusive assumption, such as that of Gilman and subsequent related work. In considering the diffusionless case, we aim to understand how the inclusion of  $\gamma$  affects such analytic results, and thus how it may act on the instability as a whole. However, as we have discussed in Chapters 2 and 3, it is possible that applying  $\gamma$  without an associated  $\beta$  effect produces a basic state that is at best unphysical, and may also be numerically problematic, given the fact that discontinuities in the basic state field can more easily arise without  $\beta$  (or the standard molecular diffusivity) to “smooth” them. Furthermore, there are other diffusive effects present in the full system, such as viscous diffusion terms. While we have assumed that these constitute relatively small effects throughout the rest of this analysis (see parameter values, Table 3.1), we have shown that especially in the absence of  $\beta$ , the molecular magnetic diffusivity is critical to being able to solve for the magnetic field basic state. Given the importance of the gradient of the basic state that we have discussed elsewhere, this may represent a significant difficulty.

## 5. AN ANALYTIC APPROACH TO THE DIFFUSIONLESS INSTABILITY

---

# Chapter 6

## Conclusions and Discussion

We have extended previous magnetic buoyancy instability studies by incorporating the effect of the overlying turbulent convection. We do this by introducing the turbulent pumping and a turbulent diffusion effects, which arise from mean field electrodynamics, in the upper part of a layer of magnetic field, with a view to modelling the region of the solar tachocline. We have first considered an equilibrium state under these effects, seeking to understand the effect of choice of boundary conditions, parameters, and spatial form of the turbulent effects on this state. We have then sought to determine the scale-dependence of the instability, considering the comparative effect of the turbulent pumping and turbulent diffusion on the system. We analyse both their influence on the equilibrium basic state itself, and their effect on the perturbed linear system. Throughout this analysis, we have found that the nature of the basic state is the most important factor in determining the growth rate and horizontal and vertical spatial structure of the instability.

We have also considered the diffusionless case, using analytic methods to derive results analogous to existing relations that have been found for the instability, but with the additional effect of the turbulent pumping  $\gamma$ . We have studied the full diffusionless interchange instability, and considered model problems to understand better the effect of the addition of turbulent pumping, showing that here the presence of  $\gamma$  leads to the formation of a boundary layer. Finally, we have taken a local approximation in the diffusionless case, and derived analytic dispersion relations involving  $\gamma$  for isothermal and adiabatic systems. We also

## 6. CONCLUSIONS AND DISCUSSION

---

comment on the limit of the applicability of this local approach.

We will now discuss the results of each part of this work, as well as its limitations, and ways in which it could be extended in future.

### 6.1 Equilibrium Basic States

We have considered the mean field induction equation in the presence of turbulent diffusion and turbulent pumping, under conditions of magnetohydrostatic equilibrium. We have solved this problem subject to a variety of different boundary conditions, in an effort to try to find a physically sensible equilibrium field to use as the basic state for the full linear stability problem. We have compared numerical solutions of the second-order ODE for the equilibrium field with analytic and semi-analytic estimates in order to gain an understanding of the behaviour of the equilibrium as a function of the strength of the  $\gamma$  and  $\beta$  effects, as well as the location at which they are “switched off” within the layer.

As a result of this basic state analysis, for our instability studies we have chosen a basic state with a fixed magnetic field value of zero at the top of the layer, as well as a boundary condition that fixes the total magnetic flux within the domain. This, however, is not the only valid choice, and given the later result that the linear stability depends strongly on the basic state it would certainly be possible and valuable to extend this work by exploring more equilibrium states in greater detail, both analytically and numerically.

### 6.2 Linear Stability Analysis: Conclusions

#### 6.2.1 Action of $\gamma = \beta$ on the basic state and perturbed quantities in combination

The addition of  $\gamma$  and  $\beta$ , with “amplitude”  $\gamma_m$  representing additional turbulence in the upper part of the layer, in general has the effect of destabilising the system to magnetic buoyancy, primarily via its effect on the equilibrium field. In general,

the effect of increased levels of  $\gamma$  and  $\beta$  is to increase the growth rate of the linear instability overall — by increasing the gradient of the basic state field — and to change the most unstable mode from a 3D to an interchange mode. This latter effect, however, is more rapid with the increase in the amount of turbulence when the field strength parameter  $F$  is larger.

### 6.2.2 Effect of varying field strength $F$

We show that the most unstable mode traces out a path in  $k_x$ - $k_y$  space, from 3D (in general) to an interchange mode as  $\gamma_m$  increases. However, for higher  $F$  this transition to interchange is much faster, i.e. lower values of  $\gamma_m$  are required to make the most unstable mode an interchange mode.

### 6.2.3 Varying the relative strength of $\gamma$ and $\beta$

We consider cases where  $\gamma$  and  $\beta$  act on both the basic state and the perturbations, with the two effects proportional to one another. We find evidence that the greatest effect on the horizontal scale and growth rate of the instability comes via the effect of the field gradient of the basic state, with the perturbation profiles centred around the region where the gradient of the basic state is the highest. This is particularly well exemplified by the case of  $\beta = 0.1\gamma$ , which we have studied in more detail in Section 3.6.4.

### 6.2.4 Scale dependence of the instability

Throughout this work, we have represented the region of turbulence by the turbulent pumping and turbulent diffusion effects. By their formal derivation, however, these are strictly mean field effects. Applying  $\gamma$  and  $\beta$  equally to all scales of the instability carries the implicit assumption that all scales that are unstable are of the large, mean field scale, i.e. large compared to the typical scale of the turbulent convective motion. This is likely not to be the case at the base of the convection zone. Therefore, we seek to understand the effect of applying  $\gamma$  and  $\beta$  preferentially to the larger scales of the instability.

## 6. CONCLUSIONS AND DISCUSSION

---

Given that the mean field — by definition the largest scale of variation in the system — can be said to correspond to the basic state in the terminology of the linear stability problem, we have considered the comparative action of the  $\gamma$  and  $\beta$  effects on the basic state versus their influence on the perturbations. By comparing cases where the turbulent effects are applied to the basic state only, to the basic state and preferentially to the large-scale perturbations, or to the perturbed quantities alone (an artificial case meant for comparison only) we demonstrate that the primary factor affecting the instability and how it interacts with  $\gamma$  and  $\beta$  is the basic state.

### 6.2.5 Prescribed basic states

For the sake of comparison, we also consider prescribed basic states that do not depend on  $\gamma$  and  $\beta$ . First, as discussed above, we consider perturbations acted upon by  $\gamma$  and  $\beta$ , but applied to the linear equilibrium state of the field when the turbulent effects are not present. In this case, we find that the “shift” to interchange modes as the most unstable modes, which we have previously discussed, does not occur, nor does the increase in the growth rate of the instability as  $\gamma_m$  increases. In fact, we see a slight stabilising effect with increasing  $\gamma_m$ ; this suppression of the instability in the case of prescribed linear basic state, however, is small compared with the change in the growth rate via the action of  $\gamma$  and  $\beta$  on the equilibrium field.

We also consider the action of  $\gamma$  and  $\beta$  on a prescribed “top hat” field, motivated by the instances within the literature when such fields have been used as the basis for linear stability analysis and nonlinear simulation. We find that in the case of this form of basic state field, subject to  $\gamma$  and  $\beta$  on the perturbed quantities, 2D undular modes (those with  $k_y = 0$ ) are increasingly destabilised with increasing  $\gamma_m$ . This leads to a secondary local maximum of the growth rate in  $k_x$ - $k_y$  space, which becomes even more unstable than the most unstable interchange mode if large enough  $\gamma$  and  $\beta$  effects are introduced. This change in the form of the instability from interchange to 2D undular only occurs in this case of all those we have studied, and is likely due to the high field gradient at the upper

and lower boundaries of the “top hat” function basic state.

Note that the top hat function prescribed in this case does not represent an equilibrium field under the effects of  $\gamma$  and  $\beta$ , but was chosen following the choice of functional form of magnetic field by [Barker \*et al.\* \(2012\)](#) as the initial state for their nonlinear simulation. As we showed in [Section 2.12](#), however, it is possible to produce a top hat field that represents equilibrium for some functional forms of  $\gamma$  and  $\beta$ . The forms of  $\gamma$  and  $\beta$  required, however, do not model a physical system where a downwards turbulent pumping velocity and an associated turbulent diffusion is present in the upper part of a layer but not below, and so we do not use the associated magnetic field profile as the basic state for the linear stability problem. However, it may also be valuable as a comparison to address the stability problem with a top hat basic state field with the  $\gamma$  and  $\beta$  profiles shown to sustain it as an equilibrium, in order to fully understand the stability of the system under these conditions.

In general, we conclude that the effect of turbulent transport on the basic state field is the primary determining factor in the stability of the system to magnetic buoyancy, and using a self-consistent equilibrium field is expected to be invaluable if we seek to understand the properties of the instability.

## 6.3 Diffusionless Case: Conclusions

### 6.3.1 Diffusionless, small scale limit

We have sought to find an analogous result to that of [Gilman \(1970\)](#) for the interchange instability in the asymptotic limit  $k_y \rightarrow 0$ , with an additional  $\gamma$  effect. We find that, where Gilman derived an algebraic “dispersion relation” depending on the basic states of the system, with  $\gamma$  present the vertical derivatives cannot be eliminated in the same way. Instead we obtain a first order ODE in terms of the vertical velocity perturbation, with  $\gamma$  multiplying the derivative term. Note, however, that the criterion for marginal stability is not explicitly changed by the addition of  $\gamma$ . This implies that the onset of instability at least, in this case, is

## 6. CONCLUSIONS AND DISCUSSION

---

only implicitly affected by  $\gamma$ , via the action of  $\gamma$  on the equilibrium states. This can be said to be broadly consistent with what we find in the preceding numerical work, where  $\gamma$  primarily affects the instability via its effect on the equilibrium basic state.

### 6.3.2 Diffusionless interchange instability

We also consider the diffusionless interchange instability without the small-scale assumption, in order to better understand how this limiting case relates to the full system. By analogy to the initial approach of [Mizerski \*et al.\* \(2013\)](#), before making any assumption about the size of  $k_y$  we consider the diffusionless instability with the addition of a  $\gamma$  effect. Without  $\gamma$  the system is second order; adding  $\gamma$ , however, makes the equation for the vertical velocity a third order ODE. This increase in the order of the equation implies a boundary layer solution as  $\gamma \rightarrow 0$ . Owing to the complex dependence of the coefficients on  $\gamma$  in the full system, we consider two model problems that exhibit equivalent asymptotic behaviour in order to understand the effect of  $\gamma$  on such a system. We solve these model systems for several different choices of boundary condition, and find analytic and numerical solutions.

### 6.3.3 Local Analysis

By a similar approach to that applied by [Acheson \(1979\)](#) and [Hughes \(1985\)](#), we take a local approximation to the system, and assume periodicity of perturbed quantities in the vertical direction as well as the horizontal. This assumption allows the linearised equations to be written as an algebraic system, which then allows the derivation of a dispersion relation, and of criteria for instability. We include the  $\gamma$  and  $\beta$  effects in the induction equation, to understand their effects on the instability in analytical terms. We consider two types of system, in the case of zero viscous and molecular magnetic diffusion terms; first, an “isothermal” system, in which the thermal diffusivity is effectively infinite and therefore temperature perturbations cannot grow, but rather decay fast enough that they are not included in the system. Despite this, the background temperature profile may still be vertically stratified. In this case, for interchange modes we find that the

### 6.3 Diffusionless Case: Conclusions

---

dispersion relation is quartic, becoming biquadratic for the case of  $\gamma = \beta = 0$ . We also derive the associated criterion for stationary instability of interchange modes, and derive the perturbation to the solutions to the  $\gamma = \beta = 0$  dispersion relation in the asymptotic limit of small  $\gamma$  and  $\beta$ , showing that the turbulent effects can be stabilising or destabilising, and, indeed, are capable of destabilising oscillatory modes as well as the growing instability. In addition, we find that the 3D dispersion relation is seventh order, with coefficients presented in full in Appendix B.

We also consider the case of the adiabatic interchange instability with the addition of  $\gamma$  and  $\beta$ . In this case we obtain a quintic dispersion relation, which again reduces to a biquadratic form when  $\gamma = \beta = 0$ . We solve this perturbatively in the case of small  $\gamma$  and  $\beta$ , and show that again the effect of the perturbations may be stabilising or destabilising, in a way that depends on a complex function of the basic states of the system. In addition to this, we show that the criterion for marginal stability is given by a different function of the basic states in the case of non-zero  $\gamma$  and/or  $\beta$ , as opposed to the equivalent criterion when  $\gamma = \beta = 0$ . We also show that although the addition of  $\gamma$  and  $\beta$  changes the criterion for the onset of interchange instability, nevertheless all of the dependence on  $\gamma$  and  $\beta$  in this criterion is implicit, introduced via the assumption that the basic state field  $\bar{B}$  is a function of  $\gamma$  and  $\beta$ .

The results of such a local approximation, however, must be treated with caution under these circumstances. As discussed in Section 5.5.4, in order to correctly impose the more stringent condition that we are considering the onset of absolute, rather than merely convective instability — required by the reflectional symmetry breaking that results from the presence of the downwards advection velocity  $\gamma$ , for a finite domain such as that of our analysis — we strictly require a complex wavenumber  $k_z$  in order to impose the condition that the system must have a double root at the onset of absolute instability.

## 6.4 Limitations

### 6.4.1 Parameter Regime

As is inevitably the case with numerical work in this area, we are not able to access true astrophysical parameter regimes in such a study, specifically in terms of the magnetic and fluid Reynolds numbers. Converting into our notation and using the definitions of our dimensionless parameters (see Section 1.5.3) to find the magnetic Reynolds number, we have

$$Rm \sim \frac{UL}{\eta} \sim \frac{\sqrt{RT_o}d\rho_o c_p}{\kappa\zeta_o} \sim \frac{1}{C_k\zeta_o} \sim 10^4,$$

and a fluid Reynolds number of

$$Re \sim \frac{UL}{\nu} \sim \frac{\sqrt{RT_o}d\rho_o c_p}{\kappa\sigma} \sim \frac{1}{C_k\sigma} \sim 2 \times 10^4,$$

as well as the magnetic Prandtl number,

$$Pm \sim \frac{Rm}{Re} \sim 0.5,$$

for our parameter values of  $\zeta_o = 0.01$ ,  $C_k = 0.01$ , and  $\sigma = 0.005$ . However, in the case of the solar convection zone the values of these quantities are expected to fall within ranges of  $Rm \sim 10^6 - 10^{10}$ ,  $Re \sim 10^9 - 10^{13}$ , and  $Pm \sim 10^{-3} - 10^{-6}$  (Hood & Hughes (2011), Ossendrijver, 2003). The fact that the physically correct parameter range is currently numerically inaccessible is an issue that is persistent for analyses such as this. However, we may at least reach the parameter ranges of  $Rm, Re \gg 1$  and  $Pm < 1$ , allowing us to gain some insight into the characteristics of such instabilities in astrophysical contexts.

### 6.4.2 Validity of the Mean Field Approximation

Throughout this work, we have assumed that the turbulent convection exhibits a separation of scales, i.e., that the largest scale of the field (the mean field) is much larger than the scale of turbulent variation, such that over an intermediate scale the turbulent fluctuations average to zero. However, there is no reason why such a clear division should be present in the solar convection zone, in which we see a spectrum of scales of variation in the region of turbulent convection.

### 6.4.3 Basic state boundary conditions

When calculating the basic state, we chose the boundary condition  $\bar{B}(0) = 0$ , as well as fixing the integrated magnetic flux over the interval concerned. Given that it is not fully known what the “real” boundary conditions are in this region of the Sun, the conditions we have chosen may be as physically realistic as any other choice we may make. With this in mind, the boundary conditions were chosen because they produced physically meaningful basic states that are not inconsistent with what we know of the magnetic field in the solar convection zone, rather than because the boundary conditions are inherently physically meaningful or imposed by some specific property of the region in themselves. Fixing the flux prevents the numerical scheme from arriving at the zero solution. It also prevents the value of the field gradient from increasing by orders of magnitude at the base of the layer when additional  $\gamma$  and  $\beta$  are added: that is to say, it places an upper limit on the amount of field “drawn in” from above, which is a physically reasonable requirement even though it is imposed artificially.

The  $\bar{B}(0) = 0$  boundary condition, meanwhile, was chosen because fixing the value of the field at the top of the layer was found preferable to fixing its gradient, as in the latter case the application of higher levels of  $\gamma$  and  $\beta$  can give rise to large increases in the field gradient for some levels of turbulence. It is not a physical scenario to have the field tend to  $-\infty$  for some given finite value of  $\gamma_m$  and reverse before becoming finite again, and so the boundary condition  $\bar{B}(0) = 0$  was chosen because it provided “well behaved” solutions that did not exhibit this property. However, it may also be valuable to consider equilibrium fields with Dirichlet boundary conditions fixed at the bottom of the layer, as it may be more physically reasonable for the field to be “fixed” in the radiative zone, below the level of the tachocline, than in the convection zone above.

More research is needed to be able to fix a boundary condition that more accurately represents the physical reality in this region, especially given the result that the gradient of the equilibrium basic state — determined by solving with  $\gamma$  and  $\beta$  — strongly determines the linear stability to magnetic buoyancy.

## 6.5 Extensions of the Research

### 6.5.1 Rotation

None of the analysis in this thesis has involved rotation. In the real solar convection zone, however, rotation and the Coriolis effect may be significant. We may consider the importance of rotation by comparing the growth time of the instability to the rotation time of the Sun, which is on the order of about 27 days when an average is taken over the differential rotation profile, with a minimum value of approximately 24.5 days at the equator as discussed in Chapter 1. Let us consider the growth rates of the instability found in Chapters 3 and 4 (see Figures 3.13 and 4.1). We may scale the growth time of the instability (given by  $\Re(s)^{-1}$ ) with the sound travel time, to produce a dimensional growth time. We consider the linear growth of the instability within the tachocline region. The sound travel time across this region, which makes up approximately 0.04% of the solar radius, is given by:

$$\tau_s = \frac{0.04R_\odot}{c_s} \approx 121 \text{ seconds,}$$

where the solar radius  $R_\odot = 6.96 \times 10^8$  m, and the sound speed in the region of the solar tachocline  $c_s = 2.3 \times 10^5 \text{ ms}^{-1}$  (Gough, 2007). From this, we find that the maximum dimensionless growth rate of the instability that we find,  $\Re(s) \sim 1.5$  (for  $F = 10^{-1}$ , in Figure 3.13), gives a growth time on the order of 1.3 minutes. This is much less than the average rotational period, over which rotational effects become significant, so they can be neglected in this case. Likewise, for the case of  $F = 10^{-3}$ , with typical growth rates of the order  $\Re(s) \sim 0.1$ , we find a typical growth time of approximately 20.2 minutes, a timescale over which the rotation is similarly insignificant. By contrast, however, in the case of  $F = 10^{-5}$ , we obtain a typical growth rate  $\Re(s) \sim 10^{-4}$ , giving a growth time of approximately 14 days. This, clearly, is closer to being on the order of the timescale of the rotation period, and so in the case of low field strength  $F$ , rotation may be a significant factor in the evolution of the instability and should not be neglected in this parameter regime.

In general, future work could include a Coriolis term in the momentum equation in order to quantify its effect on the instability under the turbulent effects we have studied. In addition, the  $\gamma$  and  $\beta$  effects themselves are understood to depend on rotation, so future research on similar systems would benefit from considering its effect regardless.

### 6.5.2 $\alpha$ Effect

This analysis has included the  $\gamma$  and  $\beta$  effects that result from applying the mean field approximation in order to characterise the turbulence in the region considered. However, it does not include the  $\alpha$  effect present in Equation (1.25). The reason for this is that the consideration of  $\alpha$  would have introduced another level of complexity, and is outside the scope of this analysis. Including it, however, may constitute a logical progression of this work.

### 6.5.3 Nonlinear Regime

All the results presented here have been obtained under the assumption of a linear stability analysis. Once such instabilities have been allowed to evolve for a time, however, nonlinear effects quickly begin to become significant. Therefore, there is also a need to extend this work into the nonlinear regime, to build on the results presented here by means of time-dependent simulation. Future work could make use of an equilibrium state similar to the one we have discussed, and simulate its time evolution under the effect of turbulence.

## 6.6 Concluding Remarks

The study of the solar magnetic field is a current and rapidly expanding area of research, driven by ever-improving computational power. Understanding magnetohydrodynamic instabilities under the action of turbulence, and modelling turbulent convection with the mean field approach is but one small aspect of this. In future, we hope that numerical, theoretical, and observational lines of enquiry will be combined to improve our understanding of such instability processes, and how they relate to the solar dynamo. Furthermore, owing to the Sun's

## 6. CONCLUSIONS AND DISCUSSION

---

proximity we have a relative abundance of observational evidence to inform and support our theoretical understanding of the dynamo process.

Of course, with an understanding of the solar dynamo we pave the way for understanding other astrophysical dynamo processes such as planetary dynamos, or stellar dynamos for stars of different mass and convective structure than our own, or the dynamo processes occurring in astrophysical discs. Instabilities drive such processes, and studying them broadens our understanding of astrophysical objects and how their magnetic fields are produced and maintained.

# Appendix A

## Analytic solution for step functions $\gamma = \beta$ , $\bar{B}'(0) = \lambda$ , $\phi(1) = 1$

We consider a case analogous to that of Section 2.6.1, though instead of  $\bar{B}'(0) = 0$ , we take the more general boundary condition  $\bar{B}'(0) = \lambda$ . With this and the constant flux condition  $\phi(1) = 1$ , we solve the equilibrium induction equation, (2.2), for step functions  $\gamma$  and  $\beta$  with jump conditions (2.9) and (2.10), using the same method as in Section 2.6.1.

Recall that for equilibrium,

$$(\zeta_0 C_k + \beta)\bar{B}'' + (\beta' - \gamma)\bar{B}' - \gamma'\bar{B} = 0,$$

and we assume:

$$\beta = \gamma = \begin{cases} \gamma_m = \text{constant} & 0 \leq z < z_i \\ 0 & z_i < z \leq 1 \end{cases}.$$

The chosen boundary conditions are

$$\phi(1) = \int_0^1 \bar{B}(z) dz = 1, \quad (\text{A.1})$$

$$\bar{B}'(0) = \lambda, \quad (\text{A.2})$$

where  $\lambda$  is a constant. As before, we solve for each region of the domain separately and obtain

$$\bar{B} = \begin{cases} P + Q \exp\left(\frac{\gamma_m z}{\zeta_0 C_k + \gamma_m}\right) & 0 \leq z < z_i \\ R + Sz & z_i < z \leq 1 \end{cases}.$$

**A. ANALYTIC SOLUTION FOR STEP FUNCTIONS**  $\gamma = \beta$ ,  
 $\bar{B}'(0) = \lambda$ ,  $\phi(1) = 1$

---

Applying the boundary condition  $\bar{B}'(0) = \lambda$  gives an expression for  $Q$ :

$$Q = \frac{\lambda(\zeta_o C_k + \gamma_m)}{\gamma_m}. \quad (\text{A.3})$$

We then apply the jump condition (2.9) to find

$$P + Q \exp\left(\frac{\gamma_m z_i}{\zeta_o C_k + \gamma_m}\right) - R - S z_i = 0. \quad (\text{A.4})$$

Applying (2.10) gives

$$\gamma_m P + \zeta_o C_k S = 0. \quad (\text{A.5})$$

Finally, we may apply the constant flux boundary condition  $\phi(1) = 1$  to obtain

$$P z_i + Q \left(\frac{\zeta_o C_k + \gamma_m}{\gamma_m}\right) \left(\exp\left(\frac{\gamma_m z_i}{\zeta_o C_k + \gamma_m}\right) + 1\right) + R(1 - z_i) + \frac{S}{2}(1 - z_i^2) = 1. \quad (\text{A.6})$$

Solving these equations simultaneously in the same way as in Section 2.6.1, we find:

$$S = \frac{\left(1 - \frac{\lambda(\zeta_o C_k + \gamma_m)}{\gamma_m} \left(\left(\frac{\zeta_o C_k}{\gamma_m} + 2 - z_i\right) \exp\left(\frac{\gamma_m z}{\zeta_o C_k + \gamma_m}\right) - \frac{\zeta_o C_k}{\gamma_m} - 1\right)\right)}{\left(-\frac{\zeta_o C_k}{\gamma_m} + \frac{(1 - z_i)^2}{2}\right)}, \quad (\text{A.7})$$

$$P = -\frac{\zeta_o C_k}{\gamma_m} S, \quad (\text{A.8})$$

$$R = \frac{\lambda(\zeta_o C_k + \gamma_m)}{\gamma_m} \exp\left(\frac{\gamma_m z_i}{\zeta_o C_k + \gamma_m}\right) - \left(z_i + \frac{\zeta_o C_k}{\gamma_m}\right) S, \quad (\text{A.9})$$

$$Q = \frac{\lambda(\zeta_o C_k + \gamma_m)}{\gamma_m}. \quad (\text{A.10})$$

Note that as expected, these coefficients reduce to the forms (2.16) – (2.18), as well as  $Q = 0$ , when  $\lambda \rightarrow 0$ , which is the case discussed in Section 2.6.1. The case considered numerically in Section 2.5 is approximated in the analytical ( $a \rightarrow 0$ ) limit by the solution presented here with  $\lambda = 1$ .

## Appendix B

# Coefficients of the dispersion relation for the 3D isothermal instability

For Equation (5.133) in Chapter 5, the coefficient functions  $g_0 - g_7$ , derived by means of symbolic computation, are given by

$$\begin{aligned} g_0 = & \bar{B}^2 F^2 \bar{\rho} k_x^2 (\bar{B}^2 \bar{T} \gamma' k_x^4 - \bar{T} \beta \bar{B}'^2 k_y^4 - \bar{T} \bar{B}'^2 \gamma' k_y^2 + \bar{T} \bar{B}'^2 \beta' k_y^2 k_z i) \quad (\text{B.1}) \\ & - \bar{T} \bar{B}'^2 \gamma k_x^2 k_z i - \bar{T} \bar{B}'^2 \gamma k_y^2 k_z i + \bar{B}^2 \bar{T} \beta k_x^2 k_y^4 + \bar{B}^2 \bar{T} \beta k_x^4 k_y^2 \\ & + \bar{B}^2 \bar{T} \beta k_x^2 k_z^4 + \bar{B}^2 \bar{T} \beta k_x^4 k_z^2 + \bar{B}^2 \bar{T} \gamma' k_x^2 k_y^2 + \bar{B}^2 \bar{T} \gamma k_x^2 k_z^3 i \\ & - \bar{T} \beta \bar{B}'^2 k_x^2 k_y^2 - \bar{T} \beta \bar{B}'^2 k_x^2 k_z^2 - \bar{T} \beta \bar{B}'^2 k_y^2 k_z^2 + \bar{B} \bar{T} \bar{B}' \beta' k_x^4 \\ & + \bar{B} \beta \bar{B}' \bar{T}' k_y^4 + \bar{B} \bar{B}' \bar{T}' \gamma' k_x^2 + \bar{B} \bar{B}' \bar{T}' \gamma' k_y^2 - \bar{B} \beta \bar{B}' k_y^4 \theta(m+1) \\ & - \bar{B} \bar{B}' \gamma' k_x^2 \theta(m+1) - \bar{B} \bar{B}' \gamma' k_y^2 \theta(m+1) + \bar{B}^2 \bar{T} \gamma k_x^4 k_z i \\ & - \bar{B} \bar{B}' \bar{T}' \beta' k_x^2 k_z i - \bar{B} \bar{B}' \bar{T}' \beta' k_y^2 k_z i + \bar{B} \bar{B}' \bar{T}' \gamma k_x^2 k_z i + \bar{B} \bar{B}' \bar{T}' \gamma k_y^2 k_z i \\ & + \bar{B} \bar{B}' \beta' k_x^2 k_z \theta(m+1) i + \bar{B} \bar{B}' \beta' k_y^2 k_z \theta(m+1) i - \bar{B} \bar{B}' \gamma k_x^2 k_z \theta(m+1) i \\ & - \bar{B} \bar{B}' \gamma k_y^2 k_z \theta(m+1) i + 2 \bar{B}^2 \bar{T} \beta k_x^2 k_y^2 k_z^2 - \bar{B} \bar{T} \beta \bar{B}' k_x^2 k_z^3 i \\ & + \bar{B} \bar{T} \bar{B}' \beta' k_x^2 k_y^2 + \bar{B} \bar{T} \bar{B}' \beta' k_x^2 k_z^2 + \bar{B} \bar{T} \bar{B}' \gamma k_x^2 k_z^2 + \bar{B} \beta \bar{B}' \bar{T}' k_x^2 k_y^2 \\ & + \bar{B} \beta \bar{B}' \bar{T}' k_x^2 k_z^2 + \bar{B} \beta \bar{B}' \bar{T}' k_y^2 k_z^2 - \bar{B} \beta \bar{B}' k_x^2 k_y^2 \theta(m+1) \\ & - \bar{B} \beta \bar{B}' k_x^2 k_z^2 \theta(m+1) - \bar{B} \beta \bar{B}' k_y^2 k_z^2 \theta(m+1) + \bar{B}^2 \bar{T} \gamma k_x^2 k_y^2 k_z i \\ & + \bar{B} \bar{T} \bar{B}' \gamma' k_x^2 k_z i - \bar{B} \bar{T} \beta \bar{B}' k_x^2 k_y^2 k_z i), \end{aligned}$$

## B. COEFFICIENTS OF THE DISPERSION RELATION FOR THE 3D ISOTHERMAL INSTABILITY

---

$$\begin{aligned}
g_1 = & \bar{T} \beta^3 \bar{\rho}^3 k_y^8 + \bar{T} \beta^3 \bar{\rho}^3 k_z^8 - \bar{T} \bar{\rho}^3 \gamma^3 k_z^5 i - \beta^3 \bar{T}' \bar{\rho}^3 k_z^7 i - \bar{T}' \bar{\rho}^3 \gamma^3 k_z^4 \quad (\text{B.2}) \\
& + \beta^3 \bar{\rho}^3 k_z^7 \theta(m+1) i + \bar{\rho}^3 \gamma^3 k_z^4 \theta(m+1) + \bar{B}^4 F^2 \bar{\rho} \gamma' k_x^4 - \bar{T} \beta \beta'^2 \bar{\rho}^3 k_z^6 \\
& - \bar{T} \beta^2 \beta' \bar{\rho}^3 k_z^7 2i - \bar{T} \beta^3 \bar{\rho}' \bar{\rho}^2 k_z^7 i + \bar{T} \beta \bar{\rho}^3 \gamma'^2 k_y^4 + 2\bar{T} \beta^2 \bar{\rho}^3 \gamma' k_y^6 \\
& + \bar{T} \beta \bar{\rho}^3 \gamma'^2 k_z^4 + 2\bar{T} \beta^2 \bar{\rho}^3 \gamma' k_z^6 - 3\bar{T} \beta \bar{\rho}^3 \gamma^2 k_z^6 + \bar{T} \beta^2 \bar{\rho}^3 \gamma k_z^7 3i \\
& + \bar{T} \beta' \bar{\rho}^3 \gamma^2 k_z^5 2i - \bar{T} \beta'^2 \bar{\rho}^3 \gamma k_z^5 i - \bar{T} \bar{\rho}' \bar{\rho}^2 \gamma^3 k_z^4 + \bar{T} \bar{\rho}^3 \gamma'^2 \gamma k_z^3 i \\
& - 2\bar{T} \bar{\rho}^3 \gamma' \gamma^2 k_z^4 + \beta \bar{T}' \beta'^2 \bar{\rho}^3 k_z^5 i - 2\beta^2 \bar{T}' \beta' \bar{\rho}^3 k_z^6 - \beta^3 \bar{T}' \bar{\rho}' \bar{\rho}^2 k_y^6 \\
& - \beta^3 \bar{T}' \bar{\rho}' \bar{\rho}^2 k_z^6 - \beta \bar{T}' \bar{\rho}^3 \gamma'^2 k_z^3 i - \beta^2 \bar{T}' \bar{\rho}^3 \gamma' k_z^5 2i + \beta \bar{T}' \bar{\rho}^3 \gamma^2 k_z^5 3i \\
& + 3\beta^2 \bar{T}' \bar{\rho}^3 \gamma k_z^6 + 2\bar{T}' \beta' \bar{\rho}^3 \gamma^2 k_z^4 - \bar{T}' \beta'^2 \bar{\rho}^3 \gamma k_z^4 + \bar{T}' \bar{\rho}' \bar{\rho}^2 \gamma^3 k_z^3 i \\
& + \bar{T}' \bar{\rho}^3 \gamma'^2 \gamma k_z^2 + \bar{T}' \bar{\rho}^3 \gamma' \gamma^2 k_z^3 2i - \beta^3 \bar{T}' \bar{\rho}^3 k_y^6 k_z i - \beta \beta'^2 \bar{\rho}^3 k_z^5 \theta(m+1) i \\
& + 2\beta^2 \beta' \bar{\rho}^3 k_z^6 \theta(m+1) + \beta^3 \bar{\rho}' \bar{\rho}^2 k_y^6 \theta(m+1) + \beta^3 \bar{\rho}' \bar{\rho}^2 k_z^6 \theta(m+1) \\
& + \beta \bar{\rho}^3 \gamma'^2 k_z^3 \theta(m+1) i + \beta^2 \bar{\rho}^3 \gamma' k_z^5 \theta(m+1) 2i - \beta \bar{\rho}^3 \gamma^2 k_z^5 \theta(m+1) 3i \\
& - 3\beta^2 \bar{\rho}^3 \gamma k_z^6 \theta(m+1) - 2\beta' \bar{\rho}^3 \gamma^2 k_z^4 \theta(m+1) + \beta'^2 \bar{\rho}^3 \gamma k_z^4 \theta(m+1) \\
& - \bar{\rho}' \bar{\rho}^2 \gamma^3 k_z^3 \theta(m+1) i - \bar{\rho}^3 \gamma'^2 \gamma k_z^2 \theta(m+1) - \bar{\rho}^3 \gamma' \gamma^2 k_z^3 \theta(m+1) 2i \\
& + \beta^3 \bar{\rho}^3 k_y^6 k_z \theta(m+1) i + \bar{T} \beta^3 \bar{\rho}^3 k_x^2 k_y^6 + \bar{T} \beta^3 \bar{\rho}^3 k_x^2 k_z^6 + 4\bar{T} \beta^3 \bar{\rho}^3 k_y^2 k_z^6 \\
& + 6\bar{T} \beta^3 \bar{\rho}^3 k_y^4 k_z^4 + 4\bar{T} \beta^3 \bar{\rho}^3 k_y^6 k_z^2 - \bar{T} \bar{\rho}^3 \gamma^3 k_x^2 k_z^3 i - \bar{T} \bar{\rho}^3 \gamma^3 k_y^2 k_z^3 i \\
& - \beta^3 \bar{T}' \bar{\rho}^3 k_y^2 k_z^5 3i - \beta^3 \bar{T}' \bar{\rho}^3 k_y^4 k_z^3 3i + \beta^3 \bar{\rho}^3 k_y^2 k_z^5 \theta(m+1) 3i \\
& + \beta^3 \bar{\rho}^3 k_y^4 k_z^3 \theta(m+1) 3i + \bar{B}^4 F^2 \beta \bar{\rho} k_x^2 k_y^4 + \bar{B}^4 F^2 \beta \bar{\rho} k_x^4 k_y^2 \\
& + \bar{B}^4 F^2 \beta \bar{\rho} k_x^2 k_z^4 + \bar{B}^4 F^2 \beta \bar{\rho} k_x^4 k_z^2 + \bar{B}^4 F^2 \bar{\rho} \gamma' k_x^2 k_y^2 + \bar{B}^4 F^2 \bar{\rho} \gamma k_x^2 k_z^3 i \\
& - \bar{T} \beta \beta'^2 \bar{\rho}^3 k_x^2 k_z^4 - \bar{T} \beta^2 \beta' \bar{\rho}^3 k_x^2 k_z^5 2i - 2\bar{T} \beta \beta'^2 \bar{\rho}^3 k_y^2 k_z^4 - \bar{T} \beta \beta'^2 \bar{\rho}^3 k_y^4 k_z^2 \\
& - \bar{T} \beta^2 \beta' \bar{\rho}^3 k_y^2 k_z^5 6i - \bar{T} \beta^2 \beta' \bar{\rho}^3 k_y^4 k_z^3 6i - \bar{T} \beta^3 \bar{\rho}' \bar{\rho}^2 k_y^2 k_z^5 3i \\
& - \bar{T} \beta^3 \bar{\rho}' \bar{\rho}^2 k_y^4 k_z^3 3i + \bar{T} \beta \bar{\rho}^3 \gamma'^2 k_x^2 k_y^2 + 2\bar{T} \beta^2 \bar{\rho}^3 \gamma' k_x^2 k_y^4 + \bar{T} \beta \bar{\rho}^3 \gamma'^2 k_x^2 k_z^2 \\
& + 2\bar{T} \beta^2 \bar{\rho}^3 \gamma' k_x^2 k_z^4 + 2\bar{T} \beta \bar{\rho}^3 \gamma'^2 k_y^2 k_z^2 + 6\bar{T} \beta^2 \bar{\rho}^3 \gamma' k_y^2 k_z^4 + 6\bar{T} \beta^2 \bar{\rho}^3 \gamma' k_y^4 k_z^2 \\
& - 3\bar{T} \beta \bar{\rho}^3 \gamma^2 k_x^2 k_z^4 + \bar{T} \beta^2 \bar{\rho}^3 \gamma k_x^2 k_z^5 3i - 6\bar{T} \beta \bar{\rho}^3 \gamma^2 k_y^2 k_z^4 - 3\bar{T} \beta \bar{\rho}^3 \gamma^2 k_y^4 k_z^2 \\
& + \bar{T} \beta^2 \bar{\rho}^3 \gamma k_y^2 k_z^5 9i + \bar{T} \beta^2 \bar{\rho}^3 \gamma k_y^4 k_z^3 9i + \bar{T} \beta' \bar{\rho}^3 \gamma^2 k_x^2 k_z^3 2i - \bar{T} \beta'^2 \bar{\rho}^3 \gamma k_x^2 k_z^3 i \\
& + \bar{T} \beta' \bar{\rho}^3 \gamma^2 k_y^2 k_z^3 2i - \bar{T} \beta'^2 \bar{\rho}^3 \gamma k_y^2 k_z^3 i - 2\bar{T} \bar{\rho}^3 \gamma' \gamma^2 k_x^2 k_z^2 - 2\bar{T} \bar{\rho}^3 \gamma' \gamma^2 k_y^2 k_z^2 \\
& + \beta \bar{T}' \beta'^2 \bar{\rho}^3 k_y^2 k_z^3 i - 4\beta^2 \bar{T}' \beta' \bar{\rho}^3 k_y^2 k_z^4 - 2\beta^2 \bar{T}' \beta' \bar{\rho}^3 k_y^4 k_z^2 - 3\beta^3 \bar{T}' \bar{\rho}' \bar{\rho}^2 k_y^2 k_z^4 \\
& - 3\beta^3 \bar{T}' \bar{\rho}' \bar{\rho}^2 k_y^4 k_z^2 - \beta^2 \bar{T}' \bar{\rho}^3 \gamma' k_y^2 k_z^3 4i + \beta \bar{T}' \bar{\rho}^3 \gamma^2 k_y^2 k_z^3 3i + 6\beta^2 \bar{T}' \bar{\rho}^3 \gamma k_y^2 k_z^4 \\
& + 3\beta^2 \bar{T}' \bar{\rho}^3 \gamma k_y^4 k_z^2 - \beta \beta'^2 \bar{\rho}^3 k_y^2 k_z^3 \theta(m+1) i + 4\beta^2 \beta' \bar{\rho}^3 k_y^2 k_z^4 \theta(m+1) \\
& + 2\beta^2 \beta' \bar{\rho}^3 k_y^4 k_z^2 \theta(m+1) + 3\beta^3 \bar{\rho}' \bar{\rho}^2 k_y^2 k_z^4 \theta(m+1) + 3\beta^3 \bar{\rho}' \bar{\rho}^2 k_y^4 k_z^2 \theta(m+1) \\
& + \beta^2 \bar{\rho}^3 \gamma' k_y^2 k_z^3 \theta(m+1) 4i - \beta \bar{\rho}^3 \gamma^2 k_y^2 k_z^3 \theta(m+1) 3i - 6\beta^2 \bar{\rho}^3 \gamma k_y^2 k_z^4 \theta(m+1)
\end{aligned}$$

---


$$\begin{aligned}
& - 3\beta^2\bar{\rho}^3\gamma k_y^4 k_z^2 \theta(m+1) - \bar{T}\beta\beta'\bar{\rho}^3\gamma'k_z^5 2i + 4\bar{T}\beta\beta'\bar{\rho}^3\gamma k_z^6 + \bar{T}\beta\bar{\rho}^3\gamma'\gamma k_z^5 4i \\
& + 2\bar{T}\beta'\bar{\rho}^3\gamma'\gamma k_z^4 - 2\beta\bar{T}'\beta'\bar{\rho}^3\gamma'k_z^4 - \beta\bar{T}'\beta'\bar{\rho}^3\gamma k_z^5 4i + 4\beta\bar{T}'\bar{\rho}^3\gamma'\gamma k_z^4 \\
& - \bar{T}'\beta'\bar{\rho}^3\gamma'\gamma k_z^3 2i - \bar{T}'\bar{\rho}'\bar{\rho}^2\gamma'^2\gamma k_z i + 2\beta\beta'\bar{\rho}^3\gamma'k_z^4 \theta(m+1) + 3\bar{B}^2 F\bar{T}\bar{\rho}^2\gamma'k_x^4 \\
& + \beta\beta'\bar{\rho}^3\gamma k_z^5 \theta(m+1) 4i - 4\beta\bar{\rho}^3\gamma'\gamma k_z^4 \theta(m+1) + \beta'\bar{\rho}^3\gamma'\gamma k_z^3 \theta(m+1) 2i \\
& + \bar{\rho}'\bar{\rho}^2\gamma'^2\gamma k_z \theta(m+1) i + 3\bar{T}\beta^3\bar{\rho}^3 k_x^2 k_y^2 k_z^4 + 3\bar{T}\beta^3\bar{\rho}^3 k_x^2 k_y^4 k_z^2 \\
& + \bar{B}^3 F^2 \bar{B}'\beta'\bar{\rho} k_x^4 + \bar{B}^4 F^2 \bar{\rho}\gamma k_x^4 k_z i - 2F\bar{T}\beta\bar{B}'\bar{\rho}^2 k_y^4 - F\bar{T}\bar{B}'\bar{\rho}^2\gamma'k_x^2 \\
& - F\bar{T}\bar{B}'\bar{\rho}^2\gamma'k_y^2 + \bar{T}\beta\beta'^2\bar{\rho}'\bar{\rho}^2 k_z^5 i - 2\bar{T}\beta^2\beta'\bar{\rho}'\bar{\rho}^2 k_z^6 - \bar{T}\beta\bar{\rho}'\bar{\rho}^2\gamma'^2 k_z^3 i \\
& - \bar{T}\beta^2\bar{\rho}'\bar{\rho}^2\gamma'k_z^5 2i + \bar{T}\beta\bar{\rho}'\bar{\rho}^2\gamma'^2 k_z^5 3i + 3\bar{T}\beta^2\bar{\rho}'\bar{\rho}^2\gamma k_z^6 + 2\bar{T}\beta'\bar{\rho}'\bar{\rho}^2\gamma'^2 k_z^4 \\
& - \bar{T}\beta'^2\bar{\rho}'\bar{\rho}^2\gamma k_z^4 + \bar{T}\bar{\rho}'\bar{\rho}^2\gamma'^2\gamma k_z^2 + \bar{T}\bar{\rho}'\bar{\rho}^2\gamma'\gamma'^2 k_z^3 2i - \bar{T}\beta^2\beta'\bar{\rho}^3 k_y^6 k_z 2i \\
& - \bar{T}\beta^3\bar{\rho}'\bar{\rho}^2 k_y^6 k_z i + \bar{T}\beta^2\bar{\rho}^3\gamma k_y^6 k_z 3i + \bar{T}\bar{\rho}^3\gamma'^2\gamma k_x^2 k_z i + \bar{T}\bar{\rho}^3\gamma'^2\gamma k_y^2 k_z i \\
& + \beta\bar{T}'\beta'^2\bar{\rho}'\bar{\rho}^2 k_z^4 + \beta^2\bar{T}'\beta'\bar{\rho}'\bar{\rho}^2 k_z^5 2i - \beta\bar{T}'\bar{\rho}'\bar{\rho}^2\gamma'^2 k_y^2 - 2\beta^2\bar{T}'\bar{\rho}'\bar{\rho}^2\gamma'k_y^4 \\
& - \beta\bar{T}'\bar{\rho}'\bar{\rho}^2\gamma'^2 k_z^2 - 2\beta^2\bar{T}'\bar{\rho}'\bar{\rho}^2\gamma'k_z^4 + 3\beta\bar{T}'\bar{\rho}'\bar{\rho}^2\gamma'^2 k_z^4 - \beta^2\bar{T}'\bar{\rho}'\bar{\rho}^2\gamma k_z^5 3i \\
& - \bar{T}'\beta'\bar{\rho}'\bar{\rho}^2\gamma'^2 k_z^3 2i + \bar{T}'\beta'^2\bar{\rho}'\bar{\rho}^2\gamma k_z^3 i + 2\bar{T}'\bar{\rho}'\bar{\rho}^2\gamma'\gamma'^2 k_z^2 - \beta\bar{T}'\bar{\rho}^3\gamma'^2 k_y^2 k_z i \\
& - \beta^2\bar{T}'\bar{\rho}^3\gamma'k_y^4 k_z 2i - \beta\beta'^2\bar{\rho}'\bar{\rho}^2 k_z^4 \theta(m+1) - \beta^2\beta'\bar{\rho}'\bar{\rho}^2 k_z^5 \theta(m+1) 2i \\
& + \beta\bar{\rho}'\bar{\rho}^2\gamma'^2 k_y^2 \theta(m+1) + 2\beta^2\bar{\rho}'\bar{\rho}^2\gamma'k_y^4 \theta(m+1) + \beta\bar{\rho}'\bar{\rho}^2\gamma'^2 k_z^2 \theta(m+1) \\
& + 2\beta^2\bar{\rho}'\bar{\rho}^2\gamma'k_z^4 \theta(m+1) - 3\beta\bar{\rho}'\bar{\rho}^2\gamma'^2 k_z^4 \theta(m+1) + \beta^2\bar{\rho}'\bar{\rho}^2\gamma k_z^5 \theta(m+1) 3i \\
& + \beta'\bar{\rho}'\bar{\rho}^2\gamma'^2 k_z^3 \theta(m+1) 2i - \beta'^2\bar{\rho}'\bar{\rho}^2\gamma k_z^3 \theta(m+1) i - 2\bar{\rho}'\bar{\rho}^2\gamma'\gamma'^2 k_z^2 \theta(m+1) \\
& + \beta\bar{\rho}^3\gamma'^2 k_y^2 k_z \theta(m+1) i + \beta^2\bar{\rho}^3\gamma'k_y^4 k_z \theta(m+1) 2i - 3\bar{T}\beta\bar{\rho}^3\gamma^2 k_x^2 k_y^2 k_z^2 \\
& + \bar{T}\beta^2\bar{\rho}^3\gamma k_x^2 k_y^2 k_z^3 6i - \bar{B}^2 F\bar{T}'\bar{\rho}^2\gamma'k_x^2 k_z i + \bar{B}^2 F\bar{\rho}^2\gamma'k_x^2 k_z \theta(m+1) i \\
& + F\bar{T}\bar{B}'\bar{\rho}^2\beta'\bar{\rho}^2 k_x^2 k_z i + F\bar{T}\bar{B}'\bar{\rho}^2\beta'\bar{\rho}^2 k_y^2 k_z i - F\bar{T}\bar{B}'\bar{\rho}^2\gamma k_x^2 k_z 2i \\
& - F\bar{T}\bar{B}'\bar{\rho}^2\gamma k_y^2 k_z 2i - \bar{T}\beta\beta'\bar{\rho}^3\gamma'k_x^2 k_z^3 2i - \bar{T}\beta\beta'\bar{\rho}^3\gamma'k_y^2 k_z^3 4i \\
& - \bar{T}\beta\bar{\rho}'\bar{\rho}^2\gamma'^2 k_y^2 k_z i - \bar{T}\beta^2\bar{\rho}'\bar{\rho}^2\gamma'k_y^4 k_z 2i + 4\bar{T}\beta\beta'\bar{\rho}^3\gamma k_x^2 k_z^4 \\
& + 8\bar{T}\beta\beta'\bar{\rho}^3\gamma k_y^2 k_z^4 + 4\bar{T}\beta\beta'\bar{\rho}^3\gamma k_y^4 k_z^2 + \bar{T}\beta\bar{\rho}^3\gamma'\gamma k_x^2 k_z^3 4i + \bar{T}\beta\bar{\rho}^3\gamma'\gamma k_y^2 k_z^3 8i \\
& + 2\bar{T}\beta'\bar{\rho}^3\gamma'\gamma k_x^2 k_z^2 + 2\bar{T}\beta'\bar{\rho}^3\gamma'\gamma k_y^2 k_z^2 + \beta^2\bar{T}'\beta'\bar{\rho}'\bar{\rho}^2 k_y^4 k_z 2i \\
& - 2\beta\bar{T}'\beta'\bar{\rho}^3\gamma'k_y^2 k_z^2 - \beta\bar{T}'\beta'\bar{\rho}^3\gamma k_y^2 k_z^3 4i - \beta^2\bar{T}'\bar{\rho}'\bar{\rho}^2\gamma k_y^4 k_z 3i \\
& + 4\beta\bar{T}'\bar{\rho}^3\gamma'\gamma k_y^2 k_z^2 + 4\bar{B}^2 F\bar{T}\beta\bar{\rho}^2 k_x^2 k_y^4 + 4\bar{B}^2 F\bar{T}\beta\bar{\rho}^2 k_x^4 k_y^2 \\
& + 4\bar{B}^2 F\bar{T}\beta\bar{\rho}^2 k_x^2 k_z^4 + 4\bar{B}^2 F\bar{T}\beta\bar{\rho}^2 k_x^4 k_z^2 - \beta^2\beta'\bar{\rho}'\bar{\rho}^2 k_y^4 k_z \theta(m+1) 2i \\
& + 2\beta\beta'\bar{\rho}^3\gamma'k_y^2 k_z^2 \theta(m+1) - \bar{B}^2 F\bar{T}'\beta'\bar{\rho}^2 k_x^2 k_z^3 2i + 3\bar{B}^2 F\bar{T}\bar{\rho}^2\gamma'k_x^2 k_y^2 \\
& + 2\bar{B}^2 F\bar{T}\bar{\rho}^2\gamma'k_x^2 k_z^2 + \beta\beta'\bar{\rho}^3\gamma k_y^2 k_z^3 \theta(m+1) 4i + \beta^2\bar{\rho}'\bar{\rho}^2\gamma k_y^4 k_z \theta(m+1) 3i
\end{aligned}$$

## B. COEFFICIENTS OF THE DISPERSION RELATION FOR THE 3D ISOTHERMAL INSTABILITY

---

$$\begin{aligned}
& - 4\beta\bar{\rho}^3\gamma'\gamma k_y^2 k_z^2 \theta(m+1) + \bar{B}^2 F \bar{T} \bar{\rho}^2 \gamma k_x^2 k_z^3 4i - \bar{B}^3 F^2 \beta \bar{B}' \bar{\rho} k_x^2 k_z^3 2i \\
& - \bar{B}^2 F \beta \bar{T}' \bar{\rho}^2 k_x^2 k_z^3 2i + \bar{B}^3 F^2 \bar{B}' \beta' \bar{\rho} k_x^2 k_y^2 - \bar{B}^2 F \bar{T}' \beta' \bar{\rho}^2 k_x^2 k_z^2 \\
& - \bar{B}^2 F^2 \bar{B}' \bar{\rho} \gamma k_x^2 k_z i + 2\bar{B}^3 F^2 \bar{B}' \bar{\rho} \gamma k_x^2 k_z^2 + 2\bar{B}^2 F \bar{T}' \bar{\rho}^2 \gamma k_x^2 k_z^2 \\
& + \bar{B}^4 F^2 \bar{\rho} \gamma k_x^2 k_y^2 k_z i + \bar{B}^2 F \beta \bar{\rho}^2 k_x^2 k_z^3 \theta(m+1) 2i - 2F \bar{T} \beta \bar{B}' \bar{\rho}^2 k_x^2 k_y^2 \\
& - 2F \bar{T} \beta \bar{B}' \bar{\rho}^2 k_x^2 k_z^2 - 2F \bar{T} \beta \bar{B}' \bar{\rho}^2 k_y^2 k_z^2 + \bar{B}^2 F \beta' \bar{\rho}^2 k_x^2 k_z^2 \theta(m+1) \\
& - 2\bar{B}^2 F \bar{\rho}^2 \gamma k_x^2 k_z^2 \theta(m+1) + \bar{B} F \bar{T} \bar{B}' \beta' \bar{\rho}^2 k_x^4 + \bar{T} \beta \beta' \bar{\rho}' \bar{\rho}^2 k_y^2 k_z^3 i \\
& - 4\bar{T} \beta^2 \beta' \bar{\rho}' \bar{\rho}^2 k_y^2 k_z^4 - 2\bar{T} \beta^2 \beta' \bar{\rho}' \bar{\rho}^2 k_y^4 k_z^2 - \bar{T} \beta^2 \bar{\rho}' \bar{\rho}^2 \gamma' k_y^2 k_z^3 4i \\
& + \bar{T} \beta \bar{\rho}' \bar{\rho}^2 \gamma^2 k_y^2 k_z^3 3i + 6\bar{T} \beta^2 \bar{\rho}' \bar{\rho}^2 \gamma k_y^2 k_z^4 + 3\bar{T} \beta^2 \bar{\rho}' \bar{\rho}^2 \gamma k_y^4 k_z^2 \\
& - \bar{T} \beta^2 \beta' \bar{\rho}^3 k_x^2 k_y^4 k_z 2i + 2\bar{B} F \beta \bar{B}' \bar{T}' \bar{\rho}^2 k_y^4 - 2\bar{B}^2 F \beta \bar{T}' \bar{\rho}' \bar{\rho} k_y^4 \\
& + \bar{T} \beta^2 \bar{\rho}^3 \gamma k_x^2 k_y^4 k_z 3i + 2\bar{B} F \bar{B}' \bar{T}' \bar{\rho}^2 \gamma' k_x^2 + \bar{B} F \bar{B}' \bar{T}' \bar{\rho}^2 \gamma' k_y^2 - \bar{B}^2 F \bar{T}' \bar{\rho}' \bar{\rho} \gamma' k_x^2 \\
& - \bar{B}^2 F \bar{T}' \bar{\rho}' \bar{\rho} \gamma' k_y^2 + \beta \bar{T}' \beta' \bar{\rho}' \bar{\rho}^2 k_y^2 k_z^2 + \beta^2 \bar{T}' \beta' \bar{\rho}' \bar{\rho}^2 k_y^2 k_z^3 4i \\
& - 4\beta^2 \bar{T}' \bar{\rho}' \bar{\rho}^2 \gamma' k_y^2 k_z^2 + 3\beta \bar{T}' \bar{\rho}' \bar{\rho}^2 \gamma^2 k_y^2 k_z^2 - \beta^2 \bar{T}' \bar{\rho}' \bar{\rho}^2 \gamma k_y^2 k_z^3 6i \\
& - 2\bar{B} F \beta \bar{B}' \bar{\rho}^2 k_y^4 \theta(m+1) + 2\bar{B}^2 F \beta \bar{\rho}' \bar{\rho} k_y^4 \theta(m+1) - 2\bar{B} F \bar{B}' \bar{\rho}^2 \gamma' k_x^2 \theta(m+1) \\
& - \bar{B} F \bar{B}' \bar{\rho}^2 \gamma' k_y^2 \theta(m+1) + \bar{B}^2 F \bar{\rho}' \bar{\rho} \gamma' k_x^2 \theta(m+1) + \bar{B}^2 F \bar{\rho}' \bar{\rho} \gamma' k_y^2 \theta(m+1) \\
& - \beta \beta^2 \bar{\rho}' \bar{\rho}^2 k_y^2 k_z^2 \theta(m+1) - \beta^2 \beta' \bar{\rho}' \bar{\rho}^2 k_y^2 k_z^3 \theta(m+1) 4i + 4\beta^2 \bar{\rho}' \bar{\rho}^2 \gamma' k_y^2 k_z^2 \theta(m+1) \\
& - 3\beta \bar{\rho}' \bar{\rho}^2 \gamma^2 k_y^2 k_z^2 \theta(m+1) + \beta^2 \bar{\rho}' \bar{\rho}^2 \gamma k_y^2 k_z^3 \theta(m+1) 6i - \bar{B}^2 F^2 \beta \bar{B}' \bar{\rho} k_x^2 k_y^2 \\
& - \bar{B}^2 F^2 \beta \bar{B}' \bar{\rho} k_x^2 k_z^2 + 2\bar{B}^4 F^2 \beta \bar{\rho} k_x^2 k_y^2 k_z^2 - 2\bar{T} \beta \beta' \bar{\rho}' \bar{\rho}^2 \gamma' k_x^4 - \bar{T} \beta \beta' \bar{\rho}' \bar{\rho}^2 \gamma k_z^5 4i \\
& + 4\bar{T} \beta \bar{\rho}' \bar{\rho}^2 \gamma' \gamma k_z^4 - \bar{T} \beta' \bar{\rho}' \bar{\rho}^2 \gamma' \gamma k_z^3 2i - \bar{T} \beta \beta' \bar{\rho}^3 \gamma' k_y^4 k_z 2i + \bar{T} \beta \bar{\rho}^3 \gamma' \gamma k_y^4 k_z 4i \\
& + \beta \bar{T}' \beta' \bar{\rho}' \bar{\rho}^2 \gamma' k_z^3 2i - 4\beta \bar{T}' \beta' \bar{\rho}' \bar{\rho}^2 \gamma k_z^4 - \beta \bar{T}' \bar{\rho}' \bar{\rho}^2 \gamma' \gamma k_z^3 4i - 2\bar{T}' \beta' \bar{\rho}' \bar{\rho}^2 \gamma' \gamma k_z^2 \\
& - \beta \beta' \bar{\rho}' \bar{\rho}^2 \gamma' k_z^3 \theta(m+1) 2i + 4\beta \beta' \bar{\rho}' \bar{\rho}^2 \gamma k_z^4 \theta(m+1) + \beta \bar{\rho}' \bar{\rho}^2 \gamma' \gamma k_z^3 \theta(m+1) 4i \\
& + 2\beta' \bar{\rho}' \bar{\rho}^2 \gamma' \gamma k_z^2 \theta(m+1) - \bar{B}^2 F \bar{T} \beta' \bar{\rho}^2 k_x^4 k_z 2i + \bar{B}^2 F \bar{T} \bar{\rho}^2 \gamma k_x^4 k_z 4i \\
& - \bar{T} \beta \beta^2 \bar{\rho}^3 k_x^2 k_y^2 k_z^2 - \bar{T} \beta^2 \beta' \bar{\rho}^3 k_x^2 k_y^2 k_z^3 4i + 4\bar{T} \beta^2 \bar{\rho}^3 \gamma' k_x^2 k_y^2 k_z^2 \\
& + 4\bar{T} \beta \beta' \bar{\rho}^3 \gamma k_x^2 k_y^2 k_z^2 - \bar{B} F \bar{B}' \bar{T}' \beta' \bar{\rho}^2 k_x^2 k_z 2i - \bar{B} F \bar{B}' \bar{T}' \beta' \bar{\rho}^2 k_y^2 k_z i \\
& + \bar{B}^2 F \bar{T}' \beta' \bar{\rho}' \bar{\rho} k_x^2 k_z i + \bar{B}^2 F \bar{T}' \beta' \bar{\rho}' \bar{\rho} k_y^2 k_z i + \bar{B} F \bar{B}' \bar{T}' \bar{\rho}^2 \gamma k_x^2 k_z 2i \\
& + \bar{B} F \bar{B}' \bar{T}' \bar{\rho}^2 \gamma k_y^2 k_z 2i - \bar{B}^2 F \bar{T}' \bar{\rho}' \bar{\rho} \gamma k_x^2 k_z 2i - \bar{B}^2 F \bar{T}' \bar{\rho}' \bar{\rho} \gamma k_y^2 k_z 2i \\
& + \bar{B} F \bar{B}' \beta' \bar{\rho}^2 k_x^2 k_z \theta(m+1) 2i + \bar{B} F \bar{B}' \beta' \bar{\rho}^2 k_y^2 k_z \theta(m+1) i \\
& - \bar{B}^2 F \beta' \bar{\rho}' \bar{\rho} k_x^2 k_z \theta(m+1) i - \bar{B}^2 F \beta' \bar{\rho}' \bar{\rho} k_y^2 k_z \theta(m+1) i \\
& - \bar{B} F \bar{B}' \bar{\rho}^2 \gamma k_x^2 k_z \theta(m+1) 2i - \bar{B} F \bar{B}' \bar{\rho}^2 \gamma k_y^2 k_z \theta(m+1) 2i \\
& + \bar{B}^2 F \bar{\rho}' \bar{\rho} \gamma k_x^2 k_z \theta(m+1) 2i + \bar{B}^2 F \bar{\rho}' \bar{\rho} \gamma k_y^2 k_z \theta(m+1) 2i
\end{aligned}$$

---


$$\begin{aligned}
& + 8\bar{B}^2 F\bar{T}\beta\bar{\rho}^2 k_x^2 k_y^2 k_z^2 + \beta\bar{T}'\beta'\bar{\rho}'\bar{\rho}^2\gamma'k_y^2 k_z^2 2i - \beta\bar{T}'\bar{\rho}'\bar{\rho}^2\gamma'\gamma k_y^2 k_z^2 4i \\
& - \bar{B}F\bar{T}\beta\bar{B}'\bar{\rho}^2 k_x^2 k_z^3 2i - \bar{B}^2 F\bar{T}\beta\bar{\rho}'\bar{\rho}k_x^2 k_z^3 2i - \beta\beta'\bar{\rho}'\bar{\rho}^2\gamma'k_y^2 k_z^2 \theta(m+1)2i \\
& + \bar{B}F\bar{T}\bar{B}'\beta'\bar{\rho}^2 k_x^2 k_y^2 - \bar{B}^2 F\bar{T}\beta'\bar{\rho}'\bar{\rho}k_x^2 k_z^2 + \beta\bar{\rho}'\bar{\rho}^2\gamma'\gamma k_y^2 k_z^2 \theta(m+1)4i \\
& + 2\bar{B}F\bar{T}\bar{B}'\bar{\rho}^2\gamma k_x^2 k_z^2 + 2\bar{B}^2 F\bar{T}\bar{\rho}'\bar{\rho}\gamma k_x^2 k_z^2 + 2\bar{B}F\beta\bar{B}'\bar{T}'\bar{\rho}^2 k_x^2 k_y^2 \\
& + 2\bar{B}F\beta\bar{B}'\bar{T}'\bar{\rho}^2 k_x^2 k_z^2 + 2\bar{B}F\beta\bar{B}'\bar{T}'\bar{\rho}^2 k_y^2 k_z^2 - 2\bar{B}^2 F\beta\bar{T}'\bar{\rho}'\bar{\rho}k_x^2 k_y^2 \\
& - 2\bar{B}^2 F\beta\bar{T}'\bar{\rho}'\bar{\rho}k_x^2 k_z^2 - 2\bar{B}^2 F\beta\bar{T}'\bar{\rho}'\bar{\rho}k_y^2 k_z^2 - 2\bar{B}F\beta\bar{B}'\bar{\rho}^2 k_x^2 k_y^2 \theta(m+1) \\
& - 2\bar{B}F\beta\bar{B}'\bar{\rho}^2 k_x^2 k_z^2 \theta(m+1) - 2\bar{B}F\beta\bar{B}'\bar{\rho}^2 k_y^2 k_z^2 \theta(m+1) \\
& + 2\bar{B}^2 F\beta\bar{\rho}'\bar{\rho}k_x^2 k_y^2 \theta(m+1) + 2\bar{B}^2 F\beta\bar{\rho}'\bar{\rho}k_x^2 k_z^2 \theta(m+1) \\
& + 2\bar{B}^2 F\beta\bar{\rho}'\bar{\rho}k_y^2 k_z^2 \theta(m+1) + 2\bar{B}F\bar{T}\beta\bar{B}'\bar{\rho}'\bar{\rho}k_y^4 + \bar{B}F\bar{T}\bar{B}'\bar{\rho}'\bar{\rho}\gamma'k_y^2 \\
& - 2\bar{T}\beta\beta'\bar{\rho}'\bar{\rho}^2\gamma'k_y^2 k_z^2 - \bar{T}\beta\beta'\bar{\rho}'\bar{\rho}^2\gamma'k_y^2 k_z^3 4i + 4\bar{T}\beta\bar{\rho}'\bar{\rho}^2\gamma'\gamma k_y^2 k_z^2 \\
& - \bar{T}\beta\beta'\bar{\rho}^3\gamma'k_x^2 k_y^2 k_z^2 2i + \bar{T}\beta\bar{\rho}^3\gamma'\gamma k_x^2 k_y^2 k_z^2 4i - 4\beta\bar{T}'\beta'\bar{\rho}'\bar{\rho}^2\gamma'k_y^2 k_z^2 \\
& + 4\beta\beta'\bar{\rho}'\bar{\rho}^2\gamma'k_y^2 k_z^2 \theta(m+1) - \bar{B}^2 F\bar{T}\beta'\bar{\rho}^2 k_x^2 k_y^2 k_z^2 2i + \bar{B}^2 F\bar{T}\bar{\rho}^2\gamma k_x^2 k_y^2 k_z^2 4i \\
& - \bar{B}^3 F^2\beta\bar{B}'\bar{\rho}k_x^2 k_y^2 k_z^2 2i - \bar{B}^2 F\beta\bar{T}'\bar{\rho}^2 k_x^2 k_y^2 k_z^2 2i + \bar{B}^2 F\beta\bar{\rho}^2 k_x^2 k_y^2 k_z^2 \theta(m+1)2i \\
& - \bar{B}^2 F\bar{T}\bar{\rho}'\bar{\rho}\gamma'k_x^2 k_z^2 i - \bar{B}F\bar{T}\bar{B}'\beta'\bar{\rho}'\bar{\rho}k_y^2 k_z^2 i + \bar{B}F\bar{T}\bar{B}'\bar{\rho}'\bar{\rho}\gamma'k_y^2 k_z^2 2i \\
& + 2\bar{B}F\bar{T}\beta\bar{B}'\bar{\rho}'\bar{\rho}k_y^2 k_z^2 - \bar{B}F\bar{T}\beta\bar{B}'\bar{\rho}^2 k_x^2 k_y^2 k_z^2 2i - \bar{B}^2 F\bar{T}\beta\bar{\rho}'\bar{\rho}k_x^2 k_y^2 k_z^2 2i,
\end{aligned}$$

$$\begin{aligned}
g_2 = & \bar{T}\beta^3\bar{\rho}^3 k_y^8 + \bar{T}\beta^3\bar{\rho}^3 k_z^8 - \bar{T}\bar{\rho}^3\gamma^3 k_z^5 i - \beta^3\bar{T}'\bar{\rho}^3 k_z^7 i - \bar{T}'\bar{\rho}^3\gamma^3 k_z^4 \quad (B.3) \\
& + \beta^3\bar{\rho}^3 k_z^7 \theta(m+1)i + \bar{\rho}^3\gamma^3 k_z^4 \theta(m+1) + \bar{B}^4 F^2\bar{\rho}\gamma'k_x^4 - \bar{T}\beta\beta'^2\bar{\rho}^3 k_z^6 \\
& - \bar{T}\beta^2\beta'\bar{\rho}^3 k_z^7 2i - \bar{T}\beta^3\bar{\rho}'\bar{\rho}^2 k_z^7 i + \bar{T}\beta\bar{\rho}^3\gamma'^2 k_y^4 + 2\bar{T}\beta^2\bar{\rho}^3\gamma'k_y^6 \\
& + \bar{T}\beta\bar{\rho}^3\gamma'^2 k_z^4 + 2\bar{T}\beta^2\bar{\rho}^3\gamma'k_z^6 - 3\bar{T}\beta\bar{\rho}^3\gamma^2 k_z^6 + \bar{T}\beta^2\bar{\rho}^3\gamma k_z^7 3i \\
& + \bar{T}\beta'\bar{\rho}^3\gamma^2 k_z^5 2i - \bar{T}\beta'^2\bar{\rho}^3\gamma k_z^5 i - \bar{T}\bar{\rho}'\bar{\rho}^2\gamma^3 k_z^4 + \bar{T}\bar{\rho}^3\gamma'^2\gamma k_z^3 i \\
& - 2\bar{T}\bar{\rho}^3\gamma'\gamma^2 k_z^4 + \beta\bar{T}'\beta'^2\bar{\rho}^3 k_z^5 i - 2\beta^2\bar{T}'\beta'\bar{\rho}^3 k_z^6 - \beta^3\bar{T}'\bar{\rho}'\bar{\rho}^2 k_y^6 \\
& - \beta^3\bar{T}'\bar{\rho}'\bar{\rho}^2 k_z^6 - \beta\bar{T}'\bar{\rho}^3\gamma'^2 k_z^3 i - \beta^2\bar{T}'\bar{\rho}^3\gamma'k_z^5 2i + \beta\bar{T}'\bar{\rho}^3\gamma^2 k_z^5 3i \\
& + 3\beta^2\bar{T}'\bar{\rho}^3\gamma k_z^6 + 2\bar{T}'\beta'\bar{\rho}^3\gamma^2 k_z^4 - \bar{T}'\beta'^2\bar{\rho}^3\gamma k_z^4 + \bar{T}'\bar{\rho}'\bar{\rho}^2\gamma^3 k_z^3 i \\
& + \bar{T}'\bar{\rho}^3\gamma'^2\gamma k_z^2 + \bar{T}'\bar{\rho}^3\gamma'\gamma^2 k_z^3 2i - \beta^3\bar{T}'\bar{\rho}^3 k_y^6 k_z i - \beta\beta'^2\bar{\rho}^3 k_z^5 \theta(m+1)i \\
& + 2\beta^2\beta'\bar{\rho}^3 k_z^6 \theta(m+1) + \beta^3\bar{\rho}'\bar{\rho}^2 k_y^6 \theta(m+1) + \beta^3\bar{\rho}'\bar{\rho}^2 k_z^6 \theta(m+1) \\
& + \beta\bar{\rho}^3\gamma'^2 k_z^3 \theta(m+1)i + \beta^2\bar{\rho}^3\gamma'k_z^5 \theta(m+1)2i - \beta\bar{\rho}^3\gamma^2 k_z^5 \theta(m+1)3i
\end{aligned}$$

## B. COEFFICIENTS OF THE DISPERSION RELATION FOR THE 3D ISOTHERMAL INSTABILITY

---

$$\begin{aligned}
& - 3\beta^2 \bar{\rho}^3 \gamma k_z^6 \theta(m+1) - 2\beta' \bar{\rho}^3 \gamma^2 k_z^4 \theta(m+1) + \beta'^2 \bar{\rho}^3 \gamma k_z^4 \theta(m+1) \\
& - \bar{\rho}' \bar{\rho}^2 \gamma^3 k_z^3 \theta(m+1) i - \bar{\rho}^3 \gamma'^2 \gamma k_z^2 \theta(m+1) - \bar{\rho}^3 \gamma' \gamma^2 k_z^3 \theta(m+1) 2i \\
& + \beta^3 \bar{\rho}^3 k_y^6 k_z \theta(m+1) i + \bar{T} \beta^3 \bar{\rho}^3 k_x^2 k_y^6 + \bar{T} \beta^3 \bar{\rho}^3 k_x^2 k_z^6 + 4\bar{T} \beta^3 \bar{\rho}^3 k_y^2 k_z^6 \\
& + 6\bar{T} \beta^3 \bar{\rho}^3 k_y^4 k_z^4 + 4\bar{T} \beta^3 \bar{\rho}^3 k_y^6 k_z^2 - \bar{T} \bar{\rho}^3 \gamma^3 k_x^2 k_z^3 i - \bar{T} \bar{\rho}^3 \gamma^3 k_y^2 k_z^3 i \\
& - \beta^3 \bar{T}' \bar{\rho}^3 k_y^2 k_z^5 3i - \beta^3 \bar{T}' \bar{\rho}^3 k_y^4 k_z^3 3i + \beta^3 \bar{\rho}^3 k_y^2 k_z^5 \theta(m+1) 3i \\
& + \beta^3 \bar{\rho}^3 k_y^4 k_z^3 \theta(m+1) 3i + \bar{B}^4 F^2 \beta \bar{\rho} k_x^2 k_y^4 + \bar{B}^4 F^2 \beta \bar{\rho} k_x^4 k_y^2 \\
& + \bar{B}^4 F^2 \beta \bar{\rho} k_x^2 k_z^4 + \bar{B}^4 F^2 \beta \bar{\rho} k_x^4 k_z^2 + \bar{B}^4 F^2 \bar{\rho}' \gamma' k_x^2 k_y^2 + \bar{B}^4 F^2 \bar{\rho}' \gamma' k_x^2 k_z^3 i \\
& - \bar{T} \beta \beta'^2 \bar{\rho}^3 k_x^2 k_z^4 - \bar{T} \beta^2 \beta' \bar{\rho}^3 k_x^2 k_z^5 2i - 2\bar{T} \beta \beta'^2 \bar{\rho}^3 k_y^2 k_z^4 - \bar{T} \beta \beta'^2 \bar{\rho}^3 k_y^4 k_z^2 \\
& - \bar{T} \beta^2 \beta' \bar{\rho}^3 k_y^2 k_z^5 6i - \bar{T} \beta^2 \beta' \bar{\rho}^3 k_y^4 k_z^3 6i - \bar{T} \beta^3 \bar{\rho}' \bar{\rho}^2 k_y^2 k_z^5 3i \\
& - \bar{T} \beta^3 \bar{\rho}' \bar{\rho}^2 k_y^4 k_z^3 3i + \bar{T} \beta \bar{\rho}^3 \gamma'^2 k_x^2 k_y^2 + 2\bar{T} \beta^2 \bar{\rho}^3 \gamma' k_x^2 k_y^4 + \bar{T} \beta \bar{\rho}^3 \gamma'^2 k_x^2 k_z^2 \\
& + 2\bar{T} \beta^2 \bar{\rho}^3 \gamma' k_x^2 k_z^4 + 2\bar{T} \beta \bar{\rho}^3 \gamma'^2 k_y^2 k_z^2 + 6\bar{T} \beta^2 \bar{\rho}^3 \gamma' k_y^2 k_z^4 \\
& + 6\bar{T} \beta^2 \bar{\rho}^3 \gamma' k_y^4 k_z^2 - 3\bar{T} \beta \bar{\rho}^3 \gamma^2 k_x^2 k_z^4 + \bar{T} \beta^2 \bar{\rho}^3 \gamma k_x^2 k_z^5 3i \\
& - 6\bar{T} \beta \bar{\rho}^3 \gamma^2 k_y^2 k_z^4 - 3\bar{T} \beta \bar{\rho}^3 \gamma^2 k_y^4 k_z^2 + \bar{T} \beta^2 \bar{\rho}^3 \gamma k_y^2 k_z^5 9i \\
& + \bar{T} \beta^2 \bar{\rho}^3 \gamma k_y^4 k_z^3 9i + \bar{T} \beta' \bar{\rho}^3 \gamma^2 k_x^2 k_z^3 2i - \bar{T} \beta'^2 \bar{\rho}^3 \gamma k_x^2 k_z^3 i \\
& + \bar{T} \beta' \bar{\rho}^3 \gamma^2 k_y^2 k_z^3 2i - \bar{T} \beta'^2 \bar{\rho}^3 \gamma k_y^2 k_z^3 i - 2\bar{T} \bar{\rho}^3 \gamma' \gamma^2 k_x^2 k_z^2 \\
& - 2\bar{T} \bar{\rho}^3 \gamma' \gamma^2 k_y^2 k_z^2 + \beta \bar{T}' \beta'^2 \bar{\rho}^3 k_y^2 k_z^3 i - 4\beta^2 \bar{T}' \beta' \bar{\rho}^3 k_y^2 k_z^4 \\
& - 2\beta^2 \bar{T}' \beta' \bar{\rho}^3 k_y^4 k_z^2 - 3\beta^3 \bar{T}' \bar{\rho}' \bar{\rho}^2 k_y^2 k_z^4 - 3\beta^3 \bar{T}' \bar{\rho}' \bar{\rho}^2 k_y^4 k_z^2 \\
& - \beta^2 \bar{T}' \bar{\rho}^3 \gamma' k_y^2 k_z^3 4i + \beta \bar{T}' \bar{\rho}^3 \gamma^2 k_y^2 k_z^3 3i + 6\beta^2 \bar{T}' \bar{\rho}^3 \gamma k_y^2 k_z^4 \\
& + 3\beta^2 \bar{T}' \bar{\rho}^3 \gamma k_y^4 k_z^2 - \beta \beta'^2 \bar{\rho}^3 k_y^2 k_z^3 \theta(m+1) i + 4\beta^2 \beta' \bar{\rho}^3 k_y^2 k_z^4 \theta(m+1) \\
& + 2\beta^2 \beta' \bar{\rho}^3 k_y^4 k_z^2 \theta(m+1) + 3\beta^3 \bar{\rho}' \bar{\rho}^2 k_y^2 k_z^4 \theta(m+1) + 3\beta^3 \bar{\rho}' \bar{\rho}^2 k_y^4 k_z^2 \theta(m+1) \\
& + \beta^2 \bar{\rho}^3 \gamma' k_y^2 k_z^3 \theta(m+1) 4i - \beta \bar{\rho}^3 \gamma^2 k_y^2 k_z^3 \theta(m+1) 3i - 6\beta^2 \bar{\rho}^3 \gamma k_y^2 k_z^4 \theta(m+1) \\
& - 3\beta^2 \bar{\rho}^3 \gamma k_y^4 k_z^2 \theta(m+1) - \bar{T} \beta \beta' \bar{\rho}^3 \gamma' k_z^5 2i + 4\bar{T} \beta \beta' \bar{\rho}^3 \gamma k_z^6 + \bar{T} \beta \bar{\rho}^3 \gamma' \gamma k_z^5 4i \\
& + 2\bar{T} \beta' \bar{\rho}^3 \gamma' \gamma k_z^4 - 2\beta \bar{T}' \beta' \bar{\rho}^3 \gamma' k_z^4 - \beta \bar{T}' \beta' \bar{\rho}^3 \gamma k_z^5 4i + 4\beta \bar{T}' \bar{\rho}^3 \gamma' \gamma k_z^4 \\
& - \bar{T}' \beta' \bar{\rho}^3 \gamma' \gamma k_z^3 2i - \bar{T}' \bar{\rho}' \bar{\rho}^2 \gamma'^2 \gamma k_z i + 2\beta \beta' \bar{\rho}^3 \gamma' k_z^4 \theta(m+1) + 3\bar{B}^2 F \bar{T} \bar{\rho}^2 \gamma' k_x^4 \\
& + \beta \beta' \bar{\rho}^3 \gamma k_z^5 \theta(m+1) 4i - 4\beta \bar{\rho}^3 \gamma' \gamma k_z^4 \theta(m+1) + \beta' \bar{\rho}^3 \gamma' \gamma k_z^3 \theta(m+1) 2i \\
& + \bar{\rho}' \bar{\rho}^2 \gamma'^2 \gamma k_z \theta(m+1) i + 3\bar{T} \beta^3 \bar{\rho}^3 k_x^2 k_y^2 k_z^4 + 3\bar{T} \beta^3 \bar{\rho}^3 k_x^2 k_y^4 k_z^2 \\
& + \bar{B}^3 F^2 \bar{B}' \beta' \bar{\rho} k_x^4 + \bar{B}^4 F^2 \bar{\rho}' \gamma k_x^4 k_z i - 2F \bar{T} \beta \bar{B}'^2 \bar{\rho}^2 k_y^4 - F \bar{T} \bar{B}'^2 \bar{\rho}^2 \gamma' k_x^2 \\
& - F \bar{T} \bar{B}'^2 \bar{\rho}^2 \gamma' k_y^2 + \bar{T} \beta \beta'^2 \bar{\rho}' \bar{\rho}^2 k_z^5 i - 2\bar{T} \beta^2 \beta' \bar{\rho}' \bar{\rho}^2 k_z^6 - \bar{T} \beta \bar{\rho}' \bar{\rho}^2 \gamma'^2 k_z^3 i
\end{aligned}$$

---


$$\begin{aligned}
& - \bar{T}\beta^2\bar{\rho}'\bar{\rho}^2\gamma'k_z^52i + \bar{T}\beta\bar{\rho}'\bar{\rho}^2\gamma^2k_z^53i + 3\bar{T}\beta^2\bar{\rho}'\bar{\rho}^2\gamma k_z^6 + 2\bar{T}\beta'\bar{\rho}'\bar{\rho}^2\gamma^2k_z^4 \\
& - \bar{T}\beta^2\bar{\rho}'\bar{\rho}^2\gamma k_z^4 + \bar{T}\bar{\rho}'\bar{\rho}^2\gamma'^2\gamma k_z^2 + \bar{T}\bar{\rho}'\bar{\rho}^2\gamma'\gamma'^2k_z^32i - \bar{T}\beta^2\beta'\bar{\rho}^3k_y^6k_z2i \\
& - \bar{T}\beta^3\bar{\rho}'\bar{\rho}^2k_y^6k_zi + \bar{T}\beta^2\bar{\rho}^3\gamma k_y^6k_z3i + \bar{T}\bar{\rho}^3\gamma'^2\gamma k_x^2k_zi + \bar{T}\bar{\rho}^3\gamma'^2\gamma k_y^2k_zi \\
& + \beta\bar{T}'\beta'^2\bar{\rho}'\bar{\rho}^2k_z^4 + \beta^2\bar{T}'\beta'\bar{\rho}'\bar{\rho}^2k_z^52i - \beta\bar{T}'\bar{\rho}'\bar{\rho}^2\gamma'^2k_y^2 - 2\beta^2\bar{T}'\bar{\rho}'\bar{\rho}^2\gamma'k_y^4 \\
& - \beta\bar{T}'\bar{\rho}'\bar{\rho}^2\gamma'^2k_z^2 - 2\beta^2\bar{T}'\bar{\rho}'\bar{\rho}^2\gamma'k_z^4 + 3\beta\bar{T}'\bar{\rho}'\bar{\rho}^2\gamma^2k_z^4 - \beta^2\bar{T}'\bar{\rho}'\bar{\rho}^2\gamma k_z^53i \\
& - \bar{T}'\beta'\bar{\rho}'\bar{\rho}^2\gamma^2k_z^32i + \bar{T}'\beta^2\bar{\rho}'\bar{\rho}^2\gamma k_z^3i + 2\bar{T}'\bar{\rho}'\bar{\rho}^2\gamma'\gamma^2k_z^2 - \beta\bar{T}'\bar{\rho}^3\gamma'^2k_y^2k_zi \\
& - \beta^2\bar{T}'\bar{\rho}^3\gamma'k_y^4k_z2i - \beta\beta'^2\bar{\rho}'\bar{\rho}^2k_z^4\theta(m+1) - \beta^2\beta'\bar{\rho}'\bar{\rho}^2k_z^5\theta(m+1)2i \\
& + \beta\bar{\rho}'\bar{\rho}^2\gamma'^2k_y^2\theta(m+1) + 2\beta^2\bar{\rho}'\bar{\rho}^2\gamma'k_y^4\theta(m+1) + \beta\bar{\rho}'\bar{\rho}^2\gamma'^2k_z^2\theta(m+1) \\
& + 2\beta^2\bar{\rho}'\bar{\rho}^2\gamma'k_z^4\theta(m+1) - 3\beta\bar{\rho}'\bar{\rho}^2\gamma^2k_z^4\theta(m+1) + \beta^2\bar{\rho}'\bar{\rho}^2\gamma k_z^5\theta(m+1)3i \\
& + \beta'\bar{\rho}'\bar{\rho}^2\gamma^2k_z^3\theta(m+1)2i - \beta'^2\bar{\rho}'\bar{\rho}^2\gamma k_z^3\theta(m+1)i - 2\bar{\rho}'\bar{\rho}^2\gamma'\gamma^2k_z^2\theta(m+1) \\
& + \beta\bar{\rho}^3\gamma'^2k_y^2k_z\theta(m+1)i + \beta^2\bar{\rho}^3\gamma'k_y^4k_z\theta(m+1)2i - 3\bar{T}\beta\bar{\rho}^3\gamma^2k_x^2k_y^2k_z^2 \\
& + \bar{T}\beta^2\bar{\rho}^3\gamma k_x^2k_y^2k_z^36i - \bar{B}^2F\bar{T}'\bar{\rho}^2\gamma'k_x^2k_zi + \bar{B}^2F\bar{\rho}^2\gamma'k_x^2k_z\theta(m+1)i \\
& + F\bar{T}\bar{B}'\beta'\bar{\rho}^2k_x^2k_zi + F\bar{T}\bar{B}'\beta'\bar{\rho}^2k_y^2k_zi - F\bar{T}\bar{B}'\bar{\rho}^2\gamma k_x^2k_z2i \\
& - F\bar{T}\bar{B}'\bar{\rho}^2\gamma k_y^2k_z2i - \bar{T}\beta\beta'\bar{\rho}^3\gamma'k_x^2k_z^32i - \bar{T}\beta\beta'\bar{\rho}^3\gamma'k_y^2k_z^34i \\
& - \bar{T}\beta\bar{\rho}'\bar{\rho}^2\gamma'^2k_y^2k_zi - \bar{T}\beta^2\bar{\rho}'\bar{\rho}^2\gamma'k_y^4k_z2i + 4\bar{T}\beta\beta'\bar{\rho}^3\gamma k_x^2k_z^4 \\
& + 8\bar{T}\beta\beta'\bar{\rho}^3\gamma k_y^2k_z^4 + 4\bar{T}\beta\beta'\bar{\rho}^3\gamma k_y^4k_z^2 + \bar{T}\beta\bar{\rho}^3\gamma'\gamma k_x^2k_z^34i \\
& + \bar{T}\beta\bar{\rho}^3\gamma'\gamma k_y^2k_z^38i + 2\bar{T}\beta'\bar{\rho}^3\gamma'\gamma k_x^2k_z^2 + 2\bar{T}\beta'\bar{\rho}^3\gamma'\gamma k_y^2k_z^2 \\
& + \beta^2\bar{T}'\beta'\bar{\rho}'\bar{\rho}^2k_y^4k_z2i - 2\beta\bar{T}'\beta'\bar{\rho}^3\gamma'k_y^2k_z^2 - \beta\bar{T}'\beta'\bar{\rho}^3\gamma k_y^2k_z^34i \\
& - \beta^2\bar{T}'\bar{\rho}'\bar{\rho}^2\gamma k_y^4k_z3i + 4\beta\bar{T}'\bar{\rho}^3\gamma'\gamma k_y^2k_z^2 + 4\bar{B}^2F\bar{T}\beta\bar{\rho}^2k_x^2k_y^4 \\
& + 4\bar{B}^2F\bar{T}\beta\bar{\rho}^2k_x^4k_y^2 + 4\bar{B}^2F\bar{T}\beta\bar{\rho}^2k_x^2k_z^4 + 4\bar{B}^2F\bar{T}\beta\bar{\rho}^2k_x^4k_z^2 \\
& - \beta^2\beta'\bar{\rho}'\bar{\rho}^2k_y^4k_z\theta(m+1)2i + 2\beta\beta'\bar{\rho}^3\gamma'k_y^2k_z^2\theta(m+1) - \bar{B}^2F\bar{T}\beta'\bar{\rho}^2k_x^2k_z^32i \\
& + 3\bar{B}^2F\bar{T}\bar{\rho}^2\gamma'k_x^2k_y^2 + 2\bar{B}^2F\bar{T}\bar{\rho}^2\gamma'k_x^2k_z^2 + \beta\beta'\bar{\rho}^3\gamma k_y^2k_z^3\theta(m+1)4i \\
& + \beta^2\bar{\rho}'\bar{\rho}^2\gamma k_y^4k_z\theta(m+1)3i - 4\beta\bar{\rho}^3\gamma'\gamma k_y^2k_z^2\theta(m+1) + \bar{B}^2F\bar{T}\bar{\rho}^2\gamma k_x^2k_z^34i \\
& - \bar{B}^3F^2\beta\bar{B}'\bar{\rho}k_x^2k_z^32i - \bar{B}^2F\beta\bar{T}'\bar{\rho}^2k_x^2k_z^32i + \bar{B}^3F^2\bar{B}'\beta'\bar{\rho}k_x^2k_y^2 \\
& - \bar{B}^2F\bar{T}'\beta'\bar{\rho}^2k_x^2k_z^2 - \bar{B}^2F^2\bar{B}'\bar{\rho}\gamma k_x^2k_zi + 2\bar{B}^3F^2\bar{B}'\bar{\rho}\gamma k_x^2k_z^2 \\
& + 2\bar{B}^2F\bar{T}'\bar{\rho}^2\gamma k_x^2k_z^2 + \bar{B}^4F^2\bar{\rho}\gamma k_x^2k_y^2k_zi + \bar{B}^2F\beta\bar{\rho}^2k_x^2k_z^3\theta(m+1)2i \\
& - 2F\bar{T}\beta\bar{B}'\bar{\rho}^2k_x^2k_y^2 - 2F\bar{T}\beta\bar{B}'\bar{\rho}^2k_x^2k_z^2 - 2F\bar{T}\beta\bar{B}'\bar{\rho}^2k_y^2k_z^2
\end{aligned}$$

## B. COEFFICIENTS OF THE DISPERSION RELATION FOR THE 3D ISOTHERMAL INSTABILITY

---

$$\begin{aligned}
& + \bar{B}^2 F \beta' \bar{\rho}^2 k_x^2 k_z^2 \theta(m+1) - 2\bar{B}^2 F \bar{\rho}^2 \gamma k_x^2 k_z^2 \theta(m+1) + \bar{B} F \bar{T} \bar{B}' \beta' \bar{\rho}^2 k_x^4 \\
& + \bar{T} \beta \beta'^2 \bar{\rho}' \bar{\rho}^2 k_y^2 k_z^3 i - 4\bar{T} \beta^2 \beta' \bar{\rho}' \bar{\rho}^2 k_y^2 k_z^4 - 2\bar{T} \beta^2 \beta' \bar{\rho}' \bar{\rho}^2 k_y^4 k_z^2 \\
& - \bar{T} \beta^2 \bar{\rho}' \bar{\rho}^2 \gamma' k_y^2 k_z^3 4i + \bar{T} \beta \bar{\rho}' \bar{\rho}^2 \gamma^2 k_y^2 k_z^3 3i + 6\bar{T} \beta^2 \bar{\rho}' \bar{\rho}^2 \gamma k_y^2 k_z^4 \\
& + 3\bar{T} \beta^2 \bar{\rho}' \bar{\rho}^2 \gamma k_y^4 k_z^2 - \bar{T} \beta^2 \beta' \bar{\rho}^3 k_x^2 k_y^4 k_z 2i + 2\bar{B} F \beta \bar{B}' \bar{T}' \bar{\rho}^2 k_y^4 \\
& - 2\bar{B}^2 F \beta \bar{T}' \bar{\rho}' \bar{\rho} k_y^4 + \bar{T} \beta^2 \bar{\rho}^3 \gamma k_x^2 k_y^4 k_z 3i + 2\bar{B} F \bar{B}' \bar{T}' \bar{\rho}^2 \gamma' k_x^2 \\
& + \bar{B} F \bar{B}' \bar{T}' \bar{\rho}^2 \gamma' k_y^2 - \bar{B}^2 F \bar{T}' \bar{\rho}' \bar{\rho} \gamma' k_x^2 - \bar{B}^2 F \bar{T}' \bar{\rho}' \bar{\rho} \gamma' k_y^2 + \beta \bar{T}' \beta'^2 \bar{\rho}' \bar{\rho}^2 k_y^2 k_z^2 \\
& + \beta^2 \bar{T}' \beta' \bar{\rho}' \bar{\rho}^2 k_y^2 k_z^3 4i - 4\beta^2 \bar{T}' \bar{\rho}' \bar{\rho}^2 \gamma' k_y^2 k_z^2 + 3\beta \bar{T}' \bar{\rho}' \bar{\rho}^2 \gamma^2 k_y^2 k_z^2 \\
& - \beta^2 \bar{T}' \bar{\rho}' \bar{\rho}^2 \gamma k_y^2 k_z^3 6i - 2\bar{B} F \beta \bar{B}' \bar{\rho}^2 k_y^4 \theta(m+1) + 2\bar{B}^2 F \beta \bar{\rho}' \bar{\rho} k_y^4 \theta(m+1) \\
& - 2\bar{B} F \bar{B}' \bar{\rho}^2 \gamma' k_x^2 \theta(m+1) - \bar{B} F \bar{B}' \bar{\rho}^2 \gamma' k_y^2 \theta(m+1) + \bar{B}^2 F \bar{\rho}' \bar{\rho} \gamma' k_x^4 \theta(m+1) \\
& + \bar{B}^2 F \bar{\rho}' \bar{\rho} \gamma' k_y^2 \theta(m+1) - \beta \beta'^2 \bar{\rho}' \bar{\rho}^2 k_y^2 k_z^2 \theta(m+1) \\
& - \beta^2 \beta' \bar{\rho}' \bar{\rho}^2 k_y^2 k_z^3 \theta(m+1) 4i + 4\beta^2 \bar{\rho}' \bar{\rho}^2 \gamma' k_y^2 k_z^2 \theta(m+1) \\
& - 3\beta \bar{\rho}' \bar{\rho}^2 \gamma^2 k_y^2 k_z^2 \theta(m+1) + \beta^2 \bar{\rho}' \bar{\rho}^2 \gamma k_y^2 k_z^3 \theta(m+1) 6i \\
& - \bar{B}^2 F^2 \beta \bar{B}'^2 \bar{\rho} k_x^2 k_y^2 - \bar{B}^2 F^2 \beta \bar{B}'^2 \bar{\rho} k_x^2 k_z^2 + 2\bar{B}^4 F^2 \beta \bar{\rho} k_x^2 k_y^2 k_z^2 \\
& - 2\bar{T} \beta \beta' \bar{\rho}' \bar{\rho}^2 \gamma' k_z^4 - \bar{T} \beta \beta' \bar{\rho}' \bar{\rho}^2 \gamma k_z^5 4i + 4\bar{T} \beta \bar{\rho}' \bar{\rho}^2 \gamma' \gamma k_z^4 \\
& - \bar{T} \beta' \bar{\rho}' \bar{\rho}^2 \gamma' \gamma k_z^3 2i - \bar{T} \beta \beta' \bar{\rho}^3 \gamma' k_y^4 k_z 2i + \bar{T} \beta \bar{\rho}^3 \gamma' \gamma k_y^4 k_z 4i \\
& + \beta \bar{T}' \beta' \bar{\rho}' \bar{\rho}^2 \gamma' k_z^3 2i - 4\beta \bar{T}' \beta' \bar{\rho}' \bar{\rho}^2 \gamma k_z^4 - \beta \bar{T}' \bar{\rho}' \bar{\rho}^2 \gamma' \gamma k_z^3 4i \\
& - 2\bar{T}' \beta' \bar{\rho}' \bar{\rho}^2 \gamma' \gamma k_z^2 - \beta \beta' \bar{\rho}' \bar{\rho}^2 \gamma' k_z^3 \theta(m+1) 2i + 4\beta \beta' \bar{\rho}' \bar{\rho}^2 \gamma k_z^4 \theta(m+1) \\
& + \beta \bar{\rho}' \bar{\rho}^2 \gamma' \gamma k_z^3 \theta(m+1) 4i + 2\beta' \bar{\rho}' \bar{\rho}^2 \gamma' \gamma k_z^2 \theta(m+1) - \bar{B}^2 F \bar{T} \beta' \bar{\rho}^2 k_x^4 k_z 2i \\
& + \bar{B}^2 F \bar{T} \bar{\rho}^2 \gamma k_x^4 k_z 4i - \bar{T} \beta \beta'^2 \bar{\rho}^3 k_x^2 k_y^2 k_z^2 - \bar{T} \beta^2 \beta' \bar{\rho}^3 k_x^2 k_y^2 k_z^3 4i \\
& + 4\bar{T} \beta^2 \bar{\rho}^3 \gamma' k_x^2 k_y^2 k_z^2 + 4\bar{T} \beta \beta' \bar{\rho}^3 \gamma k_x^2 k_y^2 k_z^2 - \bar{B} F \bar{B}' \bar{T}' \beta' \bar{\rho}^2 k_x^2 k_z 2i \\
& - \bar{B} F \bar{B}' \bar{T}' \beta' \bar{\rho}^2 k_y^2 k_z i + \bar{B}^2 F \bar{T}' \beta' \bar{\rho}' \bar{\rho} k_x^2 k_z i + \bar{B}^2 F \bar{T}' \beta' \bar{\rho}' \bar{\rho} k_y^2 k_z i \\
& + \bar{B} F \bar{B}' \bar{T}' \bar{\rho}^2 \gamma k_x^2 k_z 2i + \bar{B} F \bar{B}' \bar{T}' \bar{\rho}^2 \gamma k_y^2 k_z 2i - \bar{B}^2 F \bar{T}' \bar{\rho}' \bar{\rho} \gamma k_x^2 k_z 2i \\
& - \bar{B}^2 F \bar{T}' \bar{\rho}' \bar{\rho} \gamma k_y^2 k_z 2i + \bar{B} F \bar{B}' \beta' \bar{\rho}^2 k_x^2 k_z \theta(m+1) 2i \\
& + \bar{B} F \bar{B}' \beta' \bar{\rho}^2 k_y^2 k_z \theta(m+1) i - \bar{B}^2 F \beta' \bar{\rho}' \bar{\rho} k_x^2 k_z \theta(m+1) i \\
& - \bar{B}^2 F \beta' \bar{\rho}' \bar{\rho} k_y^2 k_z \theta(m+1) i - \bar{B} F \bar{B}' \bar{\rho}^2 \gamma k_x^2 k_z \theta(m+1) 2i \\
& - \bar{B} F \bar{B}' \bar{\rho}^2 \gamma k_y^2 k_z \theta(m+1) 2i + \bar{B}^2 F \bar{\rho}' \bar{\rho} \gamma k_x^2 k_z \theta(m+1) 2i \\
& + \bar{B}^2 F \bar{\rho}' \bar{\rho} \gamma k_y^2 k_z \theta(m+1) 2i + 8\bar{B}^2 F \bar{T} \beta \bar{\rho}^2 k_x^2 k_y^2 k_z^2 \\
& + \beta \bar{T}' \beta' \bar{\rho}' \bar{\rho}^2 \gamma' k_y^2 k_z 2i - \beta \bar{T}' \bar{\rho}' \bar{\rho}^2 \gamma' \gamma k_y^2 k_z 4i - \bar{B} F \bar{T} \beta \bar{B}' \bar{\rho}^2 k_x^2 k_z^3 2i \\
& - \bar{B}^2 F \bar{T} \beta \bar{\rho}' \bar{\rho} k_x^2 k_z^3 2i - \beta \beta' \bar{\rho}' \bar{\rho}^2 \gamma' k_y^2 k_z \theta(m+1) 2i + \bar{B} F \bar{T} \bar{B}' \beta' \bar{\rho}^2 k_x^2 k_y^2
\end{aligned}$$

---


$$\begin{aligned}
& - \bar{B}^2 F \bar{T} \bar{\rho}' \bar{\rho} k_x^2 k_z^2 + \beta \bar{\rho}' \bar{\rho}^2 \gamma' \gamma k_y^2 k_z \theta(m+1) 4i + 2 \bar{B} F \bar{T} \bar{B}' \bar{\rho}^2 \gamma k_x^2 k_z^2 \\
& + 2 \bar{B}^2 F \bar{T} \bar{\rho}' \bar{\rho} \gamma k_x^2 k_z^2 + 2 \bar{B} F \beta \bar{B}' \bar{T}' \bar{\rho}^2 k_x^2 k_y^2 + 2 \bar{B} F \beta \bar{B}' \bar{T}' \bar{\rho}^2 k_x^2 k_z^2 \\
& + 2 \bar{B} F \beta \bar{B}' \bar{T}' \bar{\rho}^2 k_y^2 k_z^2 - 2 \bar{B}^2 F \beta \bar{T}' \bar{\rho}' \bar{\rho} k_x^2 k_y^2 - 2 \bar{B}^2 F \beta \bar{T}' \bar{\rho}' \bar{\rho} k_x^2 k_z^2 \\
& - 2 \bar{B}^2 F \beta \bar{T}' \bar{\rho}' \bar{\rho} k_y^2 k_z^2 - 2 \bar{B} F \beta \bar{B}' \bar{\rho}^2 k_x^2 k_y^2 \theta(m+1) \\
& - 2 \bar{B} F \beta \bar{B}' \bar{\rho}^2 k_x^2 k_z^2 \theta(m+1) - 2 \bar{B} F \beta \bar{B}' \bar{\rho}^2 k_y^2 k_z^2 \theta(m+1) \\
& + 2 \bar{B}^2 F \beta \bar{\rho}' \bar{\rho} k_x^2 k_y^2 \theta(m+1) + 2 \bar{B}^2 F \beta \bar{\rho}' \bar{\rho} k_x^2 k_z^2 \theta(m+1) \\
& + 2 \bar{B}^2 F \beta \bar{\rho}' \bar{\rho} k_y^2 k_z^2 \theta(m+1) + 2 \bar{B} F \bar{T} \beta \bar{B}' \bar{\rho}' \bar{\rho} k_y^4 + \bar{B} F \bar{T} \bar{B}' \bar{\rho}' \bar{\rho} \gamma' k_y^2 \\
& - 2 \bar{T} \beta \beta' \bar{\rho}' \bar{\rho}^2 \gamma' k_y^2 k_z^2 - \bar{T} \beta \beta' \bar{\rho}' \bar{\rho}^2 \gamma k_y^2 k_z^3 4i + 4 \bar{T} \beta \bar{\rho}' \bar{\rho}^2 \gamma' \gamma k_y^2 k_z^2 \\
& - \bar{T} \beta \beta' \bar{\rho}^3 \gamma' k_x^2 k_y^2 k_z^2 2i + \bar{T} \beta \bar{\rho}^3 \gamma' \gamma k_x^2 k_y^2 k_z^2 4i - 4 \beta \bar{T}' \beta' \bar{\rho}' \bar{\rho}^2 \gamma k_y^2 k_z^2 \\
& + 4 \beta \beta' \bar{\rho}' \bar{\rho}^2 \gamma k_y^2 k_z^2 \theta(m+1) - \bar{B}^2 F \bar{T} \beta' \bar{\rho}^2 k_x^2 k_y^2 k_z^2 2i + \bar{B}^2 F \bar{T} \bar{\rho}^2 \gamma k_x^2 k_y^2 k_z^2 4i \\
& - \bar{B}^3 F^2 \beta \bar{B}' \bar{\rho} k_x^2 k_y^2 k_z^2 2i - \bar{B}^2 F \beta \bar{T}' \bar{\rho}^2 k_x^2 k_y^2 k_z^2 2i \\
& + \bar{B}^2 F \beta \bar{\rho}^2 k_x^2 k_y^2 k_z^2 \theta(m+1) 2i - \bar{B}^2 F \bar{T} \bar{\rho}' \bar{\rho} \gamma' k_x^2 k_z^2 i \\
& - \bar{B} F \bar{T} \bar{B}' \beta' \bar{\rho}' \bar{\rho} k_y^2 k_z^2 i + \bar{B} F \bar{T} \bar{B}' \bar{\rho}' \bar{\rho} \gamma k_y^2 k_z^2 2i + 2 \bar{B} F \bar{T} \beta \bar{B}' \bar{\rho}' \bar{\rho} k_y^2 k_z^2 \\
& - \bar{B} F \bar{T} \beta \bar{B}' \bar{\rho}^2 k_x^2 k_y^2 k_z^2 2i - \bar{B}^2 F \bar{T} \beta \bar{\rho}' \bar{\rho} k_x^2 k_y^2 k_z^2 2i,
\end{aligned}$$

$$\begin{aligned}
g_3 = & 3 \bar{T} \beta^2 \bar{\rho}^3 k_y^6 + 3 \bar{T} \beta^2 \bar{\rho}^3 k_z^6 - \bar{T} \beta'^2 \bar{\rho}^3 k_z^4 + \bar{T} \bar{\rho}^3 \gamma'^2 k_x^2 & (B.4) \\
& + \bar{T} \bar{\rho}^3 \gamma'^2 k_y^2 + \bar{T} \bar{\rho}^3 \gamma'^2 k_z^2 - 3 \bar{T} \bar{\rho}^3 \gamma^2 k_z^4 - \beta^2 \bar{T}' \bar{\rho}^3 k_z^5 3i \\
& + \bar{T}' \beta'^2 \bar{\rho}^3 k_z^3 i + \bar{T}' \bar{\rho}^3 \gamma^2 k_z^3 3i + \beta^2 \bar{\rho}^3 k_z^5 \theta(m+1) 3i \\
& - \beta'^2 \bar{\rho}^3 k_z^3 \theta(m+1) i - \bar{\rho}^3 \gamma^2 k_z^3 \theta(m+1) 3i - \bar{T}' \bar{\rho}' \bar{\rho}^2 \gamma'^2 \\
& - \bar{T}' \bar{\rho}^3 \gamma'^2 k_z i + \bar{\rho}' \bar{\rho}^2 \gamma'^2 \theta(m+1) + \bar{\rho}^3 \gamma'^2 k_z \theta(m+1) i \\
& + \bar{B}^4 F^2 \bar{\rho} k_x^4 - \bar{T} \beta \beta' \bar{\rho}^3 k_z^5 4i + 4 \bar{T} \beta \bar{\rho}^3 \gamma' k_y^4 + 4 \bar{T} \beta \bar{\rho}^3 \gamma' k_z^4 \\
& - \bar{T} \beta' \bar{\rho}^3 \gamma' k_z^3 2i - \bar{T} \bar{\rho}' \bar{\rho}^2 \gamma'^2 k_z i + \bar{T} \beta \bar{\rho}^3 \gamma k_z^5 6i + 4 \bar{T} \beta' \bar{\rho}^3 \gamma k_z^4 \\
& + \bar{T} \bar{\rho}^3 \gamma' \gamma k_z^3 4i - 4 \beta \bar{T}' \beta' \bar{\rho}^3 k_z^4 - \beta \bar{T}' \bar{\rho}^3 \gamma' k_z^3 4i - 2 \bar{T}' \beta' \bar{\rho}^3 \gamma' k_z^2 \\
& + 6 \beta \bar{T}' \bar{\rho}^3 \gamma k_z^4 - \bar{T}' \beta' \bar{\rho}^3 \gamma k_z^3 4i + 4 \bar{T}' \bar{\rho}^3 \gamma' \gamma k_z^2 + 4 \beta \beta' \bar{\rho}^3 k_z^4 \theta(m+1) \\
& + \beta \bar{\rho}^3 \gamma' k_z^3 \theta(m+1) 4i + 2 \bar{B}^2 F \bar{T} \bar{\rho}^2 k_x^4 + 2 \beta' \bar{\rho}^3 \gamma' k_z^2 \theta(m+1) \\
& - 6 \beta \bar{\rho}^3 \gamma k_z^4 \theta(m+1) + \beta' \bar{\rho}^3 \gamma k_z^3 \theta(m+1) 4i - 4 \bar{\rho}^3 \gamma' \gamma k_z^2 \theta(m+1) \\
& - F \bar{T} \bar{B}' \bar{\rho}^2 k_x^2 - F \bar{T} \bar{B}' \bar{\rho}^2 k_y^2 - \bar{T} \beta^2 \bar{\rho}' \bar{\rho}^2 k_z^5 3i + \bar{T} \beta'^2 \bar{\rho}' \bar{\rho}^2 k_z^3 i \\
& + \bar{T} \bar{\rho}' \bar{\rho}^2 \gamma^2 k_z^3 3i - 3 \beta^2 \bar{T}' \bar{\rho}' \bar{\rho}^2 k_y^4 - 3 \beta^2 \bar{T}' \bar{\rho}' \bar{\rho}^2 k_z^4 + \bar{T}' \beta'^2 \bar{\rho}' \bar{\rho}^2 k_z^2
\end{aligned}$$

## B. COEFFICIENTS OF THE DISPERSION RELATION FOR THE 3D ISOTHERMAL INSTABILITY

---

$$\begin{aligned}
& + 3\bar{T}'\bar{\rho}'\bar{\rho}^2\gamma^2k_z^2 - \beta^2\bar{T}'\bar{\rho}^3k_y^4k_z^3i + 3\beta^2\bar{\rho}'\bar{\rho}^2k_y^4\theta(m+1) \\
& + 3\beta^2\bar{\rho}'\bar{\rho}^2k_z^4\theta(m+1) - \beta'^2\bar{\rho}'\bar{\rho}^2k_z^2\theta(m+1) - 3\bar{\rho}'\bar{\rho}^2\gamma^2k_z^2\theta(m+1) \\
& + \beta^2\bar{\rho}^3k_y^4k_z\theta(m+1)3i + \bar{B}^2F\beta^2\bar{\rho}^2k_y^6 + \bar{B}^2F\beta^2\bar{\rho}^2k_z^6 \\
& - \bar{B}^2F^2\bar{B}'^2\bar{\rho}k_x^2 + \bar{B}^2F\bar{\rho}^2\gamma'^2k_x^2 - \bar{B}^2F\bar{\rho}^2\gamma^2k_z^4 + \bar{B}^4F^2\bar{\rho}k_x^2k_y^2 \\
& + \bar{B}^4F^2\bar{\rho}k_x^2k_z^2 - F\beta^2\bar{B}'^2\bar{\rho}^2k_y^4 - F\beta^2\bar{B}'^2\bar{\rho}^2k_z^4 + F\bar{B}'^2\bar{\rho}^2\gamma^2k_z^2 \\
& + 3\bar{T}\beta^2\bar{\rho}^3k_x^2k_y^4 + 3\bar{T}\beta^2\bar{\rho}^3k_x^2k_z^4 + 9\bar{T}\beta^2\bar{\rho}^3k_y^2k_z^4 + 9\bar{T}\beta^2\bar{\rho}^3k_y^4k_z^2 \\
& - \bar{T}\beta'^2\bar{\rho}^3k_x^2k_z^2 - \bar{T}\beta'^2\bar{\rho}^3k_y^2k_z^2 - 3\bar{T}\bar{\rho}^3\gamma^2k_x^2k_z^2 - 3\bar{T}\bar{\rho}^3\gamma^2k_y^2k_z^2 \\
& - \beta^2\bar{T}'\bar{\rho}^3k_y^2k_z^36i + \beta^2\bar{\rho}^3k_y^2k_z^3\theta(m+1)6i + \bar{T}'\beta'\bar{\rho}'\bar{\rho}^2\gamma'k_z^2i \\
& - \bar{T}'\bar{\rho}'\bar{\rho}^2\gamma'\gamma k_z^4i - \beta'\bar{\rho}'\bar{\rho}^2\gamma'k_z\theta(m+1)2i + \bar{\rho}'\bar{\rho}^2\gamma'\gamma k_z\theta(m+1)4i \\
& - \bar{T}\beta^2\bar{\rho}'\bar{\rho}^2k_y^2k_z^36i + \bar{B}F\bar{B}'\bar{T}'\bar{\rho}^2k_x^2 + \bar{B}F\bar{B}'\bar{T}'\bar{\rho}^2k_y^2 - \bar{B}^2F\bar{T}'\bar{\rho}'\bar{\rho}k_x^2 \\
& - \bar{B}^2F\bar{T}'\bar{\rho}'\bar{\rho}k_y^2 - 6\beta^2\bar{T}'\bar{\rho}'\bar{\rho}^2k_y^2k_z^2 - \bar{B}F\bar{B}'\bar{\rho}^2k_x^2\theta(m+1) \\
& - \bar{B}F\bar{B}'\bar{\rho}^2k_y^2\theta(m+1) + \bar{B}^2F\bar{\rho}'\bar{\rho}k_x^2\theta(m+1) + \bar{B}^2F\bar{\rho}'\bar{\rho}k_y^2\theta(m+1) \\
& + 6\beta^2\bar{\rho}'\bar{\rho}^2k_y^2k_z^2\theta(m+1) + 2\bar{B}^2F\beta^2\bar{\rho}^2k_x^2k_y^4 + 2\bar{B}^2F\beta^2\bar{\rho}^2k_x^2k_z^4 \\
& + 3\bar{B}^2F\beta^2\bar{\rho}^2k_y^2k_z^4 + 3\bar{B}^2F\beta^2\bar{\rho}^2k_y^4k_z^2 - F\bar{B}'^2\bar{\rho}^2\gamma'k_z^2i \\
& - 2\bar{B}^2F\bar{\rho}^2\gamma^2k_x^2k_z^2 - \bar{B}^2F\bar{\rho}^2\gamma^2k_y^2k_z^2 - 4\bar{T}\beta\beta'\bar{\rho}'\bar{\rho}^2k_z^4 \\
& - \bar{T}\beta\bar{\rho}'\bar{\rho}^2\gamma'k_z^34i - 2\bar{T}\beta'\bar{\rho}'\bar{\rho}^2\gamma'k_z^2 + 6\bar{T}\beta\bar{\rho}'\bar{\rho}^2\gamma k_z^4 - \bar{T}\beta'\bar{\rho}'\bar{\rho}^2\gamma k_z^34i \\
& + 4\bar{T}\bar{\rho}'\bar{\rho}^2\gamma'\gamma k_z^2 - \bar{T}\beta\beta'\bar{\rho}^3k_y^4k_z^4i - \bar{T}\beta'\bar{\rho}^3\gamma'k_x^2k_z^2i \\
& - \bar{T}\beta'\bar{\rho}^3\gamma'k_y^2k_z^2i + \bar{T}\beta\bar{\rho}^3\gamma k_y^4k_z^6i + \bar{T}\bar{\rho}^3\gamma'\gamma k_x^2k_z^4i \\
& + \bar{T}\bar{\rho}^3\gamma'\gamma k_y^2k_z^4i + \beta\bar{T}'\beta'\bar{\rho}'\bar{\rho}^2k_z^34i - 4\beta\bar{T}'\bar{\rho}'\bar{\rho}^2\gamma'k_y^2 - 4\beta\bar{T}'\bar{\rho}'\bar{\rho}^2\gamma'k_z^2 \\
& - \beta\bar{T}'\bar{\rho}'\bar{\rho}^2\gamma k_z^36i - 4\bar{T}'\beta'\bar{\rho}'\bar{\rho}^2\gamma k_z^2 - \beta\bar{T}'\bar{\rho}^3\gamma'k_y^2k_z^4i \\
& - 2F\beta^2\bar{B}'^2\bar{\rho}^2k_y^2k_z^2 - \beta\beta'\bar{\rho}'\bar{\rho}^2k_z^3\theta(m+1)4i + 4\beta\bar{\rho}'\bar{\rho}^2\gamma'k_y^2\theta(m+1) \\
& + 4\beta\bar{\rho}'\bar{\rho}^2\gamma'k_z^2\theta(m+1) + \beta\bar{\rho}'\bar{\rho}^2\gamma k_z^3\theta(m+1)6i + 4\beta'\bar{\rho}'\bar{\rho}^2\gamma k_z^2\theta(m+1) \\
& + \beta\bar{\rho}^3\gamma'k_y^2k_z\theta(m+1)4i + 6\bar{T}\beta^2\bar{\rho}^3k_x^2k_y^2k_z^2 - \bar{B}F\beta^2\bar{B}'\bar{\rho}^2k_z^52i \\
& - \bar{B}^2F\beta\beta'\bar{\rho}^2k_z^5i + \bar{B}^2F\beta\bar{\rho}^2\gamma'k_y^4 + \bar{B}^2F\beta\bar{\rho}^2\gamma'k_z^4 + \bar{B}^2F\beta\bar{\rho}^2\gamma k_z^52i \\
& + \bar{B}F\bar{B}'\bar{\rho}^2\gamma^2k_z^32i + \bar{B}^2F\beta'\bar{\rho}^2\gamma k_z^4 + \bar{B}^2F\bar{\rho}^2\gamma'\gamma k_z^3i - \bar{B}^3F^2\bar{B}'\bar{\rho}k_x^2k_z^2i \\
& - \bar{B}^2F\bar{T}'\bar{\rho}^2k_x^2k_z^2i + \bar{B}^2F\bar{\rho}^2k_x^2k_z^2\theta(m+1)i + F\beta\bar{B}'^2\beta'\bar{\rho}^2k_z^3i
\end{aligned}$$

---


$$\begin{aligned}
& - F\beta\bar{B}'^2\bar{\rho}^2\gamma'k_y^2 - F\beta\bar{B}'^2\bar{\rho}^2\gamma'k_z^2 - F\beta\bar{B}'^2\bar{\rho}^2\gamma k_z^3 2i - F\bar{B}'^2\beta'\bar{\rho}^2\gamma k_z^2 \\
& - \bar{T}\beta\beta'\bar{\rho}^3k_x^2k_z^3 4i - \bar{T}\beta\beta'\bar{\rho}^3k_y^2k_z^3 8i - \bar{T}\beta^2\bar{\rho}'\bar{\rho}^2k_y^4k_z 3i \\
& + 4\bar{T}\beta\bar{\rho}^3\gamma'k_x^2k_y^2 + 4\bar{T}\beta\bar{\rho}^3\gamma'k_x^2k_z^2 + 8\bar{T}\beta\bar{\rho}^3\gamma'k_y^2k_z^2 + \bar{T}\beta\bar{\rho}^3\gamma k_x^2k_z^3 6i \\
& + \bar{T}\beta\bar{\rho}^3\gamma k_y^2k_z^3 12i + 4\bar{T}\beta'\bar{\rho}^3\gamma k_x^2k_z^2 + 4\bar{T}\beta'\bar{\rho}^3\gamma k_y^2k_z^2 - 4\beta\bar{T}'\beta'\bar{\rho}^3k_y^2k_z^2 \\
& + 6\beta\bar{T}'\bar{\rho}^3\gamma k_y^2k_z^2 + 4\beta\beta'\bar{\rho}^3k_y^2k_z^2\theta(m+1) + 2\bar{B}^2F\bar{T}\bar{\rho}^2k_x^2k_y^2 \\
& + 2\bar{B}^2F\bar{T}\bar{\rho}^2k_x^2k_z^2 - 6\beta\bar{\rho}^3\gamma k_y^2k_z^2\theta(m+1) - \bar{B}F\beta^2\bar{B}'\bar{\rho}^2k_y^4k_z 2i \\
& - \bar{B}^2F\beta\beta'\bar{\rho}^2k_y^4k_z i - \bar{B}F\bar{B}'\beta^2\bar{\rho}^2k_x^2k_z i - \bar{B}^2F\beta'\bar{\rho}^2\gamma'k_x^2k_z i \\
& + \bar{B}^2F\beta\bar{\rho}^2\gamma k_y^4k_z 2i + \bar{B}^2F\bar{\rho}^2\gamma'k_x^2k_z 3i + \bar{B}^2F\bar{\rho}^2\gamma'k_y^2k_z i \\
& + F\beta\bar{B}'^2\beta'\bar{\rho}^2k_y^2k_z i - F\beta\bar{B}'^2\bar{\rho}^2\gamma k_y^2k_z 2i + 4\bar{B}^2F\beta^2\bar{\rho}^2k_x^2k_y^2k_z^2 \\
& + \bar{B}F\bar{T}\bar{B}'\bar{\rho}'\bar{\rho}k_y^2 - 4\bar{T}\beta\beta'\bar{\rho}'\bar{\rho}^2k_y^2k_z^2 + 6\bar{T}\beta\bar{\rho}'\bar{\rho}^2\gamma k_y^2k_z^2 \\
& - \bar{T}\beta\beta'\bar{\rho}^3k_x^2k_y^2k_z 4i + \bar{T}\beta\bar{\rho}^3\gamma k_x^2k_y^2k_z 6i - \bar{B}F\beta^2\bar{B}'\bar{\rho}^2k_y^2k_z^3 4i \\
& - \bar{B}^2F\beta\beta'\bar{\rho}^2k_x^2k_z^3 2i - \bar{B}^2F\beta\beta'\bar{\rho}^2k_y^2k_z^3 2i + 3\bar{B}^2F\beta\bar{\rho}^2\gamma'k_x^2k_y^2 \\
& + 3\bar{B}^2F\beta\bar{\rho}^2\gamma'k_x^2k_z^2 + 2\bar{B}^2F\beta\bar{\rho}^2\gamma'k_y^2k_z^2 + \bar{B}^2F\beta\bar{\rho}^2\gamma k_x^2k_z^3 4i \\
& + \bar{B}^2F\beta\bar{\rho}^2\gamma k_y^2k_z^3 4i + 2\bar{B}^2F\beta'\bar{\rho}^2\gamma k_x^2k_z^2 + \bar{B}^2F\beta'\bar{\rho}^2\gamma k_y^2k_z^2 \\
& - \bar{B}F\bar{T}\bar{B}'\bar{\rho}^2k_x^2k_z i - \bar{B}^2F\bar{T}\bar{\rho}'\bar{\rho}k_x^2k_z i - 2\bar{B}F\beta\bar{B}'\beta'\bar{\rho}^2k_z^4 \\
& - \bar{B}F\beta\bar{B}'\bar{\rho}^2\gamma'k_z^3 2i + \bar{B}F\bar{B}'\beta'\bar{\rho}^2\gamma'k_x^2 + 4\bar{B}F\beta\bar{B}'\bar{\rho}^2\gamma k_z^4 \\
& - \bar{B}F\bar{B}'\beta'\bar{\rho}^2\gamma k_z^3 2i + 2\bar{B}F\bar{B}'\bar{\rho}^2\gamma'k_z^2 - \bar{T}\beta\bar{\rho}'\bar{\rho}^2\gamma'k_y^2k_z 4i \\
& + \beta\bar{T}'\beta'\bar{\rho}'\bar{\rho}^2k_y^2k_z 4i - \beta\bar{T}'\bar{\rho}'\bar{\rho}^2\gamma k_y^2k_z 6i - \beta\beta'\bar{\rho}'\bar{\rho}^2k_y^2k_z\theta(m+1) 4i \\
& + \beta\bar{\rho}'\bar{\rho}^2\gamma k_y^2k_z\theta(m+1) 6i - \bar{B}F\beta\bar{B}'\bar{\rho}^2\gamma'k_y^2k_z 2i + \bar{B}F\bar{B}'\beta'\bar{\rho}^2\gamma k_x^2k_z i \\
& + \bar{B}F\beta\bar{B}'\beta'\bar{\rho}^2k_x^2k_y^2 + \bar{B}F\beta\bar{B}'\beta'\bar{\rho}^2k_x^2k_z^2 - 2\bar{B}F\beta\bar{B}'\beta'\bar{\rho}^2k_y^2k_z^2 \\
& + 4\bar{B}F\beta\bar{B}'\bar{\rho}^2\gamma k_y^2k_z^2 - \bar{B}^2F\beta\beta'\bar{\rho}^2k_x^2k_y^2k_z 2i + \bar{B}^2F\beta\bar{\rho}^2\gamma k_x^2k_y^2k_z 4i,
\end{aligned}$$

$$\begin{aligned}
g_4 = & \bar{\rho}^2 (\beta^3\bar{\rho}k_y^6 + \beta^3\bar{\rho}k_z^6 - \bar{\rho}\gamma^3k_z^3 i - 2\bar{T}'\bar{\rho}'\gamma' + 2\bar{\rho}'\gamma'\theta(m+1)) \quad (B.5) \\
& - F\bar{B}'^2\gamma' - \beta'\bar{\rho}'k_z\theta(m+1) 2i + \bar{\rho}\gamma'k_z\theta(m+1) 2i + \bar{\rho}'\gamma k_z\theta(m+1) 3i \\
& + 3\beta^3\bar{\rho}k_y^2k_z^4 + 3\beta^3\bar{\rho}k_y^4k_z^2 + F\bar{B}'^2\beta'k_z i - F\bar{B}'^2\gamma k_z 2i \\
& - \bar{T}\beta\bar{\rho}'k_z^3 3i + 3\bar{T}\beta\bar{\rho}k_y^4 + 3\bar{T}\beta\bar{\rho}k_z^4 - 2\bar{T}\beta'\bar{\rho}'k_z^2 - \bar{T}\beta'\bar{\rho}k_z^3 2i \\
& + 2\bar{T}\bar{\rho}\gamma'k_x^2 + 2\bar{T}\bar{\rho}\gamma'k_y^2 + 2\bar{T}\bar{\rho}\gamma'k_z^2 + 3\bar{T}\bar{\rho}'\gamma k_z^2 + \bar{T}\bar{\rho}\gamma k_z^3 3i \\
& - 3\beta\bar{T}'\bar{\rho}'k_y^2 - 3\beta\bar{T}'\bar{\rho}'k_z^2 - \beta\bar{T}'\bar{\rho}k_z^3 3i - 2\bar{T}'\beta'\bar{\rho}k_z^2 + 3\bar{T}'\bar{\rho}\gamma k_z^2 \\
& + \bar{\rho}\gamma'^2\gamma k_z i + 3\beta\bar{\rho}'k_y^2\theta(m+1) + 3\beta\bar{\rho}'k_z^2\theta(m+1) + \beta\bar{\rho}k_z^3\theta(m+1) 3i
\end{aligned}$$

## B. COEFFICIENTS OF THE DISPERSION RELATION FOR THE 3D ISOTHERMAL INSTABILITY

---

$$\begin{aligned}
& + 2\beta'\bar{\rho}k_z^2\theta(m+1) - 3\bar{\rho}\gamma k_z^2\theta(m+1) + 2\bar{B}^2F\beta k_y^4 + 2\bar{B}^2F\beta k_z^4 \\
& - \bar{B}^2F\beta'k_z^3i + 3\bar{B}^2F\gamma'k_x^2 + \bar{B}^2F\gamma'k_y^2 + \bar{B}^2F\gamma'k_z^2 + \bar{B}^2F\gamma k_z^32i \\
& - 2F\beta\bar{B}'^2k_y^2 - 2F\beta\bar{B}'^2k_z^2 - \beta\beta'^2\bar{\rho}k_z^4 - \beta^2\beta'\bar{\rho}k_z^52i + \beta\bar{\rho}\gamma'^2k_y^2 \\
& + 2\beta^2\bar{\rho}\gamma'k_y^4 + \beta\bar{\rho}\gamma'^2k_z^2 + 2\beta^2\bar{\rho}\gamma'k_z^4 - 3\beta\bar{\rho}\gamma^2k_z^4 + \beta^2\bar{\rho}\gamma k_z^53i \\
& + \beta'\bar{\rho}\gamma^2k_z^32i - \beta'^2\bar{\rho}\gamma k_z^3i - 2\bar{\rho}\gamma'\gamma^2k_z^2 - \bar{T}\bar{\rho}'\gamma'k_z2i + \bar{T}'\beta'\bar{\rho}'k_z2i \\
& - \bar{T}'\bar{\rho}\gamma'k_z2i - \bar{T}'\bar{\rho}'\gamma k_z3i + 3\bar{T}\beta\bar{\rho}k_x^2k_y^2 + 3\bar{T}\beta\bar{\rho}k_x^2k_z^2 + 6\bar{T}\beta\bar{\rho}k_y^2k_z^2 \\
& - \bar{B}F\bar{B}'\gamma'k_z2i - \beta^2\beta'\bar{\rho}k_y^4k_z2i + \beta^2\bar{\rho}\gamma k_y^4k_z3i + 4\bar{B}^2F\beta k_x^2k_y^2 \\
& + 4\bar{B}^2F\beta k_x^2k_z^2 + 4\bar{B}^2F\beta k_y^2k_z^2 - \bar{B}F\beta\bar{B}'k_z^34i + \bar{B}F\bar{B}'\beta'k_x^2 \\
& - 2\bar{B}F\bar{B}'\beta'k_z^2 + 4\bar{B}F\bar{B}'\gamma k_z^2 - \beta\beta'^2\bar{\rho}k_y^2k_z^2 - \beta^2\beta'\bar{\rho}k_y^2k_z^34i \\
& + 4\beta^2\bar{\rho}\gamma'k_y^2k_z^2 - 3\beta\bar{\rho}\gamma^2k_y^2k_z^2 + \beta^2\bar{\rho}\gamma k_y^2k_z^36i - \bar{T}\beta\bar{\rho}'k_y^2k_z3i \\
& - \bar{T}\beta'\bar{\rho}k_x^2k_z2i - \bar{T}\beta'\bar{\rho}k_y^2k_z2i + \bar{T}\bar{\rho}\gamma k_x^2k_z3i + \bar{T}\bar{\rho}\gamma k_y^2k_z3i \\
& - \beta\beta'\bar{\rho}\gamma'k_z^32i + 4\beta\beta'\bar{\rho}\gamma k_z^4 + \beta\bar{\rho}\gamma'\gamma k_z^34i + 2\beta'\bar{\rho}\gamma'\gamma k_z^2 \\
& - \beta\bar{T}'\bar{\rho}k_y^2k_z3i + \beta\bar{\rho}k_y^2k_z\theta(m+1)3i - \bar{B}^2F\beta'k_x^2k_z2i - \bar{B}^2F\beta'k_y^2k_zi \\
& + \bar{B}^2F\gamma k_x^2k_z4i + \bar{B}^2F\gamma k_y^2k_z2i - \beta\beta'\bar{\rho}\gamma'k_y^2k_z2i + \beta\bar{\rho}\gamma'\gamma k_y^2k_z4i \\
& + 4\beta\beta'\bar{\rho}\gamma k_y^2k_z^2 - \bar{B}F\beta\bar{B}'k_y^2k_z4i),
\end{aligned}$$

$$\begin{aligned}
g_5 = \bar{\rho}^2 & \left( \bar{\rho}'\theta(m+1) - \bar{T}'\bar{\rho}' - F\bar{B}'^2 + \bar{\rho}\gamma'^2 + 2\bar{B}^2Fk_x^2 + \bar{B}^2Fk_y^2 \right. \\
& + \bar{B}^2Fk_z^2 + 3\beta^2\bar{\rho}k_y^4 + 3\beta^2\bar{\rho}k_z^4 - \beta'^2\bar{\rho}k_z^2 - 3\bar{\rho}\gamma^2k_z^2 - \bar{T}\bar{\rho}'k_zi \\
& - \bar{T}'\bar{\rho}k_zi + \bar{\rho}k_z\theta(m+1)i + \bar{T}\bar{\rho}k_x^2 + \bar{T}\bar{\rho}k_y^2 + \bar{T}\bar{\rho}k_z^2 + 6\beta^2\bar{\rho}k_y^2k_z^2 \\
& - \beta\beta'\bar{\rho}k_z^34i + 4\beta\bar{\rho}\gamma'k_y^2 + 4\beta\bar{\rho}\gamma'k_z^2 + \beta\bar{\rho}\gamma k_z^36i + 4\beta'\bar{\rho}\gamma k_z^2 \\
& \left. - \bar{B}F\bar{B}'k_z2i - \beta'\bar{\rho}\gamma'k_z2i + \bar{\rho}\gamma'\gamma k_z4i - \beta\beta'\bar{\rho}k_y^2k_z4i + \beta\bar{\rho}\gamma k_y^2k_z6i \right),
\end{aligned} \tag{B.6}$$

$$g_6 = \bar{\rho}^3 (2\gamma' + ik_z(3\gamma - 2\beta') + 3\beta(k_y^2 + k_z^2)), \tag{B.7}$$

$$g_7 = \bar{\rho}^3. \tag{B.8}$$

# References

- ABRAMOWITZ, M. & STEGUN, I. (1964). *Handbook of Mathematical Functions*. United States Department of Commerce/National Bureau of Standards. [157](#)
- ACHESON, D. (1978). On the instability of toroidal magnetic fields and differential rotation in stars. *Philosophical Transactions of the Royal Society of London*, **289**, 459–500. [171](#)
- ACHESON, D. (1979). Instability by magnetic buoyancy. *Solar Physics*, **62**, 23–50. [10](#), [12](#), [13](#), [26](#), [137](#), [164](#), [171](#), [184](#)
- BARKER, A., SILVERS, L., PROCTOR, M. & WEISS, N. (2012). Magnetic buoyancy instabilities in the presence of magnetic flux pumping at the base of the solar convection zone. *Monthly Notices of the Royal Astronomical Society*, **424**, 115–127. [14](#), [24](#), [29](#), [33](#), [67](#), [75](#), [86](#), [130](#), [183](#)
- BASU, S., ANTIA, H. & NARASIMHA, D. (1994). Helioseismic measurement of the extent of overshoot below the solar convection zone. *Monthly Notices of the Royal Astronomical Society*, **267**, 209–224. [6](#)
- BRIGGS, R. (1964). *Electron-Stream Interaction with Plasmas*. MIT Press. [174](#)
- BROWN, T. (1985). Solar rotation as a function of depth and latitude. *Nature*, **317**, 591–594. [6](#)
- BROWN, T. (1989). Inferring the sun’s angular velocity from observed p-mode frequency splittings. *The Astrophysical Journal*, **343**, 526–546. [6](#)
- BROWN, T. & MORROW, C. (1987). Depth and latitude dependence of solar rotation. *The Astrophysical Journal*, **314**, L21–L26. [6](#)

## REFERENCES

---

- CATTANEO, F. & HUGHES, D. (1988). The nonlinear breakup of a magnetic layer: instability to interchange modes. *Journal of Fluid Mechanics*, **196**, 323–344. [14](#), [26](#), [29](#)
- CATTANEO, F. & HUGHES, D. (2006). Dynamo action in a rotating convective layer. *Journal of Fluid Mechanics*, **553**, 401–418. [22](#)
- CATTANEO, F. & HUGHES, D. (2009). Problems with kinematic mean field electrodynamics at high magnetic reynolds numbers. *Monthly Notices of the Royal Astronomical Society*, **395**, L48L51. [21](#)
- CATTANEO, F., HUGHES, D. & PROCTOR, M. (1988). Mean advection effects in turbulence. *Geophysical & Astrophysical Fluid Dynamics*, **41**, 335–342. [22](#)
- CHARBONNEAU, P., CHRISTENSEN-DALSGAARD, J., HENNING, R., LARSEN, R., SCHOU, J., THOMPSON, M. & TOMCZYK, S. (1999). Helioseismic constraints on the structure of the solar tachocline. *The Astrophysical Journal*, **527**, 445–460. [6](#)
- CHOUDHURI, A., SCHÜSSLER, M. & DIKPATI, M. (1995). The solar dynamo with meridional circulation. *Astronomy and Astrophysics*, **303**, L29–L32. [17](#)
- CHRISTENSEN-DALSGAARD, J., GOUGH, D. & THOMPSON, M. (1991). The depth of the solar convection zone. *The Astrophysical Journal*, **378**, 413–437. [5](#)
- COUAIRO, A. & CHOMAZ, J. (1997). Pattern selection in the presence of a cross flow. *Physical Review Letters*, **79**, 2666–2669. [175](#)
- COWLING, T. (1933). The magnetic field of sunspots. *Monthly Notices of the Royal Astronomical Society*, **94**, 39–48. [19](#)
- DAVIES, C. & HUGHES, D. (2011). The mean electromotive force resulting from magnetic buoyancy instability. *The Astrophysical Journal*, **727**, 112, 12 pp. [23](#)
- DORMY, E. & SOWARD, A. (2007). *Mathematical Aspects of Natural Dynamos*. CRC Press/Taylor & Francis. [18](#)

## REFERENCES

---

- DROBYSHEVSKI, E. & YUFEREV, V. (1974). Topological pumping of magnetic flux by three-dimensional convection. *Journal of Fluid Mechanics*, **65**, 33–44. [22](#)
- DUVALL, T., DZIEMBOWSKI, W., GOODE, P., GOUGH, D., HARVEY, J. & LEIBACHER, J. (1984). Internal rotation of the sun. *Nature*, **310**, 22–25. [6](#)
- DUVALL, T., HARVEY, J. & POMERANTZ, M. (1986). Latitude and depth variation of solar rotation. *Nature*, **321**, 500–501. [6](#)
- DZIEMBOWSKI, W. (1989). The radial gradient in the sun’s rotation. *The Astrophysical Journal*, **337**, L53–L57. [6](#)
- GILMAN, P. (1970). Instability of magnetohydrostatic stellar interiors from magnetic buoyancy. i. *The Astrophysical Journal*, **162**, 1019–1029. [11](#), [13](#), [25](#), [137](#), [140](#), [142](#), [156](#), [167](#), [175](#), [183](#)
- GILMAN, P., MORROW, C. & DELUCA, E. (1989). Angular momentum transport and dynamo action in the sun: implications of recent oscillation measurements. *The Astrophysical Journal*, **338**, 528–537. [6](#)
- GLATZMAIER, G. & ROBERTS, P. (1995). A three-dimensional convective dynamo solution with rotating and finitely conducting inner core and mantle. *Physics of the Earth and Planetary Interiors*, **91**, 63–75. [17](#)
- GOLUB, L., ROSNER, R., VAIANA, G. & WEISS, N. (1981). Solar magnetic fields: the generation of emerging flux. *The Astrophysical Journal*, **243**, 309–316. [6](#), [20](#)
- GOUGH, D. (2007). *The Solar Tachocline*, ed. Hughes, D.W., Rosner, R., & Weiss, N., chap. An Introduction to the Solar Tachocline. Cambridge University Press. [188](#)
- HALE, G. (1908). On the probable existence of a magnetic field in sunspots. *The Astrophysical Journal*, **28**, 315–343. [2](#)
- HOOD, A. & HUGHES, D. (2011). Solar magnetic fields. *Physics of the Earth and Planetary Interiors*, **187**, 78–91. [23](#), [186](#)

## REFERENCES

---

- HUERRE, P. & MONKEWITZ, P. (1990). Local and global instabilities in spatially developing flows. *Annual Review of Fluid Mechanics*, **22**, 473–537. [174](#)
- HUGHES, D. (1985). Magnetic buoyancy instabilities for a static plane layer. *Geophysical & Astrophysical Fluid Dynamics*, **32:3-4**, 273–316. [13](#), [164](#), [171](#), [172](#), [184](#)
- HUGHES, D. (2007). *The Solar Tachocline*, ed. Hughes, D.W., Rosner, R., & Weiss, N., chap. Magnetic buoyancy instabilities in the tachocline. Cambridge University Press. [9](#), [12](#)
- HUGHES, D. (2018). Mean field electrodynamics: triumphs and tribulations. *Journal of Plasma Physics*, **84**. [21](#), [23](#)
- HUGHES, D. & CATTANEO, F. (1987). A new look at the instability of a stratified horizontal magnetic field. *Geophysical & Astrophysical Fluid Dynamics*, **39**, 65–81. [11](#), [13](#), [88](#), [134](#)
- HUGHES, D. & CATTANEO, F. (2008). The alpha-effect in rotating convection: size matters. *Journal of Fluid Mechanics*, **594**, 445461. [23](#)
- HUGHES, D. & PROCTOR, M. (2010). Turbulent magnetic diffusivity tensor for time-dependent mean fields. *Physical Review Letters*, **104**, 024503. [23](#)
- KERSALÉ, E., HUGHES, D. & TOBIAS, S. (2007). The nonlinear evolution of instabilities driven by magnetic buoyancy: a new mechanism for the formation of coherent magnetic structures. *The Astrophysical Journal*, **663**, L113–L116. [14](#), [31](#)
- KOSOVICHEV, A. (1988). The internal rotation of the sun from helioseismological data. *Soviet Astronomy Letters*, **14**, 145–149. [6](#)
- KRAUSE, F. & RÄDLER, K.H. (1980). *Mean field magnetohydrodynamics and dynamo theory*. Pergamon Press. [18](#)
- KRUSKAL, M. & SCHWARZSCHILD, M. (1954). Some instabilities of a completely ionized plasma. *Proceedings of the Royal Society of London. Series A, Mathematical and Physical Sciences*, **223**, 348–360. [12](#)

## REFERENCES

---

- MASON, J., HUGHES, D. & TOBIAS, S. (2008). The effects of flux transport on interface dynamos. *Monthly Notices of the Royal Astronomical Society*, **391**, 467480. [23](#)
- MATTHEWS, P., HUGHES, D. & PROCTOR, M. (1995). Magnetic buoyancy, vorticity, and three-dimensional flux-tube formation. *The Astrophysical Journal*, **448**, 938–941. [14](#), [29](#), [31](#)
- MEUNIER, N., PROCTOR, M., SOKOLOFF, D., SOWARD, A. & TOBIAS, S. (1997). Asymptotic properties of a nonlinear  $\alpha\omega$ -dynamo wave: Period, amplitude and latitude dependence. *Geophysical & Astrophysical Fluid Dynamics*, **86**, 249–285. [175](#)
- MIZERSKI, K., DAVIES, C. & HUGHES, D. (2013). Short-wavelength magnetic buoyancy instability. *The Astrophysical Journal*, **205**. [13](#), [26](#), [137](#), [142](#), [143](#), [146](#), [156](#), [157](#), [176](#), [184](#)
- MOFFATT, H. (1978). *Magnetic field generation in electrically conducting fluids*. Cambridge University Press. [17](#), [19](#), [20](#), [22](#)
- MOFFATT, H. (1983). Transport effects associated with turbulence with particular attention to the influence of helicity. *Reports on Progress in Physics*, **46**, 621–664. [22](#)
- MOFFATT, H. & DORMY, E. (2019). *Self-Exciting Fluid Dynamos*. Cambridge University Press. [18](#), [21](#)
- NEWCOMB, W. (1961). Convective instability induced by gravity in a plasma with a frozen-in magnetic field. *Physics of Fluids*, **4**, 391–396. [11](#), [12](#), [137](#)
- OSSENDRIJVER, M. (2003). The solar dynamo. *The Astronomy and Astrophysics Review*, **11**, 287–367. [23](#), [186](#)
- OSSENDRIJVER, M., STIX, M., BRANDENBURG, A. & RÜDIGER, G. (2002). Magnetoconvection and dynamo coefficients ii. field-direction dependent pumping of magnetic field. *Astronomy & Astrophysics*, **394**, 735–745. [22](#)

## REFERENCES

---

- PARKER, E. (1955a). Formation of sunspots from the solar toroidal field. *The Astrophysical Journal*, **121**, 491–507. [9](#), [15](#)
- PARKER, E. (1955b). Hydromagnetic dynamo models. *The Astrophysical Journal*, **122**, 293–314. [19](#)
- PARKER, E. (1975). The generation of magnetic fields in astrophysical bodies. x. magnetic buoyancy and the solar dynamo. *The Astrophysical Journal*, **198**, 205–209. [13](#)
- PARKER, E. (1993). A solar dynamo surface wave at the interface between convection and nonuniform rotation. *The Astrophysical Journal*, **408**, 707–719. [7](#)
- PLUNIAN, F. & RÄDLER, K.H. (2002). Subharmonic dynamo action in the roberts flow. *Geophysical & Astrophysical Fluid Dynamics*, **96**, 115–133. [22](#)
- ROBERTS, G. (1970). Spatially periodic dynamos. *Philosophical Transactions of the Royal Society of London. Series A, Mathematical and Physical Sciences*, **266**, 535–558. [22](#)
- ROBERTS, P. & STIX, M. (1971). *The turbulent dynamo: a translation of a series of papers by F. Krause, K.-H. Rädler and M. Steenbeck*. NCAR, Boulder, Colorado. [17](#)
- SOWARD, A. & JONES, C. (1983). The linear stability of the flow in the narrow gap between two concentric rotating spheres. *The Quarterly Journal of Mechanics and Applied Mathematics*, **36**, 1942. [175](#)
- SPIEGEL, E. (1972). *Physics of the solar system*, ed. Rasool, S.I., chap. A History of Solar Rotation. NASA SP-300. [6](#)
- SPIEGEL, E. & WEISS, N. (1980). Magnetic activity and variations in solar luminosity. *Nature*, **287**, 616–617. [6](#)
- SPIEGEL, E. & ZAHN, J.P. (1992). The solar tachocline. *Astronomy & Astrophysics*, **265**, 106–114. [6](#)

## REFERENCES

---

- STEENBECK, M., KRAUSE, F. & RÄDLER, K.H. (1966). A calculation of the mean electromotive force in an electrically conducting fluid in turbulent motion, under the influence of coriolis forces. *Zeitschrift für Naturforschung*, **21a**, 369–376. [17](#), [19](#)
- TAYLER, R. (1973). The adiabatic stability of stars containing magnetic fields - i toroidal fields. *Monthly Notices of the Royal Astronomical Society*, **161**, 365–380. [13](#)
- THOMAS, J. & NYE, A. (1975). Convective instability in the presence of a nonuniform horizontal magnetic field. *The Physics of Fluids*, **18**, 490–491. [11](#), [12](#)
- TOBIAS, S., BRUMMELL, N., CLUNE, T. & TOOMRE, J. (1998a). Pumping of magnetic fields by turbulent penetrative convection. *The Astrophysical Journal*, **502**, L177–L180. [24](#)
- TOBIAS, S., PROCTOR, M. & KNOBLOCH, E. (1998b). Convective and absolute instabilities of fluid flows in finite geometry. *Physica D*, **113**, 43–72. [175](#)
- TREFETHEN, L. (2000). *Spectral Methods in Matlab*. Society for Industrial and Applied Mathematics. [85](#)
- VASIL, G. & BRUMMELL, N. (2008). Magnetic buoyancy instabilities of a shear-generated magnetic layer. *The Astrophysical Journal*, **686**, 709–730. [14](#)
- WISSINK, J., HUGHES, D., MATTHEWS, P. & PROCTOR, M. (2000). The three-dimensional breakup of a magnetic layer. *Monthly Notices of the Royal Astronomical Society*, **318**, 501–510. [14](#)